Slovenian Veterinary Research

Slovenski veterinarski zbornik

THE SCIENTIFIC JOURNAL OF THE VETERINARY FACULTY UNIVERSITY OF LJUBLJANA

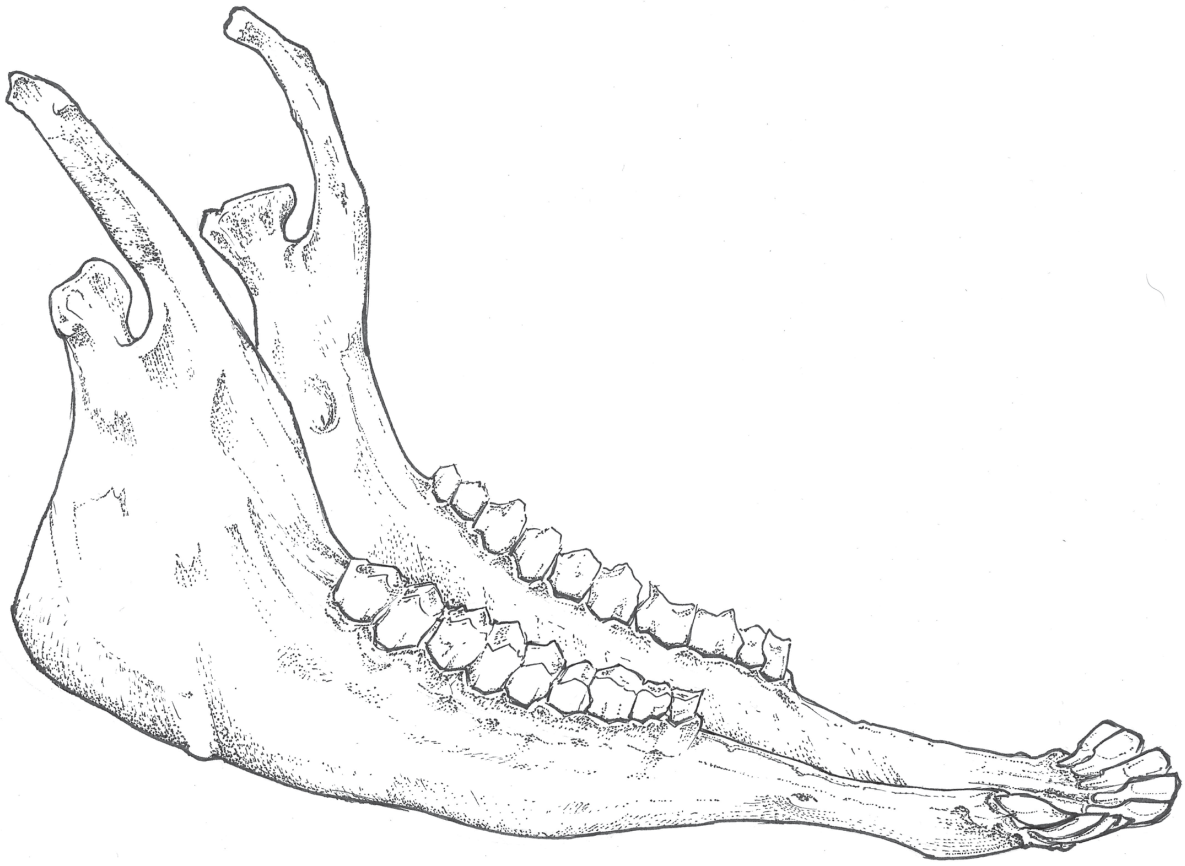

ISSN 1580-4003

Slov Vet Res, Ljubljana, Volume 62, Number 3, Pages 125–240

Slovenian Veterinary Research

Slovenski veterinarski zbornik

THE SCIENTIFIC JOURNAL OF THE VETERINARY FACULTY UNIVERSITY OF LJUBLJANA

Slov Vet Res, Ljubljana, Volume 62, Number 3, Pages 125–240

The Scientific Journal of the Veterinary Faculty University of Ljubljana

Slovenian Veterinary Research

Slovenski veterinarski zbornik

Previously: RESEARCH REPORTS OF THE VETERINARY FACULTY UNIVERSITY OF LJUBLJANA
Prej: ZBORNIK VETERINARSKE FAKULTETE UNIVERZA V LJUBLJANI

4 issues per year / Izhaja štirikrat letno
Volume 62, Number 3 / Letnik 62, Številka 3

Published by / Založila	University of Ljubljana Press / Založba Univerze v Ljubljani
For the Publisher / Za založbo	Gregor Majdič, Rector of the University of Ljubljana / Rektor Univerze v Ljubljani
Issued by / Izdala	Veterinary Faculty University of Ljubljana / Veterinarska fakulteta Univerze v Ljubljani
For the Issuer / Za izdajatelja	Breda Jakovac Strajn, Dean of the Veterinary Faculty / Dekanja Veterinarske fakultete
Address	Veterinary Faculty, Gerbičeva 60, 1000 Ljubljana, Slovenia
Naslov	Veterinarska fakulteta, Gerbičeva 60, 1000 Ljubljana, Slovenija
Phone / Telefon	+386 (0)1 4779 100
E-mail	slovetres@vf.uni-lj.si
Sponsored by / Sofinancira	The Slovenian Research Agency / Javna agencija za raziskovalno dejavnost Republike Slovenije
Printed by / Tisk	DZS, d.d., Ljubljana, September/September 2025
Number of copies printed / Naklada	220
Indexed in / Indeksirano v	Agris, Biomedicina Slovenica, CAB Abstracts, IVSI Urlich's International Periodicals Directory, Science Citation Index Expanded, Journal Citation Reports – Science Edition
	https://www.slovetres.si/
	ISSN 1580-4003 2385-8761 (on-line)

The cover illustration by Pšenica Kovačič provides an artistic interpretation of the goat mandible, inspired by the comparative anatomy article featured in this issue, "*Morphometric Analysis of the Mandible in Sheep, Goat, and Rabbit*" by Evcim and Kara.

Table of Content

Slov Vet Res
DOI 10.26873/SVR-2320-2025
UDC 591.4:636.09:378:159.938.363.6
Pages: 129–37

Editorial

The Language of Bodies: Comparative Anatomy as a Unifying Science for Education, Research, and One Health

Ko telo spregovori: primerjalna anatomija kot povezovalna znanost v izobraževanju, raziskovanju in okviru koncepta Eno zdravje

Key words

comparative anatomy;
education;
research;
one health

Accepted: 26 September 2025

Valentina Kubale[1*§], William Perez[2¥], and Catrin S. Rutland[3†]

[1]Veterinary faculty, University of Ljubljana, Slovenia, [2]National Research System and PEDECIBA, Montevideo, Uruguay, [3]School of Veterinary Medicine and Science, Faculty of Medicine and Health Sciences, University of Nottingham, Nottingham, United Kingdom , *Co-Editor, Slovenian Veterinary Research journal, [§]Secretary general of European association of veterinary anatomists (EAVA), [¥]President of World Association of Veterinary Anatomists (WAVA), [†]President of European Association of veterinary anatomists (EAVA)

***Corresponding Author:** valentina.kubaledvojmoc@vf.uni-lj.si

Comparative anatomy, the study of structural similarities and differences between animals and humans, remains one of the oldest and most enduring foundations of veterinary and medical science (1). From the dissections of Aristotle, Galen, and Vesalius through to the anatomical theatres and museums of the 19th century and beyond, comparative examination has shaped our understanding of the living world (2, 3, 4). It is no coincidence that the very roots of biology, medicine, and veterinary science are deeply embedded in this discipline. Examining the horse's limb, the ruminant stomach, or the avian lung not only satisfies scientific curiosity but also provides veterinarians with essential knowledge for diagnosis, surgery, and disease prevention, while at the same time revealing important parallels with human medicine (5, 6), and *vice versa*.

For veterinary students, comparative anatomy is far more than an abstract subject or a purely theoretical exercise. It provides a framework for connecting the immense diversity of animals they will encounter in practice, from farm and companion animals to wildlife and exotic animals, with

Primerjalna anatomija, veda o strukturnih podobnostih in razlikah med živalmi in človekom, ostaja ena najstarejših in najtrdnejših osnov veterinarske in medicinske znanosti (1). Od disekcij Aristotela, Galena in Vesaliusa do anatomskih gledališč in muzejev 19. stoletja ter kasneje je primerjalno proučevanje oblikovalo naše razumevanje živega sveta (2, 3, 4). Ni naključje, da so prav v tej disciplini korenine biologije, medicine in veterinarske znanosti. Proučevanje okončine konja, želodca prežvekovalcev ali pljuč ptic ne zadovoljuje le znanstvene radovednosti, temveč veterinarjem zagotavlja temeljno znanje za diagnostiko, kirurgijo in preprečevanje bolezni, hkrati pa razkriva pomembne vzporednice s človeško medicino (5, 6) in obratno.

Za študente veterine je primerjalna anatomija veliko več kot abstrakten predmet ali zgolj teoretična vaja. Predstavlja okvir, s katerim povezujejo izjemno raznolikost živali, s katerimi se bodo srečevali v praksi, od domačih in rejnih živali do prostoživečih in eksotičnih vrst, z osnovnimi strukturnimi in funkcionalnimi načeli. Hkrati deluje kot univerzalni jezik, ki jih uči, kako »brati« telesa številnih vrst, s katerimi bodo delali. V

general structural and functional principles. It also serves as a universal language, teaching them how to "read" the bodies of the many species they will work with. Throughout history comprehensive comparative anatomy has also supported societies during extreme crisis periods. Proficiency in this area has supported veterinary professionals required to work within human healthcare settings, such as during times of war and in epidemics and pandemics. These situations are rare, but arguably the most important rationale for comparative anatomy are the everyday implications and uses.

By understanding differences in the avian respiratory system, the reptilian cardiovascular system, or the mammalian gastrointestinal tract, students learn to adapt their anatomical and clinical knowledge across species. Comparative anatomy trains them to identify differences that have practical implications, for instance, why intubation techniques vary between ruminants and carnivores, while also appreciating the shared features that unify vertebrate structure. In this way, it not only reinforces conceptual understanding but also fosters intellectual flexibility. Once students grasp the underlying blueprint of the vertebrate body, they can extend and adapt their anatomical knowledge, connected to clinical skills to almost any animal they encounter.

The significance of comparative anatomy extends well beyond veterinary medicine. Increasingly, it is recognized as a crucial bridge between animal and human health. The concept of Zoobiquity, popularized in recent years, underscores the fact that many diseases transcend species boundaries (7). Heart disease in chimpanzees, obesity in cats, mammary cancer in dogs, and cruciate ligament tears in horses all mirror conditions familiar in human medicine. Research highlighting the comparative nature of these, and many more conditions, are evidencing the similarities and differences in numerous species. Veterinarians, physicians, and research scientists share common foundations in anatomy, physiology, and pathology, and by approaching these conditions comparatively, all of these, and allied, professions gain valuable insights. Comparative anatomy provides the shared vocabulary for this dialogue. It reminds us that the human body is not unique in its vulnerabilities and that novel solutions may emerge when we look beyond our own species (7, 8).

Within the broader framework of One Health, comparative anatomy has established a great importance and provides the evidence base that links clinical practice, public health, and evolutionary adaptation. It is not merely an academic pursuit, but a dynamic, applied science that connects bodies across species and domains (8, 9). Understanding comparative anatomy highlights interspecies connections and clarifies disease mechanisms and zoonotic pathways. Numerous examples illustrate this integrative potential. Canine models for ocular disease, such as the Swiss Briard dog with Leber congenital amaurosis, have led to human gene therapies like Luxturna®. Cavalier King Charles Spaniels with spontaneous Chiari malformation provide insights into human neurology

zgodovini je celovito poznavanje primerjalne anatomije podpiralo družbe tudi v obdobjih hudih kriz. Usposobljenost na tem področju je omogočala veterinarskim strokovnjakom delovanje tudi v humanem zdravstvenem sistemu, na primer v času vojn, epidemij in pandemij. Takšne situacije so sicer redke, vendar je mogoče trditi, da je najpomembnejši pomen primerjalne anatomije videti v njeni vsakodnevni uporabi in rezultatih.

Z razumevanjem razlik v dihalnem sistemu ptic, srčno-žilnem sistemu plazilcev ali prebavnem traktu sesalcev se študenti učijo prilagajati svoje anatomsko in klinično znanje različnim vrstam. Primerjalna anatomija jih uri v prepoznavanju razlik s praktičnimi posledicami, npr. zakaj se tehnike intubacije razlikujejo med prežvekovalci in mesojedimi živalmi, hkrati pa jih spodbuja k razumevanju skupnih značilnosti, ki povezujejo zgradbo vretenčarjev. Na ta način ne le krepi konceptualno razumevanje, temveč tudi spodbuja intelektualno prožnost. Ko študenti enkrat razumejo osnovni »načrt« telesa vretenčarjev, lahko svoje anatomsko znanje povežejo s kliničnimi spretnostmi in ga uporabijo pri skoraj katerikoli živali, s katero se srečajo.

Pomen primerjalne anatomije sega daleč preko meja veterinarske medicine. Vedno pogosteje jo prepoznavamo kot ključen most med zdravjem živali in človeka. Koncept Zoobiquity, ki je v zadnjih letih pridobil veliko pozornosti, poudarja dejstvo, da številne bolezni presegajo meje posameznih živalskih vrst (7). Srčne bolezni pri šimpanzih, debelost pri mačkah, rak mlečne žleze pri psih in poškodbe križnih vezi pri konjih so le nekateri primeri stanj, ki so dobro poznana tudi v humani medicini. Raziskave, ki izpostavljajo primerjalno naravo teh in številnih drugih bolezni, razkrivajo podobnosti in razlike med različnimi vrstami. Veterinarji, zdravniki in raziskovalci si delijo skupne temelje v anatomiji, fiziologiji in patologiji, in ko k tem stanjem pristopijo primerjalno, te stroke pridobijo dragocene vpoglede. Primerjalna anatomija zagotavlja skupen jezik za tak dialog. Spominja nas, da človeško telo ni edinstveno v svojih ranljivostih in da se lahko nove rešitve pojavijo, ko pogled usmerimo preko meja lastne vrste (7, 8).

Širše gledano ima v okvirju koncepta Eno zdravje (iz angl. One Health) primerjalna anatomija izjemen pomen, saj predstavlja znanstveno podlago, ki povezuje klinično prakso, javno zdravje in evolucijsko prilagoditev. Ni zgolj akademska disciplina, temveč dinamična, uporabna znanost, ki povezuje telesa različnih vrst in področij (8, 9). Razumevanje primerjalne anatomije poudarja medvrstne povezave ter pojasnjuje mehanizme bolezni in poti zoonotskih okužb. Številni primeri ponazarjajo njen povezovalni potencial. Pasji modeli za očesne bolezni, kot je švicarski briard z Leberjevo hereditarno optično nevropatijo, so omogočili razvoj genskih terapij pri ljudeh, med drugim zdravila Luxturna®. Španjeli, kavalirji kralja Karla, s spontano deformacijo Chiari, nudijo pomemben vpogled v človeško nevrologijo in njeno gensko terapijo. Raziskave mačjega koronavirusa (iz angl. feline infectious peritonitis, FCoV) so neposredno prispevale

and gene therapy approaches. Feline coronavirus research (feline infectious peritonitis, FCoV) directly advised treatment strategies for SARS-CoV-2 patients, with GS-441524 as a key therapeutic molecule. Comparative oncology demonstrates how elephants, with over 20 TP53 gene copies, naked mole rats, and bowhead whales naturally resist cancer, inspiring translational cancer research. Comparative reproductive biology reveals the variety of sex determination systems across vertebrates, from XY and ZW chromosomal mechanisms to sequential hermaphroditism and temperature-dependent sex in reptiles (10).

Other examples connect physiology and anatomy more closely to education. The photochemistry and molecular structure of respiratory pigments explain the diversity of oxygen dissociation curves across species, while comparisons of human and avian respiratory systems highlight the efficiency of avian gas exchange and ventilation. The eyes of mantis shrimps, with their 16 color receptors, serve as striking models for teaching eye anatomy and physiology (11). The equine auditory tube and guttural pouch offer instructive parallels to human otitis media (12). Comparative anatomy of the shoulder joint with its stability mechanisms, biomechanics, and vulnerability to dislocation provides another clinically relevant bridge.

Meat inspection demonstrates how anatomical precision underpins food safety and public trust in the food chain (13). Anatomical comparisons help develop surgical tools and techniques, used in one species and adapted for the needs of others. Whilst perhaps historically this was developed in animals to use in people, we now recognise the important of adapting practices used by physicians to support veterinary practice. Understanding anatomical similarities and differences can also help provide insight into diagnostic, prognostic and therapeutic advances across different species.

Anatomy should be recognized as the ideal entry point for One Health thinking. It is taught early in both veterinary and medical curricula, providing the foundation for later professional development. Many accreditation standards for health professions already share One Health core competencies, and these should be introduced from the very beginning of anatomy courses through real case studies and comparative examples (8, 9).

One Health examples should be embedded in lectures, dissections, practical sessions, electives, and problem-based learning. Comparative exchange days or joint projects, modelled on initiatives at Tufts and UPenn Universities, can bring together veterinary, medical, and public health students to learn side by side (14). Modern tools such as virtual anatomy platforms, 3D printing, and shared digital case libraries facilitate cross-disciplinary connections. Real-world applications, outbreak tracing, wildlife crime investigations, and meat safety inspections, should be highlighted to show how anatomical knowledge protects societies. Finally, student

k razvoju terapevtskih pristopov za bolnike s SARS-CoV-2, pri čemer je bila učinkovina GS-441524 ključna terapevtska molekula. Primerjalna onkologija razkriva, kako nekatere živalske vrste, npr. sloni z več kot 20 kopijami gena TP53, gole krtaste podgane in grenlandski kiti, naravno izkazujejo odpornost proti raku ter tako navdihujejo translacijske raziskave raka. Primerjalna reprodukcija pa odkriva raznolikost sistemov za določanje spola pri vretenčarjih od kromosomskih mehanizmov XY in ZW do zaporednega hermafroditizma ter temperaturno odvisnega določanja spola pri plazilcih (10).

Drugi primeri še tesneje povezujejo fiziologijo in anatomijo z izobraževanjem. Fotokemija in molekularna zgradba dihalnih pigmentov pojasnjujeta raznolikost disociacijskih krivulj kisika med vrstami, medtem ko primerjava dihalnega sistema človeka in ptic razkriva izjemno učinkovitost izmenjave plinov in ventilacije pri pticah. Oči rakov bogomolčarjev, ki imajo kar 16 receptorjev za barve, predstavljajo osupljive modele za poučevanje anatomije in fiziologije vida (11). Sluhovod in zračni mehur konja ponujata poučno vzporednico s človeškim vnetjem srednjega ušesa (12). Primerjalna anatomija ramenskega sklepa z mehanizmi njegove stabilnosti, biomehaniko in nagnjenostjo k izpahom predstavlja še en klinično pomemben most med živalskimi vrstami.

Inšpekcija mesa jasno kaže, kako anatomska natančnost podpira varnost hrane in zaupanje javnosti v prehransko verigo (13). Primerjalne anatomske raziskave pomagajo pri razvoju kirurških instrumentov in tehnik, ki se uporabljajo pri eni vrsti ter nato prilagodijo potrebam druge. Če je bilo v preteklosti pogosto tako, da so se postopki razvijali najprej pri živalih in nato uporabljali pri ljudeh, danes vedno bolj prepoznavamo pomen prenosa znanj tudi v obratni smeri iz humane medicine v veterinarsko prakso. Razumevanje anatomskih podobnosti in razlik tako omogoča nov vpogled v diagnostične, prognostične in terapevtske napredke pri različnih vrstah.

Anatomijo bi bilo treba prepoznati kot idealno izhodišče za razmišljanje v okviru koncepta Eno zdravje. Poučuje se že v zgodnjih fazah tako veterinarskih kot medicinskih študijskih programov in predstavlja temelj za nadaljnji strokovni razvoj. Številni akreditacijski standardi zdravstvenih poklicev že vključujejo temeljne kompetence One Health, ki bi jih bilo treba vpeljati že od samega začetka poučevanja anatomije z uporabo resničnih primerov in primerjalnih pristopov (8, 9).

Primeri koncepta Eno zdravje bi morali biti vključeni v predavanja, disekcije, praktične vaje, izbirne predmete in problemsko učenje. Dnevi primerjalne izmenjave ali skupni projekti, po vzoru iniciativ na univerzah Tufts in UPenn, lahko povežejo študente veterine, medicine in javnega zdravja pri skupnem učenju (14). Sodobna orodja, kot so virtualne anatomske platforme, 3D-tiskanje in skupne digitalne baze primerov, omogočajo učinkovite interdisciplinarne povezave. Poudariti bi bilo treba tudi praktično vrednost anatomskega

engagement should be encouraged through One Health clubs, joint research projects, and exchange opportunities, ensuring that the next generation views anatomy not only as a science of structure, but as a discipline at the core of global health and security (13).

Recently published article by Ruberte et al., 2025 (15) is highly relevant for comparative anatomy from another perspective, as it highlights the importance of consistent and comparable terminology for both animal and human biomedical research. The article points out the comparative perspective of using of mice as key models in comparative and translational research for humans and animals. The mouse remains one of the most widely used models for human diseases, yet its anatomical nomenclature is fragmented, with dozens of competing terms for the same liver lobes or muscles, frequent use of outdated eponyms, and even "do-it-yourself" descriptions by researchers unfamiliar with standard references. This terminological confusion mirrors the historical chaos in human anatomy before the introduction of Terminologia Anatomica. It also mirrors the situation seen in molecular genetics whereby genetic and protein nomenclature often differs across species due to independent historical naming events, differences in structure or function, or alternative naming conventions. To solve this nomenclature committee, database curators, identification of orthologs, bioinformatics tools and other methods are being utilised to develop more unified approaches.

With conflicting nomenclature for structures like liver lobes and muscles, cross-species comparisons risk misinterpretation. The authors stress the need for standardized terminology, expert working groups, and a centralized anatomical repository to ensure accuracy, facilitate phenotyping, and strengthen comparative anatomy as a shared scientific language. By highlighting the need for both new anatomical descriptors and a harmonized vocabulary, this work shows that comparative anatomy is not only about structural similarities but also about creating a shared language. Such efforts are vital to improve accuracy in phenotyping, enhance translational research, and strengthen the role of anatomy as a bridge across species and disciplines. They also call for the development of a centralized anatomical repository to integrate emerging knowledge, including novel structures like adipose depots or specialized nerves, which currently lack official terms (15).

This issue of Slovenian Veterinary Research offers an excellent illustration of the value of comparative anatomy and its richness. Several original research articles, spanning different species and methodologies, jointly underline how studying anatomical structures contributes to veterinary practice, translational research, and even the human medical field and can advance both veterinary and biomedical sciences.

The article by Tim Šteferl et al. explores seasonal variations in serum vitamin D levels and growth performance in

znanja, od sledenja izbruhom bolezni in forenzičnih preiskav kaznivih dejanj nad prostoživečimi živalmi do nadzora inšpekcije mesa, saj vse to jasno ponazarja, kako anatomsko znanje prispeva k varovanju zdravja in zaščiti družbe. Pomembno je tudi spodbujati aktivno vključenost študentov prek klubov v okviru koncepta Eno zdravje, skupnih raziskovalnih projektov in mednarodnih izmenjav, da bi prihodnje generacije razumele anatomijo ne le kot znanost o zgradbi, temveč kot disciplino v samem jedru globalnega zdravja in varnosti (13).

Nedavno objavljen članek avtorja Ruberte in sod. 2025 (15), je izjemno pomemben za področje primerjalne anatomije z nekoliko drugačnega vidika, saj poudarja pomen dosledne in primerljive terminologije tako za biomedicinske raziskave na živalih kot na ljudeh. Članek izpostavlja primerjalni vidik uporabe miši kot ključnega modela v primerjalnih in translacijskih raziskavah za ljudi in živali. Miš ostaja eden najpogosteje uporabljenih modelov za preučevanje človeških bolezni, vendar je njena anatomska nomenklatura razdrobljena. Za iste režnje jeter ali mišice obstajajo številni konkurenčni izrazi, pogosto se uporabljajo zastarela poimenovanja, raziskovalci pa včasih oblikujejo tudi lastne opise, ne da bi se sklicevali na standardna anatomska poimenovanja. Takšna terminološka zmeda odraža zgodovinski kaos v humani anatomiji pred uvedbo anatomske terminologije. Podobna situacija je prisotna tudi na področju molekularne genetike, kjer se imena genov in beljakovin pogosto razlikujejo med vrstami zaradi zgodovinsko neodvisnega poimenovanja, razlik v zgradbi ali funkciji, ali pa zaradi uporabe različnih poimenovalnih konvencij. Za razrešitev teh neskladij se danes vključujejo nomenklaturni odbori, skrbniki podatkovnih baz, identifikacija ortologov, bioinformacijska orodja in druge metode, s katerimi se razvijajo bolj enotni pristopi k poimenovanju.

Zaradi neenotne terminologije za strukture, kot so jetrni režnji in mišice, obstaja tveganje za napačno razlago pri medvrstnih primerjavah. Avtorji zato poudarjajo potrebo po standardizirani terminologiji, strokovnih delovnih skupinah in vzpostavitvi centralnega anatomskega repozitorija, ki bi zagotavljal natančnost, olajšal fenotipizacija in okrepil primerjalno anatomijo kot skupni znanstveni jezik. S poudarjanjem pomena tako novih anatomskih opisov kot tudi usklajenega besedišča delo kaže, da primerjalna anatomija ni le veda o strukturnih podobnostih, temveč tudi o oblikovanju skupnega jezika. Takšna prizadevanja so ključna za izboljšanje natančnosti pri fenotipizaciji, za napredek translacijskih raziskav ter za utrjevanje vloge anatomije kot mostu med vrstami in znanstvenimi disciplinami. Avtorji obenem pozivajo k razvoju centraliziranega anatomskega repozitorija, ki bi vključeval novo pridobljeno znanje, vključno z novoodkritimi strukturami, kot so maščobni depoji ali specializirani živci, ki trenutno še nimajo uradnih poimenovanj (15).

V tokratni številki revije Slovenskega Veterinarskega Zbornika sta odlično ponazorjena pomen in bogastvo primerjalne anatomije. Več izvirnih ter preglednih raziskovalnih

Krškopolje pigs raised on organic farms, linking nutritional physiology with skeletal health and animal welfare. By correlating vitamin D status, known to influence calcium metabolism, bone mineralization, and musculoskeletal robustness, with housing conditions and sunlight exposure, the study bridges biochemical and anatomical perspectives. The findings not only provide reference values for vitamin D in outdoor and indoor pigs but also highlight how environmental and anatomical factors jointly shape skeletal development, supporting a holistic One Health approach to animal morphology and welfare.

The study by Mohamed A. M. Alsafy et al. provides new insights into the horse stifle joint using advanced imaging and analytical methods, including 3D computed tomography (CT), scanning electron microscopy (SEM), and energy-dispersive X-ray (EDX) analysis. The equine stifle is one of the most clinically important joints, it is a frequent source of lameness yet is also one of the most complex anatomical regions, both structurally and functionally. By combining CT-based 3D reconstruction with microscopic and elemental analysis, the authors offer a comprehensive description of the joint's bones, ligaments, and synovial components. Their work not only provides a valuable reference for equine clinicians but also enriches the comparative understanding of synovial joints across species, including humans, where cruciate ligament injuries represent a major clinical problem.

Another contribution which focused on surgical anatomy is presented by Mohamed Marzok et al., who carried out computed tomographic and gross anatomical studies of the temporomandibular and supraorbital regions in the one-humped camel (*Camelus dromedarius*). Their detailed dissections and CT scans of camel skulls demonstrate that the extensive supraorbital fossa offers a safe and feasible surgical approach to the orbital cavity. The study highlights how comparative anatomy supports clinical innovation: in this case, facilitating orbital surgeries such as enucleation, prosthetic implantation, and tumor removal in camels. The findings not only enrich camel anatomy but also broaden the comparative understanding of orbital surgery across domestic species, showing again how structural knowledge translates into clinical advances.

From skeletal health in pigs, musculoskeletal anatomy in horses, skull study in camels the issue then turns to poultry physiology and bone biology. Ghulam Murtaza Lochi et al. examined the effects of selenium nanoparticles and chitosan on meat quality, lipid profile, mineral content, and tibial bone morphometry in heat-stressed broilers. While the primary focus was nutritional physiology, the study also emphasizes the anatomical and structural aspects of bone health. The findings that nano-selenium and chitosan supplementation improve tibial robustness and mineralization underpin how nutrition and environmental stress intersect with skeletal anatomy. This work provides not only practical applications for poultry production but also broader insights into how

člankov, ki obravnavajo različne živalske vrste in primerjave ter uporabljajo raznolike metodologije poudarja, kako proučevanje anatomskih struktur prispeva k veterinarski praksi, translacijskim raziskavam in celo k razumevanju v humani medicini, ter tako omogoča boljše razvijanje tako veterinarske medicine kot drugih biomedicinskih ved.

Članek Tima Šteferla in sod. obravnava sezonska nihanja ravni vitamina D v serumu in rastno zmogljivost krškopoljskih prašičev, vzrejenih na ekoloških kmetijah, ter povezuje prehransko fiziologijo z zdravjem okostja in dobrobitjo živali. S povezovanjem statusa vitamina D, ki vpliva na presnovo kalcija, mineralizacijo kosti in mišično-skeletno odpornost, z bivalnimi pogoji in izpostavljenostjo sončni svetlobi raziskava povezuje biokemični in anatomski vidik. Ugotovitve ne ponujajo le referenčnih vrednosti za vitamin D pri zunaj in znotraj hlevsko rejenih prašičih, temveč tudi poudarjajo, kako okoljski in anatomski dejavniki skupaj oblikujejo razvoj skeleta, s čimer prispevajo k celostnemu pristopu Eno zdravje pri preučevanju morfologije in dobrobiti živali.

Raziskava Mohameda A. M. Alsafyja in sod. prinaša nova spoznanja o kolenskem sklepu konja, pridobljena z uporabo naprednih slikovnih in analitskih metod, med katerimi so tridimenzionalna računalniška tomografija (CT), vrstična elektronska mikroskopija (SEM) ter energijsko-disperzijska rentgenska analiza (EDX). Konjski kolenski sklep je eden klinično najpomembnejših sklepov (pogost vzrok šepavosti), hkrati pa tudi eden najkompleksnejših anatomskih predelov tako po zgradbi kot po funkciji. S kombinacijo 3D rekonstrukcije na osnovi CT-posnetkov ter mikroskopske in elementne analize avtorji ponujajo celovit opis kosti, vezi in sinovialnih struktur sklepa. Njihovo delo predstavlja dragocen referenčni vir za klinične veterinarje, hkrati pa bogati primerjalno razumevanje sinovialnih sklepov pri različnih vrstah, vključno s človekom, pri katerem so poškodbe križnih vezi velik klinični problem.

Še en prispevek, osredotočen na kirurško anatomijo, predstavlja Mohamed Marzok in sod., v katerem so izvedli računalniško-tomografske in makroskopske anatomske raziskave temporomandibularnega in supraorbitalnega področja pri enogrbi kameli (*Camelus dromedarius*). Njihove podrobne disekcije in CT-posnetki kameljih lobanj so pokazali, da obsežna supraorbitalna kotanja predstavlja varen in izvedljiv kirurški dostop do orbitalne votline. Študija jasno poudarja, kako primerjalna anatomija spodbuja klinične inovacije, v tem primeru omogoča učinkovitejše orbitalne operacije, kot so enukleacija, vstavitev protez in odstranjevanje tumorjev pri kamelah. Rezultati ne le poglabljajo poznavanje anatomije kamele, temveč tudi širijo primerjalno razumevanje orbitalne kirurgije pri domačih živalih ter znova dokazujejo, kako se anatomsko znanje neposredno prevaja v klinični napredek.

Od zdravja skeleta pri prašičih, mišično-skeletne anatomije pri konjih in raziskav lobanje pri kamelah se tokratna številka nadaljuje s fiziologijo perutnine in morfologijo kosti. Ghulam

bone morphology can be modulated across species, a theme relevant for both veterinary and human bone biology.

A direct comparative anatomical perspective is offered by Bahri Evcim and Mehmet Erkut Kara, who present a morphometric analysis of the mandible in sheep, goats, and rabbits. Their research is an excellent example of how comparative anatomy updates translational and experimental studies. Rabbits and small ruminants are frequently used as animal models in oral and maxillofacial surgery research, yet significant morphological differences exist in mandibular geometry and cortical thickness. By providing detailed morphometric data, the authors help guide researchers in selecting the most appropriate model for implants, screw fixation, or bone defect studies. Their work demonstrates how comparative anatomy bridges veterinary and human medical research, ensuring that experimental surgery is both scientifically valid and clinically relevant.

Nadia Hameed Rija Al-Falahi and Ali Ghazi Atiyah present a study relating to the healing of bone defects in rabbits using eggshell hydroxyapatite powder and autologous bone marrow. Bone regeneration is one of the great challenges in both veterinary and human orthopedics. By testing natural and biologically derived materials such as eggshell hydroxyapatite, combined with stem cell-rich bone marrow aspirates, the authors contribute to the field of regenerative medicine. Their results, showing superior healing when both materials are combined, provide an important reference for translational orthopedic surgery, again underscoring how rabbits serve as a valuable comparative model.

The article by Mohamed A. M. Alsafy et al. investigates how sodium butyrate supplementation influences the microanatomy and immune architecture of the small intestine in broiler chickens. Through detailed histological and immunohistochemical analysis, the study demonstrates significant increases in villus height, crypt depth, and goblet cell number, key structural parameters that enhance nutrient absorption and mucosal defense. Notably, the expression of interleukin-22 (IL-22) and toll-like receptor 8 (TLR8) was markedly elevated, revealing how dietary factors can modulate epithelial integrity and local immunity. By linking cellular morphology, intestinal immunology, and nutritional physiology, this research exemplifies how anatomical studies continue to underpin our understanding of health, function, and disease resistance in animals.

The comparative scope of this issue extends further into aquatic species. Hakan Didinen investigates the use of tea tree and geranium essential oils as anesthetic agents in rainbow trout (*Oncorhynchus mykiss*). While focused on aquaculture and pharmacology, the study contributes towards comparative anatomy and physiology by exploring species-specific responses to anesthetic agents. Understanding how fish tissues react to plant-derived compounds not only provides safer, more sustainable methods for fish handling

Murtaza Lochi in sod. so proučevali vpliv nanodelcev selena in hitosana na kakovost mesa, lipidni profil, mineralno sestavo in morfometrijo golenice pri brojlerjih, izpostavljenih toplotnemu stresu. Čeprav je bilo glavno težišče raziskave na prehranski fiziologiji, delo hkrati poudarja anatomske in strukturne vidike zdravja kosti. Ugotovitve, da dodajanje nano-selena in hitosana izboljšuje trdnost in mineralizacijo golenice, razkrivajo, kako prehrana in okoljski stres vplivata na anatomijo skeleta. Študija ne ponuja le praktičnih aplikacij za rejo perutnine, temveč tudi širši vpogled v to, kako je mogoče obliko in zgradbo kosti modulirati med različnimi vrstami, kar je tema, pomembna tako za veterinarsko kot za humano biologijo kosti.

Neposredno primerjalno-anatomsko analizo uporabita v svojem prispevku avtorja Bahri Evcim in Mehmet Erkut Kara, v katerem predstavita morfometrično analizo mandibule pri ovcah, kozah in kuncih. Njuna raziskava je odličen primer, kako primerjalna anatomija prispeva k translacijskim in eksperimentalnim raziskavam. Kunci in mali prežvekovalci se pogosto uporabljajo kot živalski modeli v raziskavah oralne in maksilofacialne kirurgije, vendar med vrstami obstajajo pomembne morfološke razlike v geometriji mandibule in debeline kosti. Z natančnimi morfometričnimi podatki avtorja prispevata k raziskavam izbire najprimernejšega modela za študije implantatov, fiksacije z vijaki ali kostnih defektov. Njuno delo lepo ponazarja, kako primerjalna anatomija povezuje veterinarske in humane medicinske raziskave ter zagotavlja, da so eksperimentalne kirurške študije tako znanstveno utemeljene kot klinično relevantne.

Nadia Hameed Rija Al-Falahi in Ali Ghazi Atiyah predstavljata raziskavo o celjenju kostnih defektov pri kuncih z uporabo hidroksiapatitnega prahu iz jajčne lupine in avtolognega kostnega mozga. Regeneracija kosti je eden največjih izzivov tako v veterinarski kot v humani ortopediji. Z raziskovanjem naravnih in biološko pridobljenih materialov, kot je hidroksiapatit iz jajčne lupine, v kombinaciji z aspirati kostnega mozga, bogatimi z matičnimi celicami, avtorja prispevata k razvoju regenerativne medicine. Rezultati, ki kažejo na boljše celjenje ob sočasni uporabi obeh materialov, predstavljajo pomemben referenčni prispevek za translacijsko ortopedsko kirurgijo in znova potrjujejo, kako dragocen primerjalni model predstavljajo kunci.

Članek avtorja Mohameda A. M. Alsafyja in sod. proučuje, kako dodatek natrijevega butirata vpliva na mikroskopsko anatomijo in imunsko zgradbo tankega črevesa pri brojlerjih. Z natančno histološko in imunohistokemično analizo so v raziskavi pokazali pomembno povečanje višine resic, globine kript in števila čašastih celic, ključnih strukturnih parametrov, ki izboljšujejo absorpcijo hranil in obrambno funkcijo sluznice. Znatno povečano izražanje interlevkina-22 (IL-22) in Tollu podobnega receptorja 8 (TLR8) razkriva, kako lahko prehranski dejavniki vplivajo na celovitost epitelija in lokalno imunost. Z združevanjem celične morfologije, črevesne imunologije in prehranske fiziologije ta raziskava nazorno prikazuje, kako anatomske študije še naprej

but also enriches comparative knowledge on nervous system sensitivity and metabolic variation across vertebrates.

At the end of the issue case report by Eun-Jae Cho et al. presents an extended subtotal mandibulectomy in a cat with alveolar osteomyelitis showing an unusually aggressive, spiculated ("sunburst") periosteal reaction, an imaging pattern typically associated with malignant bone tumors. Through detailed radiological, surgical, and histopathological assessment, the authors demonstrate that even benign inflammatory lesions can mimic neoplastic processes in their anatomical manifestation. The study highlights how understanding bone morphology and periosteal dynamics is essential for accurate diagnosis and surgical planning. Moreover, it underscores the anatomical precision required in reconstructive and functional preservation surgeries, reaffirming the value of comparative craniofacial anatomy in advancing both veterinary and clinical medicine.

In last few years more studies supporting comparative anatomy have been published. Within the journal Slovenian Veterinary Research, a good complementary example is the study investigating Anatomical Structures in the Rabbit Carpal Tunnel: Comparison with Human (16). This work showed that rabbits share close anatomical similarities with humans in the carpal tunnel, particularly in the flexor retinaculum and tendon arrangement. These parallels make the rabbit a valuable model for studying carpal tunnel syndrome, illustrating the translational power of comparative anatomy for both veterinary and human medicine (16). Furthermore, the study Anatomical and Histological Features of Lingual Papillae in Squirrel (17) described the morphology and histology of five types of tongue papillae, comparing them with rodents. The findings reveal both similarities and species-specific differences, highlighting the role of comparative anatomy in understanding feeding adaptations and oral physiology (17). Moreover, the study Comparative Evaluation of the Komodo Dragon (*Varanus komodoensis*) and the Green Iguana (*Iguana iguana*) Skull by Three-Dimensional Computed Tomographic Reconstruction (18) used advanced 3D CT imaging to visualize and compare cranial structures in two lizard species. The results revealed distinct differences in orbital configuration and neurocranial bones, demonstrating the potential of modern imaging techniques to enhance reptile diagnostics and deepen comparative anatomical understanding of skull morphology and functional adaptation (18).

Recent studies on marine mammals provide striking examples of functional adaptations to live in the sea. Hrvoje Smodlaka et al. examined the ear anatomy and histology of the northern elephant seal (*Mirounga angustirostris*), revealing unique features of the auditory system that support underwater hearing and pressure regulation (19). In another study, the gross anatomy of the ringed seal (*Pusa hispida*) gastrointestinal tract was described, highlighting evolutionary adjustments to a carnivorous, fish-based diet in a cold marine environment (20). Additionally, histological assessment of blood vessels in phocid seals demonstrated vascular

predstavljajo temelj razumevanja zdravja, funkcije in odpornosti proti boleznim pri živalih.

Primerjava med vrstami se v tem članku nanaša tudi na vodne živali. Hakan Didinen preučuje uporabo eteričnih olj čajevca in pelargonije kot anestetikov pri mavrični postrvi (*Oncorhynchus mykiss*). Čeprav je raziskava usmerjena predvsem v akvakulturo in farmakologijo, pomembno prispeva k primerjalni anatomiji in fiziologiji, saj raziskuje vrstno specifične odzive na anestetike. Razumevanje, kako tkiva pri ribah reagirajo na spojine rastlinskega izvora, ne omogoča le varnejših in trajnostnejših metod rokovanja z ribami, temveč tudi bogati primerjalno znanje o občutljivosti živčnega sistema in presnovnih razlikah med vretenčarji.

Na koncu številke študija primera avtorja Eun-Jae Cho in sod. prikazuje izvedbo razširjene subtotalne mandibulectomije pri mački z alveolarno osteomielitisom, ki je kazal nenavadno agresivno, trnasto periostalno reakcijo ("sončni izbruh"), vzorec, ki je običajno značilen za maligne kostne tumorje. Z natančno radiološko, kirurško in histopatološko analizo so avtorji pokazali, da lahko tudi benigne vnetne spremembe anatomsko posnemajo neoplastične procese. Študija poudarja, kako pomembno je razumevanje morfologije kosti in dinamike periosta za natančno diagnostiko in kirurško načrtovanje. Poleg tega izpostavlja anatomsko natančnost, potrebno pri rekonstruktivnih in funkcionalno ohranitvenih posegih, ter znova potrjuje vrednost primerjalne kraniofacialne anatomije pri napredku veterinarske in klinične medicine.

V zadnjih letih je bilo objavljenih vse več raziskav, ki podpirajo pomen primerjalne anatomije. V okviru revije Slovenski Veterinarski Zbornik je lep dopolnilni primer raziskava z naslovom: »Anatomske strukture v karpalnem kanalu kunca: primerjava s človekom« (16). Raziskava je pokazala, da imajo kunci z ljudmi številne anatomske podobnosti tudi v zapestnem kanalu, zlasti v zgradbi fleksornega retinakluma in razporeditvi tetiv. Te vzporednice uvrščajo kunca med dragocene modele za preučevanje sindroma zapestnega kanala ter ponazarjajo translacijsko moč primerjalne anatomije tako v veterinarski kot humani medicini (16). V raziskavi z naslovom: »Anatomske in histološke značilnosti jezičnih papil na jeziku pri veverici (*Sciurus vulgaris*)« (17) opisana morfologija in histologija petih tipov jezičnih papil pri veverici ter primerjava z glodavci. Ugotovitve razkrivajo tako podobnosti kot vrstno specifične razlike in poudarjajo vlogo primerjalne anatomije pri razumevanju prilagoditev na prehrano ter fiziologijo prebave v ustni votlini (17). Raziskava z naslovom: »Primerjava lobanj komodoškega varana (*Varanus komodoensis*) in zelenega legvana (*Iguana iguana*) s pomočjo tridimenzionalne računalniške tomografske konstrukcije« (18) je uporabila napredno 3D CT-slikanje za vizualizacijo in primerjavo kranialnih struktur pri dveh vrstah kuščarjev. Rezultati so razkrili izrazite razlike v zgradbi orbitalnega področja in kosteh nevrokranija ter pokazali, kako sodobne slikovne tehnike lahko izboljšajo diagnostiko pri plazilcih in poglobijo primerjalno anatomsko razumevanje morfologije lobanje ter funkcionalne prilagoditve (18).

specializations crucial for thermoregulation and diving physiology (21). Further morphological studies, such as that by Serkan Erdoğan, Silia Villar Arias, and William Pérez (22), revealed striking interspecific differences between the South American fur seal (*Arctocephalus australis*) and sea lion (*Otaria flavescens*). Variations in the structure and distribution of lingual papillae reflect dietary and ecological adaptations, highlighting how feeding strategies and environment shape anatomical diversity among marine carnivores. Together, these studies underline how comparative and functional anatomy illuminate the complex relationships between structure, environment, and survival strategies in both terrestrial and marine species. By studying these anatomical traits, researchers gain insight not only into evolution but also into the health and conservation of these species, which are increasingly affected by pollution and climate change.

Taken together, these contributions vividly illustrate how comparative anatomy continues to serve as a unifying framework across species, systems, and scientific disciplines. Each study reveals how structural and functional diversity provides not only fascinating biological insight but also practical value for advancing diagnostics, surgery, and welfare. Far from being a limitation, anatomical variation represents a shared foundation for innovation, allowing us to translate findings between species and bridge the gap between veterinary and human medicine. Through such integrative and comparative perspectives, anatomy remains at the heart of scientific discovery, education, and clinical progress.

As veterinary science enters an era defined by One Health, digital technologies, and global collaboration, comparative anatomy remains central. It teaches us that diversity of form is not a complication but an opportunity. By embracing diversity, ranging from the horse's stifle to the broiler's tibia, from the rabbit's mandible to the trout's nervous system, we uncover the principles that unite living beings. In doing so, we not only strengthen our understanding of animals but also enrich human medicine, public health, and the broader science of life. By continuing to support comparative anatomy, we strengthen not only our scientific comprehension and knowledge but also our increase our capacity for clinical and translational breakthroughs.

Funding: We gratefully acknowledge financial support from the Slovenian Research Agency (grant number P4-0053 and V5-2315).

Nedavne raziskave morskih sesalcev ponujajo izjemne primere funkcionalnih prilagoditev na življenje v morju. Hrvoje Smodlaka s sod. je proučeval anatomijo in histologijo ušesa severnega morskega slona (*Mirounga angustirostris*) ter razkril edinstvene značilnosti slušnega sistema, ki omogočajo poslušanje pod vodo in uravnavanje tlaka (19). V drugi raziskavi je bila opisana makroskopska anatomija prebavil kolobarjastega tjulnja (*Pusa hispida*), ki kaže evolucijske prilagoditve na mesojedo, z ribami bogato prehrano v hladnem morskem okolju (20). Histološka analiza krvnih žil pri tjulnjih iz družine Phocidae pokazala posebnosti v žilnem sistemu, pomembne za termoregulacijo in fiziologijo potapljanja (21). Morfološke raziskave avtorjev Serkana Erdoğana, Silvie Villar Arias in Wiliama Péreza (22), so pokazale izrazite medvrstne razlike med južnoameriškim morskim medvedom (*Arctocephalus australis*) in morskim levom (*Otaria flavescens*). Razlike v zgradbi in razporeditvi jezičnih papil odražajo prehranske in ekološke prilagoditve ter poudarjajo, kako prehranske strategije in okoljski dejavniki oblikujejo anatomsko raznolikost morskih mesojedcev. Skupaj ti prispevki poudarjajo, kako primerjalna in funkcionalna anatomija osvetljujeta tesno povezanost med zgradbo, okoljem in preživetvenimi strategijami tako pri kopenskih kot pri morskih vrstah. S preučevanjem takšnih anatomskih značilnosti raziskovalci pridobivajo vpogled ne le v evolucijo, temveč tudi v zdravje in ohranjanje vrst, ki so vse bolj ogrožene zaradi onesnaženja in podnebnih sprememb.

Navedeni članki nazorno ponazarjajo, kako primerjalna anatomija še naprej deluje kot povezovalni okvir med vrstami, sistemi in znanstvenimi disciplinami. Vsaka raziskava razkriva, da strukturna in funkcionalna raznolikost ne ponuja le zanimivih bioloških spoznanj, temveč ima tudi praktično vrednost pri razvoju diagnostike, kirurgije in izboljševanju dobrobiti živali. Anatomska variabilnost ni slabost, temveč skupna osnova za inovacije, ki nam omogoča prenos spoznanj med vrstami in povezovanje veterinarske ter humane medicine.

Ko veterinarska znanost vstopa v obdobje, ki ga zaznamujejo koncept Eno zdravje, digitalne tehnologije in globalno sodelovanje, anatomija s celostnimi in primerjalnimi pristopi ostaja v središču znanstvenih odkritij, izobraževanja in kliničnega napredka. Uči nas, da raznolikost oblik ni omejitev, temveč priložnost. S poznavanjem različnih struktur, od konjskega kolenskega sklepa do golenice piščancev, od mandibule kunca do živčnega sistema postrvi, razkrivamo temeljna načela, ki povezujejo vsa živa bitja. S tem ne poglabljamo le razumevanja živali, temveč bogatimo tudi humano medicino, javno zdravje in širšo znanost o življenju. Z nadaljnjim razvojem in sprejemanjem primerjalne anatomije krepimo ne le svoje znanstveno razumevanje in znanje, temveč tudi svojo sposobnost za nadaljnje klinične in translacijske preboje.

Financiranje: Za finančno podporo se iskreno zahvaljujemo Jav¬ni agenciji za raziskovalno dejavnost Republike Slovenije (št. projektov P4-0053 in V5-2315).

References

1. Kardong KV. Vertebrates: comparative anatomy, function, evolution. Boston: McGraw-Hill Higher Education, 2009.
2. Cohen BJ, Loew FM. Laboratory Animal Medicine: Historical Perspectives. In: Fox JG, eds. Laboratory Animal Medicine. 2nd ed, Burlington: Academic Press, 2002: 1–17.
3. Ganz JC. Hippocrates (ca 460 BC to ca 370 BC). Prog Brain Res 2024; 284: 31–48. doi: 10.1016/bs.pbr.2024.02.004
4. Ganz JC. Rome-Galen (129 to ca. 216). Prog Brain Res 2024; 284: 65–86. doi: 10.1016/bs.pbr.2024.02.007
5. Kubale V, Perez W, Rutland CS. Teaching of anatomy: dissecting dissection in veterinary and medical education from historical perspective through today. Slo Vet Res 2024; 61(4): 225–32. doi: 10.26873/SVR-2167-2024
6. Kubale V. Veterinary illustration: science and art telling a story together. Slo Vet Res 2023; 60(1): 5–7. doi: 10.26873/SVR-1723-2023.
7. Natterson-Horowitz B. Zoobiquity: What Animals Can Teach Us about Health and the Science of Healing. Animals (Basel) 2012; 2(4): 559–63. doi: 10.3390/ani2040559
8. Lerner H, Berg C. The concept of health in One Health and some practical implications for research and education. Infect Ecol Epidemiol 2015; 5:25300. doi:10.3402/iee.v5.25300
9. Larsen RJ. Shared Curricula and Competencies in One Health and Health Professions Education. Med Sci Edu 2020; 31(1): 249–52. doi: 10.1007/s40670-020-01140-7
10. Bhattacharjee S, Ceri Davies, D, Holland JC, et al. On the importance of integrating comparative anatomy and One Health perspectives in anatomy education. J Anat 2022; 240(3): 429–46. https://doi.org/10.1111/joa.13570
11. Streets A, England H, Marshall J. Colour vision in stomatopod crustaceans: more questions than answers. J Exp Biol 2022; 225(6): jeb243699. doi: 10.1242/jeb.243699
12. Manglai D, Wada R, Endo H, et al. Macroscopic anatomy of the auditory tube diverticulum (guttural pouch) in the thoroughbred equine – a silicon mold approach. Okajimas Folia Anatom Japon 2000; 76(6): 335–46. doi: 10.2535/ofaj1936.76.6_335.
13. Kubale V, Pavlovic D, Rutland C, Dvojmoc M. One Health concept and anatomy education – The importance of comparative anatomy and (bio)security. In: Proceedings of 35th congress of the European association of veterinary anatomists (EAVA), Toulouse, France, 22-25th of July 2025.. Munich: Wiley, 2025. Anat Histol Embyrol 2025; 54(S11): 15. doi: 10.1111/ahe.70056
14. Linder D, Cardamone C, Cash SB, et al. Development, implementation, and evaluation of a novel multidisciplinary one health course for university undergraduates. One Health 2020; 9: 100121. doi: 10.1016/j.onehlt.2019.100121
15. Ruberte J, Schofield PN, Sundberg JP, Olvera-Maneu S, Carretero A. Harmonizing mouse anatomy terminology: a common language? Mamm Genome 2025; 36(4): 993–1004. doi: 10.1007/s00335-025-10156-6
16. Turker Yavas F, Dabanoglu I, Akkoc AN. Anatomical structures in the rabbit carpal tunnel: comparison with human. Slo Vet Res 2024; 61(3): 187–94. doi: 10.26873/SVR-1870-2023
17. Toprak B, Kilinç B. Anatomical and histological features of lingual papillae on tongue of squirrel (Sciurus vulgaris). Slo Vet Res 2024; 61(4): 291–7. doi: 10.26873/SVR-1792-2023
18. Pérez S, Encinoso M, Morales M, et al. Comparative evaluation of the Komodo dragon (Varanus komodoensis) and the green iguana (Iguana iguana) skull by the three-dimensional computed tomographic reconstruction. Slo Vet Res 2021; 58(3): 111–6. doi:10.26873/SVR-1330-2021
19. Smodlaka H, Khamas WA, Jungers H, et al. A novel understanding of phocidae hearing adaptations through a study of Northern elephant seal (Mirounga angustirostris) ear anatomy and histology. Anatom Rec 2019; 302(9):1605–14. doi: 10.1002/ar.24026
20. Smodlaka H, Henry RW. Gross anatomy of the ringed seal (Pusa hispida) gastro-intestinal tract. Anatom Histol Embryol 2014; 43(3): 230–8. doi: 10.1111/ahe.12066
21. Smodlaka H, Khamas W, Tkalcic S, Golub T, Palmer L. Histological assessment of selected blood vessels of the phocid seals (northern elephant and harbour seals). Anatom Histol Embryol 2010; 39(3):178–85. doi: 10.1111/j.1439-0264.2010.00994.x
22. Erdoğan S, Villar Arias S, Pérez W. Morphology of the lingual surface of South American fur seal (Arctocephalus australis) and sea lion (Otaria flavescens). Microsc Res Tech 2015; 78(2):140–7. doi: 10.1002/jemt.22456.

Slov Vet Res
DOI 10.26873/SVR-2195-2025
UDC 303.4:543.384:575.113.1:575.853:577.115:591.11:636.09
Pages: 139–43

Editorial

The Growing Potential of Extracellular Vesicle Research in Veterinary Medicine

Naraščajoči potencial raziskav zunajceličnih veziklov v veterinarski medicini

Key words

extracellular vesicles;
regenerative veterinary medicine;
biomarker,
therapy;
cargo

Accepted: 7 April 2025

Saša Koprivec

University of Ljubljana, Veterinary Faculty, Gerbičeva 60, 1000 Ljubljana, Slovenia

sasa.koprivec@vf.uni-lj.si

Extracellular vesicles (EVs) are small, information-rich subcellular structures that have attracted considerable attention in the scientific community. Their ubiquitous presence in the body and their natural role as cellular messengers make them valuable indicators of the physiological and pathological state of cells and tissues. Currently, the number of specific studies on the presence, properties and role of EVs in all life forms is increasing exponentially. In veterinary medicine, EVs are still relatively under-researched, and we have only recently begun to explore their potential.

EVs facilitate communication between cells or tissues. They are information carriers that travel from cell of origin to the target cells via body fluids. Their diverse cargo includes a plethora of proteins, lipids, DNA and other small nucleic acids, all of which reflect the state of the donor cell (1). As a result, EV research is rapidly expanding, particularly within the One Health concept, which aims at interlinked health outcomes for humans, animals and the environment (2). The integrated approach of the One Health concept emphasizes the importance of the link between veterinary and human medicine. Research on selected animal models provides valuable insights that can be transferred to human research in many clinical areas, and vice versa (3). Key areas of interest include understanding the role of EVs in physiology

Zunajcelični vezikli (ZV) so majhne, informacijsko bogate subcelične strukture, ki so v znanstveni skupnosti pritegnile veliko pozornosti. Zaradi njihove vsesplošne prisotnosti v telesu in njihove naravne vloge kot prenašalci informacij so dragoceni pokazatelji fiziološkega in patološkega stanja celic in tkiv. V tem trenutku število študij o prisotnosti, lastnostih in vlogi ZV v vseh oblikah življenja eksponentno narašča. V veterinarski medicini so ZV še vedno razmeroma slabo proučeni in šele pred kratkim smo začeli bolj natančno raziskovati njihov potencial.

ZV omogočajo komunikacijo med celicami ali tkivi. So nosilci informacij, ki prek telesnih tekočin potujejo od matične do tarčnih celic. Njihov raznovrsten tovor vključuje številne proteine, lipide, DNA in druge majhne nukleinske kisline, ki odražajo stanje celice, iz katere izvirajo (1). Zato se raziskave ZV hitro širijo, zlasti v okviru koncepta Eno zdravje, ki obravnava medsebojno povezanost zdravja ljudi, živali in okolja (2). Celostni pristop koncepta Eno zdravje poudarja pomen povezave med veterinarsko in humano medicino. Raziskave na izbranih živalskih modelih zagotavljajo dragocena spoznanja, ki jih je mogoče prenesti na številna področja raziskav v humani medicini, in obratno (3). Ključna področja zanimanja vključujejo razumevanje vloge ZV v fiziologiji in patofiziologiji, potencialno uporabo

and pathophysiology, potential use as disease biomarkers, exploring their potential as therapeutics or vaccine carriers, and applications in regenerative veterinary medicine (4). Currently, EV research is focused on cattle, pigs, dogs, birds, horses and cats, as well as some small ruminants and exotic animals (5).

Despite tremendous progress in a short period of time, some critical challenges remain if we are to take EV research in veterinary medicine to the next level. These include the standardization of isolation and characterization methods, the optimization of dosing and storage conditions, and the identification of species-specific EV markers and reference genes. In contrast to EV research in human medicine, where many protocols are already established, there is a greater variability in starting materials for EV isolation in veterinary applications, which makes the transfer of protocols difficult. In addition, there are few functional studies on EVs in animals (5). The challenges are being relentlessly addressed by the scientific community, particularly thorough the work of the International Society for Extracellular Vesicles (ISEV), which is continuously updating minimal requirements for standardization of workflows in this field (6).

The lipid bilayer envelope of EVs ensures the stability of their cargo, making them excellent candidates for non-invasive diagnostics. EVs can be isolated from various minimally invasive samples, such as blood, urine or saliva. Their cargo reflects the state of the donor cell and enables early detection and monitoring of diseases in different areas of veterinary medicine (7). Tumor-derived EVs contain specific proteins and RNAs that can be used to differentiate between healthy and tumor cells or even between different tumor phenotypes. Zamboni and colleagues (8) showed a correlation between elevated levels of miR-21-5p in EVs from canine plasma and mast cell tumors. Using bioinformatic analysis of RNA sequencing data, Özmen and colleagues (9) also identified miR-21-5p as a potential marker for hepatic hemangiosarcoma in dogs. EVs may contain pro-inflammatory cytokines and microRNAs indicative of inflammatory conditions. In horses, the presence of pro-inflammatory cytokines such as TNF-α or IL-6 in synovial fluid EVs is associated with joint inflammation and arthritis and could be used to monitor disease status (10, 11). EVs may contain specific pathogenderived molecules that allow identification of infections. For example, Palacios and colleagues (12) showed that mycobacteria-derived EV-associated lipoprotein LpqH in blood samples can help distinguish between Mycobacterium bovis and Mycobacterium avium subsp. paratuberculosis infection. We can use EVs to detect organ damage or stress in specific tissues. NGAL has been presented as a promising biomarker of kidney damage in canine urine (13), and in humans, Ugarte and colleagues (14) have already linked the presence of EV-derived NGAL to diabetic kidney disease. Similarly, liver damage in pets can be detected clinically by determining various hepatic markers in blood, but further studies are needed to link them to EVs and evaluate which markers are most suitable for the early detection of liver failure. Elevated

kot biomarkerjev bolezni, raziskovanje njihovega potenciala za prenos in tarčno dostavo zdravil ali kot nosilcev cepiv ter uporabo v regenerativni veterinarski medicini (4). Trenutno so raziskave ZV osredotočene na govedo, prašiče, pse, ptice, konje in mačke ter nekatere male prežvekovalce in eksotične živali (5).

Kljub izjemnemu napredku področja v kratkem času, ostajajo nekateri kritični izzivi nerešeni, predvsem, če želimo raziskave ZV v veterinarski medicini dvigniti na naslednjo raven. Ti vključujejo standardizacijo metod izolacije in karakterizacije, optimizacijo pogojev doziranja in shranjevanja ter opredelitev vrstno specifičnih označevalcev ZV in referenčnih genov. V nasprotju z raziskavami ZV v humani medicini, kjer so številni protokoli že uveljavljeni, so izhodni materiali za izolacijo EV v veterini bolj raznoliki, kar otežuje direktni prenos protokolov. Poleg tega je število funkcionalnih študij o ZV pri živalih nizko (5). Znanstvena skupnost se s temi izzivi vztrajno ukvarja, pomembne temelje pa postavlja Mednarodno združenje za zunajcelične vezikle (ISEV), ki nenehno posodablja minimalne zahteve za standardizacijo delovnih postopkov na tem področju (6).

Lipidni dvosloj ZV zagotavlja stabilnost njihovega tovora, zato so odlični kandidati za neinvazivno diagnostiko. ZV lahko izoliramo iz različnih minimalno invazivnih vzorcev, kot so kri, urin ali slina. Njihov tovor odraža stanje starševske celice in omogoča zgodnje odkrivanje in spremljanje bolezni na različnih področjih veterinarske medicine (7). ZV, ki izvirajo iz tumorjev, vsebujejo specifične proteine in RNA molekule, ki jih je mogoče uporabiti za razlikovanje med zdravimi in tumorskimi celicami ali celo med različnimi tumorskimi fenotipi. Zamboni in sodelavci (8) so pokazali povezavo med povišanimi ravnmi miR-21-5p v ZV iz plazme psov in tumorjev mastocitov. Özmen in sodelavci (9) so z bioinformacijsko analizo podatkov sekvenciranja RNA prav tako identificirali miR-21-5p kot potencialni označevalec prisotnosti jetrnega hemangiosarkoma pri psih. ZV lahko vsebujejo vnetne citokine in mikroRNA, ki kažejo na prisotnost vnetnega stanja. Pri konjih je prisotnost vnetnih citokinov, kot sta TNF-α ali IL-6, v ZV sinovialne tekočine povezana z vnetjem sklepov in artritisom ter se lahko uporablja za spremljanje stanja bolezni (10, 11). ZV lahko vsebujejo specifične molekule, ki izvirajo iz patogenov in omogočajo identifikacijo okužb. Npr. Palacios in sodelavci (12) so pokazali, da lahko z mikobakterijami povezan lipoprotein LpqH iz ZV v vzorcih krvi pomaga razlikovati med okužbo z Mycobacterium bovis in Mycobacterium avium subsp. paratuberculosis. ZV lahko uporabimo za odkrivanje poškodb organov ali stresa v določenih tkivih. NGAL je bil predstavljen kot obetaven biomarker poškodbe ledvic v pasjem urinu (13), pri ljudeh pa so Ugarte in sodelavci (14) prisotnost NGAL iz ZV že povezali z diabetično ledvično boleznijo. Podobno lahko poškodbe jeter pri hišnih ljubljenčkih klinično zaznamo z določanjem različnih jetrnih označevalcev v krvi, vendar so potrebne nadaljnje študije za njihovo povezavo z ZV in oceno, kateri označevalci so najprimernejši za zgodnje odkrivanje odpovedi jeter. Pri različnih možganskih motnjah so opazili

levels of the protein S100B in CSF have been observed in various brain disorders and are therefore gaining attention as a possible biomarker for neuroinflammation in animals (15). Piibor and colleagues (16) investigated the association between EVs in the uterine fluid and reproductive disorders in cows and specifically showed differences in EV protein profiles between healthy cows and cows with subclinical or clinical endometritis. These are only a few examples as several other potential biomarkers from different body fluids are being investigated in basic research and clinical studies in different animal species.

Another interesting research direction in the field is the use of EVs in different therapeutic approaches. EVs can be loaded or modified to deliver therapeutic agents – drugs, proteins or nucleic acids – directly to the target tissue (17). While the natural origin of EVs reduces the risk of immune reactions, the transferred bioactive molecules can influence proliferation, differentiation or apoptosis in target tissues (18). By introducing carefully selected modifications, we can bind specific ligands to the EV surface, enhance their natural abilities, optimize delivery to target cells and reduce off-target effects (19). Many applications include the treatment of cancer, infections and various inflammatory diseases. EVs from immune cells can modulate the immune response, offering new potential treatments for autoimmune diseases, allergies and other immune-related diseases in animals. Many current treatments are based on symptom relief, but EVs offer an alternative treatment focused on influencing the cause of the disease. Thanks to their natural presence in the body, EVs are less likely to trigger an immune response, especially compared to some synthetic nanoparticles. Since EVs can be derived from autologous cells, there is less risk of rejection. This also opens numerous possibilities for personalized treatments (20). Of particular interest is the investigation of the influence of EVs on fertility enhancement, e.g. in economically important animals. As EVs contribute to the regulation of sperm and oocyte maturation and are an important part of the embryonic development microenvironment, we can use them to support embryonic development and improve reproductive outcomes in assisted reproductive techniques (21). It has also been shown that different cryopreservation protocols for sperm and oocytes need to be thoroughly investigated and improved (22, 23). For example, Pedrosa and colleagues (24) recently showed that certain miRNAs present in EVs from seminal plasma indicate low sperm cryotolerance in boars and may serve as predictive factors for the success of the cryopreservation process.

The development of vaccines based on EVs is promising from several points of view. EVs are natural carriers of biomolecules, and the lipid bilayer suitably protects the cargo. Novel techniques for vaccine production aim at products with a better safety profile and targeted immunogenicity. EVs are superior to synthetic nanoparticles in this respect, and their small size even allows them to overcome certain biological barriers that were previously considered insurmountable (25). Furthermore, novel vaccine production options represent an

povišane ravni proteina S100B v cerebrospinalni tekočini, zato so le-ta omenja kot možen biomarker nevrovnetja pri živalih (15). Piibor in sodelavci (16) so raziskovali povezavo med ZV v maternici in reproduktivnimi motnjami pri kravah ter posebej pokazali razlike v proteinskih profilih ZV med zdravimi kravami ter kravami s subkliničnim ali kliničnim endometritisom. Naštetih je le nekaj primerov. Še veliko več drugih potencialnih biomarkerjev, prisotnih v ZV iz različnih telesnih tekočin, se preučuje v temeljnih raziskavah in kliničnih študijah na različnih živalskih vrstah.

Druga zanimiva raziskovalna smer na tem področju je uporaba ZV v različnih terapevtskih pristopih. ZV lahko izboljšamo oz. spremenimo tako, da omogočajo tarčno dostavo terapevtskih snovi - zdravila, proteine ali nukleinske kisline - neposredno v ciljno tkivo (17). Medtem, ko naravni izvor ZV zmanjšuje tveganje za pojav neželenih imunskih reakcij, lahko prenesene bioaktivne molekule vplivajo na proliferacijo, diferenciacijo ali apoptozo v tarčnem tkivu (18). Z uvajanjem skrbno izbranih modifikacij, lahko na površino ZV vežemo specifične molekule, povečamo njihove naravne sposobnosti, optimiziramo dostavo v ciljne celice in zmanjšamo neželene učinke (19). Številne aplikacije vključujejo zdravljenje raka, okužb in različnih vnetnih bolezni. ZV imunskih celic lahko modulirajo imunski odziv, kar ponuja nove možnosti zdravljenja avtoimunskih bolezni, alergij in drugih, z imunskim sistemom povezanih bolezni pri živalih. Številna trenutna zdravljenja teh obolenj temeljijo predvsem na lajšanju simptomov, ZV pa ponujajo alternativo, ki se osredotoča na zdravljenje vzroka bolezni. Zaradi svoje naravne prisotnosti v telesu ZV manj verjetno sprožijo imunski odziv, zlasti v primerjavi z nekaterimi sintetičnimi nanodelci. Ker lahko ZV pridobivamo iz avtolognih celic, je tveganje zavrnitvene reakcije manjše. To odpira tudi številne možnosti za personalizirano zdravljenje (20). Posebno zanimive so raziskave vpliva ZV na izboljšanje plodnosti, npr. pri gospodarsko pomembnih živalih. Ker ZV prispevajo k uravnavanju zorenja spermijev in jajčnih celic ter so pomemben del mikrookolja embrionalnega razvoja, jih lahko uporabimo za podporo embrionalnega razvoja in izboljšanje reproduktivnih rezultatov pri tehnikah oploditve z biomedicinsko pomočjo (21). Obstaja potreba po raziskavah na področju optimizacije protokolov za kriokonzervacijo spermijev in jajčec (22, 23). Pedrosa in sodelavci (24) so na primer nedavno pokazali, da nekatere miRNA molekule, ki so prisotne v ZV v semenski plazmi, kažejo na nizko stopnjo kriotolerance sperme pri merjascih in lahko služijo kot napovedni dejavnik za uspešnost postopka krioprezervacije.

Razvoj cepiv, ki temeljijo na ZV, je obetaven z več vidikov. ZV so naravni nosilci biomolekul, lipidni dvosloj pa ustrezno ščiti tovor. Eden izmed pomembnih ciljev novih tehnik za proizvodnjo cepiv je priprava izdelkov z boljšim varnostnim profilom in usmerjeno imunogenostjo. V tem pogledu so ZV boljši od sintetičnih nanodelcev, njihova velikost pa jim omogoča premagovanje nekaterih bioloških ovir, ki so prej veljale za nepremostljive (25). Nadalje, nova cepiva predstavljajo alternativo uporabi antibiotikov (26). Zmanjšanje

alternative to the use of antibiotics (26). Reducing the use of antibiotics is an urgent issue in animal husbandry, food-producing species and overall, which is closely linked to the One Health initiative.

Last, but not least, in regenerative veterinary medicine efforts are shifting towards cell-free therapies, focusing on the need for readily available off-the-shelf products. Such products offer more safety and customized treatments. Compared to cell-based therapies, EVs offer several advantages (27). EVs derived from medicinal/mesenchymal stem cells are of particular interest. It is now clear that EVs are the cellular fraction of medicinal/mesenchymal stem cells that influence immunomodulation of damaged tissue.

The EV cargo is protected in body fluids, which is reflected in and extended shelf life of EV-based products. On the other hand, preparations from living cells require stringent viability conditions that are not easy or cheap to maintain.

Their anti-inflammatory properties may reduce the need for long-term medication. Also, boosting immune response can be helpful in cancer therapies or in fighting infections. An important factor compared to cell therapies is the lower risk of tumor formation, as EVs do not carry the risk of uncontrolled cell proliferation (5, 28). All these positive properties favor the active research of EVs, which are used in various areas of regenerative veterinary medicine, e.g. neurodegeneration, joint and cartilage diseases, wound healing and skin regeneration, autoimmune diseases and fertility therapies (29).

While EVs offer immense promises and applications, challenges such as standardizing isolation techniques, optimizing the high cost/low yield ratio, improving detection sensitivity and performing species-specific studies still need to be addressed to unlock their full potential in veterinary medicine. A new era has begun, and the increasing number of publications highlights the promising applications of EVs in non-invasive diagnostics, targeted delivery of molecules and regenerative treatments. With their remarkable versatility, EVs are uniquely positioned to revolutionize the way we think about veterinary medicine.

uporabe antibiotikov je pomembna iniciativa v živinoreji, pri živalskih vrstah za proizvodnjo hrane in je hkrati tesno povezano s pobudo Eno zdravje.

Nenazadnje se na področju regenerativne veterinarske medicine prizadevanja usmerjajo v uvedbo brezceličnih terapij, pri čemer se osredotočamo na potrebo po lahko dostopnih izdelkih, ki so na voljo za takojšnjo uporabo v kliniki. Želimo, da takšni izdelki zagotavljajo večjo varnost in omogočajo zdravljenje po meri. V primerjavi s celičnimi terapijami imajo ZV več prednosti (27). ZV, pridobljene iz medicinskih/mezenhimskih matičnih celic, so še posebej zanimivi. Zdaj je jasno, da so ZV tista celična frakcija medicinskih/mezenhimskih matičnih celic, ki vpliva na imunomodulacijo poškodovanega tkiva.

Tovor ZV je v telesnih tekočinah zaščiten, kar se odraža v podaljšanem roku uporabnosti izdelkov na osnovi ZV. Po drugi strani pa pripravki iz živih celic zahtevajo stroge pogoje vzdrževanja viabilnosti, ki jih je težko in ekonomsko neučinkovito vzdrževati.

Protivnetne lastnosti ZV lahko zmanjšajo potrebo po dolgotrajni uporabi zdravil. Spodbujanje delovanja imunskega odziva je lahko koristno pri zdravljenju raka ali v boju proti okužbam. Pomemben dejavnik v primerjavi s celičnimi terapijami je manjše tveganje za nastanek tumorjev, saj ZV ne prinašajo tveganja nenadzorovane proliferacije celic (5, 28). Vse te pozitivne lastnosti spodbujajo aktivne raziskave na področju ZV, ki izkazujejo potencial za uporabo na različnih področjih regenerativne veterinarske medicine, npr. pri nevrodegeneraciji, boleznih sklepov in hrustanca, celjenju ran in regeneraciji kože, avtoimunskih boleznih in zdravljenju plodnosti (29).

Čeprav so ZV izjemno obetavni in uporabni, je treba za sprostitev njihovega celokupnega potenciala v veterinarski medicini še vedno obravnavati izzive, kot so standardizacija tehnik izolacije, optimizacija razmerja med visokimi stroški in nizkimi donosi, izboljšanje občutljivosti zaznavanja in izvajanje študij, specifičnih za posamezne vrste. Začelo se je novo obdobje in vedno večje število publikacij poudarja obetavno uporabo ZV v neinvazivni diagnostiki, ciljani dostavi molekul in regenerativnem zdravljenju. Zaradi svoje izjemne vsestranskosti so ZV v edinstvenem položaju, da korenito spremenijo naš pogled na veterinarsko medicino.

References

1. van Niel G, D'Angelo G, Raposo G. Shedding light on the cell biology of extracellular vesicles. Nat Rev Mol Cell Biol 2018; 19(4): 213-28. doi: 10.1038/nrm.2017.125
2. Espejo C, Ezenwa VO. Extracellular vesicles: an emerging tool for wild immunology. Discov Immunol 2024;3(1):kyae011. doi: 10.1093/discim/kyae011
3. Tozon N. Translation Oncology throught the One Health Perspective. Slov Vet Res 2025; 62(Suppl. 27): 9–12. doi: 10.26873/SVR-2180-2024
4. Yáñez-Mó M, Siljander PR, Andreu Z, et al. Biological properties of extracellular vesicles and their physiological functions. J Extracell Vesicles 2015; 4: 27066. doi: 10.3402/jev.v4.27066
5. Moccia V, Sammarco A, Cavicchioli L, Castagnaro M, Bongiovanni L, Zappulli V. Extracellular Vesicles in Veterinary Medicine. Animals (Basel) 2022; 12(19): 2716. doi: 10.3390/ani12192716
6. Welsh JA, Goberdhan DCI, O'Driscoll L, et al. Minimal information for studies of extracellular vesicles (MISEV2023): from basic to advanced approaches. J Extracell Vesicles 2024; 13(2): e12404. doi: 10.1002/jev2.12404
7. Kumar MA, Baba SK, Sadida HQ, et al. Extracellular vesicles as tools and targets in therapy for diseases. Signal Transduct Target Ther 2024; 9(1): 27. doi: 10.1038/s41392-024-01735-1
8. Zamboni C, Zamarian V, Stefanello D, et al. Plasma small extracellular vesicles from dogs affected by cutaneous mast cell tumors deliver high levels of miR-21-5p. Front Vet Sci 2022; 9: 1083174. doi: 10.3389/fvets.2022.1083174
9. Özmen Ö, Kaya B, Karaman K. Transcriptome analysis and bioinformatics characterization of canine hemangiosarcoma: potential therapeutic targets. Slov Vet Res 2025; 62: 41–52. doi: 10.26873/SVR-1797-2024
10. Elashry MI, Speer J, De Marco I, Klymiuk MC, Wenisch S, Arnhold S. Extracellular vesicles: a novel diagnostic tool and potential therapeutic approach for equine osteoarthritis. Curr Issues Mol Biol 2024; 46(11): 13078–104. doi: 10.3390/cimb46110780
11. Varela L, van de Lest CHA, van Weeren PR, Wauben MHM. Synovial fluid extracellular vesicles as arthritis biomarkers: the added value of lipid-profiling and integrated omics. Extracell Vesicles Circ Nucl Acids 2024 ;5(2): 276–96. doi: 10.20517/evcna.2024.14
12. Palacios A, Sampedro L, Sevilla IA, et al. Mycobacterium tuberculosis extracellular vesicle-associated lipoprotein LpqH as a potential biomarker to distinguish paratuberculosis infection or vaccination from tuberculosis infection. BMC Vet Res 2019; 15(1): 188. doi: 10.1186/s12917-019-1941-6
13. Monari E, Troìa R, Magna L, et al. Urine neutrophil gelatinase-associated lipocalin to diagnose and characterize acute kidney injury in dogs. J Vet Intern Med 2020; 34(1): 176–85. doi: 10.1111/jvim.15645
14. Ugarte F, Santapau D, Gallardo V, et al. Urinary extracellular vesicles as a source of ngal for diabetic kidney disease evaluation in children and adolescents with type 1 diabetes mellitus. Front Endocrinol (Lausanne) 2021; 12: 654269. doi: 10.3389/fendo.2021.654269
15. Cerón JJ, Ortín-Bustillo A, López-Martínez MJ, et al. S-100 Proteins: basics and applications as biomarkers in animals with special focus on calgranulins (S100A8, A9, and A12). Biology (Basel) 2023; 12(6): 881. doi: 10.3390/biology12060881
16. Piibor J, Waldmann A, Prasadani M, et al. Investigation of uterine fluid extracellular vesicles' proteomic profiles provides novel diagnostic biomarkers of bovine endometritis. Biomolecules 2024; 14(6): 626. doi: 10.3390/biom14060626
17. Yeo RW, Lai RC, Zhang B, Tan SS, Yin Y, Teh BJ, et al. Mesenchymal stem cell: an efficient mass producer of exosomes for drug delivery. Adv Drug Deliv Rev 2013; 65(3): 336–41. doi: 10.1016/j.addr.2012.07.001
18. Amina SJ, Azam T, Dagher F, Guo B. A review on the use of extracellular vesicles for the delivery of drugs and biological therapeutics. Expert Opin Drug Deliv 2024; 21(1): 45-70. doi: 10.1080/17425247.2024.2305115
19. Xiong Y, Lou P, Xu C, Han B, Liu J, Gao J. Emerging role of extracellular vesicles in veterinary practice: novel opportunities and potential challenges. Front Vet Sci 2024; 11: 1335107. doi: 10.3389/fvets.2024.1335107
20. Kim HI, Park J, Zhu Y, Wang X, Han Y, Zhang D. Recent advances in extracellular vesicles for therapeutic cargo delivery. Exp Mol Med 2024; 56(4): 836–49. doi: 10.1038/s12276-024-01201-6
21. Gervasi MG, Soler AJ, González-Fernández L, Alves MG, Oliveira PF, Martín-Hidalgo D. Extracellular Vesicles, the Road toward the Improvement of ART Outcomes. Animals (Basel) 2020; 10(11): 2171. doi: 10.3390/ani10112171
22. Ba-Awadh HA, Olarinre IO, Alowaimer AN, Saadeldin IM, Swelum AA. Comparison between rapid and slow cryopreservation protocols for ram semen. Slov Vet Res 2023; 60: 249-57. doi: 10.26873/SVR-1586-2022
23. Mogas T, García-Martínez T, Martínez-Rodero I. Methodological approaches in vitrification: enhancing viability of bovine oocytes and in vitro-produced embryos. Reprod Domest Anim 2024; 59 (Suppl. 3) : e14623. doi: 10.1111/rda.14623
24. Pedrosa AC, Andrade Torres M, Vilela Alkmin D, et al. Spermatozoa and seminal plasma small extracellular vesicles miRNAs as biomarkers of boar semen cryotolerance. Theriogenology 2021; 174: 60–72. doi: 10.1016/j.theriogenology.2021.07.022
25. Santos P, Almeida F. Exosome-based vaccines: history, current state, and clinical trials. Front Immunol 2021; 12: 711565. doi: 10.3389/fimmu.2021.711565
26. Hoelzer K, Bielke L, Blake DP, et al. Vaccines as alternatives to antibiotics for food producing animals. Part 2: new approaches and potential solutions. Vet Res 2018; 49(1): 70. doi: 10.1186/s13567-018-0561-7
27. El-Husseiny HM, Mady EA, Helal MAY, Tanaka R. the pivotal role of stem cells in veterinary regenerative medicine and tissue engineering. Vet Sci 2022; 9(11): 648. doi: 10.3390/vetsci9110648
28. Pirisinu M. The long journey of extracellular vesicles towards global scientific acclamation. Adv Pharm Bull 2023; 13(3): 489–501. doi: 10.34172/apb.2023.049
29. Koprivec S, Majdič G. Extracellular vesicles in domestic animals: cellular communication in health and disease. Adv Exp Med Biol 2024; 1450: 39-57. doi: 10.1007/5584_2023_779

Slov Vet Res

DOI 10.26873/SVR-2202-2025
UDC 636.4:577.161.2:612.015.6:591.143
Pages: 145–55

Original Research Article

Evaluating Seasonal Serum Vitamin D Levels and Growth Performance in Pigs From Organic Farms

Key words

vitamin D;
serum concentrations;
pigs welfare;
organic farm;
growth performance

Tim Šteferl[1]*, Melita Hajdinjak[2], Eva Nadlučnik[1], Irena Golinar Oven[1], Marina Štukelj[1], Ožbalt Podpečan[1]

[1]Clinic for Reproduction and Large Animals, Clinic for Ruminants and Pigs, Nacional Centre for Animal Welfare, Veterinary Faculty, University of Ljubljana, Gerbičeva ulica 60, [2]Laboratory of Applied Mathematics and Statistics, Faculty of Electrical Engineering, University of Ljubljana, Tržaška cesta 25, 1000 Ljubljana, Slovenia

***Corresponding author:** tim.steferl@vf.uni-lj.si

Abstract: Vitamin D is an essential micronutrient in pig production as it plays an important role in many physiological functions. The aim of this study was to determine serum vitamin D concentration and growth performance in pigs reared on organic farms in different seasons. A total of 109 Krškopolje pigs were selected for this study. Pigs were divided into three groups: low altitude outdoor group A (N = 39), high altitude outdoor group B (N = 36) and indoor group C (N = 34). Blood samples and body weights were collected seasonally in 2022 and 2023. Serum vitamin D levels peaked in summer for outdoor groups A (69.3 ±2.6 ng/ml) and B (65.3 ±4.4 ng/ml) and were the lowest in winter (group A 21.5 ±2.2, group B 35.2 ±2.5). Altitude had no significant effect on vitamin D levels except in winter ($p<0.001$). Housing type significantly influenced vitamin D levels in every season between groups B and C, and in spring, summer, and autumn between groups A and C. Pigs in the outdoor group A showed higher average final body weights (151.2 ±7.5 kg in 2022 and 146.8 ±3.8 kg in 2023) than those in group C (132.7 ±11.3 kg and 118.5 ±6.9 kg), though this should be interpreted cautiously given variability in initial weights.

Received: 27 February 2025
Accepted: 9 July 2025

Introduction

Vitamin D comprises a group of fat-soluble steroid compounds with a similar chemical structure and a variety of physiological functions. It is best known for its role in the homeostasis of calcium in bone formation by increasing calcium absorption from the intestine, stimulating calcium reabsorption in the distal renal tubules, and mobilising calcium stored in bone (1, 2).

The two main forms of vitamin D are ergocalciferol (vitamin D_2) and cholecalciferol (vitamin D_3). Vitamin D_3 is formed in the skin after exposure to ultraviolet radiation from sunlight (UVB). Vitamin D_3 is then hydroxylated in the liver to 25-hydroxyvitamin D_3 ($25(OH)D_3$). This metabolite is present in serum, and its concentration is measured to determine vitamin D status in an individual (3). $25(OH)D_3$ is further hydroxylated in the kidney to 1, 25-dihydroxyvitamin D_3 or calcitriol, the biologically active form of vitamin D (1, 2). Vitamin D_2 is formed from ergosterol under UVB radiation in fungi and plants (2, 4) and must be ingested with food. Studies have shown differences in the physiological effects of both variants of vitamin D, with vitamin D_3 being more stable, more potent, and more effective in raising serum vitamin D levels than vitamin D_2 (3).

Like many other animals and humans (1, 5, 6), pigs are also able to synthesise vitamin D in their skin. However, as pigs in intensive pork production are mostly raised indoors without access to sunlight, they are dependent on dietary intake of vitamin D. Chronic vitamin D deficiency in pigs may lead to certain metabolic bone diseases (7, 8). Vitamin

D deficiency affects bone strength in grower pigs, leading to lameness, rickets with flared growth plates, and bone fractures. Hypocalcemic paresis, tremors, and even sudden death can occur. Swine with clinical rickets generally have serum vitamin D concentrations lower than 5 ng/ml, whereas swine with concentrations above 15 ng/ml appear to be clinically healthy (9). Piglets are most susceptible to hypovitaminosis D, as they are born with the lowest blood concentrations of vitamin D (8).

Vitamin D supplementation positively impacts growth performance, bone formation and immunity (10, 11, 12), meaning it also has an impact on production parameters in the pig industry. In humans, recommendations for adequate serum vitamin D concentrations have already been established (13). In pigs, vitamin D concentrations of 30 ng/ml in the blood are considered minimal standard, but 50 – 80 is required for optimal development (14). Some authors report reference serum vitamin D concentrations for individual categories of pigs (7, 8). To our knowledge, there is only one previous study evaluating serum vitamin D concentrations in organic pig farms (3), which suggested a reference value of 35–99 ng/ml for weaned sows.

In Slovenia, intensive pig farming is in decline (15). However, there are many backyard farms with one or two pigs kept for home consumption, and recently, there has been a surge of organic pig farms. There are 365 organic pig farms registered in the country, keeping around 3000 pigs of all categories (16). Many of these pigs are often reared outdoors or have the possibility of outside access, which gives us the opportunity to study the effects of sun-derived vitamin D in pigs, which is not normally possible in intensive pig production. The aims of this study were to determine the seasonal serum concentrations of vitamin D as well as growth performance of pigs reared on organic farms, and to see whether there is a connection between sun-derived vitamin D and growth performance of pigs.

Materials and methods

Ethics

This study was carried out as part of the ERA-Net CORE Organic Cofound project - RObust Animals in sustainable Mixed Free-range systems project (ROAM-FREE). The study was ethically approved by the Slovenian Ministry of Agriculture, Forestry and Food (U34401-

6/2022/11). The overall objective of the ROAM-FREE project is to investigate how mixed freerange production systems can improve animal welfare, robustness, environmental and economic sustainability and biodiversity in organic pig farming.

Experimental design

A total of 109 grower-to-finisher pigs were selected for this study and were reared in two consecutive years: 2022 and 2023. All animals were Krškopolje pigs, the only autochthonous Slovenian pig breed. Krškopolje pigs are mostly black, medium-sized pigs with a distinctive white belt running across shoulders and forelimbs. The breed was historically reared in modest conditions and is therefore characterised by extreme resilience, great adaptability, adequate reproductive capacity, and quality of meat and fat (17). All this means that Krškopolje pigs are mostly reared in extensive conditions and can be reared outdoors even in winter. All pigs in this study were born on the same organic pig farm in the Littoral-Inner Carniola region in southwestern Slovenia. Pigs were bred to provide organic meat products for consumption. Pigs were divided into groups A, B, and C and distributed to three locations for further rearing.

Based on the live weights recorded at the beginning of the experiment, as shown in Tables 5 and 6, and given that the exact ages of the pigs at the time of measurement are unknown, it is not possible to determine their precise age at the start of the experiment. The experiment began on the 21s^{t} of April 2022 and ended on the 12th of October 2023, when the last batch of pigs was sampled (Table 1).

Table 1: Dates in which blood was sampled in 2022 and 2023

Season	2022	N	2023	N
Spring	21st April	57	5th May	52
Summer	8th August	57	19th July	52
Autumn	7th October	46	12th October	51
Winter	25th November	36	24th February	52

Figure 1: Outdoor pigs in group A with a visible dugout (Photo: M. Štukelj)

Figure 2: High altitude pigs of group B together with sheep. Pigs are visibly sunburned on the white part of their bodies (Photo: M. Štukelj)

Figure 3: Pigs in group C (control group) in the barn (Photo: M. Štukelj)

Housing and feed

Pigs were divided into three groups: low-altitude outdoor pigs (Group A, N = 39), high-altitude outdoor pigs (Group B, N = 36), and a group of indoor pigs (Group C, N = 34). Pigs in group A were kept in a large, fenced pasture (9000 m^2) with access to direct sunlight. There were no trees in the pasture, but there were two straw-bedded dugouts (13.5 m^2 each) (Figure 1), and a larger straw-bedded, roofed pen (65 m^2) where pigs in group A were housed in winter. Feeders and nipple drinkers were available. Pigs in this group shared the pasture with cattle.

Pigs in group B were reared outdoors on a large grass pasture (12600 m^2) with live wire fencing. Less than half of the pasture area (5400 m^2) was overgrown with trees and bushes. Animals had access to a roofed shelter (40 m^2) and a pigloo. The shelter had straw bedding, one water trough and one feed trough inside. Pigs in this group shared the pasture with sheep (Figure 2).

Pigs in group C (i.e. control group) were housed in two pens (50 m^2 each) within a large barn, without access to sunlight, yet not entirely isolated from daylight (Figure 3). The barn had straw bedding; feeders and nipple drinkers were available for the animals. Natural ventilation was provided year-round, and the building was not heated in winter.

Pigs in groups A and C were kept at an altitude of 550 metres, pigs in group B were kept at an altitude of 820 metres. Approximate altitudes were obtained from publicly available data provided by Surveying and Mapping Authority of the Republic of Slovenia (18). Pigs in groups A and B grazed freely on the pasture, constantly coming in contact with, and possibly ingesting parts of bushes and grass.

All groups of pigs were fed the same organically produced feed, which consisted of 60% barley, 30% wheat, and 10% sunflower meal. Feed was grown on site. Pigs in group B were fed twice a day; approximately 35 kilogrammes of feed per group in the morning, and 15 kilogrammes of feed per group in the afternoon (circa 350 kilogrammes every week). Pigs in groups A and C were fed *ad libitum* and consumed approximately 700 kilogrammes of feed each week (or 350 kilogrammes per week each). No additives of any kind were added to the feed, including mineral or vitamin premixes.

Animal welfare, health assessment and treatment

Pigs in this study were reared in accordance with Regulation (EU) 2018/848 of the European Parliament and of the Council of 30th May 2018 on organic production and labelling of organic products (19), as well as the currently valid animal welfare laws and regulations of the state (20). The welfare of the animals and their health status were regularly assessed prior to each sampling in 2022 and 2023.

All pigs in this study were vaccinated against *Erysipelothrix rhusiopathiae* and received a complete treatment against ecto- and endoparasites before the start of the study. The pig herd was certified free of African swine fever, Classical swine fever, Aujeszky's disease, Porcine reproductive and respiratory syndrome (PRRS), *Clostridium perfringens C*, *Brachyspira hyodysenteriae*, and *Salmonella spp.* The herd was certified as free of African swine fever, Classical swine fever, and Aujeszky's disease based on laboratory tests carried out under the annual national Order on monitoring of animal health status, animal disease eradication programmes and vaccinations of animals (21), the rest was tested at the request of the farm's owner. During each visit to the herd, pigs were clinically examined, their welfare was assessed, and weight was calculated. Before each blood sample was taken, the length of the pig's body from the auricular region to the base of the tail and the chest circumference were measured using a tape measure. Weight of each animal in groups A, B and C was calculated using: (*chest circumference (meters)*)^2 x (*body length (meters)*) x *69.3* (22). The weight of the individual animal is given in kilogrammes. Calculations using this method are reported to be accurate to within 3%.

Blood sampling and transport

Blood sampling was performed in four periods, once every season in year 2022 and replicated in 2023, as shown in Table 1. We defined individual seasons as follows: Spring (March, April, May), Summer (June, July, August), Autumn (September, October, November), Winter (December, January, February). The exact sampling dates were set depending on the availability of the owner of the farm and the veterinary staff, however, they had to fall within the three-month period of each defined season. The only exception was November 25, 2022, which did not align with the seasonal schedule but was selected as it was the only feasible date for both the veterinary staff and the farmer. Due to its close proximity to December, it was categorized as part of Winter.

Pigs were restrained using steel wire snout snare. Blood samples were obtained by puncturing the cranial vena cava with a needle of 15 G – 1.80 x 160 needle (TIK, Slovenia) and a 10/12 ml disposable syringe (KRUUSE, Denmark). Sampled blood was stored in serum tubes (BD-Plymouth, UK) and transported to the laboratory at the ambient temperature of the respective season. Samples in spring and summer were transported in a cool bag. Blood samples were centrifuged at 2500 RPM for 10 minutes and the serum was transferred to separate vials, which were then stored at – 20 °C until analysis. Samples were analysed using Vidas 25 OH Vitamin D TOTAL (Biomerieux, France), an automated quantitative test for the determination of total 25-hydroxyvitamin D (25(OH)D_T) in serum or plasma samples using the ELFA (Enzyme Linked Fluorescent Assay) technique.

Statistical analysis

Measured serum vitamin D levels were arranged by group, sampling date and season and mean values for every season were calculated using Excel (Microsoft, USA).

Data was statistically analysed using statistical software R version 4.3.2. (GiltHub, USA). Gathered data was checked for differences using analysis of variance (ANOVA) and Tukey's HSD test or Welch's t-test, depending on the results of the Bartlett's test for homoscedasticity. We compared data to check for differences in mean values of serum vitamin D between seasons for each group of pigs. We also compared seasonal mean values of vitamin D between groups A and B to determine the effect of different altitudes on serum vitamin D levels and between groups A and C and B and C to see whether different types of housing affect levels of serum vitamin D in pigs. Considering slight imbalance in a few group comparisons, we fitted linear mixed-effects models (LMMs) with Satterthwaite degrees-of-freedom corrections. Initial weight, age (highly correlated with weight), and sex were tested as potential confounders in nested LMMs but none improved model fit. The resulting LMM p-values were marginally larger than those from the standard ANOVA, yet the numerical differences were negligible with our moderate sample sizes. This confirms that, in the absence of meaningful confounders and with all ANOVA assumptions met, the standard factorial ANOVA with Tukey's HSD provides valid and robust inference.

In addition, reference intervals were estimated using the R-package refineR, which implements the recently published, state-of-the-art indirect method (23). It takes routine measurements of diagnostic tests as input and uses sophisticated statistical methods to derive a model describing the distribution of the non-pathological samples. This distribution is then used to derive reference intervals. Mean body weight of pigs between groups A and C in every measurement was checked for differences using Welch's t-test to determine, if the means were statistically significant.

Results

Clinical examinations

Animals showed no apparent signs of disease and were clinically healthy prior to sampling in every season in 2022 and 2023. Pigs in groups A and B were sunburned on the non-pigmented parts of their bodies in the summer of 2022 and 2023 (Figure 2).

Mean values of serum vitamin D

The mean values of total serum vitamin D concentrations in sampled Krškopolje pigs for every season are shown in Table 2 and Figure 4. Statistical significance was found between all seasonal mean values of serum 25(OH)D_T for every pig group.

When evaluating the effect of altitude on total serum 25(OH)D_T concentrations by comparing means of groups A and B, no statistical significance was found in any season other than winter, when the mean value of group B was

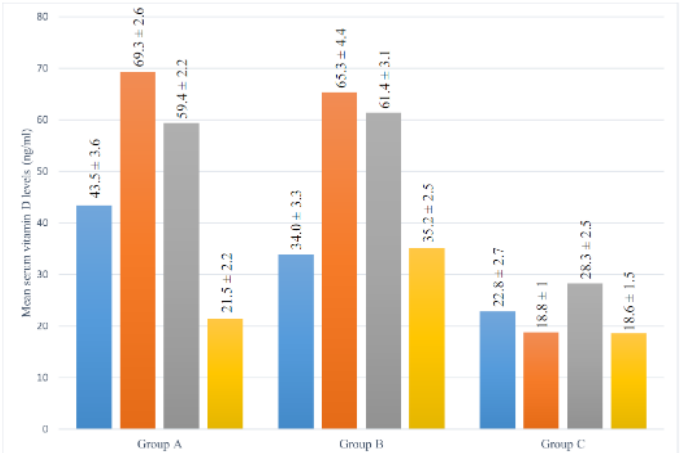

Figure 4: Seasonal serum 25(OH)D_T concentrations for groups A, B, and C

Table 2: Mean total serum 25(OH)D_T concentrations of different groups of pigs sampled each season

Mean 25(OH)D_T	GROUP A (Range)	GROUP B (Range)	GROUP C (Range)	p-values			
				Overall	AB	AC	BC
Spring (ng/ml) Min –max	N = 39[1] 43.5 ± 3.6 (11.3–64.6)	N = 36 34.0 ± 3.3 (11.4–89.0)	N = 34[2] 22.8 ± 2.7 (8.1–51.4)	<0.001	0.13	<0.001	0.023
Summer (ng/ml) Min –max	N = 39 69.3 ± 2.6 (28.1–103.9)	N = 36 65.3 ± 4.4[A] (33.1–124.9)	N = 34[3] 18.8 ± 1.0 (10.6–29.4)	<0.001	0.45	<0.001	<0.001
Autumn (ng/ml) Min –max	N = 37 59.4 ± 2.2 (26.9–79.1)	N = 36 61.4 ± 3.1 (26.3–105.2)	N = 24 28.3 ± 2.5 (12.9–62.8)	<0.001	0.84	<0.001	<0.001
Winter (ng/ml) Min –max	N = 30[4] 21.5 ± 2.2 (8.8–45.7)	N = 36 35.2 ± 2.5 (17.3–70.5)	N = 22 18.6 ± 1.5 (8.9–34.1)	<0.001	<0.001	0.28	<0.001

GROUP A: low altitude outdoor pigs; GROUP B: high altitude outdoor pigs; GROUP C: indoor pigs; 1:19 out of 544 20 blood samples taken in spring 2023 yielded results < 8.1 ng /ml and were excluded; 2: One blood sample in 545 spring 2023 yielded < 8.1 ng/ml and was excluded; 3: One of the pigs was not sampled; 4: One blood sample in 546 winter 2023 yielded < 8.1 ng/ml and was excluded; ± Standard error of the mean; N: Number of animals. The 547 number of animals sampled in groups A and C decreased over the seasons as animals were slaughtered

greater (p<0.001) than that of group A. When evaluating the effect of outdoor/indoor housing of pigs between groups A and C on serum 25(OH)D_T concentrations, means were significantly greater in all seasons in group A, except winter (p=0.28), whereas between groups B and C, means in every season were significantly greater in group B (Table 2).

Reference intervals

Reference intervals were evaluated from combined seasonal values of serum 25(OH)D_T levels together for both groups of outdoor grower-to-finisher pigs (groups A and B) and separately for indoor grower-to-finisher pigs (group C). Reference intervals are shown in Table 3.

Growth performance of pigs in groups A, B, and C

All groups of pigs were measured at the same time as shown in Table 1. Calculated weight, seasonal growth values, average daily gain (ADG), average daily feed intake (ADFI), and feed conversion ratios (FCR) are shown in Tables 4 and 5. Values were compared only between groups A and C, since they were both fed *ad libitum*.

Table 3: Evaluated reference intervals of combined seasonal values

Reference intervals	Lower limit (2, 5% perc.)	Median (50, 0% perc.)	Upper limit (97, 5% perc.)
Outdoor pigs (ng/ml) Groups A and B N = 269	25.1	55	104
Indoor pigs (ng/ml) Group C N = 112	6.7	16.8	40.6

GROUP A: low altitude outdoor pigs; GROUP B: high altitude outdoor pigs; GROUP C: indoor pigs; N: Combined number of samples from all seasons

Statistical significance between mean body weights in groups A and C (2022) was not found in any measurements other than the third measurement (p=0.015), where the mean body weights were noticeably greater in group A compared to group C (Table 4).

Mean body weights between groups A and C (2023) were significantly greater in group A in every measurement (Table 5).

Discussion

This study is the first to investigate total serum vitamin D concentrations in extensively reared Krškopolje pigs on an organic farm and, as far as we are aware, the first study to investigate serum vitamin D in pigs in every season of the year. Studies on serum vitamin D in pigs are lacking, especially in pigs from organic herds. However, there are reported reference values for serum vitamin D concentrations for each individual category of indoor pigs (7, 8). The mean values of 25(OH)D_T serum concentrations for groups A and B peaked in summer with values of 69.3 ± 2.6 ng/ml and 65.3 ± 4.4 ng/ml, respectively. Our results in these two groups correspond with serum 25(OH)D_3 levels of 67 ± 16 ng/ml measured at approximately the same time of year in outdoor sows of the Danish Landrace and Yorkshire cross breeds in organic herds in Denmark in August 2020 (3), as well as serum 25(OH)D_3 levels of 57.2 ± 2.8 ng/ml in outdoor black-skinned sows and 61.1 ± 6.56 ng/ml in outdoor white-skinned grower pigs in the upper Midwest of the United States in June 2011 (8). The aforementioned studies report specifically on serum levels of sun-derived 25(OH)D_3, which means that our results are not directly comparable to theirs, as our study reports total serum vitamin D concentrations (both sun- and feed

Table 4: Growth performance of pigs in Group A, B, and C in 2022

Growth performance	GROUP A	GROUP B	GROUP C	p-values			
				Overall	AB	AC	BC
First measurement Weight (kg) Range (kg) 21st April 2022	N = 19 44.7 ± 2.4 22.3–65.9	N = 19 26.9 ± 2.6 10.8–45.6	N = 19 41.2 ± 2.8 18.2–63.9	<0.001	<0.001	0.61	<0.001
Second measurement Weight (kg) Range (kg) ADG (g/day) ADFI (kg/day) FCR 8th August 2022	N = 19 96.1 ± 3.6 50.5–116.8 467.3 2.6 5.6	N = 19 48.5 ± 3.7 23.1–74.5 181.5 2.4 13.3	N = 19[1] 83.9 ± 5.6 40.5–129.0 388.2 2.7 7.5	<0.001	<0.001	0.13	<0.001
Third measurement Weight (kg) Range (kg) ADG (g/day) ADFI (kg/day) FCR 7th October 2022	N = 17 133.5 ± 5.0 87.3–172.7 613.1 2.2 4.7	N = 19 65.4 ± 5.3 30.0–117.8 277.0 1.5 9.3	N = 10 108.1 ± 6.7 56.1–127.9 396.7 4.9 12.4	<0.001	<0.001	0.015	<0.001
Fourth measurement Weight (kg) Range (kg) ADG (g/day) ADFI (kg/day) FCR 25th November 2022	N = 10 151.2 ± 7.5 121.5–199.4 354.0 4.9 13.8	N = 19 80.6 ± 5.8 45.0–127.8 304.0 2.6 8.5	N = 7 132.7 ± 11.3 81.8–168.0 492.0 7.0 14.2	<0.001	<0.001	0.32	<0.001

GROUP A: low altitude outdoor pigs; GROUP B: high altitude outdoor pigs; GROUP C: indoor pigs; [1]: One pig was not measured; N: Number of animals. Number of animals in groups A and C dropped through measurements, due to animals being slaughtered; ADG: Average daily gain between two measurements; ADFI: Average daily feed intake of individual pig; FCR: Average feed conversion ratio of individual pig; ±: Standard error of the mean (SEM); p-value vas calculated between mean weights of groups A and C

derived). We do not know what the exact ratio between $25(OH)D_2$ and $25(OH)D_3$ in our samples is; however, it has been reported in humans that vitamin D_2 is less effective in raising total serum vitamin D (24). In our study, pigs did not receive vitamin D supplements in their feed, meaning that serum $25(OH)D_2$ levels are likely to be low. This was also reported in the Danish study, in which serum $25(OH)D_2$ levels contributed insignificantly to overall vitamin D status (3).

We noticed a slow decline in serum $25(OH)D_T$ levels in autumn, and the lowest levels were observed in the winter. The latter was likely due to the fact that Slovenia is geographically located in the Northern Hemisphere at a latitude above 40°, where there is a lack of UVB radiation under which vitamin D can be synthesised (25). Group C had the lowest average serum

$25(OH)D_T$ concentrations; interestingly, however, levels in this group peaked in autumn (28.3 ± 2.5 ng/ml). Another factor plays an important role in the synthesis of sun-derived vitamin D in pigs studied: the pigmentation of their skin. Krškopolje pigs are predominantly black-skinned (Figures 1 to 3), i.e. they have larger amounts of melanin. Studies in humans have shown that increased melanin levels effectively reduce vitamin D synthesis in the skin, which in turn lowers serum vitamin D concentrations (26, 27). This would mean that the observed serum vitamin D concentrations in Krškopolje pigs are lower than would be expected if we included whiteskinned pig breeds (e.g. Landrace) under the same conditions. The number of pig sera sampled gradually decreased in each subsequent season. This was due to the fact that the pigs were taken to slaughter. In the spring of 2023, 19 blood samples from group A yielded results below 8.1 ng/ml, which is beneath the minimum detection threshold of the Vidas 25 OH Vitamin D TOTAL assay. As the exact $25(OH)D_T$ concentrations could not be determined, these samples were excluded from the study. Excluded samples showed moderate to severe hemolysis.

Serum $25(OH)D_T$ concentrations of Krškopolje pigs show a high variation within groups A and B (Table 2), with the highest ranges observed in summer (28.1–103.9 ng/ml and 33.1–124.9 ng/ml), which is comparable to the 32–134 ng/ml reported in the sera of newly weaned sows in Danish organic farms (3). Pigs in the outdoor groups A and B were housed in fenced areas containing trees, bushes, pens, and a pigloo, allowing them constant access to shelter from direct sunlight. However, we had no data on individual

Table 5: Growth performance of pigs in Group A, B, and C in 2023

Growth performance	GROUP A	GROUP B	GROUP C	p-values			
				Overall	AB	AC	BC
First measurement Weight (kg) Range (kg) 24th February 2023	N = 20 34.5 ± 1.4 26.2–45.1	N = 17 18.7 ± 1.3 13.2–33.7	N = 15 18.3 ± 1.3 11.9–26.5	<0.001	<0.001	<0.001	0.97
Second measurement Weight (kg) Range (kg) ADG (g/day) ADFI (kg/day) FCR 5th May 2023	N = 20 59.1 ± 2. 40.5–79.5 346.7 2.5 7.1	N = 17 39.7 ± 2.6 27.3–68.6 295.8 2.9 11.1	N = 15 45.3 ± 3.1 26.2–61.2 380.3 3.3 8.6	<0.001	<0.001	0.0012	0.57
Third measurement Weight (kg) Range (kg) ADG (g/day) ADFI (kg/day) FCR 19th July 2023	N = 20 94.2 ± 3.3 70.7–127.9 461.8 2.5 5.3	N = 17 68.0 ± 4.1 46.7–109.1 372.4 2.9 7.8	N = 15 77.3 ± 5.4 41.2–119.7 421.1 3.3 7.8	<0.001	<0.001	0.0097	0.49
Fourth measurement Weight (kg) Range (kg) ADG (g/day) ADFI (kg/day) FCR 12th October 2023	N = 20 146.8 ± 3.8 118.8–184.5 611.6 2.5 4.0	N = 17 107.3 ± 5.0 74.7–149.9 466.0 2.9 6.3	N = 14 118.5 ± 6.9 72.1–155.5 478.5 3.5 7.3	<0.001	<0.001	<0.001	0.56

GROUP A: low altitude outdoor pigs; GROUP B: high altitude outdoor pigs; GROUP C: indoor pigs; N: Number of animals. Number of animals in groups A and C dropped through measurements, due to animals being slaughtered; ADG: Average daily gain between two measurements; ADFI: Average daily feed intake of individual pig; FCR: Average feed conversion ratio of individual pig; ±: Standard error of the mean (SEM); p-value vas calculated between mean weights of groups A and C

sunlight exposure, solar intensity, day length, or weather conditions (e.g., cloud cover or storms). During summer and autumn, many of the tested pigs exhibited mild to moderate sunburns on non-pigmented skin areas (Figure 2), suggesting prolonged exposure to direct sunlight. These environmental and behavioural factors may account for the substantial variation in serum 25(OH)D_T concentrations among individual pigs.

Groups of outdoor pigs were reared at different altitudes, providing an opportunity to investigate whether altitude affects serum 25(OH)D_T concentrations. In humans, higher altitude has been reported to be associated with increased vitamin D production (25). Pigs in group A were reared at an altitude of 550 meters, while those in group B were raised at 820 meters. A statistically significant difference was observed only when comparing mean serum 25(OH)D_T concentrations between groups A and B in winter ($p<0.001$), with higher values in group B. No significant differences were found between groups during the other seasons. Therefore, we conclude that altitude had no effect on serum 25(OH)D_T concentrations in spring, summer, and autumn—likely because the difference in altitude was not substantial enough to have a meaningful impact. In winter, however, the mean values were higher in group B, which may be attributed to more effective UVB exposure at the higher altitude, resulting in a slower decline in vitamin D levels during this season. Pigs in group B only had a pigloo and a smaller shelter (40 m^2) available, while the pigs in group A had a larger shelter available (65 m^2), which means that the pigs in group B most likely spent more time in the sun, even in winter. To our knowledge, no similar studies have been conducted in pigs. However, one study examining the influence of altitude on vitamin D status in lactating sheep and goats (28) also reported no significant effect. We compared the effect of housing on serum 25(OH)D_T concentrations between outdoor and indoor pigs. Mean values across all seasons were significantly higher in group A compared to group C, except in winter, where no significant difference was observed ($p=0.28$). In contrast, mean serum concentrations in group B were significantly higher than those in group C across all seasons. These results confirm that pigs housed outdoors have higher serum vitamin D levels than those kept indoors. This corresponds with the results from the

Midwest of the United States, where authors also reported significantly greater serum vitamin D levels in outdoor pigs compared to pigs raised in confinement (8). One study did a similar comparison of serum vitamin D levels in White

Landrace-Duroc and Yorkshire-DurocLandrace crossbred pigs by exposing them to sunlight in summer and autumn (28). They similarly reported higher post-exposure levels compared to pigs housed indoors, but interestingly, serum levels in that study were higher in pigs exposed in autumn than in summer.

Krškopolje pigs in our study were clinically examined prior to every sampling, and none of them showed any clinical signs of hypovitaminosis. Mean seasonal values of all groups are within or higher than previously reported reference levels of serum vitamin D for confined grower pigs (10–30 ng/ml) (7, 8). In this study, values from groups A and B from all four seasons in 2022 and 2023 were combined; the same was done with values from group C. Reference intervals were subsequently evaluated for outdoor pigs (groups A and B) and indoor pigs, respectively (Table 4). As all animals were clinically healthy, these results could serve as reference levels for total serum vitamin D for outdoor grower-to-finisher pigs (25.1–104 ng/ml) and indoor grower-to-finisher pigs (6.7–40.6 ng/ml) reared on organic farms.

Pigs were examined by a veterinarian prior to every blood sampling and were clinically healthy throughout the entire study. All pigs were measured, and subsequently their mean seasonal body weight, ADG, ADFI, and FCR were calculated separately for 2022 and 2023 (Tables 4 and 5). Pigs in groups A and C were reared at the same location and received the same diet, with housing conditions being the only planned difference—group A was kept outdoors, while group C was housed indoors. Although group A pigs generally showed higher average body weights than group C pigs across seasons in both 2022 and 2023, these differences should be interpreted with caution due to the considerable variability in initial body weights, the unknown and likely differing ages of the animals, and the unknown sex distribution within groups. Pigs in group A reached the highest average body weight among all groups in the final (fourth) measurement.

In 2022, the greatest ADG in group A occurred in the third measurement, whereas the greatest ADG was observed in the fourth measurement. A statistically significant difference between the mean body weights of groups A and C was detected only in the third measurement ($p=0.015$), where pigs in group A had significantly higher average body weights. In 2023, a different growth pattern emerged: ADG generally increased across the measurement periods, with the most substantial growth occurring between the third and fourth measurements.

Statistically significant differences between the groups were found in all measurement periods in 2023, with pigs in group A consistently exhibiting higher average body weights than those in group C. Nonetheless, these outcomes should be viewed in the context of the study's limitations, including the lack of data on the animals' exact ages and sexes, as well as the initial variability in body weight.

In 2023, FCR corresponded with ADG in the individual measurements; the FCR values were lowest when ADG were highest. Lower FCR values indicate better conversion of feed into body tissue (30). This was not the case in 2022. This could be explained by animals being sent to slaughter, meaning less animals were able to consume feed. Normally, pigs undergo rapid growth in the early stages, until reaching a maximum. At higher weights, growth rate declines as pigs are reaching maturity (S-shaped growth curve) (31). Different trends in growth in 2022 and 2023 could be explained by the fact that the individual measurements were not carried out at the exact same time in both years. In group B, both seasonal body weights were noticeably lower than in groups A and C. This was likely due to the fact, that pigs in group B were fed twice a day, whereas pigs in groups A and C were fed *ad libitum*. This would have allowed pigs in groups A and C prolonged access to feed, resulting in greater body weights and weight gains compared to pigs in group B. In all measurements, there was a rather large range in body weight within every pig group. The reason for this was likely that individual animals spent more time feeding than others; there could also have been some pathogens present in the herd (e.g., porcine circovirus 2), which could decrease growth performance, or it could be related to physiological differences between individual animals. At the start of the study, pigs were not of equal body weight, and those with smaller initial weights normally did not grow as fast as their peers. Pigs in groups A and B were reared outdoors and were thus able to express their natural behaviour. Pigs under natural conditions spend up to 75% of their daily activity engaged in rooting and foraging (32), which means they likely spent more time searching for food and could therefore ingest extra food in addition to the feed they were given daily. Expression of natural behaviour could be one of the reasons that pigs in group A reached larger body weights than their indoor peers. Some studies have shown that adding vitamin D_3 to the feed impacts production parameters by increasing body weight and weight gain in pigs (33) and broilers (34). Pigs in our study received no dietary supplement of vitamin D; however, pigs in group A also had higher serum vitamin D concentrations than group C. Even though pigs in group A showed better production parameters (e.g., reaching larger weights and having lower FCR), this study cannot directly confirm that pigs from group A exhibited better production parameters due to higher serum vitamin D levels, but it is a question that should definitely be investigated further.

Our study is not the first to evaluate growth parameters in Krškopolje pigs. In 2017, Tomažin et al. (35) compared Krškopolje pigs reared under extensive and intensive conditions. Contrary to our findings, they reported that Krškopolje pigs reared under intensive conditions exhibited significantly higher growth rates and reached heavier slaughter weight (120 kg) compared to pigs reared under extensive conditions (88 kg). It is worth noting, however, that intensively reared pigs in that study were fed a complete feed mixture, whereas extensively reared pigs were only fed

traditional cooked feed with some ground grains. Another study from 2024, Škrlep et al. (36) compared Krškopolje pigs with modern hybrid breeds. Krškopolje pigs showed slower growth rates compared to modern breeds, but were, interestingly, less affected by reductions of dietary protein levels, indicating lower protein requirement and better adaptability.

Throughout the study, the Krškopolje pigs were exposed to challenging environmental conditions, as well as the rugged Karst terrain, and yet they showed excellent health status, good serum vitamin D concentrations, adequate feed conversion, and good growth. For this reason, the Krškopolje pigs can be described as "robust". The term "robustness" was defined by Knap (37) as the ability to combine high production potential with resilience to stress factors, allowing for expression of high production potential under a variety of environmental conditions. Krškopolje pigs owe their robustness to the modest environmental conditions in which they were historically reared. Of course, their production parameters are not comparable to those of intensive pork production, but their resilience and robustness make them well-suited for organic pig farming.

Conclusion

We reported total serum vitamin D concentrations in 109 grower-to-finisher pigs reared outdoors and indoors in organic pig farms. Sampling was performed once every season in 2022 and 2023. Serum vitamin D concentrations in outdoor pigs were highest in summer and lowest in winter. Values in both outdoor groups showed high individual variation. When evaluating the effects of altitude on serum vitamin D concentrations, we concluded that altitude did not significantly affect serum vitamin D concentrations in either group of outdoor pigs in any season, except winter. We concluded that serum vitamin D levels were significantly higher in outdoor pigs than in indoor pigs. Reference intervals calculated in this study could serve as reference levels of total serum vitamin D for outdoor and indoor organic grower-to-finisher pigs. Outdoor pigs in group A tended to achieve higher final body weights compared to indoor pigs in group C; however, this apparent difference in growth performance should be interpreted with caution due to considerable variability in initial body weights, unknown ages, and unrecorded sex distribution among the animals. These findings highlight the benefits of outdoor rearing for vitamin D status and growth performance in pigs.

Acknowledgements

We would like to thank the Slovenian Ministry of Agriculture, Forestry and Food and the Slovenian Research Agency for providing financial support for the study. We wish to express our gratitude to Jan Plut, farm personnel, farm owners and veterinary students for their help in conducting this study.

Funding. This work was supported by the European Union under the ERA-NET CORE Organic project Robust Animals in sustainable Mixed FREE-range systems and the Slovenian Research and Innovation Agency (ARIS) under the research programmes P4-0092 – animal health, environment, and food safety.

Conflict of Interests. The authors declare no conflicts of interest.

References

1. Lips P. Vitamin D physiology. Prog Biophys Mol Biol 2006; 92: 4–8. doi: 10.1016/j.pbiomolbio.2006.02.016
2. Janoušek J, Pilařová V, Macáková K, et al. Vitamin D: sources, physiological role, biokinetics, deficiency, therapeutic use, toxicity, and overview of analytical methods for detection of vitamin D and its metabolites. Crit Rev Clin Lab Sci 2022; 59: 517–54. doi: 10.1080/10408363.2022.2070595
3. Jakobsen SS, Jakobsen J, Nielsen JP. Vitamin D Levels in Sows from Five Danish Outdoor Herds. Animals (Basel) 2022; 12: 299. doi: 10.3390/ ani12030299
4. Bikle DD. Vitamin D metabolism, mechanism of action, and clinical applications. Chem Biol 2014; 21: 319–29. doi: 10.1016/ j.chembiol.2013.12.016
5. Schutkowski A, Krämer J, Kluge H, et al. UVB exposure of farm animals: study on a food-based strategy to bridge the gap between current vitamin D intakes and dietary targets. PLoS One 2013; 8: e69418. doi: 10.1371/journal. pone.0069418.
6. Casas E, Lippolis JD, Kuehn LA, Reinhardt TA. Seasonal variation in vitamin D status of beef cattle reared in the central United States. Domest Anim Endocrinol 2015; 52: 71–4. doi: 10.1016/j. domaniend.2015.03. 003
7. Madson DM, Ensley SM, Gauger PC, et al. Rickets: case series and diagnostic review of hypovitaminosis D in swine. J Vet Diagn Invest 2012; 24: 1137–44. 10.1177/1040638712461487.
8. Arnold J, Madson D, Ensley S, et al. Survey of serum Vitamin D status across stages of swine production and evaluation of supplemental bulk Vitamin D premixes used in swine diets. J Swine Health Prod 2015; 23: 28–34. doi: 10.54846/jshap/862
9. Madson D, Goff J. Vitamin D deficiency syndromes in swine. Ripoll: pig 33.com. https://www.pig333.com/articles/vitamin-d-deficiency-syndromes-in-swine-i_5470/ (1. 8. 2024).
10. Yang P, Ma Y. Recent advances of vitamin D in immune, reproduction, performance for pig: a review. Anim Health Res Rev 2021; 22: 85–5. doi: 10.1017/S1466252321000049.
11. Zhang Z, Zhang G, Cao J, Qiu B, Qin X, Zhao J. Effects of 25(OH)VD_3 on Growth performance, pork quality and calcium deposit in growing-finishing pigs. Animals (Basel) 2022; 13: 86. doi: 10.3390/ani13010086
12. Hasan M, Oster M, Reyer H, Wimmers K, Fischer DC. Efficacy of dietary vitamin D_3 and 25(OH)D_3 on reproductive capacities, growth performance, immunity and bone development in pigs. Br J Nutr 2023; 130: 1298–307. doi: 10.1017/S0007114523000442.
13. NIH. Vitamin D. Rockledge: National Institutes of Health, 2024. https://ods.od.nih.gov/factsheets/VitaminD-HealthProfessional/ (14. 6. 2024).

14. DSM-Firmenich. VitaminD deficiency in Swine. https://www.dsm.com/anh/news/feed-talks/articles/vitamin-d-deficiency-in-swine.html (1. 8. 2024).

15. Statistical Office of the Republic of Slovenia. The number of pigs continues to decline. 2024. https://www.stat.si/StatWeb/en/News/Index/ 12676 (14. 6. 2024).

16. Ministry of Agriculture, Forestry and Food, 2022. Data on organic pig farms and number of pigs on farms was obtained upon request from the Ministry of Agriculture, Forestry and Food of the Republic of Slovenia.

17. Malovrh Š, Kovač M. Pasma krškopoljski prašič. Ljubljana: Biotehniška fakulteta, 2015. https://agri.bf.uni-lj.si/Enota/html/revija/KP/KP_01.pdf (29. 6. 2024).

18. Ministary of natural resources and spatial planing. Access to geodetic data. Ljubljana: MNRSP, 2024. https://www.e-prostor.gov.si/en/access-to-geodetic-data/ (13. 6. 2024).

19. The European Parliament. Regulation (EU) 2018/848 of the European Parliament and of the Council of 30 May 2018 on organic production and labelling of organic products and repealing Council Regulation (EC) No 834/2007. Off J Eur Union 2018; L150: 1–92. https://eur-lex.europa.eu/legal-content/EN/TXT/PDF/?uri=CELEX:32018R0848

20. Official Gazette of the Republic of Slovenia. Rules on the protection of farm animals. The Official Gazette of the Republic of Slovenia: Ljubljana, Slovenia, 2010.

21. Official Gazette of the Republic of Slovenia. Order on monitoring of animal health status, animal disease eradication programmes and vaccinations of animals in 2023. The Official Gazette of the Republic of Slovenia: Ljubljana, Slovenia, 2023.

22. The Pig Site. Weighing a Pig Without a Scale. 2002. Available online: https://www.thepigsite.com/articles/weighing-a-pig-without-a-scale (accessed on 6 August 2024).

23. Ammer T, Schützenmeister A, Prokosch HU, Rauh M, Rank CM, Zierk J. refineR: a novel algorithm for reference interval estimation from real-world data. Sci Rep 2021; 11: 16023. doi: 10.1038/s41598-021-95301-2

24. Tripkovic L, Lambert H, Hart K, et al. Comparison of vitamin D_2 and vitamin D_3 supplementation in raising serum 25-hydroxyvitamin D status: a systematic review and meta-analysis. Am J Clin Nutr 2012; 95: 1357–64. doi: 10.3945/ajcn.111.031070

25. Mendes MM, Darling AL, Hart KH, Morse S, Murphy RJ, Lanham-New SA. Impact of high latitude, urban living and ethnicity on 25-hydroxyvitamin D status: a need for multidisciplinary action? J Steroid Biochem Mol Biol 2019; 188: 95–102. doi: 10.1016/j.jsbmb.2018.12.012

26. Clemens TL, Adams JS, Henderson SL, Holick MF. Increased skin pigment reduces the capacity of skin to synthesise vitamin D_3. Lancet 1982; 1: 74–6. doi: 10.1016/S0140-6736(82)90214-8

27. Shoenfeld N, Amital H, Shoenfeld Y. The effect of melanism and vitamin D synthesis on the incidence of autoimmune disease. Nat Clin Pract Rheumatol 2009; 5: 99–105. doi: 10.1038/ncprheum0989

28. Kohler M, Leiber F, Willems H, Merbold L, Liesegang A. Influence of altitude on vitamin D and bone metabolism of lactating sheep and goats. J Anim Sci 2013; 91: 5259–68. doi: 10.2527/jas.2013–6702

29. Larson-Meyer DE, Ingold BC, Fensterseifer SR, et al. Sun exposure in pigs increases the vitamin D nutritional quality of pork. PLoS One 2017; 12: e0187877. doi: 10.1371/journal.pone.0187877

30. Pig333.com. Feed conversion ratio. Ripoll: Pig333, 2024. https://www.pig333.com/pig-glossary/F/feed-conversion-ratio-fcr_147/ (1. 8. 2024).

31. Kansas State University. Establishing phase feeding programs and feed budgets. Manhattan: Kansas State Univerity, 2022. https://www.asi.kstate.edu/extension/swine/swinenutritionguide/growfinish/useGF3_EstablishingPhaseFeedingProgramsFeedBudgets_Final.pdf (6. 9. 2024).

32. Humane Society of the United States. About Pigs. Washington: Humane World for Animals, 2015. https://www.humanesociety.org/sites/default/files/docs/about-pigs.pdf (8. 9. 2024).

33. Zhou X, Wang L, Zhang Z, et al. 25-Hydroxyvitamin D_3 improved growth performance, bone characteristics and polyunsaturated fatty acid deposition by activating calcium ion channel proteins expression in growing pigs. J Funct Foods 2023; 105: 105581. doi: 10.1016/j.jff.2023.105581

34. Wei J, Li L, Peng Y, et al. The effects of optimal dietary vitamin D_3 on growth and carcass performance, tibia traits, meat quality, and intestinal morphology of chinese, yellow-feathered broiler chickens. Animals 2024; 14: 920. doi: 10.3390/ani14060920

35. Tomažin U, Škrlep M, Batorek Lukač N, Prevolnik Povše M, Čandek-Potokar M. Performance of Krškopolje pigs in extensive and intensive production systems. Agriculturae Conspectus Scientificus 2017; 82 (3): 211–5. https://hrcak.srce.hr/191827

36. Škrlep M, Poklukar K, Vrecl M, Brankovič J, Čandek-Potokar M. Growth performance, carcass quality, and lipid metabolism in krškopolje pigs and modern hybrid pigs: comparison of genotypes and evaluation of dietary protein reduction. Animals 2024; 14(22): 3331. doi: 10.3390/ani14223331

37. Knap P. Breeding robust pigs. Aust J Exp Agric 2005; 45: 763–73. doi: 10.1071/EA05041

Ocena sezonskih ravni vitamina D v serumu in rastne zmogljivosti pri prašičih z ekoloških kmetij

T. Šteferl, M. Hajdinjak, E. Nadlučnik, I. Golinar Oven, M. Štukelj, O. Podpečan

Izvleček: Vitamin D je bistveno mikrohranilo v prašičereji, saj ima pomembno vlogo pri številnih fizioloških funkcijah. Cilj študije je bil določiti koncentracijo vitamina D v serumu in rastno zmogljivost prašičev, vzrejenih na ekoloških kmetijah v različnih letnih časih. Za študijo je bilo izbranih skupaj 109 prašičev krškopoljske pasme. Prašiči so bili razdeljeni v tri skupine: skupino A na nizki nadmorski višini na prostem (N = 39), skupino B na visoki nadmorski višini na prostem (N = 36) in skupino C v hlevu (N = 34). Vzorci krvi in telesne mase so bili odvzeti sezonsko v letih 2022 in 2023. Raven vitamina D v serumu je bila najvišja poleti za skupini A (69,3 ± 2,6 ng/ml) in B (65,3 ± 4,4 ng/ml), ki sta bili na prostem, najnižja pa pozimi (skupina A 21,5 ± 2,2, skupina B 35,2 ± 2,5). Nadmorska višina ni imela pomembnega vpliva na raven vitamina D, razen pozimi ($p < 0,001$). Vrsta hlevov je pomembno vplivala na ravni vitamina D v vseh letnih časih med skupinama B in C ter spomladi, poleti in jeseni med skupinama A in C. Prašiči v skupini A, ki so bili na prostem, so imeli višjo povprečno končno telesno maso (151,2 ±7,5 kg v letu 2022 in 146,8 ±3,8 kg v letu 2023) kot prašiči v skupini C (132,7 ±11,3 kg in 118,5 ±6,9 kg), čeprav je to treba razlagati previdno, glede na spremenljivost začetnih mas.

Ključne besede: vitamin D; koncentracije v serumu; dobrobit prašičev; ekološka kmetija; rast

Slov Vet Res
DOI 10.26873/SVR-2205-2025
UDC 599.723.12:57.082.14:616.728:591.476:543.442
Pages: 157–68

Original Research Article

New Insights Into the Horse Stifle Joint Through 3D Computed Tomography, Scanning Electron Microscopy, and Scanning Electron Microscopy-Energy Dispersive X-ray Analysis

Key words

horse;
stifle;
3D CT;
sectional anatomy;
SEM;
SEM-EDX

Mohamed A. M. Alsafy[1]*, Ahmed K. S. El-Garhy[2], Ismail Abo-Ghanima[3], Ahmed G. Nomir[2], Samir A. A. El-Gendy[1]

[1]Anatomy and Embryology Department, Faculty of Veterinary Medicine, Alexandria University, Abis 10th P.O. 21944, Alexandria, [2]Department of Anatomy and Embryology, [3]Department of Physiology, Faculty of Veterinary Medicine, Damanhour University, Damanhour 22511, Egypt

***Corresponding author:** mohamed.alsafy@alexu.edu.eg

Abstract: The study design was prospective and descriptive of the horse stifle joint using CT, sectional anatomy, SEM, and EDX analysis. The 3D rendered-volume reconstruction CT of the horse's stifle joint allows good visualization of the large and small bony structures and ligaments, or menisci. In addition to the sagittal CT section and subsequent CT bone window cross sections, which provided detailed images of bone structures, ligaments, and muscles, the sectional CT was matched with cross and sagittal anatomical sections. The horse's stifle joint is described using SEM and EDX analysis. The synovial membrane had varied synovial villi in length and shape: long and short tongue shapes with different tip shapes and dome-shaped, in addition to single or branched folds. The scratched surface revealed a network of collagen fibers arranged in various directions, layers, and deep synoviocytes. SEM-EDX Spectra identified the following items in the stifle joint's meniscus and ligaments: The sample contained carbon, oxygen, nitrogen, sulfur, calcium, and phosphorus, with selenium replaced by sulfur at the meniscus. Four specimens were examined to determine their carbon and oxygen percentages. Calcium and phosphorus levels were measured, with the highest concentrations in the meniscus and the lowest in the collateral and patellar ligaments. The percentage of sulfur was determined, and ligaments had a higher percentage than menisci, particularly at the cruciate ligaments, whereas menisci contained silicon. Knowledge of the stifle joint's macro- and microscopic normal anatomy obtained through 3D CT, SEM, and EDX is a good guide and reference for determining the horse stifle's bony and soft tissue structures and microstructures, as well as the chemical structure of the synovial membrane, ligaments, and menisci.

Received: 3 March 2025
Accepted: 6 April 2025

Introduction

The stifle is a condylar synovial joint. It is a compound joint in structure and function (1, 2). Ligaments are tough, fibrous con-nective tissues that connect bones and provide support while limiting excessive movement. They are essential for maintaining the stability, integrity, and proper alignment of the stifle joint (3). The stifle's primary stabilizers are the cranial and caudal cruciate ligaments, which limit cranial translation and rotation of the tibia (4, 5).

The stifle joint affection is a significant cause of lameness in horse's hind limb (6, 7, 8). Because of their clinical significance, anatomically normal and pathologically altered stifle joints have been extensively studied using radiography

and ultrasonography (9, 10). Horses frequently experience hindlimb lameness and, stifle injuries are among the leading causes of this ailment (11, 12). The stifle joint, a major weight-bearing joint in the horse's hindlimb, is vulnerable to various soft tissue and ligament injuries (11). Stifle joint clinical problems usually necessitate surgical intervention in case of meniscal tears, patellar dislocation, frac-tures, and ligament sprains (13). However, appropriately diagnos-ing these specific stifle injuries remains a significant difficulty for equine veterinarians (7, 14, 15).

Computed tomography (CT) is an effective technique for produc-ing good sectional anatomical images with no superimposition of structures (16, 17). Furthermore, three-dimensional CT (3D-CT) is an effective diagnostic tool for determining the osseous anatomi-cal structures and distinguishing ligaments (18, 19, 20, 21).

Scanning electron microscopy was widely used to determine the structures and whole cell shapes of the synovial membrane and synoviocytes of an equine's joint capsule (22, 23). Although nu-merous reviews have detailed their structure, molecular composi-tion, and biomechanical properties, little attention has been paid to their trace element content (24, 25, 26). The synovial mem-brane consisted of a connective tissue layer lined by synovial cells on the surface facing the articular cavity, with two types of syno-viocytes (27). Ligaments and tendons were the main structures that promoted joint movement and stability (28). The presence of trace elements is related to their molecular composition and biomechanical properties (29). Ligaments and tendons were primarily rich in calcium, sulfur, and phosphorus, though notable differences existed between tendons and ligaments (26, 28).

The stifle joint was the largest and most compound joint in the limbs. The anatomical description of its structure has been re-ported using many detailed techniques in previously published articles, such as anatomical description, computed tomography, ultrasound, and MRI (18, 30, 31, 32, 33, 34, 35, 36).

The current study primarily focused on 3D CT reconstruction, scanning electron microscopy of synovial villi, and comparing the composition of trace minerals in various ligaments and menisci of the stifle joint in horses.

Materials and methods

Samples

Four adult horses were euthanized for other reasons unrelated to this study; the horses are owned and have been provided for teaching in the Department of Anatomy and Embryology. Horses were given a subcutaneous injection of 2 ampoules of the antico-agulant CLEXAN 20 and intravenously injected with 3 liters of sodium chloride solution to aid in thorough bleeding. Euthanasia was undertaken under general anesthesia by veterinary sur-geons via intravenous injection of 10 mg/kg thiopental sodium (EPICO, Egypt) after premedication with 1 mg/kg xylazine hydro-chloride (Xylaject; Egypt). Following euthanasia, the animals bled from the common carotid artery. All hindlimbs were disarticulat-ed at the hip joint.

Computed tomography (CT)

Four fresh hind limbs from horses underwent computed tomog-raphy 45 minutes after death. The stifle joint was scanned using a Toshiba Asteion CT scanner, four slices, 2003. The distance between the slices taken was 0.5 cm, with a voltage range of 100 kV and 200 mA. 3D reconstruction from the transverse and sagit-tal computed tomography (37, 38); in the end, all images were stacked together sequentially to obtain a 3D image model of the inspected object. The reconstruction algorithm was done with Octopus software and converted to digital imaging and commu-nications in medicine (DICOM format) (19, 39, 40, 41).

Cadaver gross sections

Four fresh hind limbs from adult horses were tightly placed in adhesive tape to prevent air entrapment and distal slippage of soft tissue structures. The freshly collected limbs were frozen (-12°C) for two days. After preservation, using an electric wood tray saw, the frozen hind limbs were carefully sliced (one limb cut transverse and one limb cut sagittal) at the stifle joint region. The slices were cut to a uniform thickness of 2 cm. Each slice was assigned a number for identification purposes. The slices were gently cleaned of debris with water and a light brushing. The cleaned slices were then promptly photographed. These slices were imaged using a Canon EOS 700D digital camera and matched with the correlated CT images (21, 23, 42).

Scanning electron microscopy (SEM)

Two horses (4 fresh hind limbs from adult horses aged 10 years old) were used to collect samples for SEM from both right and left limbs. The samples from the synovial membrane were fixed in a solution containing glutaraldehyde, formaldehyde, and sodium cacodylate (43, 44). Subsequently, they were rinsed in a sodium cacodylate solution with sucrose, treated with tannic acid, and dehydrated gradually using increasingly concentrated ethanol solutions. Afterward, the samples were desiccated with carbon dioxide, affixed to mounts, and coated with a gold-palladium mixture. The prepared samples were imaged using a JEOL JSM-IT200 SEM (45, 46, 47).

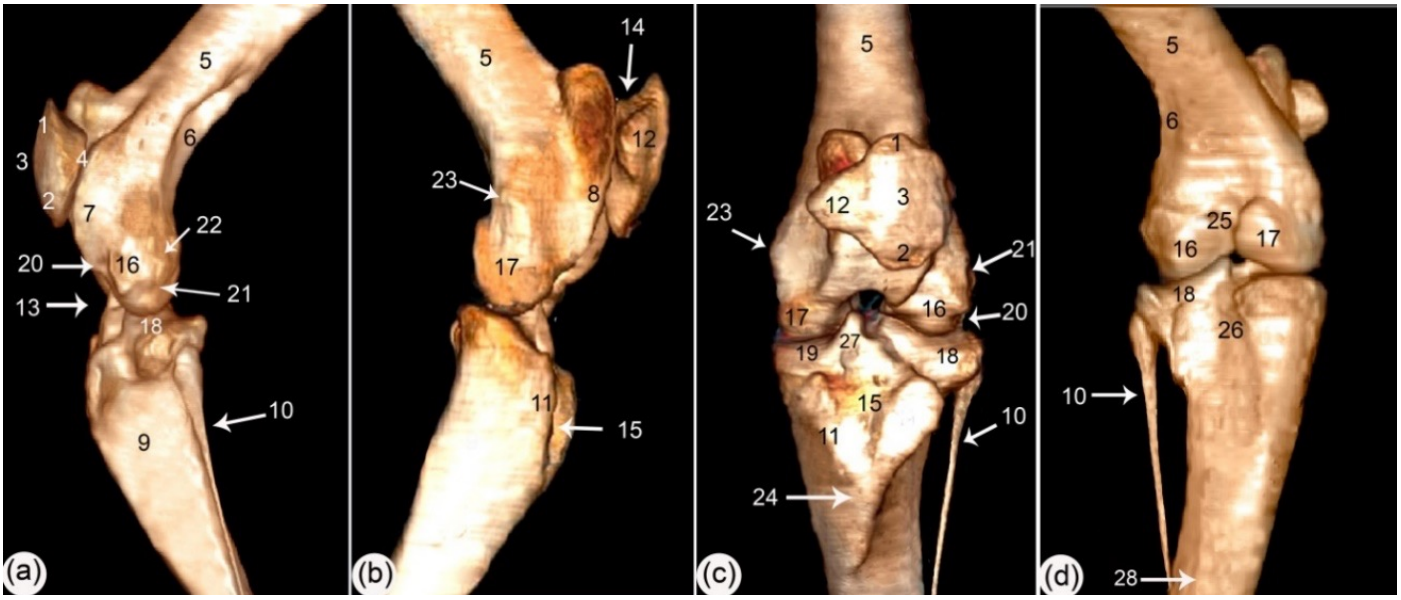

Figure 1: 3D render volume reconstruction of CT of the stifle joint bony structures. (a) lateral view. (b) medial view. (c) cranial view. (d) caudal view

1. base of the patella (*Basis patellae*); 2. apex of the patella (*Apex patellae*); 3. cranial face (*Facies cranialis*); 4. articular surface (*Facies articu-laris*); 5. Femur (*Os femoris*); 6. supracondylar fossa (*Fossa supracondylaris*); 7. lateral trochlear ridge; 8. medial trochlear ridge; 9. Tibia; 10. fibula; 11. tibial tuberosity (*Tuberositas tibiae*); 12-medial angle of patella; 13. femorotibial joint; 14. femoropatellar joint; 15-tibial sulcus (*Sulcus tuberositatis tibiae*); 16. lateral femoral condyle (*Condylus lateralis*); 17. medial femoral condyle (*Condylus medialis*); 18. lateral tibial condyle (*Tibial condylus lateralis*); 19. medial tibial condyle (*Tibial condylus medialis*); 20. extensor fossa (*Fossa extensoria*); 21. popliteal fossa (*Fossa m. poplitei*); 22. lateral epicondyle (*Epicondylus lateralis*); 23. medial epicondyle (*Epicondylus medialis*); 24. tibial crest; 25. intercondyloid fossa (*Fossa intercondylaris*); 26. popliteal notch (*Incisura poplitea*); 27. intercondyloid eminence (*Emi-nentia intercondylaris*); 28. popliteal lines (*Linea m. poplitei*).

Scanning electron microscopy-Energy Dispersive X-Ray Analysis (SEM-EDX)

The patellar ligament, collateral ligament, cruciate ligament, and menisci samples were analyzed and photographed with a JEOL JSM-IT200 scanning electron microscope at 20 kV. The quantification method was ZAF analysis. The sample distance from the detector was 10 mm, the real-time was 30.97 seconds, and the dead time was 3.00% (48, 49, 50). The EDX spectrometer was created at the Science Faculty, Alexandria University, Egypt.

Results

Computed tomography and sectional anatomy of the horse's stifle joint

The 3D rendered-volume reconstruction of the horse's stifle joint produced numerous images at 360 degrees, allowing for good visualization of the large and small bony structures, ligaments, and menisci (Figs. 1, 2). In addition to the sagittal CT section and subsequent CT bone window cross sections, which provided de-tailed images of the bones, the sectional CT was matched with cross and sagittal anatomical sections. Images revealed all bone structures, including the femur's distal diaphysis, condyles, trochlear ridges, intercondyloid fossa (*fossa intercondylaris*), extensor fossa (*fossa extensoria*), popliteal fossa (*fossa m. poplitei*), patel-la, tibial intercondylar eminence (*eminentia intercondylaris*), tibial tuberosity (*tuberositas tibiae*) (Figs. 3,

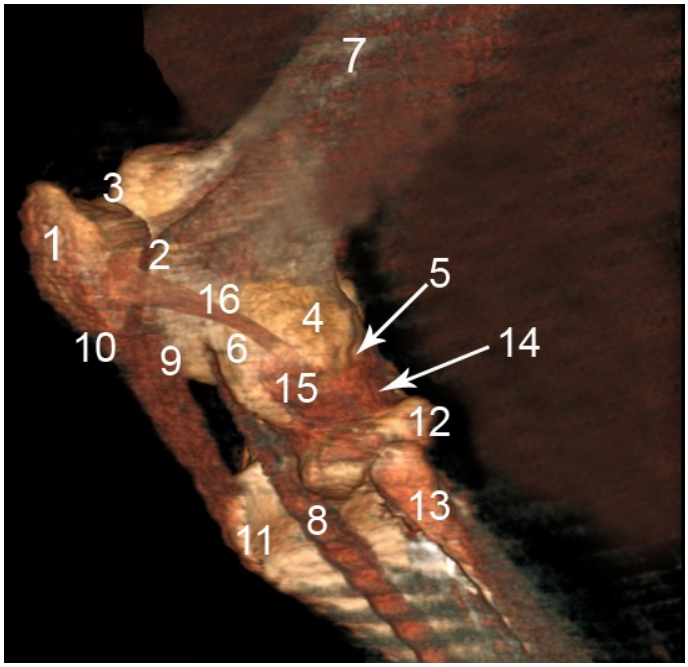

Figure 2: 3D render volume reconstruction of CT, lateral view, explains the details of the stifle joint

patella; 2. lateral trochlear ridge; 3. medial trochlear ridge; 4. lateral epicondyle (*Epicondylus lateralis*); 5. popliteal fossa (*Fossa m. pop-litei*); 6. extensor fossa (*Fossa extensoria*); 7. femur shaft (*Corpus ossis femoris*); 8. long digital extensor muscle (*Extensor digitorum longus*); 9. lateral patellar ligament (*Lig. patellae laterale*); 10. middle patellar ligament (*Lig. patellae intermedium*); 11. tibial tuberosity (*Tuberositas tibiae*); 12. lateral condyle of tibia (*Condylus medialis*); 13. fibula; 14. lateral meniscus (*Meniscus lateralis*); 15. lateral collat-eral ligament (*Lig. collaterale laterale*); 16. lateral femoropatellar ligament (*Lig. femoropatellare laterale*)

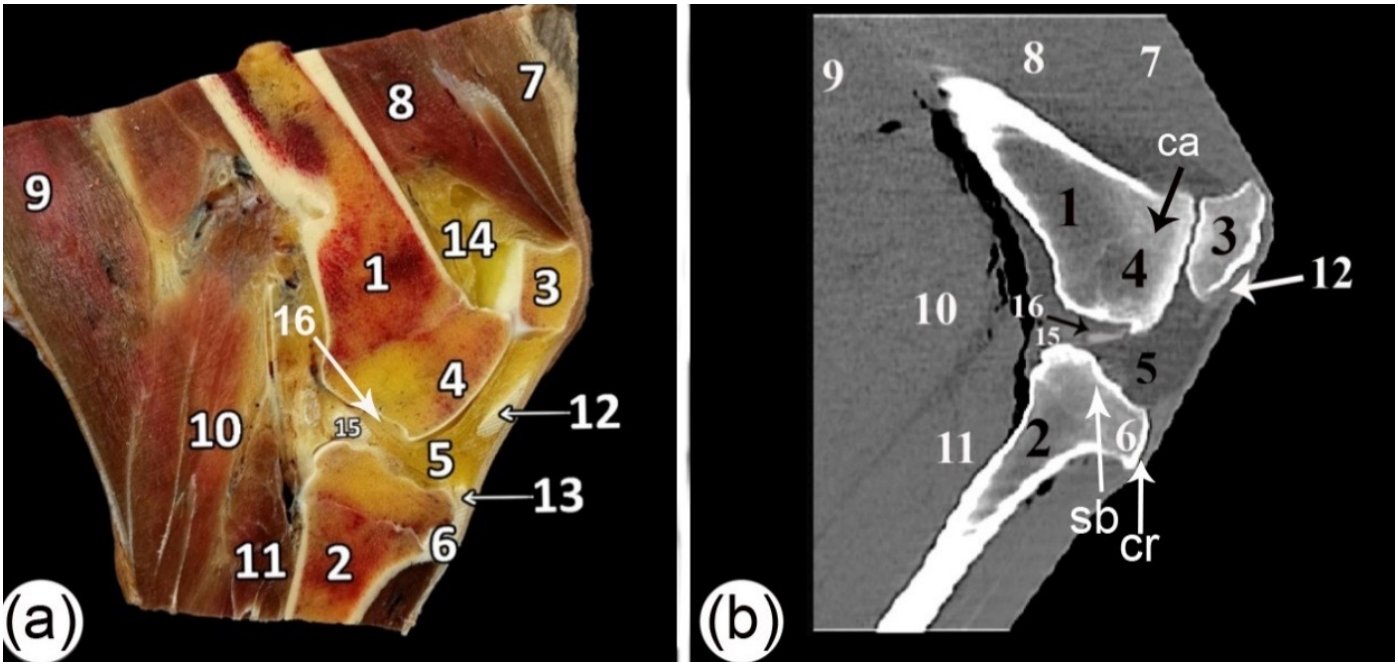

Figure 3: Sagittal sections of the stifle joint at the midline; (a) cadaver section; (b) CT scan

1. Femur (*Os femoris*); 2. tibia; 3. patella; 4. lateral ridge of the trochlear of the femur; 5. infra-patellar fat pad; 6.tibial tuberosity (*Tuberositas tibiae*); 7.rectus femoris muscle (*M. rectus femoris*); 8.vastus lateralis muscle (*M. vastus lateralis*); 9.semimembranosus muscle (*M. semi-membranosus*); 10. Lateral head of gastrocnemius muscle (*Gastrocnemius caput laterale*); 11. superficial digital flexor muscle (*M. flexor digi-torum superficialis*); 12. middle patellar ligament (*Lig. patellae intermedium*); 13. medial patellar ligament (*Lig. patellae mediale*); 14. lateral recess of the femorotibial joint; 15. caudal horn of the lateral meniscus; 16. caudal cruciate ligament (*Lig. cruciatum caudale*); (cr) cortical bone; (ca) cancellous bone (sb); subchondral bone.

4, 5, 6, 7). The infrapatellar fat pad, three patellar ligaments (*lig. patellae*), the origin of the tendinous portions of the long digital extensor muscle (*extensor digitorum longus*), and the collateral ligaments (*lig. collaterale laterale* and *lig. collaterale mediale*) of the femorotibial and fem-oropatellar joints (*articulatio femorotibialis* and *articulatio fem-oropatellaris*) were examined. The tendinous part of the popliteus muscle (*m. popliteus*), the cranial and caudal cruciate ligaments (*lig. cruciatum craniale* and *lig. cruciatum caudale*), and the me-niscotibial ligaments (*lig. meniscotibiale*) (Figs. 2, 3, 4, 5, 6, 7). In addition to explaining the patterns of the cortical, cancellous, and subchondral bones (Fig. 3).

SEM of the horse's stifle joint synovial membrane

The synovial membrane was covered with closely arranged syn-ovial villi (Fig. 8a). The villi varied in length and were classified as either long or short; the longer villi had smooth tips. The short ones had a slight wavy serration, but the surface of some villi was folded. We observed several different shapes of synovial villi, including a long tongue-like shape with a round end and a short circular and short tongue shape. Other areas of the synovial membrane's surface had folded synovial membrane; the folds were either single or branched (Fig. 8b). The synovial villi surface has a bubbling dome structure with dome-shaped synoviocytes, as well as a rough surface with microridges and pores (Fig. 8c, d). The scratched surface revealed the presence of a network of collagen fibers in various directions and layers, as well as visible deep synoviocytes (Fig. 9a, b, c, d).

SEM-EDX

The micro-elemental image of the menisci, patellar ligaments, cruciate ligament, and collateral ligament was obtained from the photon energy dispersive X-ray spectra of four specimens from two horses. EDX spectra identified the element by mass% and atom% (Figs. 10, 11, 12, 13; Table 1). We used a mass percent-age, and the EDX spectra recognized and detected the following: At our work, the SEM-EDX spectra identified the following items: menisci and various stifle joint ligaments. Carbon, oxygen, nitro-gen, sulfur, calcium, phosphorus, and silicon were replaced by sulfur in one sample of the meniscus. The calcium and phospho-rus percentages were calculated, with the menisci having the highest and the collateral and patellar ligaments having the low-est. The percentage of sulfur was higher in the ligaments than in the menisci, especially in the cruciate ligaments. The percentages of carbon and oxygen were approximately determined at four specimens and ranged from 38.7 to 42.9%, with the highest level at the menisci. Additionally, the percentages of oxygen were closely ranged from 32.6% to 36.3%, with the highest level at the cruciate ligaments. Nitrogen percentage had a higher mean at the patellar ligament.

Discussion

In our investigation, we used 3D render volume reconstruction CT of the horse's stifle joint bones, which

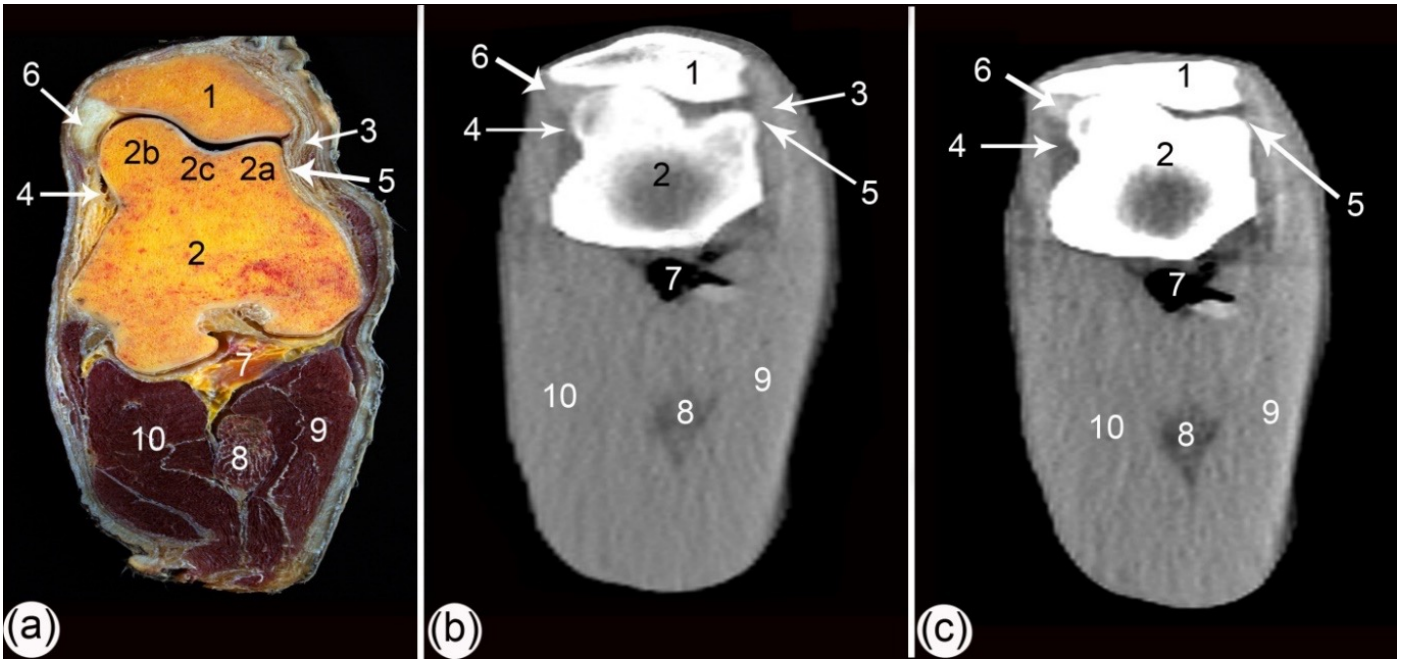

Figure 4: Cross-sections of the stifle joint proximal to the apex of the patella; (a) cadaver section; (b & c) CT scans

1. patella; 2. Femur (*Os femoris*); 2a. medial trochlear ridge; 2b. Lateral trochlear ridge; 2c. The groove of the femoral trochlear; 3. medial patellar ligament (*Lig. patellae mediale*); 4. lateral recess of femoropatellar joint; 5. medial recess of femoropatellar joint; 6. lateral patellar ligament (*Lig. collaterale laterale*); 7. joint capsule (caudal recess); 8. superficial digital flexor muscle (*M. flexor digitorum superficialis*); 9. medial head of the gastrocnemius muscle (*Gastrocnemius caput mediale*); 10. lateral head of the gastrocnemius muscle (*Gastrocnemius caput laterale*)

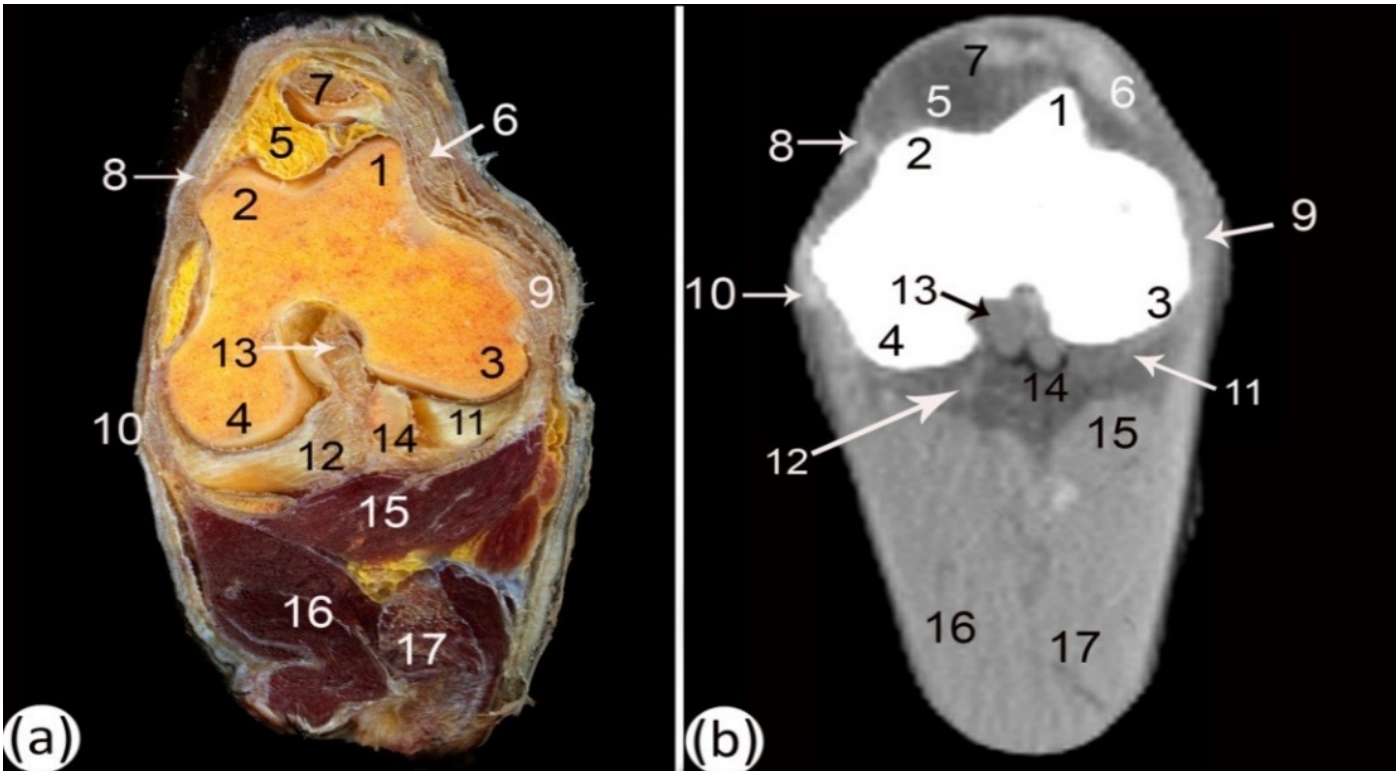

Figure 5: Cross-sections of the stifle joint through the femur intercondylar fossa; (a) cadaver section; (b) CT scan

1. medial ridge of the femoral trochlear; 2. lateral ridge of the femoral trochlear; 3. medial femoral condyle (*Condylus medialis*); 4. lateral femo-ral condyle (*Condylus lateralis*); 5. infra-patellar fat pad; 6. medial patellar ligament (*Lig. patellae mediale*); 7. middle patellar ligament (*Lig. patellae intermedium*); 8. lateral patellar ligament (*Lig. patellae laterale*); 9. medial collateral ligament (*Lig. collaterale mediale*); 10. lateral col-lateral ligament (*Lig. collaterale laterale*); 11. medial menisci (*Meniscus medialis*) 12. meniscofemoral ligament (*Lig. meniscofemorale*); 13. cranial cruciate ligament (*Lig. cruciatum craniale*); 14. caudal cruciate ligament (*Lig. cruciatum caudale*); 15. popliteus muscle (*M. popliteus*); 16. gastrocnemius muscle (*M. gastrocnemius*); 17. superficial digital flexor muscle (*M. flexor digitorum superficialis*)

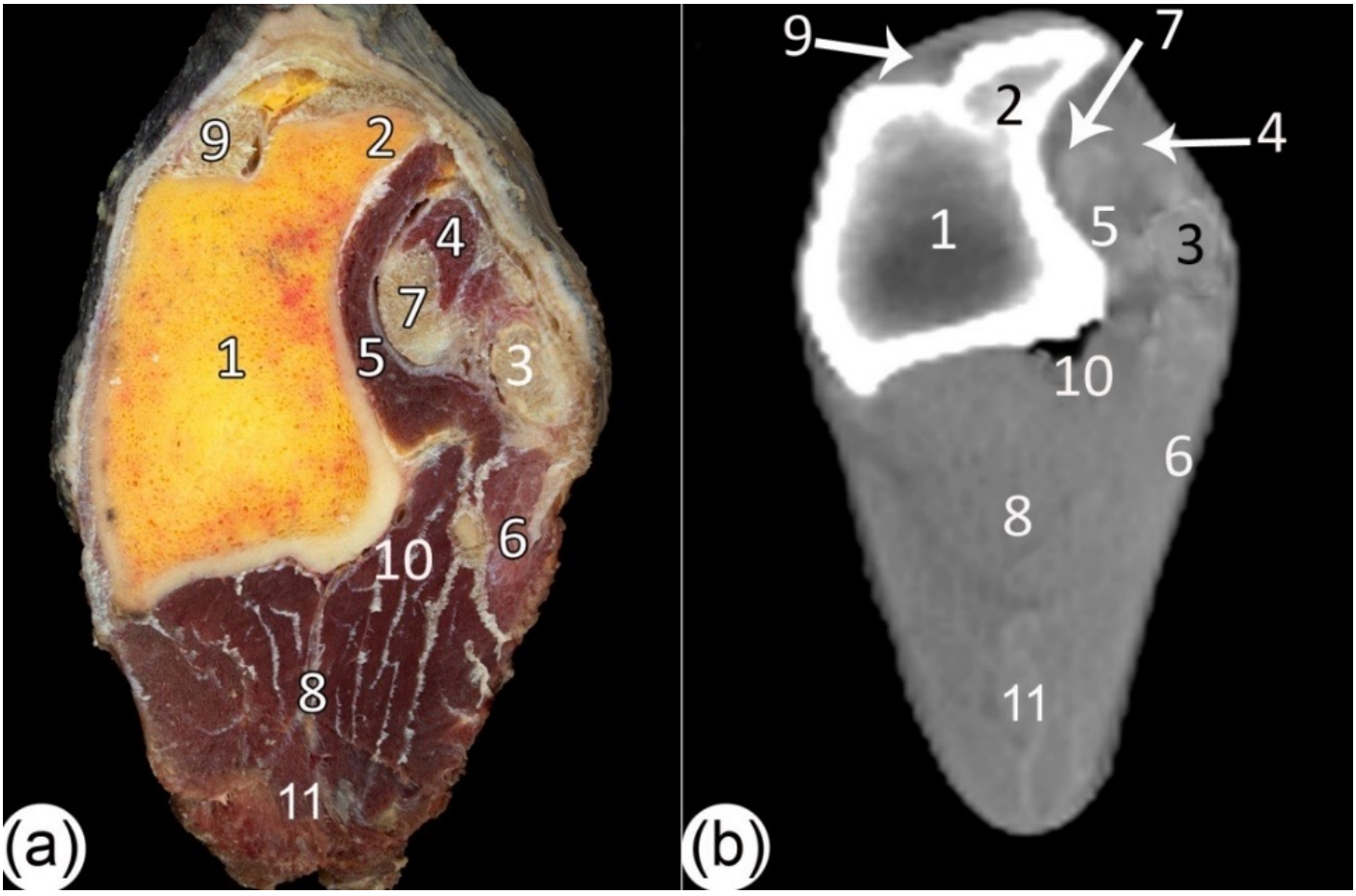

Figure 6: Cross-sections of the stifle joint at the level of the tibia proximal extremity; (a) cadaver section; (b) CT scan

1. tibia; 2. tibial crest; 3. fibula; 4. long digital extensor muscle (*M. extensor digitorum longus*); 5. tibialis cranialis muscle (*M. tibialis cranialis*); 6. lateral digital extensor muscle (*M. extensor digitorum lateralis*); 7. fibularis tertius muscle; 8. superficial digital flexor muscle (*M. flexor digitorum superficialis*); 9. middle patellar ligament (*Lig. patellae intermedium*); 10. caudal tibial artery (*A. tibialis caudalis*); 11. gastrocnemius muscle (*M. gastrocnemius*)

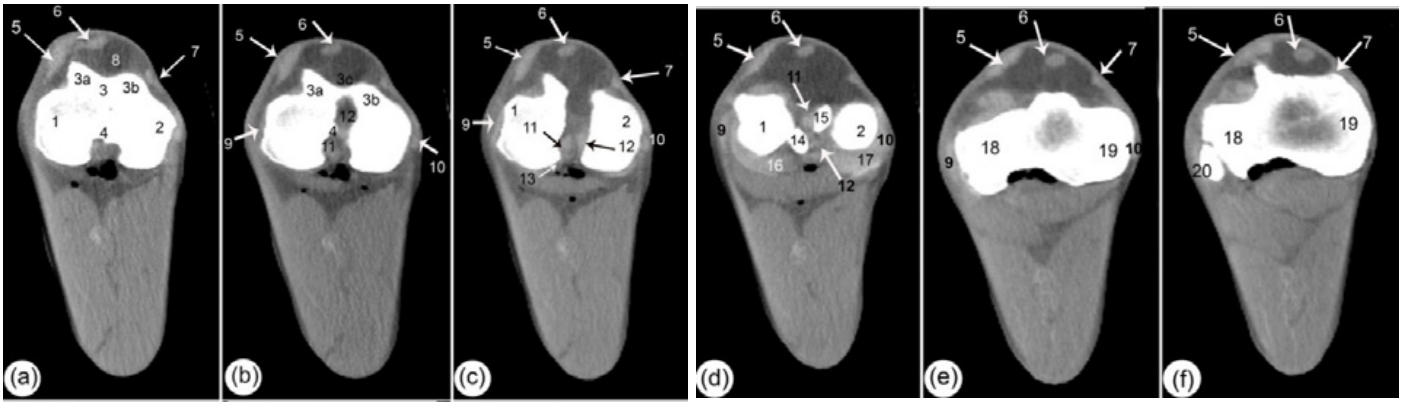

Figure 7: Transverse CT bone window scans at the femorotibial joint (Articulatio femorotibialis) (Serial sections a, b, c and d at the level of femoral condyles while e, f at the level of tibial condyles)

1. lateral femoral condyle (*Condylus lateralis*); 2. medial femoral condyle (*Condylus medialis*); 3. trochlea; 3a. lateral ridge of the femoral troch-lear; 3b. medial ridge of the femoral trochlear; 4c. trochlear groove; 5. lateral patellar ligament (*Lig. patellae laterale*); 6. middle patellar ligament (*Lig. patellae intermedium*); 7. medial patellar ligament (*Lig. patellae mediale*); 8. infra-patellar fat pad; 9. lateral collateral ligament (*Lig. collat-erale laterale*); 10. medial collateral ligament (*Lig. collaterale mediale*); 11. cranial cruciate ligament (*Lig. cruciatum craniale*); 12. caudal cruci-ate ligament (*Lig. cruciatum caudale*); 13. meniscofemoral ligament; 14. lateral tubercle of intercondyloid eminence (*Tuberculum intercon-dylare laterale*); 15. medial tubercle of intercondyloid eminence (*Tuberculum intercondylare mediale*); 16. lateral meniscus (*Meniscus lat-eralis*); 17. medial meniscus (*Meniscus medialis*); 18. lateral tibial condyle (*Condylus medialis*); 19. medial tibial condyle (*Condylus medialis*)

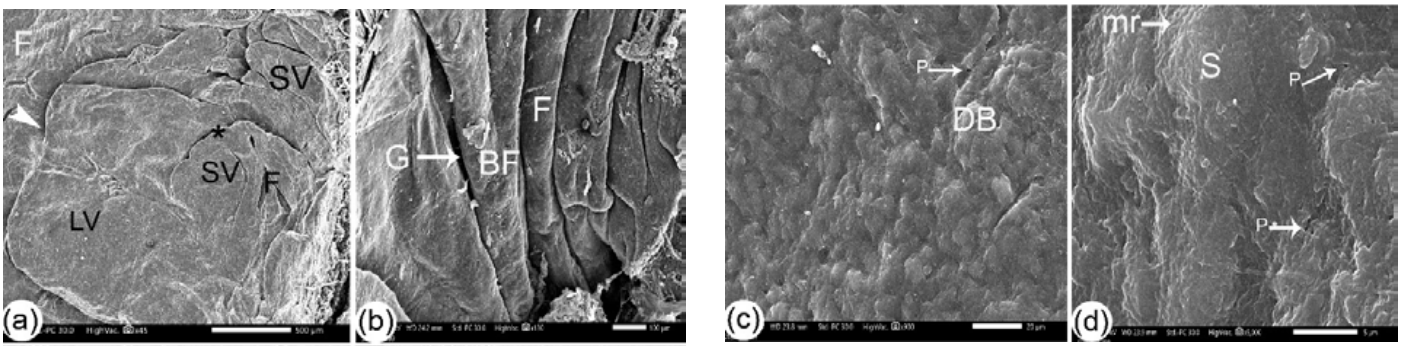

Figure 8: Scanning electron micrographs of the stifle joint synovial membrane

Long tongue-shaped villi (LV) with smooth tips (arrowhead); short circular and tongue-shaped villi (SV) with slight wavy tips (*); folds (F); branched folds (BF); dome-shaped bubbly structures (DB); dome-shaped synoviocytes (S); micro-ridges (mr); pores (P)

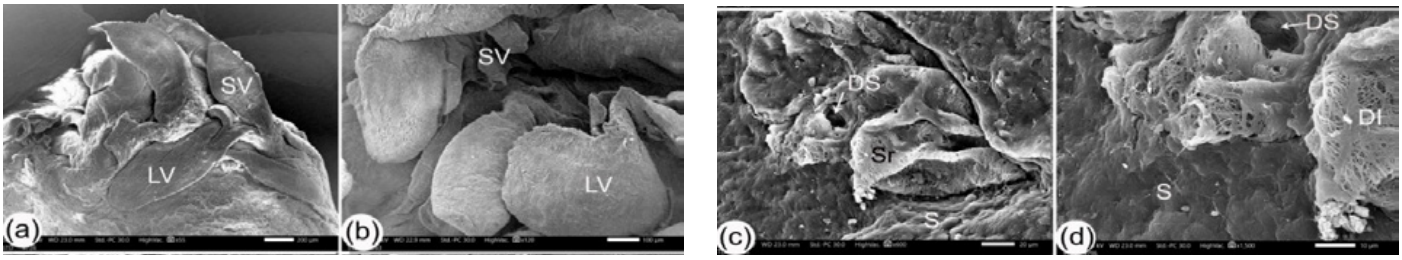

Figure 9: Scanning electron micrographs of the stifle joint synovial membrane

Long tongue-shaped villi (LV); short tongue-shaped villi (SV); dome-shaped synoviocytes (S); deep synoviocytes (DS); scratched surface (Sr); dense irregular fibers (DI)

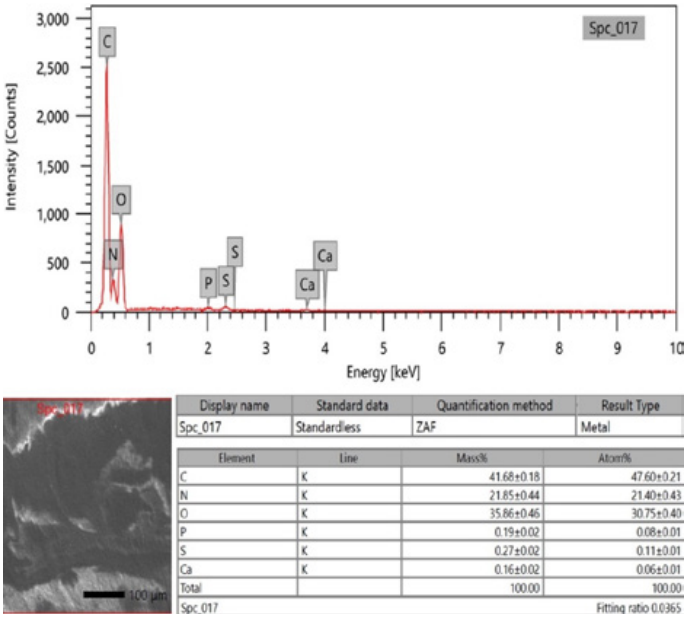

Display name	Standard data	Quantification method	Result Type
Spc_017	Standardless	ZAF	Metal

Element	Line	Mass%	Atom%
C	K	41.68±0.18	47.60±0.21
N	K	21.85±0.44	21.40±0.43
O	K	35.86±0.46	30.75±0.40
P	K	0.19±0.02	0.08±0.01
S	K	0.27±0.02	0.11±0.01
Ca	K	0.16±0.02	0.06±0.01
Total		100.00	100.00

Spc_017 Fitting ratio 0.0365

Figure 10: SEM-EDX image explaining the components at the menisci of the horse's stifle joint

The elemental composition demonstrated the following mass concentration hierarchy: carbon> oxygen > nitrogen > sulfur > phosphorus > calcium

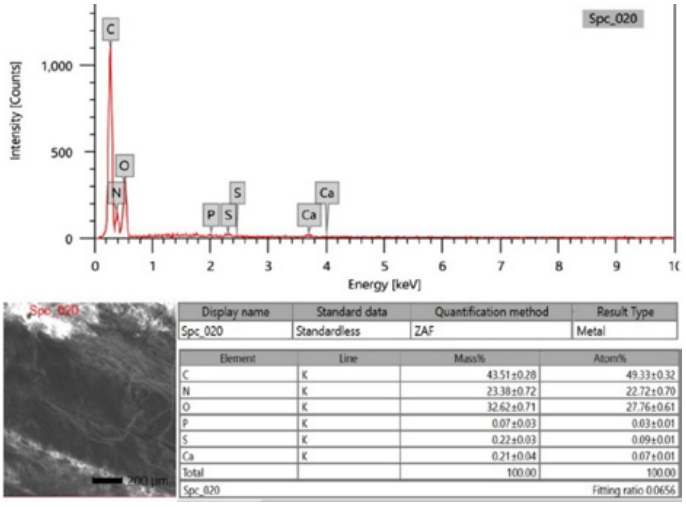

Display name	Standard data	Quantification method	Result Type
Spc_020	Standardless	ZAF	Metal

Element	Line	Mass%	Atom%
C	K	43.51±0.28	49.33±0.32
N	K	23.38±0.72	22.72±0.70
O	K	32.62±0.71	27.76±0.61
P	K	0.07±0.03	0.03±0.01
S	K	0.22±0.03	0.09±0.01
Ca	K	0.21±0.04	0.07±0.01
Total		100.00	100.00

Spc_020 Fitting ratio 0.0656

Figure 11: SEM-EDX image explaining the components of the patellar ligaments of the horse's stifle joint

The elemental composition demonstrated the following mass concentration hierarchy: carbon > oxygen > nitrogen > sulfur > calcium > phos-phorus

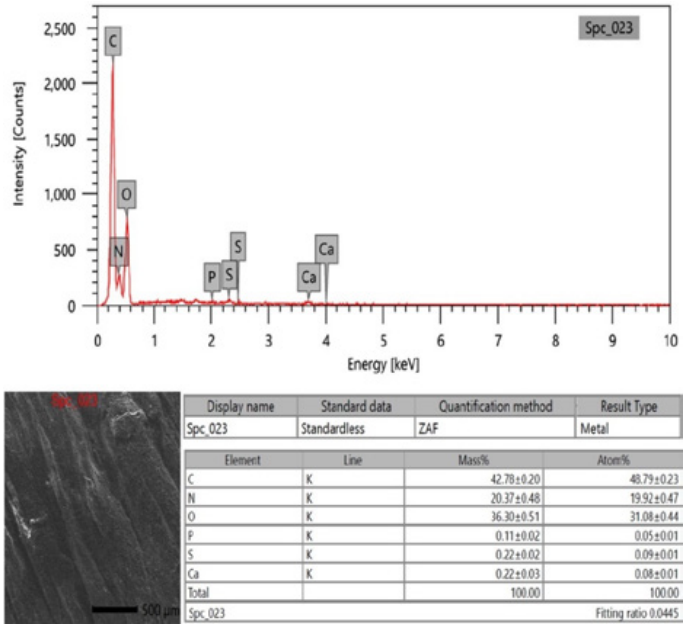

Display name	Standard data	Quantification method	Result Type
Spc_023	Standardless	ZAF	Metal

Element	Line	Mass%	Atom%
C	K	42.78±0.20	48.79±0.23
N	K	20.37±0.48	19.92±0.47
O	K	36.30±0.51	31.08±0.44
P	K	0.11±0.02	0.05±0.01
S	K	0.22±0.02	0.09±0.01
Ca	K	0.22±0.03	0.08±0.01
Total		100.00	100.00

Spc_023 Fitting ratio 0.0445

Figure 12: An SEM-EDX image explaining the components of the cruciate ligaments of the horse's stifle joint

The elemental composition demonstrated the following mass concentration hierarchy: carbon > oxygen > nitrogen > sulfur > calcium > phos-phorus.

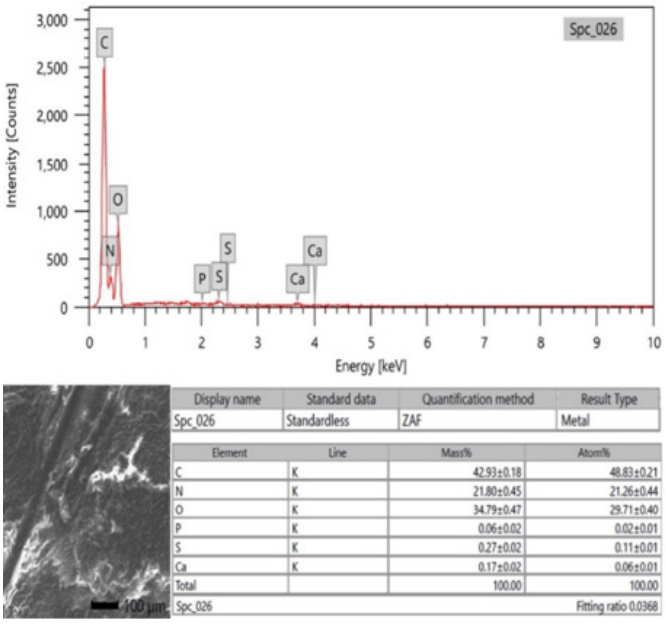

Display name	Standard data	Quantification method	Result Type
Spc_026	Standardless	ZAF	Metal

Element	Line	Mass%	Atom%
C	K	42.93±0.18	48.83±0.21
N	K	21.80±0.45	21.26±0.44
O	K	34.79±0.47	29.71±0.40
P	K	0.06±0.02	0.02±0.01
S	K	0.27±0.02	0.11±0.01
Ca	K	0.17±0.02	0.06±0.01
Total		100.00	100.00

Spc_026 Fitting ratio 0.0368

Figure 13: SEM-EDX image explaining the components of the collateral ligaments of the horse's stifle joint

The elemental composition demonstrated the following mass concentration hierarchy: carbon > oxygen > nitrogen > sulfur > calcium > phos-phorus

Table 1: The mass percentage and mean ± standard error of various elements in the menisci, patellar ligaments, cruciate ligaments, and collateral ligaments

	Menisci		Patellar ligament		Cruciate ligament		Collateral ligament	
	Horse1	**Horse2**	**Horse1**	**Horse2**	**Horse1**	**Horse2**	**Horse1**	**Horse2**
C	42.04±0.18	41.68±0.18	43.51±0.28	39.41±0.21	42.78±0.20	41.16±0.26	42.93±0.18	38.74±0.30
O	36.05±0.46	35.86±0.46	32.62±0.71	36.41±0.56	36.30±0.51	35.51±0.68	34.79±0.47	36.11±0.82
N	21.45±0.43	21.85±0.44	23.38±0.72	23.89±0.52	20.37±0.48	22.86±0.64	21.80±0.45	24.88±0.76
S		0.16±0.02	0.22±0.03	0.19±0.02	0.22±0.02	0.22±0.03	0.27±0.02	0.10±0.03
Ca	0.25±0.02	0.27±0.02	0.21±0.04	0.11±0.02	0.22±0.03	0.16±0.03	0.17±0.02	0.12±0.03
P	0.03±0.01	0.19±0.02	0.07±0.03		0.11±0.02	0.09±0.02	0.06±0.02	0.04±0.02
Si	0.18±0.02							
Ca+p	0.25	0.46	0.27	0.11	0.33	0.25	0.23	0.16

produced excellent 3D images of bones with large and small bony structures and soft structures. The 3D render volume of CT images of the bones and joints helps assess the typical fractures and dislocations (23, 39, 40, 41, 51). 3D reconstruction images improve the approach and understanding of bone anatomy and can value related diseases, allowing radiologists to identify and demonstrate individual os-seous and soft-tissue components of complex anatomy (19, 52, 53). The 3D image can be transferred to an anatomical modal cast using a 3D printer, simplifying and improving the learning process while benefiting research and diagnosis (54). CT image reconstruction into three dimensions enhances bone and joint contour assessment and delineation of fracture orientation or bone fragmentation (55, 56).

The complex stifle joint consisted of three main joint sacs: fem-oropatellar, medial, and lateral femorotibial. The ligaments of the stifle joint and meniscus were determined using a 3D reconstruc-tion CT, which provided a well-defined baseline reference image for donkey stifle joints (57).

Our study's sagittal CT sections and subsequent CT bone window cross sections provided detailed images of the bone's structures, ligaments, and muscles. The sectional CT sections were com-pared to cross and sagittal anatomical sections. The images supplied should increase the clinical use of CT to diagnose patho-logical conditions within the stifle joint that cause clinical lameness. CT scans are beneficial for evaluating menisci and cruciate ligaments (18, 58, 59, 60). CT of the equine stifle joint has shown promise as a clinically helpful technique for stifle joint injury de-tection, such as injury to the meniscus, cranial tibial ligaments of the lateral and medial menisci, and cruciate ligaments has been recognized (61). (62) used 3D radio stereometric analysis and equine cadaver stifles to determine the functional range of mo-tion. Understanding the normal kinematics of the equine stifle and the relationship between joint positions and articular contact areas may shed light on the etiology and location of common stifle joint pathologies (meniscal lesions and articular). Stifle joint injuries (meniscus and ligaments) are becoming more common in equines (63).

SEM revealed that the synovial villi varied in length, had two types, long and short, with varying tip shapes, and contained dome-shaped synoviocytes. The rest of the surface featured single or branched folds. Pig, rabbit, and rat knee joints showed blunt processes on their synovial villous surfaces (64). The char-acter of donkey carpal synovial villi exhibits the longer villi that were branched in their tips at the horse carpal (22), they were densely arranged and were longer than those of other mammals and had two types of synoviocytes; the upper half of the villi had protruded an antenna-like process into the joint cavity with tips covered with long microvilli (23). In the calf antebrachiocarpal joint, the synovial membrane consisted of type A synoviocytes that were located adjacent to the joint lumen (65). In the synovial membrane of the rabbit knee joint in the case of osteoarthritis, both types of synoviocytes increased in number and changed their morphology, indicating their elevated activities in absorp-tion and secretion (22, 23, 65, 66). Cells are abundant in synovial villi and folds and are primarily exposed to the joint cavity; they help maintain joint cavity homeostasis by phagocytosing waste and cell debris in the synovial fluid (64) in horse, (67) in human, (68) in White Leghorn chicken embryos.

Deep synoviocytes appeared at the scratched membrane; dis-tinguish between superficial and deep synoviocytes. (69) in eq-uine described the existence of multiple layers of synovial cells surrounding a dense fibrous core. The synovial membrane had two types of synoviocytes; type A-synoviocytes were spherical and possessed many processes, while type B-synoviocytes pre-sented at the luminal synovial surfaces (22, 64) in the horse, (70) in rats, rabbits, dwarf goats, sheep, pig, dog, and human. The lamina propria was dense and irregular in our sample, while the synovial membrane comprised synovial cells and lamina propria of various types: areolar, adipose, and fibrous; a similar observa-tion was stated by (69) in horse. Scanning electron microscopy revealed that human adipose and areolar tissue have a surface pattern, and blunt processes cover synovial villi (70) in human, pig, rat, and rabbit. The synovial membrane was covered with closely arranged synovial villi; other areas of the synovial membrane's surface had folded synovial membrane; the folds were either single or branched, and there were four types of gross construction at the synovial membrane of rabbit knee: accordi-on-like, lobe-like, fatty areolar, and flattened areas (71) in rabbit.

SEM-EDX detected carbon, oxygen, nitrogen, sulfur, calcium, and phosphorus in the menisci and various ligaments of the stifle joint. Selenium was replaced by sulfur in the menisci, and calcium and phosphorus were trace amounts, with the menisci having the highest percentage and the collateral and patellar ligaments having the lowest. The percentage of sulfur was also trace; liga-ments had the highest percentage compared to menisci (28). The calcium, sulfur, and phosphorus content of ligaments and tendons generally showed some exciting differences. Furthermore, sig-nificant regional variations may be associated with the presence or absence of fibrocartilage in the "wraparound." The sulfur and calcium concentrations are incredibly high, which is undoubtedly linked to elevated levels of proteoglycans (28).

The tendons and ligaments have different chemical properties. There were also more minor differences between ligaments and tendons. The findings indicate that ligaments are metabolically more active than tendons. They also have less total collagen than tendons but more glycosaminoglycans—relatively increased ligament metabolic activity (26). The relative contents of sulfur, calcium, and phosphorus in human menisci increased gradually and then decreased (72). Age-related changes in the trace ele-ment content of tendons and ligaments can aid in interpreting and evaluating morphological and biochemical changes in tissues and mechanical properties (26, 28).

Silicon plays a vital role in connective tissue, with the primary effect on bone and cartilage appearing to be the formation of the organic matrix. As a result, silicon is now required to form colla-gen and glycosaminoglycan. Silicon is involved in the biochemis-try of subcellular enzyme-containing structures and has essential interactions with other elements. The link between silicon and aging is likely due to glycosaminoglycan changes (73).

Conclusion

CT, sectional anatomy, SEM, and SEM-EDX analysis described the horse's stifle joint. The 3D render volume reconstruction CT enables clear viewing of the large and small bone features, ligaments, and meniscus. Understanding the stifle joint's macro- and microscopic normal anatomy acquired by 3D CT, SEM, and SEM-EDX is a valuable tool and reference for assessing the horse stifle's bone and soft tissue structures and microstructures

Acknowledgements

We thank Alexandria and Damanhour Universities for their help in completing this work.

Ethics approval. The study complied with the ARRIVE guidelines and followed the U.K. Animals (Scientific Procedures) Act, 1986, and associated guidelines, EU Directive 2010/63/EU for animal experiments.

All methods followed relevant guidelines and regulations with ethical permission from the Alexandria University Research Ethics Review Committee of the Faculty of Veterinary Medicine, Alex-andria University (*Approval No: Au/13/04/03/2024/096*).

We obtained informed consent and permission from the Depart-ment of Anatomy and Embryology, Faculty of Veterinary Medi-cine, Alexandria University, to use the hind limbs of euthanized horses in our study.

Availability of data and materials. The datasets used and/or analyzed during the current study are available from the corre-sponding author upon reasonable request.

Declaration of Competing Interest. The authors declare that they have no known competing financial interests or personal rela-tionships that could have appeared to influence the work report-ed in this paper.

Funding. The current study does not have any funds from any organizations or institutions.

Authors' contributions. MAMA, AKSE, and SAAE wrote the man-uscript and interpreted the results; MAMA, AKSE, IA, and AGN collected the samples and performed the CT scanning; MAMA, AKSE, and SAAE collected the samples and performed the scan-ning electron microscopy; MAMA and SAAE prepared the fig-ures, and IA and AGN assisted in interpreting the results.

Abbreviations: Computed Tomography (CT), 3D Computed To-mography (3D CT), Scanning Electron Microscopic (SEM), Scan-ning electron microscopy-Energy Dispersive X-Ray Analysis (SEM-EDX), Carbon, Oxygen, Nitrogen, Sulfur, Calcium, Phosphorus, and Silicon (C, O, N, S, Ca, P, and Si).

References

1. Carpenter Jr D, Cooper R. Mini review of canine stifle joint anatomy. Anat Histol Embryol 2000; 29 (6): 321–9.
2. Budras KD, Sack WO, Rock S, Horowitz A, Berg R. Anatomy of the Horse, Sixth Edition: Schluetersche, Germany; 2012.
3. Walmsley JP. Diagnosis and treatment of ligamentous and meniscal injuries in the equine stifle. Vet Clin North Am Equine Pract 2005; 21 (3): 651–72.
4. Judy C. The stifle. Equine MRI 2010:451-466.
5. Moore KW, Read RA. Rupture of the cranial cruciate ligament in dogs-part I. Compend Contin Educ Vet 1996; 18 (3): 223–33.
6. Jeffcott L, Kold S. Stifle lameness in the horse: a survey of 86 referred cases. Equine Vet J 1982; 14 (1): 31–9.
7. Stashak TS. Adams' lameness in horses, 4th edn: Verlag M. & H. Schaper; 2008.
8. Dyson SJ. Lameness associated with the stifle and pelvic regions. In: Proceedings of the Annual Convention of the AAEP. 2002: 387–411.
9. Jeffcott L. Interpreting radiographs 3: radiology of the stifle joint of the horse. Equine Vet J 1984; 16 (2): 81–8.
10. Butler J, Colles C, Dyson S, Kold S, Poulos P. The stifle and tibia. Clinical radiology of the horse . Ames: Wiley Blackwell, 2000:363–412.
11. McIlwraith CW, Frisbie DD, Kawcak CE, Van Weeren R. Joint disease in the horse. Amsterdam: Elsevier, 2015.
12. McIlwraith CW, Kawcak C, Baxter GM, Goodrich LR, Valberg SJ. Principles of musculoskeletal disease: joint injuries and disease and osteoarthritis. In: Baxter GM, ed. Adams and Stashak's Lameness in Horses. 7th ed. Hoboken: Wiley, 2020: 801–74.
13. Marino DJ, Loughin CA. Diagnostic imaging of the canine stifle: a review. Vet Surg 2010; 39(3): 284–95.
14. Antonacci JM, Schmidt TA, Serventi LA, et al. Effects of equine joint injury on boundary lubrication of articular cartilage by synovial fluid: role of hyaluronan. Arthritis Rheum 2012; 64(9): 2917–26.
15. Denoix J-M. Essentials of clinical anatomy of the equine locomotor system. Boca Raton: CRC press, 2019.
16. Badawy AM. Computed tomographic anatomy of the fore foot in one-humped camel (Camelus dromedrus). Glob Vet 2011; 6(4): 417–23.
17. Alsafy M, El-Kammar M, El-Gendy S. Topographical anatomy, computed tomography, and surgical approach of the guttural pouches of the donkey. J Equ Vet Sci 2008; 28 (4): 215–22.
18. Van der Vekens E, Bergman EH, Vanderperren K, et al. Computed tomographic anatomy of the equine stifle joint. Am J Vet Res 2011; 72(4): 512–21.
19. El-Gendy SA, Kamal BM, Alsafy MA. 3D render volume CT reconstruction of the bones and arteries of the hind digit of the dromedary camel (Camelus dromedarius). BMC Zool 2022; 7(1): 49.
20. El-Gendy SA, Alsafy MA, Rutland CS, Ez Elarab SM, Abd-Elhafeez HH, Kamal BM. Ossa cordis and os aorta in the one-humped camel: Computed tomography, light microscopy and morphometric analysis. Microscopy Research and Technique 2023, 86 (1):53-62.
21. El-Gendy SA, Alsafy MA, Rutland CS, El-Khamary AN, Abu-Ahmed HM, El-Kammar MH. Morphological and imaging evaluation of the metacarpophalangeal and metatarsophalangeal joints in healthy and lame donkeys. J Equ Vet Sci 2020; 88: 102904. doi: 10.1016/j.jevs.2019.102904

22. Shikichi M, Kitamura HP, Yanase H, Konno A, Takahashi-Iwanaga H, Iwanaga T. Three-dimensional ultrastructure of synoviocytes in the horse joint as revealed by the scanning electron microscope. Arch Histol Cytol 1999; 62(3): 219–29.

23. Alsafy MA, El-Gendy SA, Abou-Ahmed HM. The carpal joint of the donkey (Equus asinus): morphological investigation. Internat J Morphol 2015; 33(3): 948-54.

24. Fugazzola M, Nissinen MT, Jäntti J, et al. Composition, architecture and biomechanical properties of articular cartilage in differently loaded areas of the equine stifle. Equine Vet J 2024; 56(3): 573–85.

25. White JL, Salinas EY, Link JM, Hu JC, Athanasiou KA. Characterization of adult and neonatal articular cartilage from the equine stifle. J Equine Vet Sci 2021; 96: 103294. doi: 10.1016/j.jevs.2020.103294

26. Amiel D, Frank C, Harwood F, Fronek J, Akeson W. Tendons and ligaments: a morphological and biochemical comparison. J Orthop Res 1983; 1(3): 257–65.

27. Edwards J. The nature and origins of synovium: experimental approaches to the study of synoviocyte differentiation. J Anat 1994; 184 (3): 493–501.

28. Kumai T, Yamada G, Takakura Y, Tohno Y, Benjamin M. Trace elements in human tendons and ligaments. Biol Trace Elem Res 2006; 114(1/3): 151–61.

29. Thorpe CT, Screen HR. Tendon structure and composition. Adv Exp Med Biol 2016; 920: 3-10.

30. Ribitsch I, Peham C, Ade N, et al. Structure—Function relationships of equine menisci. PLoS One 2018; 13(3): e0194052. doi: 10.1371/journal.pone.0194052

31. Penninck DG, Nyland TG, O'Brien TR, Wheat JD, Berry CR. Ultrasonography of the equine stifle. Vet Radiol 1990; 31(6): 293–8.

32. El Sharaby AA, Alsafy MA, El-Gendy SA. Equine anatomedia: development, integration and evaluation of an e-learning resource in applied veterinary anatomy. Int J Morphol 2015; 33(4): 1577-84.

33. Holcombe SJ, Bertone AL, Biller DS, Haider V. Magnetic resonance imaging of the equine stifle. Vet Radiol Ultrasound 1995; 36(2): 119–5.

34. Hoegaerts M, Nicaise M, van Bree H, Saunders J. Cross-sectional anatomy and comparative ultrasonography of the equine medial femorotibial joint and its related structures. Equine Vet J 2005; 37(6): 520–9.

35. Maulet BEB, Mayhew I, Jones E, Booth T. Radiographic anatomy of the soft tissue attachments of the equine stifle. Equine Vet J 2005; 37(6): 530–5.

36. Dyce KM, Sack WO, Wensing CJG. Textbook of Veterinary Anatomy. St. Louis: Mosby, 2010.

37. Ali S, Esmat A, Erasha A, Yasuda M, Alsafy M. Morphology and morphometry of the inner ear of the dromedary camel and their influence on the efficiency of hearing and equilibrium. Zoo Lett 2022; 8(1): 1-12. doi: 10.1186/s40851-022-00196-0

38. Alsafy MA. Comparative morphological studies on the lacrimal apparatus of one humped camel, goat, and donkey. J Biol Sci 2010; 10(3): 224–30. doi: 10.3923/jbs.2010.224.230

39. Alsafy MA, El-Gendy SA, Kamal B. Morphological, radiographic and computed tomographic evaluation of the metatarsophalangeal joint of the one-humped camel. Anat Histol Embryol 2018; 47(6): 537–43.

40. Alsafy MA, El-Gendy SA, Kamal B. Computed tomographic and radiographic morphology of the pastern and coffin joints of One-Humped Camel (Camelus dromedarius). Anat Histol Embryol 2021; 50(1): 108–13.

41. Alsafy MAM. Computed tomography and cross-sectional anatomy of the thorax of goat. Small Rum Res 2008; 79(2/3): 158–66.

42. El-Gendy S, Alsafy M, El Sharaby A. Computed tomography and sectional anatomy of the head cavities in donkey (Equus asinus). Anat Sci Int 2014; 89(3): 140–50.

43. Alsafy MA, El-Gendy SA. Morphological investigation of the gills of the dusky grouper Epinephelus marginatus (Lowe 1834) using gross anatomy and scanning electron microscopy. Microsc Res Tech 2022; 85(5): 1891–8.

44. Alsafy MA, Seif MA, El-Gendy SA, El-Beskawy M, El Dakroury M. Ultrastructure of the oropharyngeal cavity floor of the red porgy (Pagrus pagrus) by light and scanning electron microscopy. Microsc Microanal 2023; 29(1): 273–82.

45. Ez Elarab SM, El-Gendy SA, El-Bakary NE, Alsafy MA. Ultrastructure of the palatine tonsils of the donkey (Equus asinus): new insights by light, scanning, and transmission electron microscopy. Microsc Res Tech 2022; 85(12): 3793–803.

46. El-Bakary NE, Alsafy MA, El-Gendy SA, Elarab SME. New insights into the retinal microstructure-diurnal activity relationship in the African five-lined skink (Trachylepis quinquetaeniata) (Lichtenstein, 1823). Zoological Lett 2023; 9(1) : 7. doi: 10.1186/s40851-023-00205-w

47. Alsafy M, El-Gendy S. Gastroesophageal junction of Anatolian shepherd dog; a study by topographic anatomy, scanning electron and light microscopy. Vet Res Commun 2012; 36(1): 63-9.

48. El-Gendy SAA, Derbalah A, El-Mansi AA, El Okle OS, Alsafy MAM. Light and scanning electron microscopic characterization of the Egyptian buffalo hair in relation to age with analysis by SEM-EDX. Microsc Res Tech 2023; 86(8): 955–65. doi: 10.1002/jemt.24366

49. Derbalah A, El-Gendy SA, Alsafy MA, Elghoul M. Micro-morphology of the retina of the light-adapted African catfish (Clarias gariepinus). Microsc Res Tech 2023; 86(2): 208–15.

50. Rashwan AM, El-Gendy SAA, Alsafy MAM, Haddad SS. Comparative morphological analysis of telson and uropods in Penaeus canaliculatus (Olivier, 1811), Penaeus semisulcatus (De Haan, 1844), and Metapenaeus stebbingi (Nobili, 1904) using scanning electron microscopy and EDX analysis. Micron 2024; 181: 103636. doi: 10.1016/j.micron.2024.103636

51. Rózyło-Kalinowska I, Rózyło T. Diagnostic algorithm in high (cranial) maxillofacial fractures. Ann Univ Mariae Curie Sklodowska Med 2000; 55: 309-17.

52. Alsafy MA, Elbakary RM, Bassuoni NF. A study of the shoulder and elbow joints of the donkey (Equus asinus) by gross anatomical dissection, radiography, computed tomography, and intra-articular injection. Morphologie 2022; 106(354): 177-87.

53. Fatterpekar GM, Doshi AH, Dugar M, Delman BN, Naidich TP, Som PM. Role of 3D CT in the evaluation of the temporal bone. Radiographics 2006; 26 (suppl. 1): S117-S132.

54. Jáber Mohamad JR, Carrascosa Iruzubieta CJ, Arencibia Espinosa A, Corbera Sánchez JA, Ramírez Corbera AS, Melián Limiñana C. 3-D computed tomography reconstruction: another tool to teach anatomy in the veterinary colleges. Iran J Vet Res 2018.

55. Davidson E, Ross M, Parente E. Incomplete sagittal fracture of the talus in 11 racehorses: outcome. Equine Vet J 2005; 37(5): 457–61.

56. Kelmer G, Wilson D, Essman S. Computed tomography assisted repair of a central tarsal bone slab fracture in a horse. Equine Vet Educ 2008; 20(6): 284–7.

57. Abumandour MM, Bassuoni NF, El-Gendy S, Karkoura A, El-Bakary R. Cross-anatomical, radiographic and computed tomographic study of the stifle joint of donkeys (Equus africanus asinus). Anat Histol Embryol 2020; 49(3): 402–16.

58. Buckwalter KA. Current concepts and advances: computerized tomography in sports medicine. Sports Med Arthrosc Rev 2009; 17(1): 13-20.

59. Buckwalter KA. CT arthrography. Clin Sports Med 2006; 25(4): 899–915.

60. Mutschler C, Vande Berg BC, Lecouvet FE, et al. Postoperative meniscus: assessment at dual–detector row spiral CT arthrography of the knee. Radiology 2003; 228(3): 635–41.

61. Bergman HJ, Saunders J. Equine upper limbs (carpus, tarsus, stifle). Vet Comp Tomography2011:483-501.

62. Halley S, Bey M, Haladik J, Lavagnino M, Arnoczky S. Three dimensional, radiosteriometric analysis (RSA) of equine stifle kinematics and articular surface contact: a cadaveric study. Equine Vet J 2014; 46(3): 364–9.

63. Walmsley J, Phillips T, Townsend H. Meniscal tears in horses: an evaluation of clinical signs and arthroscopic treatment of 80 cases. Equine Vet J 2003; 35 (4): 402–6.

64. Iwanaga T, Shikichi M, Kitamura H, Yanase H, Nozawa-inoue K. Morphology and functional roles of synoviocytes in the joint. Arch Histol Cytol 2000; 63(1): 17-31.

65. Leach DH, Caldwell SJ, Ferguson JG. Ultrastructural study of synovial membrane from the antebrachiocarpal joint of calves. Cells Tissues Organs 1988; 133 (3): 234–46.

66. Nio J, Yokoyama A, Okumura M, Iwanaga T. Three-dimensional ultrastructure of synoviocytes in the knee joint of rabbits and morphological changes in osteoarthritis model. Arch Histol Cytol 2002; 65(2): 189–200.

67. Esposito CI. Wear in ceramic-on-ceramic total hip replacements: mechanisms and implications of edge loading. Sydney: UNSW Sydney, 2012. doi: 10.26190/unsworks/15983

68. Williams R. Effects of mechanical strain hyaluronan metabolism of synovial cells from osteoarthritic knees. Cardiff: Cardiff University, 2004. Doctoral thesis. https://orca.cardiff.ac.uk/id/eprint/55950/

69. Updike SJ, Diesem CD. Histologic appearance and distribution of synovial membrane types in the equine stifle joint. Anat Histol Embryol 1983; 12(1): 53–9.

70. Woodward D, Gryfe A, Gardner D. Comparative study by scanning electron microscopy of synovial surfaces of four mammalian species. Experientia 1969; 25 (12): 1301–3.

71. Levanon D, Stein H. The synovial lining of the rabbit knee: a scanning electron microscopy study of specimens reinforced structurally with tannic acid. Histochem J 1992; 24: 25–32.

72. Moriwake Y, Tohno Y, Tohno S, et al. Age-related changes of element contents in the human meniscus. Biol Trace Elem Res 1998; 64: 229–35.

73. Carlisle EM. Silicon as a trace nutrient. Sci Total Environ 1988; 73(1/2): 95–106.

Nova spoznanja o konjskem kolenskem sklepu s pomočjo 3D-računalniške tomografije, vrstične elektronske mikroskopije ter vrstične elektronske mikroskopije in energijsko disperzijske rentgenske analize

M. A.M. Alsafy, A. K.S. El-Garhy, I. Abo-Ghanima, A. G. Nomir, S. A.A. El-Gendy

Izvleček: Zasnova študije konjskega kolenskega sklepa je bila prospektivna in opisna, z uporabo CT, anatomije iz rezin, SEM in analize EDX. CT konjskega kolenskega sklepa z rekonstrukcijo tridimenzionalnega upodobljenega volumna omogoča dobro vizualizacijo velikih in majhnih kostnih struktur ter vezi ali meniskusov. Poleg sagitalnih CT-rezin in naknadnih prečnih CT-rezin kosti, ki so omogočile podrobne posnetke kostnih struktur, vezi in mišic, so bili sekcijski CT-ji usklajeni s prečnimi in sagitalnimi anatomskimi prerezi. Konjski kolenski sklep je opisan z analizo SEM in EDX. Sinovialna membrana je imela različne sinovialne resice po dolžini in obliki: dolge in kratke jezičaste z različnimi konicami in kupolasto obliko, poleg tega pa tudi posamezne ali razvejene gube. Površina razkriva mrežo kolagenih vlaken, razporejenih v različnih smereh, plasteh in globoke sinoviocite. Spektri SEM-EDX so identificirali naslednje elemente v meniskusih in vezeh kolenskega sklepa: vzorec je vseboval ogljik, kisik, dušik, žveplo, kalcij in fosfor, pri čemer je selen v meniskusu zamenjal žveplo. Pregledali smo štiri vzorce, da bi določili odstotni delež ogljika in kisika. Izmerjene so bile vrednosti kalcija in fosforja, pri čemer so bile najvišje koncentracije v meniskusu, najnižje pa v kolateralnih in patelarnih vezeh. Določen je bil odstotek žvepla, ki je bil v ligamentih višji kot v meniskusih, zlasti v križnih vezeh, medtem ko so meniskusi vsebovali silicij. Poznavanje normalne makro- in mikroskopske anatomije kolenskega sklepa, pridobljene s 3D-CT, SEM in EDX, je dobro vodilo in referenca za določanje kostnih in mehkotkivnih struktur in mikrostruktur ter kemične strukture sinovialne membrane, ligamentov in meniskusov konjskega kolenskega sklepa.

Ključne besede: konj; kolenski sklep; 3D-CT; anatomska analiza iz rezin; SEM; SEM-EDX

Slov Vet Res
DOI 10.26873/SVR-2136-2025
UDC 617.7.089:616-073.7:636.295
Pages: 169–75

Original Research Article

Computed Tomography and Gross Anatomical Studies on the Temporomandibular and Supraorbital Regions of One-Humped Camel (*Camelus dromedarius*)

Key words

enucleation;
camel;
orbital surgery;
temporal fossa

Mohamed Marzok[1]*, Khalid M. Alkhodair[2], Mohamed Nazih[3], Mohamed W. El-Sherif[4]

[1]Department of Clinical Studies, College of Veterinary Medicine, King Faisal University, Al-Ahsa, KSA, [2]Department of Anatomy, College of Veterinary Medicine, King Faisal University, Al-Ahsa, KSA, [3]Department of Anatomy, Faculty of Veterinary Medicine, New Valley University, Alkharga, New Valley 25711, [4]Department of Surgery, Faculty of Veterinary Medicine, New Valley University, Alkharga, New Valley 25711, Egypt

***Corresponding author:** mmarzok@kfu.edu.sa

Abstract: The objective of this study was to investigate the detailed surgical anatomy of the temporomandibular and supraorbital regions in camels using anatomical dissection and computed tomography (CT) scanning. The study aimed to provide precise anatomical descriptions and assess the feasibility of surgical interventions within the orbital cavity via the orbital fossa. Twelve camel skulls and three fresh cadaveric heads of adult camels were procured from the faculty's morgue and a local abattoir, respectively. Descriptive anatomy of the skull and surgical anatomy of the temporo-orbital region were meticulously examined. Additionally, computed tomography of the heads was conducted to augment the dataset. Results were systematically documented to evaluate the applicability, feasibility, and safety of the orbital fossa approach to the orbital cavity. The temporal fossa of the camel was found to be significantly expansive, extending rostrally to a sizable orbital fossa. The external lining of the orbital fossa comprised skin and a subjacent thick fascia. Notably, no essential muscles or vital structures were identified. The posterior orbital cavity housed a substantial periorbital fat mass, and upon its removal, clear and safe visual access to the ocular structures was achieved, facilitating ease of approach. The orbital fossa approach was determined to be feasible and safe, enabling the performance of various surgical procedures, including enucleation, exenteration, periorbital tumor removal, prosthetic implantation, and other interventions. This approach promises enhanced cosmetic outcomes in the execution of such procedures.

Received: 24 October 2024
Accepted: 26 January 2025

Introduction

Temporal fossa formed by parietal, temporal, and frontal bones and bounded laterally by the zygomatic arch (1, 2). In camels, the temporal fossa is large and extended rostral as large orbital fossa (3-5). In animals, several surgical procedures are indicated within the orbital cavity, mainly the anesthesia administration (6, 7), ocular procedures (8, 9), retrobulbar procedures (10, 11), and post-surgical cosmetic interventions (12-14). Although less common, various conditions necessitate surgical intervention within the orbital cavity in camels (15, 16). Enucleation due to surgically untreatable conditions and removal of tumors are the most common procedures (15, 17-19). This study aims to provide a descriptive anatomy of the temporo-orbital region in camels, coupled with computed tomographic findings. The goal is to evaluate the potential use of this

region as a surgical access point to the orbital cavity and its contents.

Materials and methods

The current study was reviewed, permitted, and approved by the research ethics committee (REC) of King Faisal University, KSA (Approval NO. KFU-REC/2024- ETHICS 2,090). All methods were carried out in accordance with relevant guidelines and regulations. All methods are reported in accordance with ARRIVE guidelines.

Specimen selection and anatomical dissection

Nine cadaveric heads of adult camels (6 males and 3 females) were procured from a local abattoir to serve as specimens for the study. Employing a standardized anatomical dissection methodology, the temporo-orbital region was meticulously exposed. Special attention was dedicated to the comprehensive documentation of anatomical structures, with a specific focus on elucidating the intricacies of the orbital fossa. Additionally, morphometric assessments of pertinent anatomical features were conducted to quantify and characterize the observed structures. The utilization of freshly acquired specimens and rigorous dissection techniques ensures the precision and validity of the anatomical data obtained in this study.

Imaging techniques

Prior to anatomical dissection, the cadaveric heads underwent computed tomography (CT) scanning to enhance and complement the anatomical findings. Axial CT images were acquired utilizing parameters of 120 kV, 100-350 mAs, and a slice thickness of 5 mm. The initial recording of orbit and ocular contents was conducted in the axial plane, followed by subsequent reconstruction into multiplanar and three-dimensional (3-D) images. This comprehensive imaging approach facilitated a thorough correlation between the obtained CT images and the anatomical findings, contributing to a more nuanced and in-depth understanding of the temporo-orbital region.

Results

Gross Anatomy

The tempro-orbital fossa, also known as the supra-orbital fossa, extends dorsally from the median external parietal crest, frontal bone, and rostrally from the zygomaticofrontal process. Laterally, it extends from the zygomatic process of the zygomatic bone and the zygomaticotemporal process, while caudally it is bounded by the nuchal and temporal crests. The medial boundary is formed by the parietal, squamous part of the occipital, and squamous part of the temporal bones, along with the pterion, a point where the parietal, basisphenoid, and temporal bones converge (Figure 1). The supra-orbital fossa is directly connected rostrally to the orbital cavity, and ventrally, the pterygopalatine fossa establishes a connection between the tempro-orbital fossa and the orbital cavity. Exhibiting a nearly triangular shape with rounded ends, the outer diameter of the fossa measures approximately (5±1.5 cm). Its depth ranges from (4.8-5.2 cm) measured from the optic foramen to the mid-distance between the external parietal crest and the zygomatic arch. These anatomical details provide a comprehensive description of the spatial relationships and dimensions of the tempro-orbital fossa in the context of the surrounding cranial structures (Table 1).

Table 1: Individual measurements of the outer diameter and depth of the supraorbital fossa in a sample of nine camels

Camel No.	Outer Diameter (cm)	Depth (cm)
1	4.2	5.1
2	6.0	4.9
3	5.8	5.0
4	3.9	4.8
5	4.5	5.2
6	6.3	5.0
7	5.4	4.9
8	3.7	5.1
9	5.2	4.8

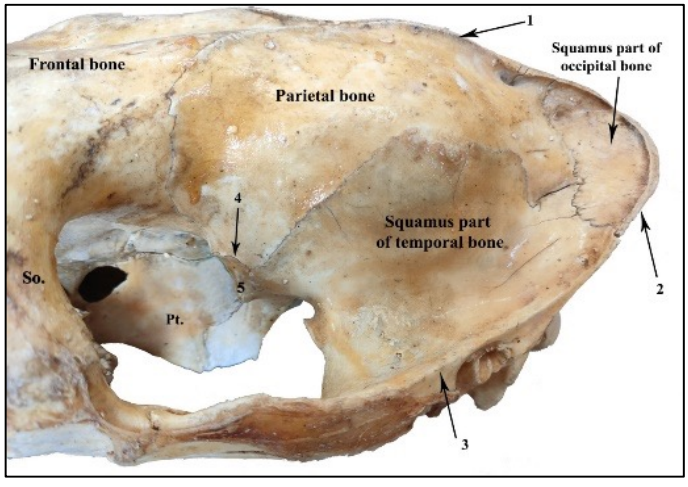

Figure 1: Dorso-lateral view of the caudal cranium of camel. 1) external parietal crest, 2) nuchal crest, 3) temporal crest, 4) pterion, 5) basisphenoid bone, So.) supra orbital process, and Pt.) pterygopalatine fossa

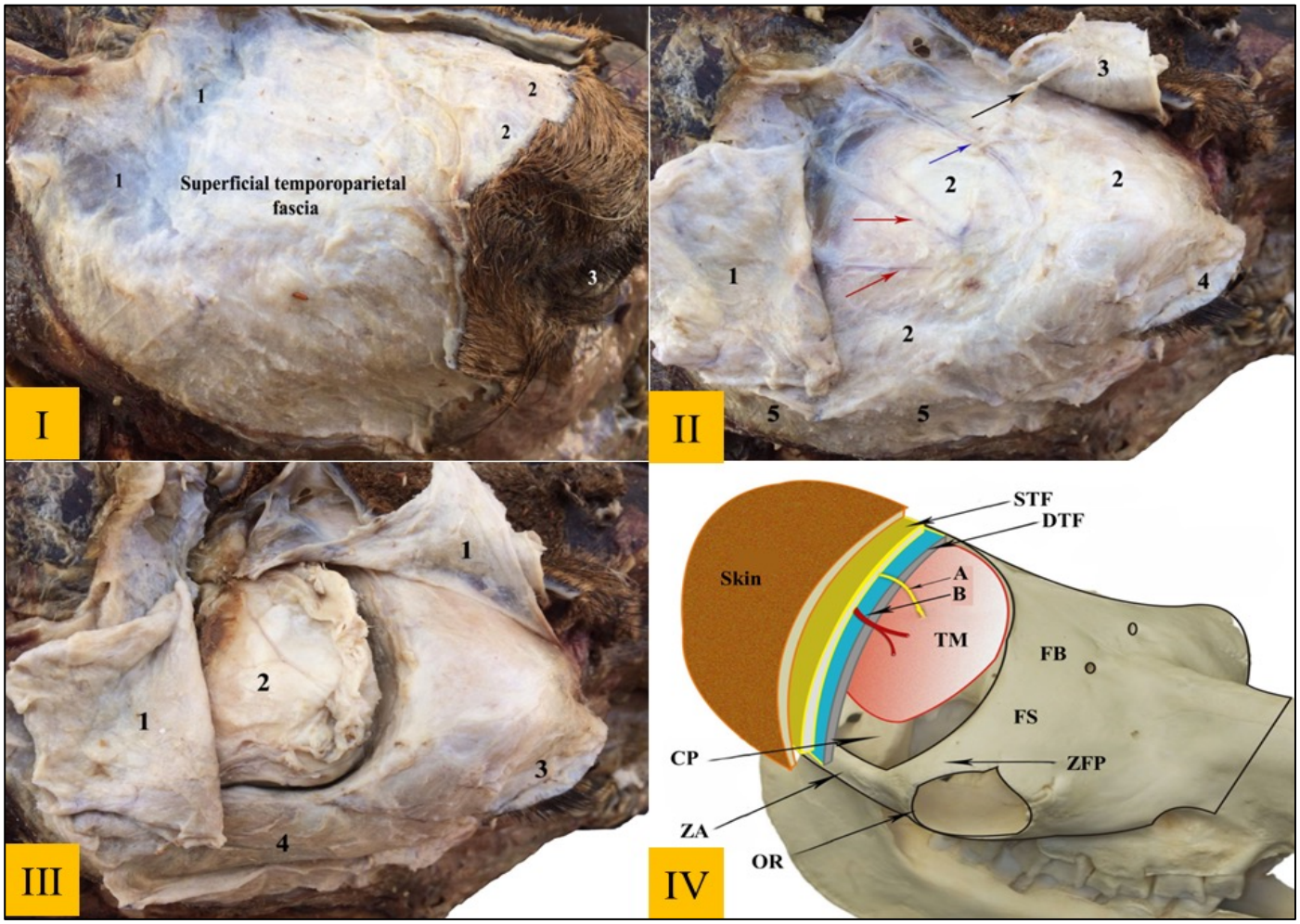

Figure 2: I) dorso-lateral view of the right caudal part of the head of camel. 1) facial part of the auricular muscles, 2) malaris muscle, and 3) upper eye lid. II) 1) superficial tempro-orbital fascia (cut), 2) deep tempro-orbital fascia, 3) malaris muscle, 4) upper eye lid, and 5) zygomatic arch. The red arrows indicate the frontal branches of the superficial temporal artery. The blue arrow indicates the superficial branch of the zygomatico temporal artery. The black arrow indicates the palpebral branch of the auriculopalpebral nerve of facial. III) 1) deep tempro-orbital fascia (cut), 2) periorbital fat, 3) upper eyelid, and 4) zygomatic arch. IV) a diagram showing the different anatomical layers on the tempro-orbital fossa. A) temporal artery and vein, B) temporal nerve, TM) temporalis muscle, STF) superficial temporoparietal fascia, DTF) deep temporoparietal fascia, CP) coronoid process, ZA) zygomatic arch, OR) orbital rim, FB) frontal bone, FS) frontal sinus, ZFP) zygomatico-frontal process

The integument covering the tempro-orbital fossa extends over the superficial temporal fascia externally (Figure 2-a, b & c). This robust layer envelops the supra-orbital fossa, extending both rostrally and dorsally in conjunction with the frontal fascia. Ventral attachment occurs at the temporal crest, providing anchorage for the frontal part of the external auricular muscles and the Malaris muscle. In deeper layers, the thinner deep tempro-orbital fascia envelops the temporalis fossa and its contents. On the external surface of this fascia, the palpebral branch of the auriculo-palpebral nerve of the facial nerve courses rostrally, passing over the Malaris muscle. Simultaneously, the frontal branch of the superficial temporal artery and the superficial branch of the zygomaticotemporal artery traverse towards the dorsolateral angle of the orbital cavity (Figure 2-d). This detailed account elucidates the intricate layers and neurovascular structures within the tempro-orbital fossa, offering a comprehensive understanding of its anatomical characteristics.

Upon removal of the deep temporo-parietal fascia, the contents of the temporal fossa become clearly delineated. Predominantly, the fossa is occupied by the temporalis muscle and periorbital fat. The temporalis muscle attaches dorsally to the parietal bone from the external sagittal crest, extending rostrally along the temporal line and inserting into the coronoid process of the mandible. In conjunction, the periorbital fat fills the space between the caudal aspect of the temporalis muscle and the rostral aspect of the orbital cavity.

This adipose tissue forms a robust, pyramidal mass with its base directed dorsally and closely related to the deep tempro-orbital fascia.

Its apex extends ventrally, reaching towards the pterygopalatine fossa. This comprehensive description elucidates the specific anatomical structures within the temporal fossa, providing a detailed understanding of their attachments, relationships, and spatial configurations. The

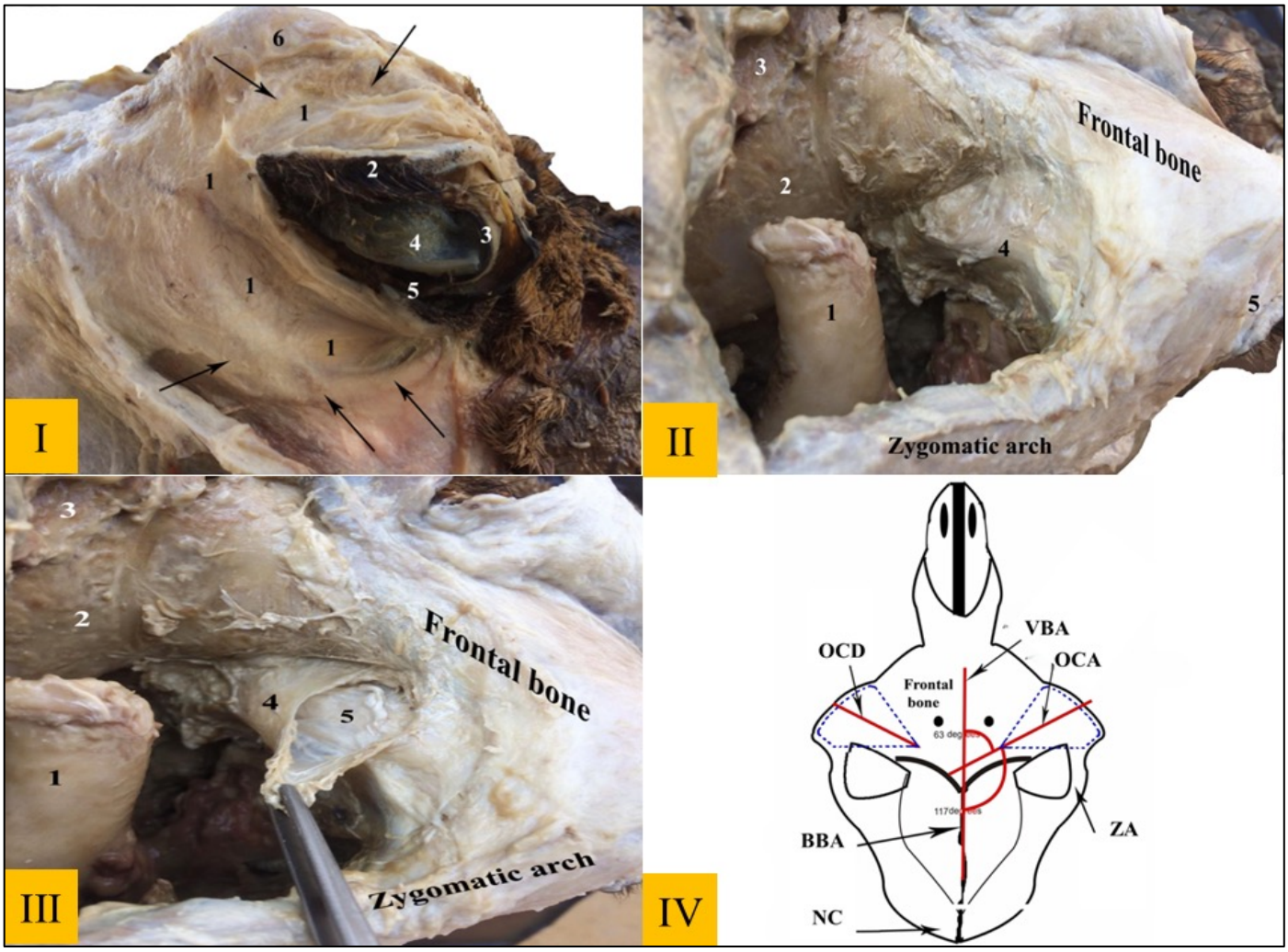

Figure 3: I) A photograph showing the entrance of the right orbital cavity. 1) orbital septum, 2) upper eyelid, 3) third eyelid, 4) cornea, and 5) lower eyelid. The black arrows indicate the orbital rim. II) a deep dissection of the right tempro-orbital fossa, dorsal view. (The periorbital fat removed). 1) coronoid process of the mandible, 2) parietal bone, 3) temporalis muscle (cut), 4) periorbital layer of the orbital fascia, and 5) upper eyelid. III) a photograph showing the right tempro-orbital fossa (deep dissection), dorsal view. (The periorbital fat removed). 1) coronoid process of the mandible, 2) parietal bone, 3) temporalis muscle (cut), 4) periorbital layer of the orbital fascia, and 5) collateral layer of the orbital fascia. IV) a diagram showing the skull of camel (dorsal view). NC) nuchal crest, BBA) basi-sphenoid bone axis, ZA) zygomatic arch, OCA) orbital cavity axis, OCD) orbital cavity depth, VBA) vomor bone axis

orbital cavity spans laterally from the orbital rim to the optic foramen medially, remaining entirely concealed ventrally by the frontal bone, sinus, and the zygomaticofrontal process. The circular perimeter of the orbital rim measures approximately (17±0.4 cm), and the depth of the orbital cavity to the optic foramen ranges from (8.7-9 cm). This cavity houses the eyeball along with its associated structures, including the lacrimal gland, eyelids, and periorbita. The periorbita, serving as the orbital fasciae and spaces, plays a crucial role in fixing and covering the eyeball and its accessories in their anatomical positions.

Comprising three superimposed layers – external periorbital, middle collateral, and internal muscular – along with orbital spaces between them, the periorbita is a key component of the orbital anatomy. The external periorbital layer takes the form of a thicker, cone-shaped capsule closely adhering to the periosteum of the orbital cavity. Caudally, it is associated with periorbital fat. Externally, the base of the cone is affixed to the orbital rim, where it reflects and inserts into the substance of the eyelids, creating the orbital septum. The apex of the cone attaches internally to the optic foramen. The longitudinal axis of the periorbital sac forms an acute angle of about (63-65 degrees) with the axis of the vomer process and approximately (117-115 degrees) with that of the basisphenoid. This detailed account provides a comprehensive understanding of the dimensions, structures, and relationships within the orbital cavity and its associated fascial components. Findings illustrated in Figure 3.

Internally, the periorbital fascia envelops the periorbital space, creating a boundary around the collateral orbital fascia. The collateral orbital fascia is thinner compared to the external fascia and encompasses the middle orbital space, extending from the sclera to the apex of the orbital cavity. The muscular coat of the eyeball (Figure 4) is composed of extraocular muscles, which encircle the eye

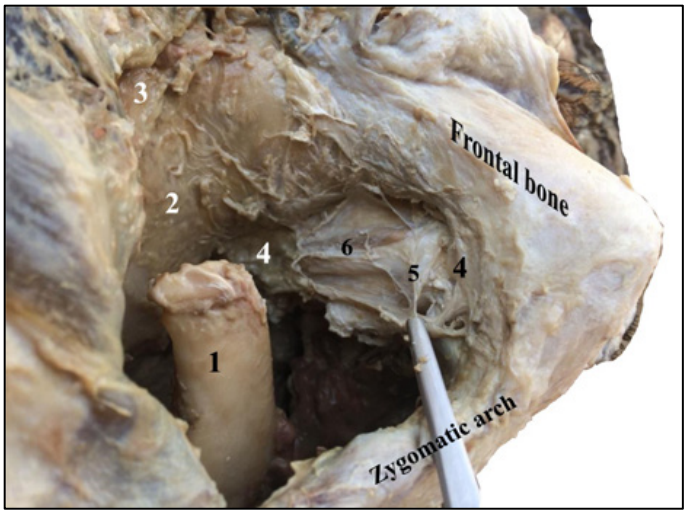

Figure 4: A photograph showing the right tempro-orbital fossa (Deep dissection), dorsal view. (The periorbital fat removed). 1) coronoid process of the mandible, 2) parietal bone, 3) temporalis muscle (cut), 4) periorbital layer of the orbital fascia, 5) collateral layer of the orbital fascia, and 6) muscular layer of the orbital fascia

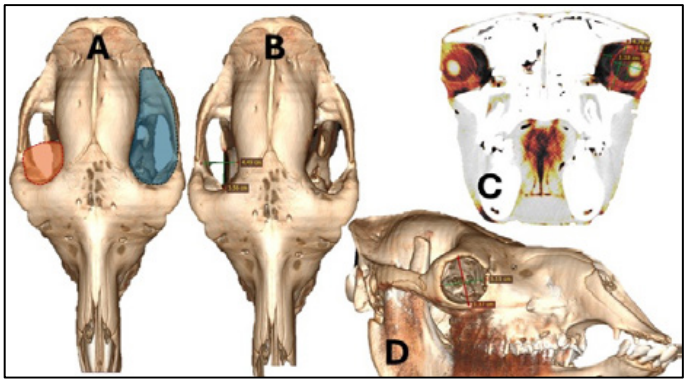

Figure 5: Showing the computed tomographic findings. A) dorsal view of the skull of camel, the orange shaded area is the orbital fossa, blue shaded area is the tempro-orbital fossa. B) dorsal view showing the dimensions of the orbital cavity. C) a slice shoeing the dimensions of the orbital cavity to that of the eye. D) lateral view showing the orbital cavity dimensions

from the rostral aspect of the sclera to the caudal extent of the optic foramen. These muscles are organized into two layers: the outer layer, which includes the recti and oblique muscles, and the inner layer closely adhering to the sclera and the optic nerve caudally. The space between these layers is termed the internal orbital space. Given the anatomical configuration of the orbital and temporo-parietal regions, it is noteworthy that surgical access to the orbital and supraorbital cavities is advantageous through the tempro-orbital fossa. Surgical interventions are indicated for a variety of vital structures, whether located in the temporo-parietal fossa or the orbital cavity. This observation underscores the clinical relevance of understanding the anatomical intricacies of these regions for precise and effective surgical procedures.

Computed tomographic findings

Computed tomographic imaging provided clear visualizations of the temporo-orbital fossa, allowing for precise measurements of the orbital fossa (Figure 5-A and B). Ocular dimensions were accurately documented and subsequently compared to those of the orbital cavity (Figure 5-C). Additionally, measurements of the orbital cavity, obtained from a lateral view, were compared with those of the supraorbital fossa (Figure 5-D). The temporal fossa in camel is extensively large and extended rostrally as orbital fossa. The mean diameter of the orbital fossa was 4.04 cm. While the mean diameter of the orbit rim was 5.24 cm. The mean diameter of the eyeball was 3.32 cm, and the mean diameter of the deep orbital cavity was 4.62 cm. The mean retrobulbar area diameter was 2.98 cm.

Discussion

The current study investigated the anatomic and computed tomographic imaging findings of the temporo-orbital region of the camel with special reference to the orbital cavity. Previous CT studies were conducted to study the paranasal sinuses in buffalos (20), head cavities in donkey (21), anatomical description of Ossimi sheep (22), and anatomy of the head of the one humped camel (23). Results of the current study were in agreement with El Allali, Achaâban (3) and Elsafy et. al., (23). The orbital fossa was large depression with a mean diameter of 4.04 cm bordered caudally with the coronoid process of the mandible, parietal bone medially and bounded by the orbital process of the frontal bone rostrally and zygomatic process laterally as mentioned in previous reports (3, 4, 23). The extensive size of the orbital fossa in camels provides a circular ceiling to the orbital cavity. The orbital fossa is covered by a dense connective tissue fascia and outer skin. There were no large blood vessels or nerves transversing this area. That makes the surgical incision applicable without essential precautions. Following the creation of a skin flap in the orbital fossa, a significantly large periorbital fat body is revealed. This fat serves as a protective cushion for the globe, easing its movements within the orbit (24). The vascularized fat requires ligation before excision to minimize bleeding. Following removal, the orbital cavity is distinctly exposed, with the Tenon's capsule clearly visible. This observation signifies the capability to access the periorbital area for the removal of extraocular lesions (10). Dissecting the Tenon's capsule reveals the extraocular muscular cone. This finding indicates ability for the correction of eye position. Through this approach, the surgeon can manipulate the eyeball both anteriorly and posteriorly. Additionally, the surgeon can readily dissect the posterior attachment of the ocular cone from the bony orbit without applying traction to the eyeball, that safeguards the optic chiasm from trauma, preventing further inflammation or blindness (25). Following the extraction of the eyeball and associated ocular structures through dissection from the bulbar conjunctiva, the

bony orbital cavity becomes fully visible, with the eyelids preserved intact. This finding allows the surgeon to easily apply an orbital prosthesis within the orbital cavity or fill the space with an appropriate sterile filler and facilitate drainage post-surgical procedures. The resulting advantages encompass enhanced healing, diminished infection and inflammation, and improved cosmetic outcomes, all of which are indicative of successful ocular surgeries (25-27). The computed tomographic findings disclosed comparable diameters of the orbit and supraorbital entrance, with a mean diameter approximately 1.2 units less than that of the orbit. This finding reinforces the viability of utilizing the supraorbital window for procedures through the orbital cavity. A continuous study is examining the experimental and clinical application of the described approach for eye enucleation and orbital prosthesis placement. Further investigations are required to assess both short-term and long-term complications associated with this approach.

Conclusion

The supraorbital fossa in camel serves as a secure surgical entrance to the orbital cavity, facilitating various procedures on the periorbital, extraocular, and ocular regions with minimized complications and improved cosmetic outcomes.

Acknowledgements

The author's sincere acknowledgment to the Deanship of Scientific Research at King Faisal University for the continuous support.

Funding. This work was supported through the Annual Funding track by the Deanship of Scientific Research, Vice Presidency for Graduate Studies and Scientific Research, King Faisal University, Saudi Arabia (Proposal Number KFU250352).

References

1. Sisson S, Grossman JD, Getty R. Sisson and Grossman's The anatomy of the domestic animals. 5th ed. Philadelphia: Saunders, 1975.
2. Dyce KM, Sack WO, Wensing CJG. Textbook of veterinary anatomy. 4th ed. St. Louis: Saunders, 2010.
3. El Allali K, Achaâban MR, Ouassat M. Anatomy of the dromedary head skeleton revisited. J Morphol Sci 2017; 34(2): 73–88. doi: 10.4322/jms.100916
4. Emam H, Aref M, Abdelbaset-Ismail A, Abdelaal A, Gouda S, Gomaa M. Description of normal head structures of the one-humped camel (Camelus dromedarius) by magnetic resonance imaging, computed tomography, and cross-sectional anatomy. Vet World 2020; 13(8): 1581–7. doi: 10.14202/vetworld.2020.1581-1587
5. Miller PE. Orbit. In: Maggs DJ, eds. Slatter's Fundamentals of veterinary ophthalmology. 4th ed. Saint Louis: W.B. Saunders, 2008: 352–73.
6. Shilo-Benjamini Y, Pascoe PJ, Maggs DJ, Kass PH, Wisner ER. Retrobulbar and peribulbar regional techniques in cats: a preliminary study in cadavers. Vet Anaesth Analg 2013; 40(6): 623–31. doi: 10.1111/vaa.12060
7. Grimm KA, eds. Veterinary anesthesia and analgesia: the fifth edition of lumb and jones. Hoboken: Wiley, 2015.
8. Berggren K, Wallin Håkansson N. A surgical approach for extensive orbital exenteration in dogs; a description of technique and its application in 4 cases. Vet Ophthalmol 2019; 22(3): 238–45. doi: 10.1111/vop.12583
9. Cheng G, Li B, Li LQ, Gao F, Ren R, Xu X, et al. Review of 1375 enucleations in the tongren eye centre, beijing. Eye 2008; 22(11): 1404–9.
10. Knickelbein KE, Holmberg BJ, Lassaline ME. Equine retrobulbar disease: diagnoses and outcomes of 15 horses with exophthalmos (1988–2017). Equine Vet Educ 2019; 31(11) :601–8. doi: 10.1111/eve.13050
11. Ludwig HC, Pucket JD, Shaw GC. Equine orbital angiomatosis. Equine Vet Educ 2017; 29(8): 426–30. doi: 10.1111/eve.12520
12. Romkes G, Eule JC. Followup of a dog with an ıntraocular silicone prosthesis combined with an extraocular glass prosthesis. Case Rep Vet Med 2012; 2012(1): 762452. doi: 10.1155/2012/762452
13. Provost PJ, Ortenburger AI, Caron JP. Silicone ocular prosthesis in horses: 11 cases (1983-1987). J Am Vet Med Assoc 1989; 194(12): 1764–6.
14. Hamor RE, Roberts SM, Severin GA, Trawnik WR, Johnson WJ. Ocular cosmetic and prosthetic devices. Vet Clin North Am Equine Pract 1992; 8(3) :637–54. doi: 10.1016/s0749-0739(17)30446-7
15. Mazhar Iqbal Siddiqui, Telfah MN. A Guide Book of Camel Surgery. Abu Dhabi: Ministary of economy, 2010.
16. Ranjan R, Nath K, Naranware S, Patil N. Ocular affections in dromedary camel-a prevalence study. Intas Polivet 2016; 17: 348–9.
17. Kassab A. Ultrasonographic and macroscopic anatomy of the enucleated eyes of the buffalo (Bos bubalis) and the one-humped camel (Camelus dromedarius) of different ages. Anat Histol Embryol 2012; 41(1): 7–11. doi: 10.1111/j.1439-0264.2011.01097.x
18. Osuobeni EP, Hamidzada WA. Ultrasonographic determination of the dimensions of ocular components in enucleated eyes of the one-humped camel (Camelus dromedarius). Res Vet Sci 1999; 67(2): 125–9. doi: 10.1053/rvsc.1998.0288
19. Kiliç N, Toplu N, Aydoğan A, Yaygingül R, Ozsoy ŞY. Corneal papilloma associated with papillomavirus in a one-humped camel (Camelus dromedarius). Vet Ophthalmol 2010; 13 Suppl.: 100–2. doi: 10.1111/j.1463-5224.2010.00795.x.
20. Alsafy MA, El-Gendy SA, El Sharaby AA. Anatomic reference for computed tomography of paranasal sinuses and their communication in the Egyptian buffalo (Bubalus bubalis). Anat Histol Embryol 2013; 42(3): 220–31. doi: 10.1111/ahe.12005
21. El-Gendy SA, Alsafy MA, El Sharaby AA. Computed tomography and sectional anatomy of the head cavities in donkey (Equus asinus). Anat Sci Int 2014; 89(3): 140–50. doi: 10.1007/s12565-013-0209-7
22. Alsafy M, Madkour N, Abumandour M, El-Gendy S, Karkoura A. Anatomical description of the head in Ossimi sheep: sectional anatomy and computed tomographic approach. Morphologie 2021; 105(348): 29–44. doi: 10.1016/j.morpho.2020.06.008
23. Alsafy MA, El-Gendy SA, Abumandour MM. Computed tomography and gross anatomical studies on the head of one-humped camel (Camelus dromedarius). Anat Rec (Hoboken) 2014; 297(4): 630–42. doi: 10.1002/ar.22865

24. Plummer CE. Equine orbital fat prolapse. Equine Vet Educ 2014; 26(11): 574–6. doi: 10.1111/eve.12251

25. Betbeze CM, Dray SM, Fontenot RL. Subconjunctival enucleation with orbital implant placement in standing horses: 20 cases (2014-2017). J Am Vet Med Assoc 2021; 258(6): 661–7. doi: 10.2460/javma.258.6.661

26. Thiry C, Holz N, Voelter K, Steiner A, Nuss K, Marchionatti E. Eye enucleation and exenteration in -cattle: a retrospective study of 38 cases (2013-2020). Schweiz Arch Tierheilkd 2022; 164(10): 687–93. doi: 10.17236/sat00368

27. Pierce KE, Townsend WM. Surgery of the globe and orbit. In: Auer JA, eds. Equine surgery. 5th ed. Amsterdam: Elsevier, 2019: 910–27.

Računalniška tomografija in grobe anatomske študije temporomandibularnega in supraorbitalnega področja enogrbe kamele (*Camelus dromedarius*)

M. Marzok, K. M. Alkhodair, M. Nazih, M. W. El-Sherif

Izvleček: Cilj študije je bil raziskati podrobno kirurško anatomijo temporomandibularnega in supraorbitalnega področja pri kamelah z anatomsko disekcijo in računalniško tomografijo (CT). Namen študije je bil zagotoviti natančne anatomske opise in oceniti izvedljivost kirurških posegov v očesni votlini prek očesne jame. Iz fakultetne secirnice in lokalne klavnice smo pridobili dvanajst kameljih lobanj in tri sveže kadavrske glave. Skrbno smo pregledali opisno anatomijo lobanje in kirurško anatomijo temporo-orbitalne regije. Poleg tega smo opravili računalniško tomografijo glav, da bi se povečal nabor podatkov. Rezultate smo sistematično dokumentirali za oceno uporabnosti, izvedljivosti in varnosti pristopa v očesno votlino iz očesne jame. Ugotovili smo, da je senčnična jama kamele precej velika in se razteza rostralno do obsežne očesne jame. Zunanja stena očesne jame je sestavljena iz kože in pod njo ležeče debele fascije. Pri tem nismo ugotovili pomembnih mišic ali vitalnih struktur. V zadnjem delu očnice se je nahajala obsežna orbitalna maščobna masa, po njeni odstranitvi pa smo dosegli jasen in varen vizualni dostop do očesnih struktur, kar je olajšalo pristop. Pristop iz očesne jame je izvedljiv in varen ter omogoča izvajanje različnih kirurških posegov, vključno z enukleacijo, eksenteracijo, odstranitvijo periorbitalnega tumorja, implantacijo proteze in drugimi posegi. Ta pristop obeta boljše estetske rezultate pri izvajanju takšnih posegov.

Ključne besede: enukleacija; kamela; kirurgija orbite; senčna jama

Slov Vet Res
DOI 10.26873/SVR-2101-2024
UDC 636.52/28:69.058.5:546.23
Pages: 177–87

Original Research Article

Effects of Selenium Nanoparticles and Chitosan on Meat Quality, Lipid Profile, Tissue Mineral Content and Tibial Bone Morphometry in Heat Stressed Broilers

Key words

selenium;
nano-selenium;
chitosan;
muscle quality;
lipid status;
tibial bone;
broiler;
heat stress

Ghulam Murtaza Lochi[1], Muhammad Ghiasuddin Shah[1]*, Jameel Ahmed Gandahi[1], Javaid Ali Gadahi[2], Syed Abdul Hadi[1], Abdul Haseeb[3], Noor Sammad Gandahi[1], Abid Hussain[3]

[1]Department of Anatomy and Histology, Faculty of Animal Husbandry & Veterinary Sciences Sindh Agriculture University Tandojam, Sindh Pakistan, [2]Department of Veterinary Parasitology, Faculty of Animal Husbandry & Veterinary Sciences Sindh Agriculture University Tandojam, Sindh Pakistan, [3]Faculty of Veterinary and Animal Sciences, Azad Jammu and Kashmir University of Bhimber, Azad Kashmir Pakistan

***Corresponding author:** ghias_shah@yahoo.com

Abstract: This study aimed to assess the effects of selenium and selenium nanoparticles with chitosan on broiler chickens during heat stress. In this study, total 336 chicks were raised. These birds were split into seven groups, each with six sets of eight birds, depending on the treatments they received. There were two control groups: one with the regular diet (negative control) and another with the regular diet plus heat stress (positive control) known as A and B Groups respectively. The remaining groups were as follows: Group-C (Basal diet+0.3mg/kg selenium), Group-D (Basal diet + 0.3mg/kg nano selenium + heat stress), Group-E (basal diet+300mg/kg chitosan+heat stress), Group-F (basal diet+0.3mg/kg selenium+300mg/kg chitosan+ heat stress) and Group-G (0.3mg nano selenium + 300mg/kg chitosan/+basal diet + heat stress). The various parameters were analyzed, including drip loss, cooking loss, lipid profiles, mineral content, and bone characteristics was significantly improved in Group G, receiving nano selenium and chitosan under heat stress. Moreover, Group G showed higher selenium, calcium, and phosphorus content in breast muscle tissue, along with tibial bone characteristics such as weight, length, wall thickness, density, and medullary canal diameter as compared to group-B. Although weight/length index showed no significant differences, Group G demonstrated the highest Tibiotarsal Index (TTI) and Robusticity Index (RI). These findings suggest the beneficial effects of nano selenium and chitosan supplementation, particularly evident under heat stress conditions.

Received: 23 August 2024
Accepted: 30 December 2024

Introduction

TDue to the environmental changes, the poultry industry is facing economic and production loss. It is associated that when the temperature crosses the normal range, birds adjust the metabolic heat to maintain their physiological status (1). Heat stress leads to physiological variation accompanied by hormonal changes and reduced feed intake that leads to a loss in production and physiological performance. Heat stress intensively enhances Reactive Oxygen Species (ROS) production in poultry that critically affects the chemical changes that indicates stress in birds (2).

Selenium is an important micro-mineral required in the trace by all animals. It plays a vital role in a wide range of physiological functions, primarily as a well-known antioxidant, used in poultry and small and large ruminants. The main source of this mineral comes from the soil present in animal feed (3).

The emergence of nanotechnology over the past three decades has revolutionized the understanding of drug delivery and its impact on livestock, particularly in poultry. This advancement has significantly contributed to Pathophysiology and treatment options (4). Due to its unique physio-chemical optical electric and thermal properties, selenium is widely used for drug delivery, enhancing bioavailability, as well as production, and performance. These physicochemical properties undergo transformation compared to the original material (5). The application of selenium nanoparticles has already demonstrated several benefits, such as enhanced absorption, enhanced bioavailability, antimicrobial activity, and positive effects on growth performance, Feed Conversion Ratio (FCR), decreased mortality rate, and minimized drip loss (6, 7). Moreover, Selenium supplementation positively effect on plasma lipid status, the lower level of Low Density Lipids (LDL), cholesterol, Triglycerides (TG) and High Density Lipids (HDL) (8).

Skeletal development plays a significant role in body growth. Recently it has been recognized that rapid body growth has adverse effects on bone mineralization (9). The carcass of certain broiler chickens exhibit distinct change in the appearance of breast meat, characterized by pale color and reduced water-holding capacity, as well as dark and dry muscles with altered functional properties (10). These alterations have significant implications for meat quality, leading to substantial economic cost and affecting's carcass characteristics, growth rate, and susceptibility to heat and transport stress during farming practices (11).

The addition of simple and selenium nanoparticles in poultry feed resulted the high absorption and an increase in selenium levels in serum and tissue (12). This improved retention of selenium has been associated with various benefits, including improved the productivity, morpho-histological architecture of intestine, lipid and immune profile, antioxidant profile, mineral absorption, and skeletal muscles and meat quality (13).

Chitosan, a natural polysaccharide derived from marine sources in the form of chitin, has gained considerable attention as a feed additive. It serve as both a drug delivery carrier and source of trace nano minerals (14). Chitosan exhibits multifunctional properties and finds application in animals nutrition (15). Supplementation of chitosan under heat-stressed conditions in poultry contributes to bone parameters (16) immune, antioxidant, performance, disease prevention, gastrointestinal health, and muscles parameters in poultry (17, 18).

Supplementation with selenium and chitosan has shown beneficial effects on poultry health and production. Therefore, this study aims to assess the impact of both selenium and nano-selenium combined with chitosan on lipid profile, meat quality, bone health, and mineral content in broiler chickens under heat stress conditions.

Material and methods

Ethics Statement

All experimental procedures involving the handling of birds in this study were conducted in concordance with the "Guidelines for Experimental Animals". The animal use protocol has been reviewed and approved by the Sindh Agriculture University Animal Ethical and Welfare Committee (DAS/2134/ of 2021).

Experiment Design

This study was performed on 336-day-old Cobb birds, purchased from the local market, and brought to the poultry experimental station, Faculty of Animal Husbandry and Veterinary Science, Sindh Agriculture University Tandojam Sindh. Before the arrival of the chicks, the proper brooding, feeding, temperature, and humidity about 35±1°C and 65% was sustained during brooding time gradually reduced thereafter according to the (19).

After the arrival of the chicks, the birds were weighed and placed together for brooding in deep litter system, all the feeding and management protocols accordance with brooding standards were followed as recommended by Aviagen, (19). On the 21st day, the chicks were divided in seven treatments groups. The treatment groups were as follows: Group-A: Negative control fed with Basal diet under normal temperature, Group-B: Positive control fed Basal diet under heat stress, Group-C: fed with 0.3mg/kg of selenium under heat stress, Group-D: fed with 0.3mg/kg selenium nanoparticles under heat stress, Group-E: fed 300mg/kg of chitosan under heat stress, Group-F: fed with selenium 0.3mg/kg and 300mg/kg of chitosan under heat stress and Group-G: fed with selenium nanoparticles 0.3mg/kg with chitosan 300mg/kg feed under heat stress.

Temperature Management

After arrival of the chicks, the temperature was maintained according the brooding standers recommended by (19). Initially temperature was maintained around 35±1°C on first day and relative humidity was about 65% and gradually decreased to reach a thermoneutral zone (26°C) after weekly reduction of 2.8°C with similar relative humidity at 21st day.

During the experiment, two environmental conditions were utilized from day 21st to 42nd day study period:

Table 1: Ingredients composition of the broiler diet

Ingredients (g/kg)	Starter/grower	Finisher
Corn	344.0	320.0
Rice polish	73.0	80.0
Canola meal	77.0	90.0
Rice tip	145.0	140
Corn gluten 60 %	35.0	40.0
Soybean meal	235.0	240.0
Limestone	11.0	10.0
D-L Methionine	1.2	1.0
L-Lysine	1.9	2.0
Threonine	1.3	1.5
Soy oil	17.0	18.5
DCP	13.0	15.0
Vitamin Premix	2.6	2.0
Molasses	43.0	40.0
Analyzed Nutritive Values		
ME, Kcal/kg	3000	3200
Dry Matter (%)	91.98	91.27
Crude protein (%)	22.93	20.40
Ash (%)	2.11	2.15
Crude fat (%)	4.01	5.05
Crude Fiber (%)	4.11	5.15

*The premix supplied per kg of diet: vit A, 12,000IU; vit-D3, 5000 IU; vit K, 2.55 mg; Vit, B1, 3 mg; Vit B2,7.5 mg; Vit B3, 51 mg, Vit B5, 13.5mg, vit B6, 4.5 mg; Vit B7, 0.2 mg, Vit B12, 0.02 mg; folic acid, 1.5 mg;; choline chloride, 250 mg

thermoneutral conditions (TN) set at 26°C and relative humidity 65±5%, where the cyclic heat stress applied to birds, with temperatures of 35°C for 8 hours and 26°C for the remaining hours of the day.

Vaccination

The vaccinations against infectious Bronchitis virus (IBV) (H120) were administered through drinking water on the first day, while vaccination against Newcastle disease were given on 8th and 21st day. Additionally, the chicks were vaccinated against flu (first day), and infectious bursal disease (IBD071IR; 14 and 23 days) during the period of study.

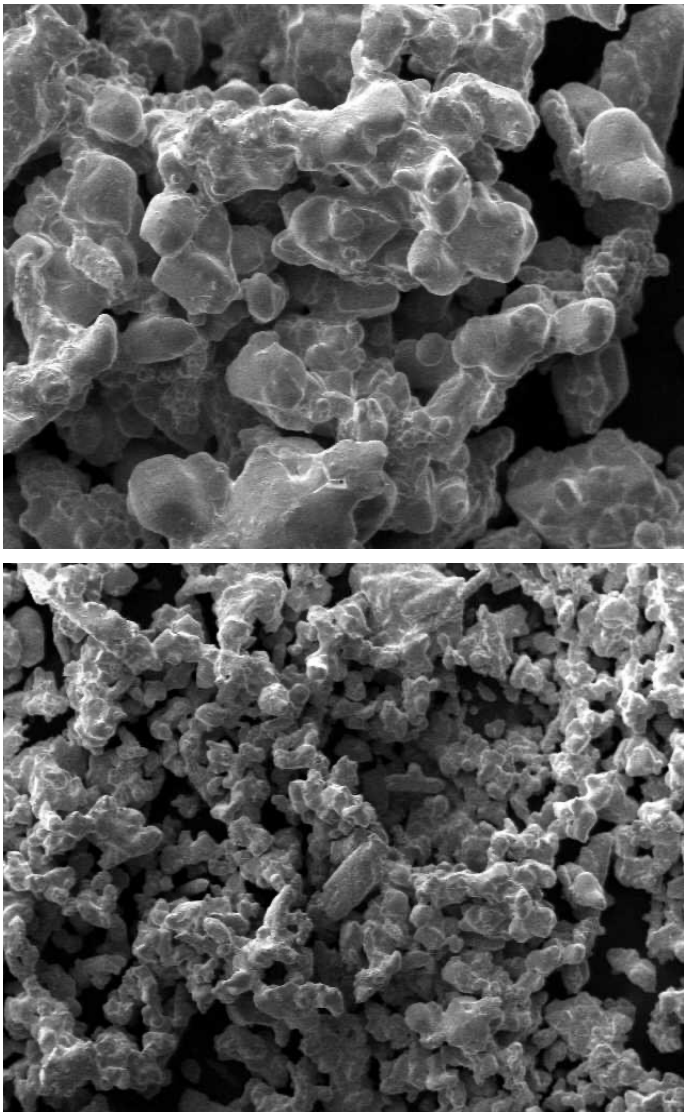

Figure 1: Scanning Electronic Microscopic (SEM) picture of selenium nano particles. Micrographs showing morphological texture of Nano particles on higher (a) and lower (b) resolution

Feeding plan

During the research, the birds were fed with commercial corn based diet according the recommendation by Aviagen, (19) from day 1st to 42nd day of the research. The birds were accessed to water and feed ad-lib. The proposed ratio of ingredients were formulated as recommended by NRC (20) guidelines (Table 1).

Simple Selenium, selenium nanoparticles and chitosan

Selenium (organic Se) was purchased from scientific store and sent to the National Centre of Excellence in Analytical Chemistry (NCEAC), University of Sindh Jamshoro for the

preparation of Nanoparticles, and for the confirmation of the synthesized, accuracy and size (range 100nm) different laboratory test were performed.

Procedure of Synthesis of selenium nanoparticles

Selenium nanoparticles were examined using low- and high-resolution scanning electron microscopy images (SEM), as shown in Figure 1 (a and b). Moreover, the elemental composition of selenium nanoparticles was analyzed using an EDX microanalysis device linked to the scanning electron microscope in chosen portions of SEM slices.

The procedure for the synthesis of simple selenium in nanoparticles separated Bovine serum, Albumin lipase and protease (*Sigma Aldrich Labs*) were purchased. Each protein aliquot (0.1g) was combined with 50 ml of sodium selenite (0.1g) and autoclaved at 121°C, and 15–20 pressure for 20 minutes under standard sterilizing conditions. Nanoparticles were purified by centrifugation at 12,000rpm for 10 minutes, and the supernatant was then discarded. The protein-containing nanoparticles were washed three times with deionized water at room temperature. Fourier-transform infrared spectroscopy and Scanning Electronic Microscopy were performed to verify the size and structure of the nanoparticles, as followed by (21);(22), and (23).

Scanning Electronic Microscopy of selenium nanoparticle

Scanning Electronic Microscopy (SEM) was employed to examine the morphology and form of selenium nanoparticles. A single drop of the nanoparticle suspension was placed on a sample holder for analysis.

Structural Analysis of Nanoparticles through Infrared

This technique was used to determine the surface characterization of selenium nanoparticles by using FTIR (Fourier Transformer Infrared) Spectrophotometer (Shimadzu 8400-Japan 1997). FTIR is a vital analytical technique that is usually used to study the surface functionalities of materials.

Sampling

On the 42nd day of the study, birds were randomly selected from each replications and after blood collection the birds were euthanized by cervical dislocation. The birds from each group (two birds from each replication) were randomly selected for sampling.

Blood samples for lipid status testing

Blood samples were collected form brachial vein before the euthanasia and the sample was shifted in the blood collecting tubes containing EDTA. For obtaining plasma, the blood samples were centrifuge at 1500rpm for 10minutes. Cholesterol concentration was determined by using cholesterol assay kit (Abcam-ab65390) following the methods (24, 25).

Water Holding Capacity (WHC)

The left superficial pectoral muscles about 1cm^3 were wrapped in a labeled in inflated plastic bags. Honikels gravimetric method (26) was used by measuring the WHC in meat through following formula.

Muscles pH

The sample of pectoral muscles were used for pH in two intervals of the time like 0 and 12hrs after slaughter, using the pH meter LOHAND Model-pH2601. The pH was obtained 2.5cm below the depth of surface.

$$\frac{WHC= W_1 - W_2 \times 100}{W_1}$$

Cooking Loss (CL) of meat

The 20gms of breast muscles (*Pectoralis Major*) samples were taken, weighted and cooked in hot water bath on internal temperature about 80°C for Cooking Loss (CL) as followed by (27). The CL was found according to the given formula.

$$\frac{CL\%= \text{Initial Weight -Final Weight} \times 100}{\text{Initial weight}}$$

Drip loss (DL) %

The collected meat sample from pectoral muscle was stored at 4°C for 24H, and expressed at the amount (%) of weight loss, this method was followed by (16, 28).

Bone parameters

The tibia bone of each broiler was separated and labeled carefully. The bone was boiled at 100°C in water for 10 minutes and cooled at room temperature. The bone were unfleshed, and air dried for 24 hours as followed by Harash et al., (29) and Yan et al., (30).

The tibia bone width and length were measured by a digital vernier caliper, and weight through electrical balance. Each bone diameter was measured outside and marked at middle of the bone body (Shaft). After breaking the bone at the mid-shaft, the diameter of the medullary canal was measured with a digital vernier caliper. The bone weight/ length index was determined by dividing the bone weight by its length and from the bone length and cube root of bone weight bone robusticity index was found outby Ndubuisi

et al., (31), Shim et al., (32) and (33)The index of tibiotarsal was determined from the diameter of the diaphysis and medullary canal (34).

Mineral concentration in muscles.

For determination of the concentration of minerals of muscles, the acid digestion of dried ash of pectoral muscles (1gram) was poured in HCl in a ratio of 1:10 and filtered with (Whatman Grade No.1) after the addition of Milli-Q water (Millipore Corporation, Bedford MA, USA) according to the method of (35, 36) and the final solution was adjusted with 50ml distilled water. The Selenium (Se) was analyzed through atomic absorption spectrophotometer (Varian SpectrAA 55B), and Calcium levels were measured through a flame photometer (Systonic-S-935), and phosphorus spectrophotometer.

Statistical Design

Data was presented as Mean ± Standard Error of Mean and was statistically analyzed using SSPSS (Version 20.0) and Turkey test was applied to determine the significant level in groups. The group means was analyzed using one-way ANOVA, with a significant level set at $p < 0.05$.

Results

Morphology and Texture Elucidation of selenium nanoparticles

SEM images show some rectangular and irregular textures of selenium nanoparticles. The EDX spectra disclosed a maximum percentage of selenium which suggests the successful nano selenium synthesis.

Fourier Transformer – Infrared Spectrophotometer (FTIR) studies

The strong absorption peaks at 1649 and 1551cm-1 signify the distinctive vibrations of amide I and C-H groups within the CH2 segments of the protein structure. These features are indicative of the presence of albumin, which serves as the stabilizing and enclosing element around the selenium nanoparticles (Figure 2).

Ultraviolet-Visible spectroscopy studies

The formation of selenium nanoparticles is observed through UV-Vis (Ultraviolet Visible Spectroscopy) with range wavelength from 200-800nm at various intervals. The UV–Visible of C spectrum protein washed with gel (SDS-Page Gel) having 30 kDa molecular weight molecular weight of 30 kDa, in this sense the peak absorption 210nm showed as peak or strong absorption in corresponding to peptide bonds and amino residues at 280nm and these reducing agents help in formation of nanoparticles (Figure 3).

Meat Quality

The effect of selenium, and nano selenium with chitosan on meat quality under heat stress shown in Table- 2. The initial and ultimate pH value of the meat were significantly improved in G followed by group F, D, E, A on the 42nd of study whereas the lowest initial and ultimate pH value (6.20±.03 and 5.43±.04) were observed in group B which was subjected to heat stress. Drip loss and cooking loss were positively affected by group-G exhibited the lowest drip loss (2.35±0.36 %) and cooking loss (35.43±1.56 %) followed by group F, D, E, A as compared with lowest values in group-B fed with basal diet and during heat stress.

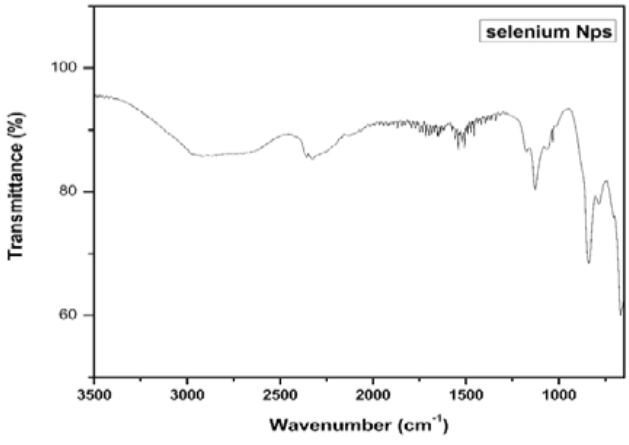

Figure 2: Fourier transformer – infrared spectrophotometer studies showed the strong absorption peaks (1649 and 1551cm-1)

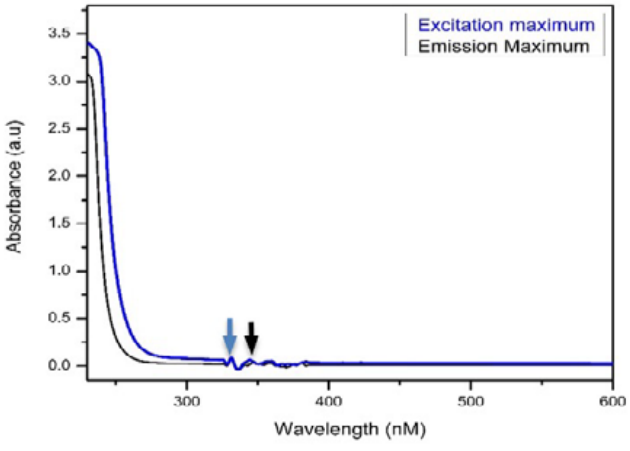

Figure 3: Ultraviolet Visible spectroscopy studies of selenium nanoparticles showing peak absorption 210 and 280nm

Table 2: Effect of selenium and nano selenium with chitosan on muscle quality and serum indices under heat stress

		Groups							P-value
		A	B	C	D	E	F	G	
Meat quality	pHi	6.30±.04^{ab}	6.20±.03^{ab}	6.44±.04^{ab}	6.58±.05^{ab}	6.34±.02^{ab}	6.46±.05^{ab}	6.56±.04^{a}	0.001
	pHf	5.96±.03^{a}	5.43±.04^{b}	5.73±.03^{ab}	5.75±.03^{ab}	5.65±.03^{ab}	5.92±.03^{ab}	6.10±.07^{a}	0.013
	WHC%	4.96 ±.29^{ab}	4.01 ±.33^{c}	4.82±.34^{b}	4.86 ±.17^{b}	4.91 ±.01^{ab}	4.97 ±.13^{a}	4.99 ±.23^{a}	0.012
	DL %	2.71±0.31^{ab}	2.95±0.62^{a}	2.65±0.33^{ab}	2.50±0.39^{bc}	2.56±0.43^{bc}	2.45±.060^{bc}	2.35±0.36^{c}	0.016
	CL %	40.42±2.4^{b}	40.90±1.21^{b}	39.15±0.32^{c}	38.98±2.21^{c}	39.57±0.41^{c}	37.34±2.96^{bc}	35.43±1.56^{d}	0.001
Serum indices	CHOL (mg/dl)	132.3±3.4^{b}	180±6.4^{a}	136.6±4.4^{bc}	130.7±6.3^{bc}	135±3.1^{bc}	115±5.6^{d}	112.6±4.6^{d}	0.023
	HDL (mg/dl)	61.7±2.3^{b}	53.5±1.5^{d}	58.1±1.2^{bc}	60.3±1.3^{bc}	59.3±1.6^{bc}	61.3±1.6^{b}	64.6±2.1^{a}	0.001
	LDL (mg/dl)	81.6±1.2^{b}	93.4±.2.1^{a}	60.2±1.3^{c}	45.4±2.1^{cd}	50.4±2.3^{cd}	41.6±1.3^{cd}	38.4±1.4^{e}	0.000
	TG (mg/dl)	60.2±2.3^{b}	63.3±1.9^{a}	56.6±2.7^{c}	54.8±2.4^{c}	55.8±1.7^{c}	51.9±.6^{cd}	50.2±.8^{d}	0.001

a–dmeans with different superscripts are significantly different(P<0.05) within the same row, HS= Heat Stress; Se= Selenium; Serum Lipids (mg/dL-1), NC* Negative Control and PC* Positive Control: NPs* Nanoparticles; WHC-Water Holding Capacity; pHi= Initial pH at 0 hour; pHu= pH Ultimate pH after 12hours; DL= Droop loss ; CL= Cooking loss, CHOL= Cholesterol, HDL-Hight Density Lipids, LDL- Low Density Lipids, TG- Triglycerides,

Table 3: Effect of selenium and nano selenium with chitosan on minerals in muscles of heat stressed of broiler

	Groups							P-value
	A	B	C	D	E	F	G	
Se (µg/g)	0.11^{f} ±0.03	0.08^{g} ±0.02	0.14^{e} ±0.01	0.21^{c} ±0.01	0.18^{d} ±0.01	0.24^{b} ±0.09	0.29^{a} ±0.01	0.01
Ca (mg/g)	0.22^{f} ±0.10	0.19^{g} ±0.09	0.23^{e} ±0.33	0.27^{c} ±0.06	0.25^{d} ±0.05	0.28^{b} ±0.03	0.29^{a} ±0.04	0.01
P (mg/g)	7.14^{f} ±0.06	6.81^{f} ±0.08	7.24^{de} ±0.06	7.37^{c} ±0.01	7.34^{cd} ±0.01	7.53^{b} ±0.02	7.66^{a} ±0.01	0.01

a–gmeans with different superscripts are significantly different(P<0.05) within the same row, HS= Heat Stress; Se= Selenium;), NC* Negative Control and PC* Positive Control: NPs* Nanoparticles; Se- Selenium, Ca- Calcium, P- Phosphorus

Serum Cholesterol Level

Table 2 presents effect of selenium and nano selenium with chitosan, on lipid status, specifically the cholesterol, under heat stress. The supplementation of nano selenium and chitosan improves the lipid profile in broilers. The cholesterol level was significantly improved in Group followed by group-F, D, C, E and A, whereas the lowest values were found in group-B.

The maximum LDL status was observed in group-G whereas, the minimum LDL level was observed in group-B fed with basal diet and heat stress. The maximum HDL level was observed in group G fed with Nanoselenium and chitosan during heat stress, while the HDL values were decreased in group B subjected to heat stress Triglyceride (TG) levels increased during heat stress, with the highest level observed in group B and the lowest level observed in group G.

Mineral indices

The deposition of minerals in breast muscle tissue content is affected by heat stress because of disturbance in absorption of minerals and physiological status. Table 3 shows breast muscle tissue selenium content was significantly higher (0.29±0.01µg/g) in group G followed by group F, D, E, C and A (0.24±0.09µg/g, 0.21±0.01 µg/g, 0.18±0.01µg/g, 0.14±0.09 and 0.11±0.03 respectively). The lower Selenium was found in group B where birds feed basal diet with heat stress (0.08±0.02µg/g). Whereas the maximum calcium content (0.29±0.04mg/g) was observed in group G followed by F, D, E, C and A resulted (0.28±0.03mg/g, 0.27±0.06, 0.25±0.05mg/g, 0.23±0.33mg/g and 0.22±0.10mg/g) respectively (Fig. 4.2). While the minimum calcium (0.19±0.09mg/g) was observed in group B fed with basal diet and heat stress. Table 3 shows the maximum phosphorous (7.66±0.01mg/g) in group G followed by group F, D, E, C and A calculated as 7.53±0.02mg/g, 7.37±0.01mg/g, 7.34±0.01 mg/g, 7.24 and 7.14±0.06mg/g respectively. While the

Table 4: Effect of selenium and nano selenium with Chitosan on tibia bone morphometry of under heat stress

Parameter	Groups							P-value
	A	B	C	D	E	F	G	
TBW (g)	5.29±.05^{ab}	4.65±.06^{d}	5.20±01^{bc}	5.33±.02^{bc}	5.10±.04^{bc}	5.90±.09^{ab}	6.15±.07^{a}	0.02
TBL (mm)	88.45±.04^{ab}	75.34±.29^{d}	85.33±.04^{c}	90.54±.15^{ab}	83.32±.06^{c}	90.67±.15^{ab}	94.55±.19^{a}	0.01
TBWT (mm)	6.57±.016^{a}	4.98±.049^{c}	5.63±.066^{b}	5..83±.013^{b}	5.59±.151^{b}	6.25.01±.042^{a}	6.65±.024^{a}	0.03
TBD (mm)	6.17±.01^{a}	5.21±.03^{c}	5.82±.05^{b}	6.12±.02^{a}	5.72±.0.8^{b}	6.47±.06^{a}	6.67±.06^{a}	0.01
MCD (mm)	4.10±.03^{ab}	3.41±.20^{c}	3.87±.04^{c}	4.09±.07^{b}	3.78±.30^{c}	4.32±.15^{ab}	4.78±.05^{a}	0.01
W/L index	46.51±.05	44.60±.02	44.91±.03	46.75±.04	45.93±.01	46.87±.13^{a}	46.97±.17	0.41
TTI	40.34±.23^{ab}	37.70±.76^{c}	39.01±.21^{ab}	41.55±.37^{ab}	40.60±.50^{ab}	41.86±.39^{ab}	43.86±.65^{a}	0.02
RI	48.22±.58^{a}	42.48±.20^{c}	46.21±.71^{b}	46.31±.51^{b}	45.53±.44^{b}	46.89±.35^{b}	48.49±.41^{a}	0.00

a–eWith in the same row, means with different superscripts are significantly different(P<0.05). Values represent the Mean ± SEM of five replicates. HS: Heat stress; COS: Chitosan ; Se: Selenium TBW- Tibia Bone Weight (TBL) Tibia Bone Length, TBWT Tibia Bone Wall Thickness; (TBD) Tibial Bone Density (MCD) Medullary Canal Diameter; (W/L I) Weight Length Index (TTI) Tibio Tarsal Index, (RI) Robusticity Index (N/C)*Negative control (PC*) Positive control. : NPs* Nanoparticle.

minimum phosphorous level (6.81±0.08mg/g) was noticed in group B. Results show that mineral indices were much affected by heat stress and selenium nanoparticles and chitosan alleviated the effects of heat stress.

Tibial bone morphometry

The tibial bone morphometry was analyzed to determine the effects of selenium and nano selenium with chitosan under heat stress, as shown in Table 4. Group-G exhibited significantly higher tibia bone weight (6.15±0.7 g) and tibia bone length (94.55±.19 mm) compared to group B, which had the lowest values (4.65±0.06 g and 75.64±0.29 mm respectively). The tibia bone wall thickness was also significantly affected by selenium and nano selenium with chitosan under heat stress. The maximum tibia bone wall thickness (6.65±0.02 mm) was observed in group G, while the minimum tibia bone wall thickness (4.98±0.49 mm) was observed in group B. Tibia bone density showed a statistically significant difference, with the highest density (6.67±0.06 mm) in group G and the lowest density (5.21±0.03 mm) in group B. The maximum medullary canal diameter (4.78±0.05 mm) was observed in group G, while the minimum diameter (3.42±0.20 mm) was observed in group B under heat stress. The weight/length index was not significantly affected by selenium and nano selenium with chitosan. The maximum tibiotarsal index (43.86±0.65) was observed in group G, while the minimum tibial tarsal index (37.70±0.76) was observed in group B. The robusticity index also showed significant differences, with the maximum index (48.49±0.41) in group G and the minimum index (42.28±0.20) in group B under heat stress.

Discussion

Selenium is an important mineral for maintaining animal health (37) as it plays various roles in physiological functions. In this study, we evaluate the effect of selenium and nano-selenium, along with chitosan on heat-stressed broiler. The hypothesis was that supplementation with different minerals and prebiotics would improve the physiological change induced by heat stress.

The results we found align with previous research. Some authors (38-40) had reported significant changes in pH and water holding capacity of muscles due to factors like lactic acid accumulation, glycolysis, ATP hydrolyzation, and hormonal release. Other research (35, 41) indicated that selenium in combination with chitosan affects the pH of the muscles, in the broiler because of the change in the muscles modulation. Wang et al., (39) concluded that heat exposure increased the release of hormones and accelerate the glycolysis resulting decline of pH. Additionally, studies by Oliveira et al., (42); Wang et al., (43), and Bakhshalinejad et al., (44) observed slight variations in meat pH within 24 hours due to the crucial role of muscle in absorbing and retaining water, which greatly impacts meat quality. Mir et al., (45) reported the pH directly influenced on meat quality aspects like tenderness, water holding capacity, color, juiciness, and shelf life and higher pH levels correspond to greater water holding capacity and that color can serve as an indicator of pH levels. However, Boiago et al., (46), and Calvo et al., (47) reported that organic selenium sources raise chicken meat pH, enhancing the muscle's ability to retain water within cells, which is crucial for muscle integrity and reduces drip loss (35, 48).

The drip loss and cooking loss values were significantly improved in group-G followed by Group-F, D, C, E and A fed with different levels of selenium and chitosan. These findings agreed with Zhou et al., (49) who concluded that birds fed 0.3 mg/kg had a lower loss due to improved cell membrane integrity. Other studies by Perić et al.,(48) and Boiago et al., (46), supported selenium's role in maintaining muscle cell integrity, promoting weight retention, and minimizing cooking losses. Cai et al.,(50) also highlighted who selenium nanoparticles improve the muscle's ability to attract and retain water within cells. Mir et al.,(45) emphasized the direct impact of water retention on muscle color and texture, considering it as crucial material for the body.

The Studies related to the muscles was mentioned by Zaboli et al., (51), Mohammadi et al., (52),and Calvo et al., (47) correlated that the breast muscle variability and color in males to pH effects, showcasing implications for shelf life, water holding capacity, and cooking loss. Observations from the study revealed that Group B (Basal Diet and Heat Stress) was highly affected by heat stress, resulting in increased drip and cooking losses. This correlates with findings from (49), (53),(1), (54),(51), and (41) indicating that heat stress decreases water absorption in muscles. Similar conclusions were drawn by Yang et al., (40) and Tahir et al., (55) showing that in broilers, selenium nano and chitosan decrease drip and cooking losses due to their water absorption capabilities.

It was observed from the present study that nano selenium has a noticeable effect on tissue selenium content. The selenium (Se), Calcium (Ca) and Phosphorus (P) content in muscles was significantly higher (P>0,05) in group-F fed with selenium nanoparticles and chitosan. The lowest tissue mineral content was found in group B (BD and HS) it may be due to slow turnover in tissue. Previous research highlighted that a dietary supplement of nano selenium at around 0.3mg/kg influenced both meat and blood selenium content (35, 56). This effect might stem from nanoparticles having better absorption rates compared to regular selenium, leading to higher elimination levels. Additionally (52),(12), and (57) reported that nano selenium enhances selenium concentration in muscle tissues, particularly during heat stress in broilers, echoing findings mentioned by Dukare et al.,(57).

Schrauzer, (58) emphasized that organic selenium deposition in tissues, especially in breast and thigh muscles, surpasses that of inorganic selenium, indicating a higher tendency for organic selenium to accumulate in these specific muscle areas.

The statistical analysis of lipid status within the groups revealed interesting trends. In Group-G, there was a notably favorable outcome for High-Density Lipoprotein (HDL), while Low-Density Lipoprotein (LDL) and Triglyceride levels were significantly higher in Group-B, followed by A, C, D, E, F, and G, in that order.

Selim et al., (2015) noted that LDL serum concentrations remained unaffected prior to heat stress, suggesting minimal changes under those conditions. Furthermore, (59) indicated that cholesterol and triglyceride levels showed significant improvements in trials involving different durations, particularly when a combination of selenium nanoparticles and increased chitosan levels was administered. Studies by Kassim et al., (60) and Bami et al., (41) supported the notion that supplementing selenium (at 0.3mg/kg feed) with chitosan resulted in higher concentrations and improved blood serum indices. Additionally, (61) reported that selenium nanoparticles had the potential to enhance plasma lipoprotein levels, particularly during heat stress, aligning with findings from Ahmad et al., (62).

Bones serve several vital roles in the body, providing support, housing blood cell generation, safeguarding organs, and storing essential minerals. These findings for bone morphometry revealed a direct correlation between bone quality and growth. Group-G showed significant improvements in weight, length, width, diameter, and bone indexes compared to other groups like group F, D, C, E and A. This indicates that the growth rate, muscle quality, and various performance parameters were notably enhanced in the group fed with selenium nano and chitosan compared to those given only selenium. This suggests that mineral intensity impacted the mineral content, length, and width of the tibial bone (63). These results agreed with Savaram et al., (64), Ndubuisi et al., (31), Shah et al., (33), and Rehman et al., (65) indicating that mineral supplementation positively affected tibial strength compared to control groups. Heat stress, as indicated by(32) alters mineral absorption, leading to more porous bones compared to treatment groups. Moreover, Shah et al., (33) and Naz et al., (66) found that mineral supplementation affected tibial length. Savaram et al.,(64) mentioned that a diet low in selenium content reduces bone volume, mineral density, and the weight of bones. Recently, Yang et al.,(67) explored the impact of nano selenium on bone health. They highlighted its importance in selenoprotein synthesis and its crucial role in proper growth and skeletal development. These collective findings underscore the significance of mineral supplementation, especially nano selenium, in enhancing bone quality, growth, and overall skeletal health.

Conclusion

In conclusion, this study demonstrated that supplementation with, selenium nano particles and chitosan had beneficial effects on hematology, muscle quality, pH, water holding capacity, drip loss, cooking loss, tissue mineral content, lipid status, and bone morphometry in heat-stressed broilers. Furthermore, this study highlights the potential

of nano selenium and chitosan as effective interventions to mitigate the negative impacts of heat stress on broiler production and performance.

Acknowledgements

Conflict of Interest. All authors have no conflict of interest.

References

1. Song D, King A. Effects of heat stress on broiler meat quality. World's Poult Sci J 2015; 71(4): 701–9. doi: 10.1017/S0043933915002421
2. Seaman C, Moritz J, Falkenstein E, Van Dyke K, Casotti G, Klandorf H. Inosine ameliorates the effects of hemin-induced oxidative stress in broilers. Comp Biochem Physiol A Mol Integr Physiol 2008; 151(4): 670–5. doi: 10.1016/j.cbpa.2008.08.014.
3. Samo, S.P., et al., Effect of Organic Selenium Supplementation in Diet on Gastrointestinal Tract Performance and Meat Quality of Goat. Pakistan J Zool 2018; 50(3): 995–1001. doi: 10.17582/journal.pjz/2018.50.3.995.1001
4. Peer D, Karp JM, Hong S, Farokhzad OC, Margalit R, Langer R. Nanocarriers as an emerging platform for cancer therapy. Nat Nanotechnol 2007; 2(7): 751–60. doi: 10.1038/nnano.2007.387
5. Hartemann P, et al. Nanosilver: Safety, health and environmental effects and role in antimicrobial resistance. Mater Today 2015; 18(3): 122–3. doi: 10.1016/j.mattod.2015.02.014
6. Tayeb İ, Qader GK. Effect of feed supplementation of selenium and vitamin E on production performance and some hematological parameters of broiler. KSÜ Doğa Bil Derg 2012; 15(3): 46–56.
7. Kumar A, Prasad KS. Role of nano-selenium in health and environment. J Biotechnol 2021; 325: 152–63. doi: 10.1016/j.jbiotec.2020.11.004
8. Iizuka, Y, Sakurai E, Tanaka Y. Effect of selenium on serum, hepatic and lipoprotein lipids concentration in rats fed on a high-cholesterol diet. Yakugaku Zasshi 2001; 121(1): 93–6. doi: 10.1248/yakushi.121.93
9. Williams B, Waddington D, Murray DH, Farquharson C. Bone strength during growth: influence of growth rate on cortical porosity and mineralization. Calcif Tissue Int 2004; 74(3): 236–45. doi: 10.1007/s00223-002-2124-0
10. Zhang ZY, Jia GQ, Zuo JJ, Zhang Y, Lei J, Ren L, Feng DY. Effects of constant and cyclic heat stress on muscle metabolism and meat quality of broiler breast fillet and thigh meat. Poult Sci 2012; 91(11): 2931–7. doi: 10.3382/ps.2012-02255
11. Trocino, A, et al. Impact of pre-slaughter transport conditions on stress response, carcass traits, and meat quality in growing rabbits. Meat Sci 2018; 146: 68–74. doi: 10.1016/j.meatsci.2018.07.035
12. Hu C, Li YI, Xiong L, Zhang HM, Song J, Xia MS. Comparative effects of nano elemental selenium and sodium selenite on selenium retention in broiler chickens. Anim Feed Sci Technol 2012; 177(3/4): 204–10. doi: 10.1016/j.anifeedsci.2012.08.010
13. Elkhateeb FSO, Ghazalah AA, Lohakare J, Abdel-Wareth AAA. Selenium nanoparticle inclusion in broiler diets for enhancing sustainable production and health. Sci Rep 2024; 14(1): 18557. doi: 10.1038/s41598-024-67399-7
14. Yadav H, Malviya R, Kaushik N. Chitosan in biomedicine: a comprehensive review of recent developments. Carbohydr Polym Technol Appl 2024; 8: 100551. doi: 10.1016/j.carpta.2024.100551
15. Uyanga VA, Ejeromedoghene O, Lambo MT. Chitosan and chitosan-based composites as beneficial compounds for animal health: impact on gastrointestinal functions and biocarrier application. J Funct Food 2023; 104: 105520. doi: 10.1016/j.jff.2023.105520
16. Khajeh Bami M, Afsharmanesh M, Espahbodi M, Esmaeilzadeh E. Effects of dietary nano-selenium supplementation on broiler chicken performance, meat selenium content, intestinal microflora, intestinal morphology, and immune response. J Trace Elem Med Biol 2022; 69: 126897. doi: 10.1016/j.jtemb.2021.126897
17. Shah SRA, Çetingül IS. Nutritional advances in production performance and product quality of poultry husbandry under heat stress. Online J Anim Feed Res 2022; 12(2): 53–65. doi: 10.51227/ojafr.2022.8
18. Chang Q, Cai H, Wei L, Lan R. Chitosan oligosaccharides alleviate acute heat stress-induced oxidative damage by activating ERK1/2-mediated HO-1 and GSH-Px gene expression in breast muscle of broilers. Poult Sci 2022; 101(1): 101515. doi: 10.1016/j.psj.2021.101515
19. Aviagen. Ross 308 broiler nutrition specifications. Huntsville: Aviagen, 2014. https://www.slideshare.net/abdelrahmanyousef/ross308-broiler-nutrition-specs
20. Sell JL, ed. Nutrient requirements of poultry. 9th rev. ed. Washington: National Academy Press, 1994.
21. Menon S, Agarwal H, Kumar V, Shanmugam. Biomemetic synthesis of selenium nanoparticles and its biomedical applications. In: Green synthesis, characterization and applications of nanoparticles. Amsterdam: Elsevier, 2019: 165-197.
22. Monesh Babu J, Preetha S. Selenium nanoparticles and its application. Annal Roman Soc Cell Biol 2021; 25(3): 5964–74.
23. Dhawan G, Singh I, Dhawan U, KumarP. Synthesis and characterization of nanoselenium: a step-by-step guide for undergraduate students. J Chem Educat 2021. 98(9): p. 2982-2989. doi: 10.1021/acs.jchemed.0c01467
24. Nuengjamnong C, Angkanaporn K. Efficacy of dietary chitosan on growth performance, haematological parameters and gut function in broilers. Ital J Anim Sci 2018; 17(2): 1–8. doi: 10.1080/1828051X.2017.1373609
25. Kim, H.J., et al., Effects of light intensity on growth performance, blood components, carcass characteristics, and welfare of broilers. J Anim Sci Technol 2022; 64(5): 985–96. doi: 10.5187/jast.2022.e47
26. Honikel KO. Reference methods for the assessment of physical characteristics of meat. Meat Sci 1998; 49(4): 447–57. doi: 10.1016/s0309-1740(98)00034-5
27. Chang Q, Lu Y, Lan R. Chitosan oligosaccharide as an effective feed additive to maintain growth performance, meat quality, muscle glycolytic metabolism, and oxidative status in yellow-feather broilers under heat stress. Poul Sci 2020; 99(10): 4824–31. doi: 10.1016/j.psj.2020.06.071
28. Christensen LB. Drip loss sampling in porcine m. longissimus dorsi. Meat Sci 2003; 63(4): 469–77. doi: 10.1016/s0309-1740(02)00106-7
29. Harash G, Richardson KC, Alshamy Z. Basic morphometry, microcomputed tomography and mechanical evaluation of the tibiotarsal bone of a dual-purpose and a broiler chicken line. PLoS One 2020; 15(3): e0230070. doi: 10.1371/journal.pone.0230070
30. Yan FF, Mohammed AA, Murugesan GR, Cheng HW. Effects of a dietary synbiotic inclusion on bone health in broilers subjected to cyclic heat stress episodes. Poult Sci 2019; 98(3): 1083–9. doi: 10.3382/ps/pey508

31. Ndubuisi D, Daudu O, Abdulrashid M. The role of selenium in ameliorating the impact of heat stress on growth, hormones, minerals and tibia measurements of broiler chickens. Nigerian J Anim Product 2021; 48(4): 176–84. doi: 10.51791/njap.v48i4.3008

32. Shim MY, Karnuah AB, Mitchell AD, Anthony NB, Pesti GM, Aggrey SE. The effects of growth rate on leg morphology and tibia breaking strength, mineral density, mineral content, and bone ash in broilers. Poult Sci 2012; 91(8): 1790–5. doi: 10.3382/ps.2011-01968

33. Shah M, Zaneb H, Masood S. Effect of single or combined supplementation of zinc and probiotics on muscle and bone characteristics and haematobiochemical profile in broilers. Vet Med 2020; 65(3): 134–42. doi: 10.17221/152/2019-VETMED

34. KOCABAĞLI N., The effect of dietary phytase supplementation at different levels on tibial bone characteristics and strength in broilers. Turk J Vet Anim Sci 2001; 25(5): 797–802.

35. Khan I, Zaneb H, Masood S, et al. Supplementation of selenium nanoparticles-loaded chitosan improves production performance, intestinal morphology, and gut microflora in broiler chickens. J Poult Sci 2022; 59(3): 272–81. doi: 10.2141/jpsa.0210026

36. Saeed AA, Sandhu MA, Khilji MS, et al. Effects of dietary chromium supplementation on muscle and bone mineral interaction in broiler chicken. J Trace Elem Med Biol 2017; 42: 25–9. doi: 10.1016/j.jtemb.2017.03.007

37. Dalia AM, Loh TC, Sazili AQ, Samsudin AA. Influence of bacterial organic selenium on blood parameters, immune response, selenium retention and intestinal morphology of broiler chickens. BMC Vet Res 2020; 16(1): 365. doi: 10.1186/s12917-020-02587-x

38. Sandercock DA, Nute GR, Hocking PM. Hocking, Quantifying the effects of genetic selection and genetic variation for body size, carcass composition, and meat quality in the domestic fowl (Gallus domesticus). Poult Sci 2009; 88(5): 923–31. doi: 10.3382/ps.2008-00376

39. Wang RH, Liang RR, Lin H. Effect of acute heat stress and slaughter processing on poultry meat quality and postmortem carbohydrate metabolism. Poult Sci 2017; 96(3): 738–46. doi: 10.3382/ps/pew329

40. Yang Y, Meng FC, Wang P. Effect of organic and inorganic selenium supplementation on growth performance, meat quality and antioxidant property of broilers. African J Biotechnol 2012; 11(12): 3031–6. doi: 10.5897/AJB11.3382

41. Bami MK, Afsharmanesh M, Salarmoini M, Ebrahimnejad H. Effects of selenium-chitosan on growth performance, carcass traits, meat quality, and blood indices of broiler chickens. Livest Sci 2021; 250: 104562. 10.1016/j.livsci.2021.104562

42. Oliveira TFB, Rivera DFR, Mesquita FR, Braga H, E.M. Ramos EM, Bertechini AG. Effect of different sources and levels of selenium on performance, meat quality, and tissue characteristics of broilers. J Appl Poult Sci 2014; 23(1): 15–22. doi: 10.3382/japr.2013-00761

43. Wang J, Liu Z, He X, et al. Selenium deficiency induces duodenal villi cell apoptosis via an oxidative stress-induced mitochondrial apoptosis pathway and an inflammatory signaling-induced death receptor pathway. Metallomics 2018; 10(10): 1390–400. doi: 10.1039/c8mt00142a

44. Bakhshalinejad R, Hassanabadi A, Swick RA. Dietary sources and levels of selenium supplements affect growth performance, carcass yield, meat quality and tissue selenium deposition in broilers. Anim Nutr 2019; 5(3): 256–63. doi: 10.1016/j.aninu.2019.03.003

45. Mir NA, Rafiq A, Kumar F, Singh V, Shukla V. Determinants of broiler chicken meat quality and factors affecting them: a review. J Food Sci Technol 2017; 54(10): 2997–3009. doi: 10.1007/s13197-017-2789-z

46. Boiago M, Borba H, Leonel FR, et al., Sources and levels of selenium on breast meat quality of broilers. Ciência Rural 2014; 44(9): 1692–8. 10.1590/0103-8478cr20131256

47. Calvo L, Toldrá F, Rodríguez AI, López-Bote C, Rey AI. Effect of dietary selenium source (organic vs. mineral) and muscle pH on meat quality characteristics of pigs. Food Sci Nutr 2017; 5(1): 94–102. doi: 10.1002/fsn3.368

48. Perić I, Milošević N, Žikić D, et al. Effect of selenium sources on performance and meat characteristics of broiler chickens. J Appl Poul Res 2009; 18(3): 403–9. doi: 10.3382/japr.2008-00017

49. Zhou X, Wang Y. Influence of dietary nano elemental selenium on growth performance, tissue selenium distribution, meat quality, and glutathione peroxidase activity in Guangxi Yellow chicken. J Poultry Science 2011; 90(3): 680–6. doi: 10.3382/ps.2010-00977

50. Cai SJ, Wu CX, Gong LM, Song T, Wu H, Zhang LY. Effects of nano-selenium on performance, meat quality, immune function, oxidation resistance, and tissue selenium content in broilers. Poult Sci 2012; 91(10): 2532–9. doi: 10.3382/ps.2012-02160

51. Zaboli G, Huang X, Feng X, Ahn DU. How can heat stress affect chicken meat quality?–a review. Poult Sci 2019; 98(3): 1551–6. doi: 10.3382/ps/pey399

52. Mohammad A, Ghazanfari S, Sharifi SD. Comparative effects of dietary organic, inorganic, and Nano-selenium complexes and rosemary essential oil on performance, meat quality and selenium deposition in muscles of broiler chickens. Livest Sci 2019; 226: 21–30. doi: 10.1016/j.livsci.2019.06.001

53. Safdari-Rostamabad M, Hosseini-Vashan SJ, Perai AH, Sarir H. Nanoselenium supplementation of heat-stressed broilers: effects on performance, carcass characteristics, blood metabolites, immune response, antioxidant status, and jejunal morphology. Biol Trace Elem Res 2017; 178(1): 105–16. doi: 10.1007/s12011-016-0899-5

54. Ashraf S, Zaneb H, Masood S. Influence of β-galacto-oligosaccharide on growth performance and components of intestinal barrier in broilers during heat stress. South Afr J Anim Sci 201; 47(5): 616–25. 10.4314/sajas.v47i5.4

55. Tahir SK, Yousaf MS, Rashid MA, et al. Supplemental chromium-loaded chitosan nanoparticles affect growth, serum metabolites and intestinal histology in broilers. S Afr J Anim Sci 2020; 49(6): 1072–2. doi: 10.4314/sajas.v49i6.11

56. Bami, M.K., et al., Effects of dietary nano-selenium supplementation on broiler chicken performance, meat selenium content, intestinal microflora, intestinal morphology, and immune response. J Trace Elem Med Biol 2022; 69: 126897. doi: 10.1016/j.jtemb.2021.126897

57. Dukare S, Mir NA, Mandal AB. A comparative study on the antioxidant status, meat quality, and mineral deposition in broiler chicken fed dietary nano zinc viz-a-viz inorganic zinc. J Food Sci Technol, 2021; 58(3): 834–43. doi: 10.1007/s13197-020-04597-x

58. Schrauzer GN. The nutritional significance, metabolism and toxicology of selenomethionine. Adv Food Nutr Res 2003; 47(1): 73–112. doi: 10.1016/s1043-4526(03)47002-2

59. Razdan A, Pettersson D. Effect of chitin and chitosan on nutrient digestibility and plasma lipid concentrations in broiler chickens. Br J Nutr 1994;72(2): 277–88. doi: 10.1079/bjn19940029

60. Kassim A, Ali AHH, Marwan T, Abdel-Wareth AAA. Selenium nanoparticles in rabbit nutrition. a review. SVU-Internat J Agricult Sci 2022; 4(1): 90–8. doi: 10.21608/svuijas.2022.117298.1171

61. Ahmadi M, Ahmadian A, Seidavi A. Effect of different levels of nano-selenium on performance, blood parameters, immunity and carcass characteristics of broilerchickens . Poult Sci J 2018; 6(1): 99–108. doi: 10.22069/psj.2018.13815.1276

62. Ahmad R, Yu YH, Hsiao FS. Influence of heat stress on poultry growth performance, intestinal inflammation, and immune function and potential mitigation by probiotics. Animals (Basel) 2022; 12(17): 2297. doi: 10.3390/ani12172297

63. Noruzi H, Hassanabadi A, Golian A, Aziz-Aliabadi F. Effects of dietary calcium and phosphorus restrictions on growth performance, intestinal morphology, nutrient retention, and tibia characteristics in broiler chickens. Br Poult Sci 2023; 64(2): 231–41. doi: 10.1080/00071668.2022.2136510

64. Savaram Venkata RR, Bhukya P, Raju MVLN, Ullengala R. Effect of dietary supplementation of organic trace minerals at reduced concentrations on performance, bone mineralization, and antioxidant variables in broiler chicken reared in two different seasons in a tropical region. Biol Trace Elem Res 2021; 199(10): 3817–24. doi: 10.1007/s12011-020-02481-5

65. Rehman H, Zaneb H, Masood S. Effect of Moringa oleifera leaf powder supplementation on pectoral muscle quality and morphometric characteristics of tibia bone in broiler chickens. Brazil J Poult Sci 2018; 20(4): 817–24. doi: 10.1590/1806-9061-2017-0609

66. Naz S, Idris M, Khalique M. The activity and use of zinc in poultry diets. World Poult Sci J 2016; 72(1): 159–67. doi: 10.1017/S0043933915002755

67. Yang T, Lee SY, Park KC, Park SH, Chung J, Lee S. The effects of selenium on bone health: From element to therapeutics. Molecules 2022; 27(2): 392. doi: 10.3390/molecules27020392

Učinki nanodelcev selena in hitozana na kakovost mesa, lipidni profil, vsebnost mineralov v tkivih in morfometrijo golenice pri toplotno obremenjenih brojlerjih

G. M. Lochi, M. G. Shah, J. A. Gandahi, J. A. Gadahi, S. A. Hadi, A. Haseeb, N. S. Gandahi, A. Hussain

Izvleček: Namen raziskave je bil oceniti učinke selena in selenovih nanodelcev s hitozanom na piščance brojlerje v času toplotnega stresa. V tej študiji je bilo vzrejenih 336 piščancev. Razdeljeni so bili v sedem skupin, vsaka je vsebovala šest enot, v katerih je bilo nastanjenih po osem piščancev, odvisno od zdravljenja, ki so ga prejeli. Bili sta dve kontrolni skupini: ena z običajno prehrano (negativna kontrola) in druga z običajno prehrano in toplotnim stresom (pozitivna kontrola), imenovani skupini A in B. Druge skupine so bile: skupina C (osnovna prehrana + 0,3 mg/kg selena), skupina D (osnovna prehrana + 0,3 mg/kg nanoselena + toplotni stres), skupina E (osnovna prehrana + 300 mg/kg hitozana + toplotni stres), skupina F (osnovna prehrana + 0,3 mg/kg selena + 300 mg/kg hitozana + toplotni stres) in skupina G (0,3 mg nanoselena + 300 mg/kg hitozana/+ osnovna prehrana + toplotni stres). Analizirani so bili različni parametri, vključno z izgubo vode iz mesa, izgubo vode pri kuhanju, lipidnimi profili, vsebnostjo mineralov in značilnostmi kosti, ki so se v skupini G, ki je prejemala nanoselen in hitozan pod vročinskim stresom, znatno izboljšali. Poleg tega so bile pri skupini G v primerjavi s skupino B ugotovljena višja vsebnost selena, kalcija in fosforja v prsni muskulaturi piščancev ter boljše lastnosti golenice, kot so masa, dolžina, debelina stene, gostota in premer medularnega kanala. Čeprav indeks mase/dolžine ni pokazal bistvenih razlik, sta bila pri skupini G ugotovljena najvišja tibiotarzalni indeks (TTI) in indeks robustnosti (RI). Te ugotovitve kažejo na ugodne učinke dodajanja nanoselena in hitozana, ki so še posebej očitni v razmerah vročinskega stresa.

Ključne besede: selen; nanoselen; hitozan; kakovost mišic; stanje lipidov; golenica; brojlerji; toplotni stres

Slov Vet Res
DOI 10.26873/SVR-2046-2024
UDC 581.41:599.325611:616-089:636.32/.38:636.39
Pages: 189–99

Original Research Article

Morphometric Analysis of the Mandibula in Sheep, Goat and Rabbit

Key words

mandible;
anatomy;
measurements;
animal models;
experimental oral surgery

Bahri Evcim*, Mehmet Erkut Kara

Sıtkı Koçman University Muğla Milas Veterinary Faculty Department of Anatomy, Turkey

***Corresponding author:** bahrievcim@mu.edu.tr

Abstract: Understanding the morphological and morphometric properties of the mandible is crucial for the selection of an appropriate animal model for applications including implants, screws, prostheses, or bone defects. The purpose of this study is to present morphological data concerning the geometrical properties of the mandible in rabbits, sheep, and goats, which are used as models in experimental oral surgery. Length and height measurements of the mandibles were made on x-ray images of the mandibles. The cortical thicknesses and inner-outer diameters were also measured on the CT sectional images. In comparison to ruminants, the mandibular canal in rabbits is relatively shorter. In rabbits, the mental foramen is positioned caudally and closer to the molar teeth, while in sheep and goats, it is located rostrally and closer to the incisive teeth. In addition, the incisive roots are very extended and curved in rabbits and extend to the caudal border of the diastema. In ruminants, the incisive tooth roots are shorter and terminate close to the rostral border of the diastema, and there is a wider working area. Sheep and goats have wider and thicker bones in the rostral, intermediary and caudal regions of the mandible. The ramus region of rabbits has a thin bone structure, which makes it difficult to apply screws and other devices. The lateral side has a thicker cortical bone towards the rostral of the rabbit mandible, while the medial side is thicker in ruminants. The morphologic and geometric data of the mandible may support a study with critical size defects and screw, plate, or other implantations in rabbits and small ruminants to avoid problems or mistakes during experimental oral surgery. Also, the supplementary files can be used by researchers to investigate mandible x-ray images and CT sections of that animal species, as well as sections in different planes based on the intended position during pre-operative planning.

Received: 11 July 2024
Accepted: 17 October 2024

Introduction

For the selection of a suitable animal model in experimental oral surgery research such as implant, screw, prosthesis, or bone defect applications, it is critical to understand the morphological and morphometric characteristics of the mandibular region (1, 2). It is very well known that no animal model can fully imitate human bones, so in experimental studies, the most appropriate model is selected for the targeted research designs (3). Rabbit is the commonly used animal in experimental orthopaedics because of easy care, low economic value, ease of working, easy creation of homogeneous breed groups, sufficient bone size compared to rodents, high bone metabolism, and rapid bone growth (1, 4-6-8). Small ruminants are also easy to find and easy to work with. Moreover, it is increasingly preferred due to reasons such as bone sizes, some histological features, and the metabolic rate and bone remodelling are similar to humans (2, 3, 7-9). Therefore, rabbit, sheep, and goat are frequently preferred as large animal models in experimental oral surgery (1, 2, 6, 9, 10, 12). Knowledge of the general morphological features of the mandible in animal species is already found in classical anatomy books (14, 15). However, there are few studies to address some morphometric evaluations from the perspective of experimental oral surgery in rabbits (1, 6), sheep (13), and goats (16). In addition, detailed information on the thickness of the cortical bone fragments to be tested for screw

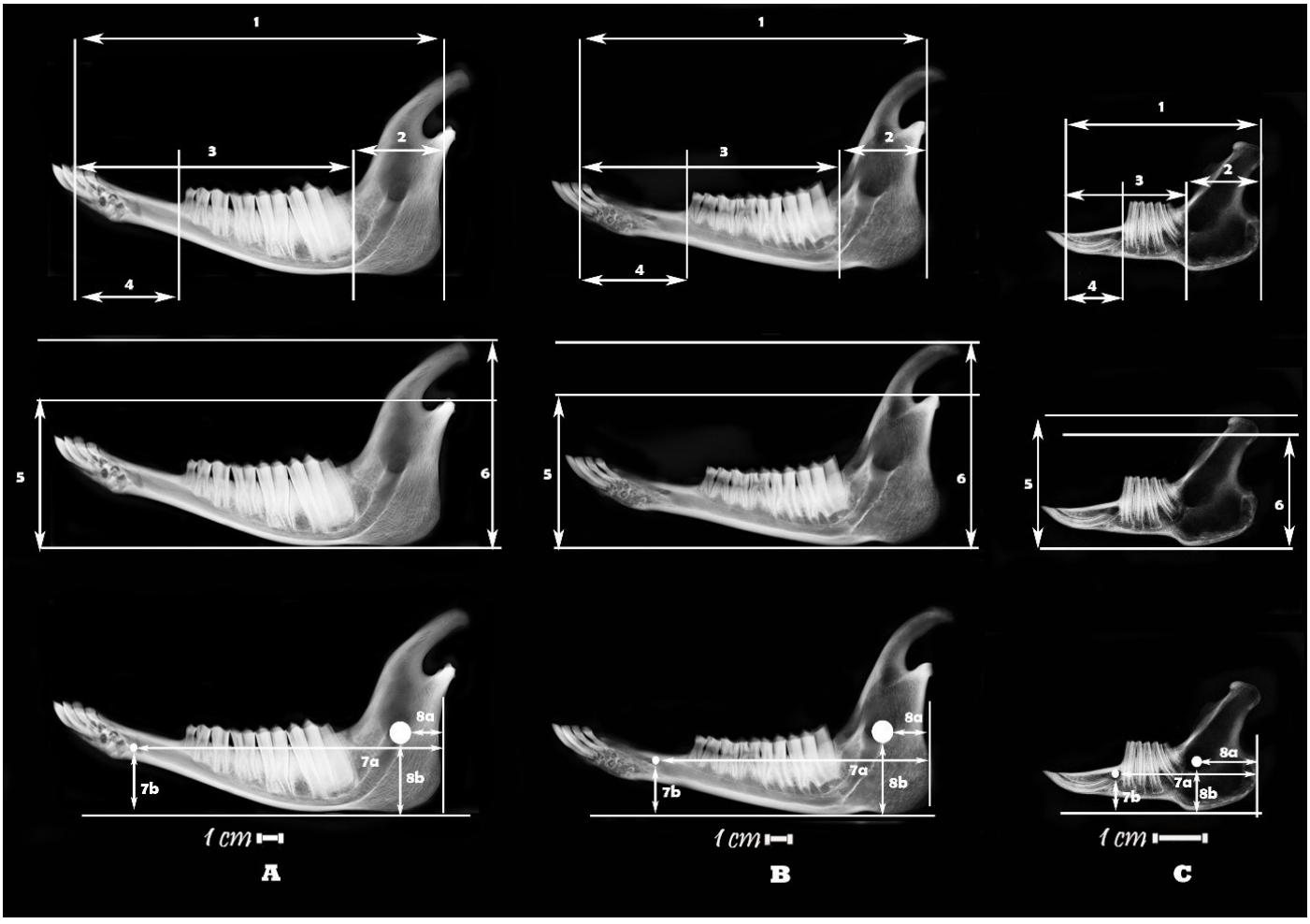

Figure 1: The distance measurements in the medio-lateral x-ray image of sheep (A), goat (B) and rabbit (C) mandibles 1; Length of the mandible, 2; Length of the ramus, 3; Length of the body 4; The diastema length, 5; Condylar height, 6; Total height, 7a; The caudal distance of the mental foramen, 7b; The ventral distance of the mental foramen, 8a; The caudal distance of the mandibular foramen, 8b; The ventral distance of the mandibular foramen

applications or bone defects is insufficient. Further studies are needed with a larger sample and in different species (6, 9). This study aims to present morphological data on the geometrical features of the mandible in rabbits, sheep, and goats, which are used as models in experimental oral and maxillofacial surgery studies in engineering and medicine.

Material and methods

In the study, the unilateral (Right side) mandibles of goats (n: 10), sheep (n: 6) and rabbits (n: 12) were used. These bones were taken from sheep (Karacabey Merino), goat (Saanen), and rabbit (New Zealand) skeletally mature female cadavers previously used for another anatomical study (TUBITAK- COST 115-O830). According to the information of this research project, the study was conducted with the permission of Adnan Menderes University Animal Experiments Ethics Committee (ADUHADYEK/2008/037 and 2014/188). The rabbits were obtained from the SYLAB experimental animal unit, and sheep and goats were obtained from local certified breeders. According to the information given by the breeders, it was noted that rabbits give birth four times on average, sheep give birth two to three times, and goats give birth three to four times. In addition, information was received from the breeder that rabbits were fed pellet feed, while sheep and goats were fed pellet feed and dry grass. The cadavers of frozen animals were thawed and the mandibles were dissected for the study. The used sheep, goats, and rabbits were 38–40, 46–48, and 14–15 months old, respectively. The average weights were also 61.1±3.87 kg, 60.3±14.10 kg, and 3.39±0.33 kg, sheep, goat and rabbit, respectively. To prepare the cadavers, euthanasia was performed under general anaesthesia via exsanguination (14). For anaesthesia, rabbits received 0.2 mg/kg/SC Atropine (Vetas Atropin®) followed by 5 mg/kg/IM xylazine (Xylazinbio®), and 35 mg/kg/IM ketamine (Alfamine®). Sheep received 0.5 mg/kg/SC atropine, followed by 0.2 mg/kg/IM xylazine and 5 mg/kg/IV ketamine. Goats received 0.1 mg/kg/IM xylazine and 5 mg/kg/IV ketamine (18, 19). Mandibles without deformities such as osteoarthritis, fractures, cracks, calluses, and developmental disorders were used. The terminology is used as medial (lingual), lateral (buccal), dorsal, ventral, rostral and caudal.

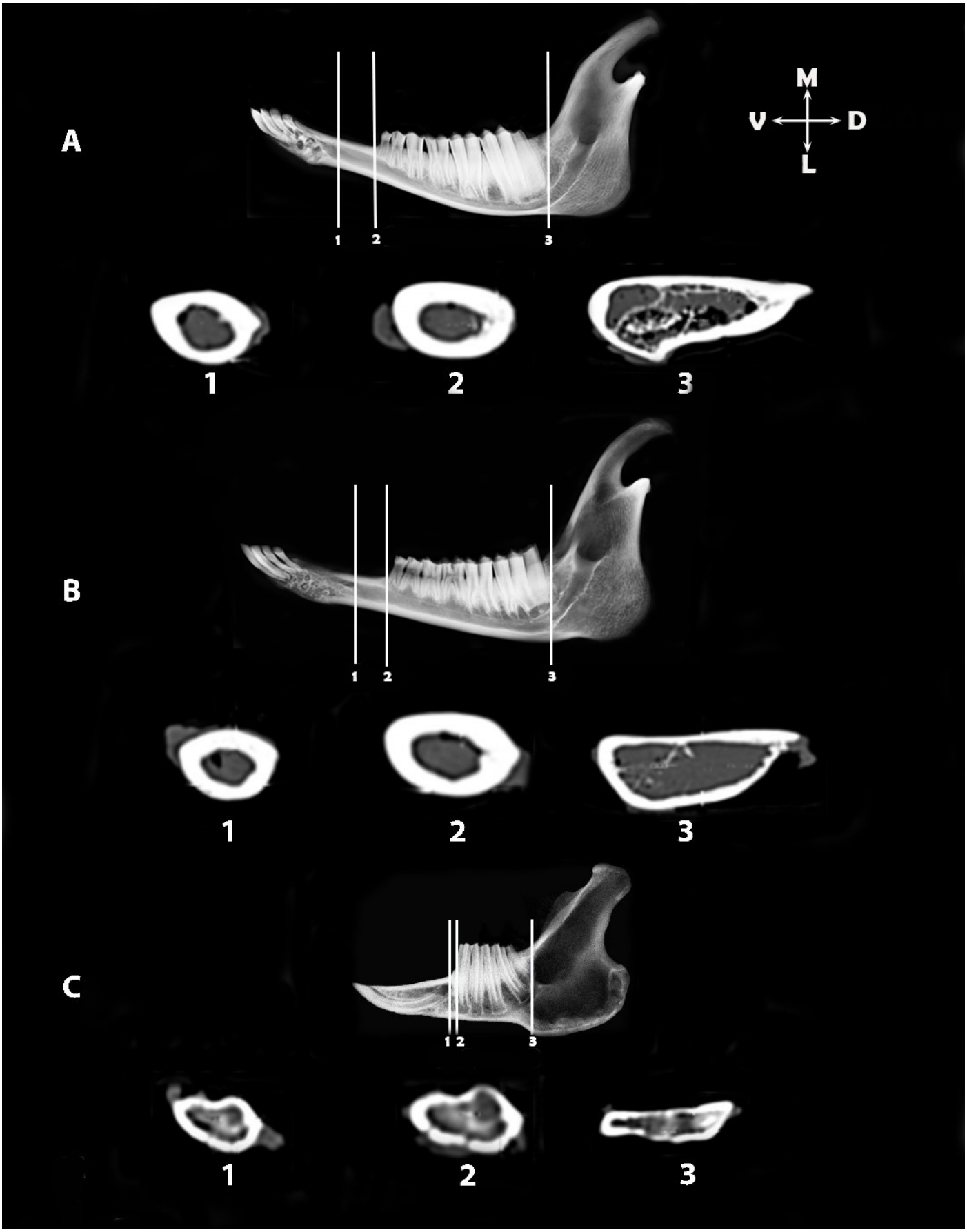

Figure 2: Cross sectional shapes in the rostral (1), intermediary (2) and caudal (3) regions of sheep, goat and rabbit mandibles M: Medial side of the mandible (Lingual side), L: Lateral side of the mandible (Buccal side), D: Dorsal side of the mandible, V: Ventral side of the mandible

Table 1: The length and height measurements of the mandible (mm)

Measurement	Rabbit (n:12)	Sheep (n:6)	Goat (n:10)
Length of mandible	74.21±2.74 (72.46-75.95)	207.03±7.43 (199.22±214.83)	201.96±10.40 (194.52±209.40)
Length of the ramus	25.92±1.36 (25.05-26.79)	46.87±10.24 (36.12-57.61)	53.06±4.76 (49.66-56.48)
The diastema length	25.31±1.31 (24.48-26.14)	54.67±5.00 (49.45-59.95)	58.73±7.78 (53.17-64.30)
The length of the body	47.41±1.67 (46.35-48.48)	156.38±8.13 (147.85-164.90)	146.32±4.80 (142.88-149.75)
Condylar height	42,87±2.18 (41,49-44,25)	86.17±3.07 (82.95-89.39)	82.72±2.64 (80.73-84.61)
Total height	37,07±1.91 (35,86-38,29)	118.06±3.64 (114.23-121.88)	115.06±3.22 (112.75-117.36)
The caudal distance of the mental foramen	48.53±1.98 (47.27-49.78)	174.04±4.49 (169.32-178.75)	148.33±33.98 (124.03-172.64)
The ventral distance of the mental foramen	11.37±1.47 (10.44-12.30)	32.85±3.85 (28.81-36.89)	24.31±6.64 (19.56-29.06)
The caudal distance of the mandibular foramen	19.94±1.46 (18.89-20.98)	21.46±2.54 (18.79-24.12)	19.91±1.86 (18.58-21.24)
The ventral distance of the mandibular foramen	12.89±1.11 (12.10-13.68)	43.16±1.40 (41.69-44.63)	41.69±1.05 (40.94-42.44)

* The data are presented as Mean value ± Standard deviation (MV±SD) and 95% confidence intervals.

Table 2. The dorso-ventral and medio-lateral diameters in the three regions of the mandible (mm)

	Region	Rabbit (n:12)	Sheep (n:6)	Goat (n:10)
Dorso-ventral inner diameter	Rostral	5.23±0.53 (4.89-5.57)	8.41±0.33 (8.06-8.75)	8.01±0.91 (7.36-8.66)
	İntermedier	7.58±0.73 (7.11-8.04)	8.44±0.75 (7.65-9.23)	8.94±1.26 (8.04-9.84)
	Caudal	13.57±1.08 (12.84-14.29)	36.32±4.46 (31.64-41)	31.34±2.13 (29.82-32.86)
Dorso-ventral outer diameter	Rostral	8.03±0.71 (7.57-8.48)	15.05±0.43 (14.60-15.50)	15.01±0.77 (14.46-15.57)
	Intermedier	11.03±0.57 (10.67-11.40)	17.66±0.48 (17.16-18.17)	17.23±0.95 (16.55-17.91)
	Caudal	16.72±1.22 (15.90-17.54)	42.66±3.64 (38.84-46.48)	37.42±1.60 (36.28-38.57)
Medio-lateral inner diameter	Rostral	3.20±0.34 (2.98-3.41)	5.61±0.73 (4.85-6.37)	5.14±0.72 (4.62-5.65)
	Intermedier	4.23±0.45 (3.94-4.52)	5.80±0.23 (5.56-6.04)	5.18±0.75 (4.64-5.71)
	Caudal	2.90±0.26 (2.74-3.07)	10.09±2.12 (7.87-12.32)	9.50±1.65 (8.32-10.68)
Medio-lateral outer diameter	Rostral	5.54±0.31 (5.35-5.74)	10.32±0.56 (9.72-10.91)	9.87±0.69 (9.38-10.36)
	Intermedier	6.36±0.47 (6.06-6.66)	11.42±0.60 (10.79-12.04)	10.42±0.56 (10.02-10.82)
	Caudal	4.84±0.20 (4.71-4.97)	13.58±2.18 (11.29-15.87)	13.54±1.20 (12.68-14.39)

* The data are presented as Mean value ± Standard deviation (MV±SD) and 95% confidence intervals

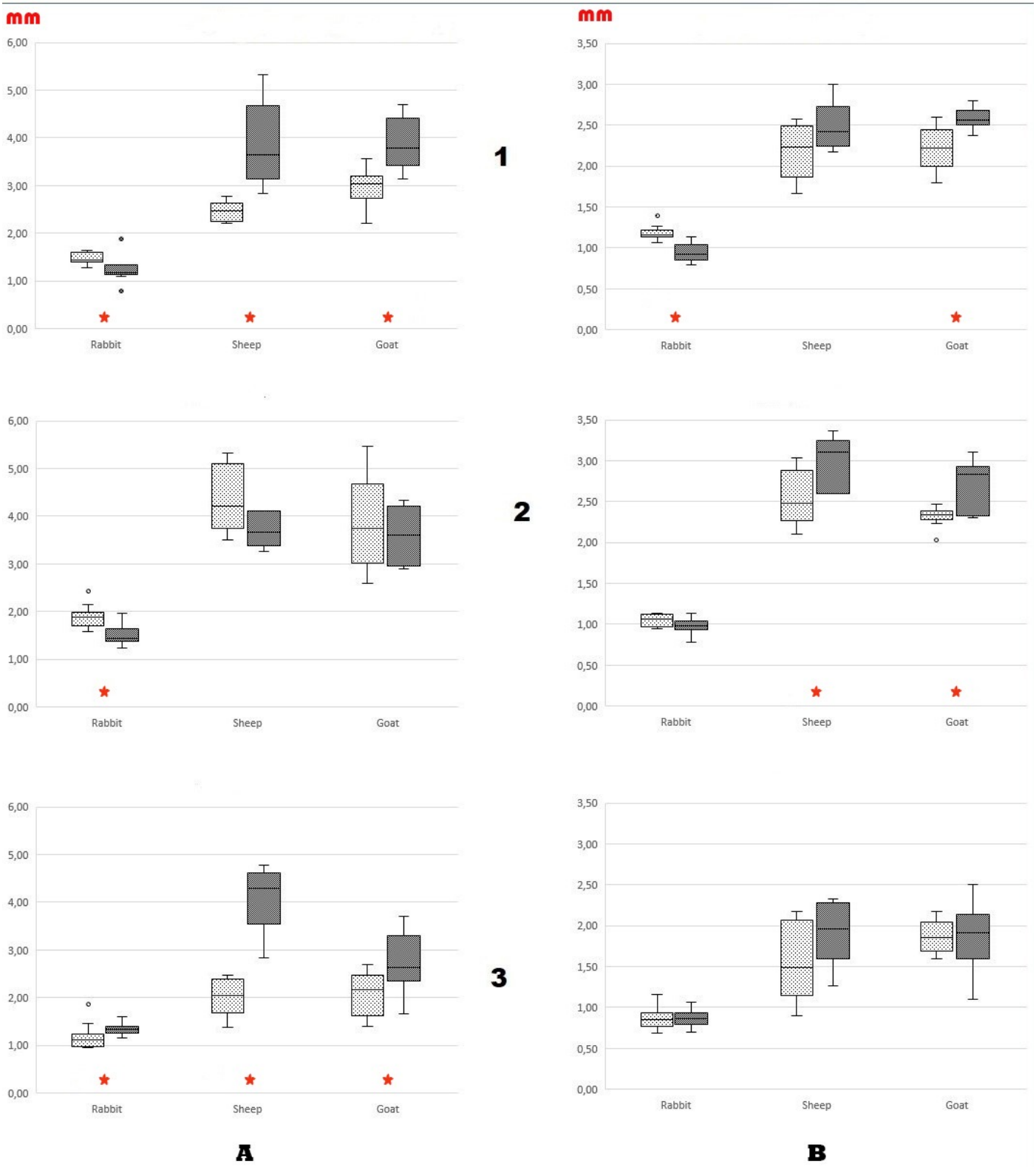

Figure 3: Comparison of the bone cortical thicknesses between dorsal-ventral and lateral-medial sides in the rostral (1), intermediary (2) and caudal (3) regions of rabbit, sheep and goat mandibles (mm). A: The white pattern demonstrates the cortical thicknesses of the dorsal side, and the dark pattern demonstrates the ventral side. B: The white pattern demonstrates the cortical thicknesses of the lateral side, and the dark pattern demonstrates the medial side

*There are statistical differences between the two sides on the cortical thicknesses ($p<0.05$)

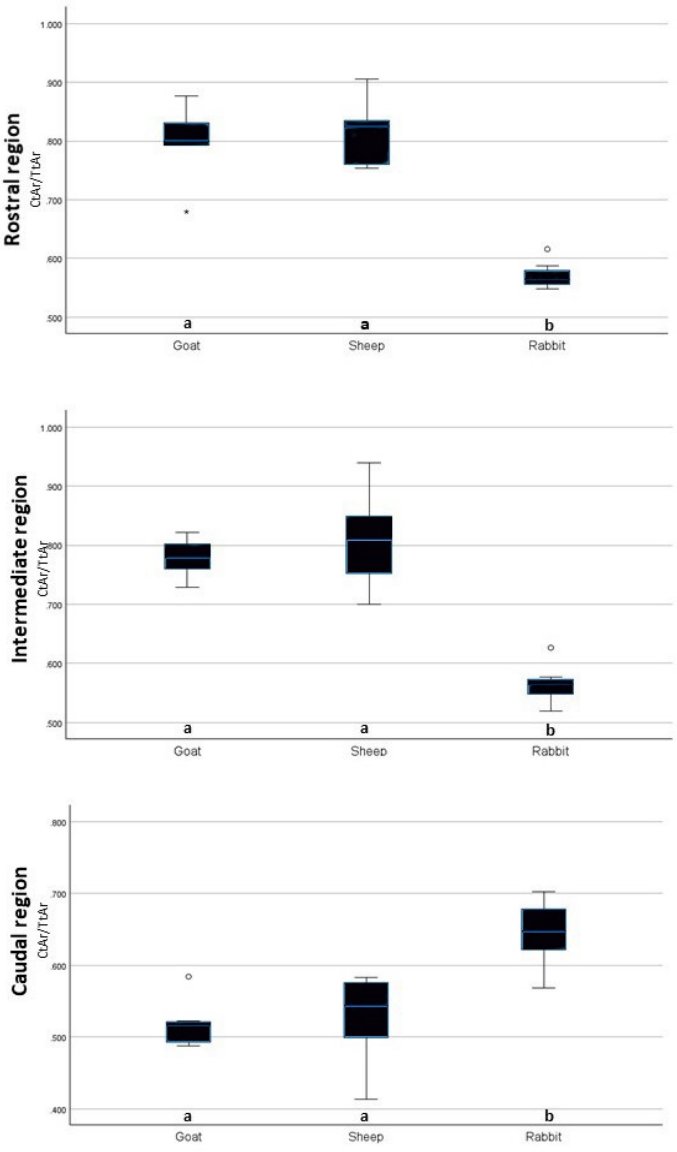

Figure 4: Figure 4. Cortical area fraction (CtAr/TtAr) in the rostral, intermediate and caudal regions of rabbit, sheep and goat mandibles

a, b Means with the same superscript across the columns were not significantly different.

Length and height measurements of mandibles were made on mediolateral radiographs. Digital x-ray images were taken with an EVA-HF750 x-ray equipment and saved in ".jpeg" format. The measurements were taken using ImageJ 1.53g version 4 December 2020 bundled with 64-bit Java 8 for windows (Figure 1).

The computed tomography (Toshiba Aquilion Premium multi-slice) was used to obtain the cross sectional images. In order to determine the bone boundaries more clearly and to align the anatomical axis, the bones were placed on the table of the device by supporting them with cotton. The sectional images were taken at 1mm thickness and 1mm interval. Cross-sectional measurements were taken in three regions that are frequently employed in experimental oral surgery studies (1, 6, 12, 18, 20-21). The caudal border of the mental foramen (Rostral region), the rostral side of the first premolar tooth (intermedier region), and the caudal border of the last molar tooth (Caudal region) were used for this aim. (Figure 2). Cortical thicknesses and diameters were made as stated in the literature (22, 23). In cross-sectional images, measurements were obtained in three consecutive sections from each region, and the average of three measurements were used as the data for the statistical analysis. The cortical thicknesses and inner-outer diameters were measured using the Sectra Pacs (Sectra Workstation IDS7, Linköping, Sweden).

Cortical area and total bone area were measured by were performed with the bone j plugin, an extension of ImageJ bundled with 64-bit Java 8, cortical area fraction was calculated as the cortical area (CtAr) / total area (TtAr) (24).

The same researcher (BE) performed all of the measurements in an attempt to eliminate any possibility of inter-observer variability. To test the reliability of the X-ray measurement methods used, all points and axes were re-determined in the X-ray image of a randomly selected bone, and measurements were taken five times. The coefficient of variation of these measurements was calculated with the formula "%CV = (Standard deviation / Average value/) x 100". The lowest coefficient of variation for the X-ray measurements was found in rabbit mandible length measurement (0.20), while the highest coefficient of variation was found in the inferior distance of the mental foramen (6.15) in sheep. Therefore, the test of repeatability suggests that the method of measurement is reliable for the study (25, 26). Since the average of the measurements taken from three consecutive slices is already used in the cortical thickness and diameter measurements obtained from the computed tomography cross-section images, the coefficient of variation for these parameters was not calculated. Statistical analyses were made using SPSS 19.0 (SPSS Inc., Chicago, IL, USA). The comparison of cortical thicknesses between dorso-ventral and medio-lateral measurements in cross-sectional images was made separately for each region. The normal distribution of the data was made using the Shapiro-Wilk test. Paired t-test was used for parametric data, and the Wilcoxon test was used for non-parametric data. The one-way analysis of variance (One-Way ANOVA) was used for statistical comparisons of the cortical area fraction data obtained from different species. The homogeneity of variances was also explored with Levene's test. Because of the normality and homogeneity of the data the one-way-ANOVA and post-hoc Bonferroni tests were used. The data are presented as Mean value ± Standard deviation (MV±SD) and 95% confidence intervals in the tables. Statistical significance was accepted as $p<0.05$.

Results

According to morphological observations, the mandibular ramus region is very thin, the trabecular bone structure is very low, and the coronoid process and mandibular notch in rabbits, those two structures cannot be seen and labelled even on rabbit's skeleton.

The mandibular canal begins near the root of the last molar, continues at the root of molar teeth, and ends in the mental foramen, which is close to the first premolar tooth at the caudal border of the diastema. It was noted that the root of the incisive teeth is very long, extending significantly to the molar teeth and mental foramen (Figure1). In sheep and goats, the region of the ramus is thicker trabecular bone structure than in rabbits. It is also noteworthy that in sheep and goats, the mandibular foramen is located more caudally and underneath the mandibular notch compared to the rabbit. In addition, the coronoid process is prominent and the mandibular notch is deeper in sheep and goats than in rabbits, but unlike rabbits, the roots of the incisors are not very prominent, the roots do not extend towards the diastema, and this group of teeth is weaker. It has been noted that the mental foramen is located rostrally on the diastema in sheep and goats.

The length and height measurements of mandibles were presented in Table 1. The length of the molar row is about 45-51% of the total length of the mandible in sheep and goats, this ratio is 31% for rabbits. The ratio of the length of the mandibular canal to the total length of the mandible is approximately 64-74% in sheep and goats, and approximately 38% in rabbits. Mental foramen is located more rostrally in sheep and goats than in rabbits. It was located approximately 16-26 % of the mandibular length behind the infradentale and approximately 29-38% of the mandibular height above the ventral base in the sheep and goat. It was located approximately 35 % caudal to the infradentale and approximately 27% dorsal to the ventral base, in the rabbit. The mandibular foramen is placed dorsally and more caudally in sheep and goats than in rabbits. It is located approximately 90 % caudal to the infradentale and approximately 50% dorsal to the ventral border of the mandible in sheep and goats. In rabbits, it is located approximately 73 % caudal to the rostral mandible and 30% dorsal to the ventral border of the mandible.

When cortical bone thickness was evaluated in cross-sectional images, it was determined that the higher cortical thickness in the rostral region was dorsal side in rabbits and ventral side in sheep and goats mandibles. For all species, the cortical thickness was found to be higher on the ventral side in the caudal region of the mandible. It was noted that while the lateral cortical thickness in the rostral region was higher than the medial cortical thickness in rabbits, the medial cortical thickness was higher in sheep and goats. It was observed that medial and lateral cortical thickness values approached each other in all species towards the caudal region of the mandible (Figure 3). The dorso-ventral and medio-lateral diameters in the three regions of the mandibles were also presented in Table 2.

Discussion

When selecting an animal model for experimental oral surgery, the convenience and size of the bone are the primary factors evaluated to ensure ease of surgical access, defect creation, or implantation (1, 6, 27). Thus, it becomes crucial to have a thorough understanding of the mandible's morphology, including its dimensions, cross-sectional diameters, and cortical thicknesses in various regions (1, 6, 27-26). Experimental studies often prefer the premolar, molar regions, or mandibular ramus (5, 6, 27-32). In this study, we present morphological comparisons, dimensions, and cortical thickness measurements for these specific regions of the mandible in three large animal models.

Knowing the differences in mandibular canal morphology between animal species may make research easier. Providing neural stimulation by minimising nerve damage is an important factor in ensuring optimal bone regeneration (31, 33). The mandibular canal is relatively short in rabbits compared to sheep and goats. Previous studies have used a 6–10 mm bone defect in the molar region in the rabbit (6, 31, 34). Considering that the average molar zone length is 22 mm in adult rabbits, it is necessary to work in an area of at least one third of the molar zone length. In this case, it may be necessary for surgeons to work very sensitively to ensure the ideal healing process by considering the proportional size of the defect for the rabbit.

Rabbits and ruminants have no canine teeth, and there is a toothless zone called the diastema between incisive and molar teeth (35). The diastema appears to be an easy and secure application area on the front of the mouth because it is about one-third the length of the mandible and toothless. Nevertheless, depending on the species, it is important to pay attention to some of the morphological features mentioned below. While the distance between the mental foramen and infradentale in sheep and goats is approximately 12–16% of the mandibular length, this ratio is 30% in rabbits. Therefore, the mental foramen is positioned caudally and closer to the molar teeth in rabbits, while in sheep and goats it is located rostrally and closer to the incisive teeth. In addition, the incisive tooth roots, which are very extended and curved in rabbits, extend to the caudal border of the diastema. In sheep and goats, incisive tooth roots are shorter and terminate close to the rostral border of the diastema. Thus, there is a wider working area in this region for ruminants.

In order to ensure the stability of an implant, it is desired that the area where the implant will be applied has the appropriate cortical bone thickness (6, 31, 36-37). Borie

et al. (6) indicated that the defects be performed with a depth of 1.2 mm and a safety margin of 0.1–0.2 mm. In rabbits, even in sections obtained just behind the molar teeth, the average mediolateral diameter is 4.84 mm, while the cortical thickness ranges between 0.80-1.35 mm. These measurements align with the rostral borders of the area where the masseter muscles attach laterally and the pterygoid muscles attach medially across all three animal species. Upon examining the DICOM files in the supplementary data, it becomes evident that cortical bone thickness decreases towards the caudal region. Specifically, in the central area where these muscles attach, the lateral and medial cortical bone layers combine to form a very thin cortical layer in rabbits. On the other hand, all regions of the sheep and goat mandible exhibit greater cortical thickness for such applications. However, in the mandibular ramus, both the medial and lateral cortical thickness measurements are generally lower compared to the rostral regions.

While direct mechanical testing is accepted as the best option to understand the bone strength, there are indirect methodologies to assess the mechanical strength of bones. Some imaging techniques (DEXA, MicroCT, pQCT etc.) are used to understand bone strength with measuring bone density. The cross-sectional geometry and ash content may also considered to assess bone strength (38). The cortical bone area and cortical bone thickness are the best predictors of the failure load for the mandible. The structural properties are also more strongly associated with changes in cross sectional geometry than in material properties (39). Cortical analysis is one of the simplest methods used for many years to determine bone strength, as it is an important data reflecting bone density (40, 41). The cortical thicknesses of the mandible were presented on the different animals and three different regions. The cortical area fraction (cortical area/total area) data were also presented. Because standard CT sections were used, the trabecular bones of the mandible were not truly marked in the sections when determining ROIs. Thus just the cortical bone area were used because there are highly significant correlation between the cortical area fraction and the bone density (42). More detailed analysis can be perform with Micro CT. The cortical area ratio is lower in rabbits on rostral and intermediate regions than ruminants. It may be related the incisive roots are very extended and curved in rabbits in this region. In the caudal region this ratio is higher in rabbits than ruminants. It may be related that the lower ratio of trabecular bone volume on the caudal side of the rabbit mandible.

The experimental bone defect or implant application can be made on either the medial or lateral sides. The cortical thicknesses on the medial and lateral sides may differ according to species, especially in rostral sections. The lateral side has a thicker cortical bone towards the rostral sides of the rabbit mandible. In ruminants, the medial side is thicker as in human (43). This should be taken into account when monitoring bone amounts in defect-gap healing or when applying screws to the cortical bone. Moreover, the bending tests are generally preferred as biomechanical testing procedures for the mandible (30, 39, 44-45). Bending causes compression on the loading side and tension on the opposite side of the bone (46). In this case, since the cortical bone thicknesses show significant differences, there may be differences in the test results when the compression direction is changed in mechanical tests, even if applied in the same region. Researchers should pay attention to the fact that the compression direction and region are the same in the mechanical tests applied in the study when they compare the bone strength values of the mechanical tests they apply with the data of other studies they refer to.

Although diameter measurements in mandible sections are generally similar for sheep and goats, it is noteworthy that the dorso-ventral outer diameter measurement taken behind the last molar tooth is smaller in goats. This can be explained by the presence of a distinct depression in the rostral-upper border of the ramus mandible behind the last molars in the goat mandible, unlike in the sheep mandible (47).

The limitation of this study is that only the right-sided mandible halves of female animals were used. As well as we know, there is no standard information available about the sex of the animals used in morphological or experimental studies related to oral surgery, as well as which side of the mandible to employ. Borie et al. (6) performed lineer measurements on the calvaria and mandible of rabbits regarding experimental surgery. They used female and male rabbits. No information regarding the gender differences was noted. There are no notable differences for length, height, or thickness measurements between the right and left sides. Campillo et al. (1) aimed to describe the anatomy of the rabbit mandible and to estimate the available bone volume for experimental studies. They use one-half of the mandible of four adult female rabbits. Wang et al. (48) used male and female rabbits to establish an animal model for a mandibular defect by using an intraoral approach and to explore the size of a critical-sized defect in the rabbit mandible. The morphometric, densitometric, and mechanical studies of the sheep mandible were carried out by Szabelska et al. (13). They used a male sheep's mandibles that was five months old. They reported no significant differences between the right and left mandibular halves' morphometric, densitometric, and mechanical properties. Carvalho et al. (2) aimed to evaluate the length and resistance of the sheep mandible under the biomechanical loading. They used mandibles from seven month old sheep collected from the abattoir. No information regarding the gender of the sheep was noted. They also stated that when using the entire mandible for biomechanical testing, the reliable simulation with freedom in the three axes in space can be more accurate, which is impossible when using the hemi-mandible. Corte et al. (49) measured the liner morphometric properties of

the mandibles of female mini-pigs and compared them to those of humans. On morphometric measurements, they could not find any statistically significant changes between the left and right hemimandibles. Cheng et al. (5) used adult male rabbits in their mandibular defect experiment. Kim et al (21) used male rabbits to analyse the customized guide and titanium implants experiments on mandibular defect. Abu-Serriah et al (50) used female sheep model to mechanical evaluation of mandibular defect study. For human mandible, sex was also found to be unrelated to cortical thickness pattern (51). Considering that there may be unilateral mastication of species, gender or individual, and that the morphometry of the mandible may also change accordingly, it may be recommended to conduct studies comparing the mandibular variations due to these characteristics. Secondly, the mean values of the measurements and the 95% confidence interval values are also presented directly in the tables. These data should be evaluated by considering the weights of the animals. Since the mandible sizes of animals of different sizes will also differ, comparison of direct measurement data with the results of different studies without an index (6) may lead to inaccurate assessments. Moreover, calculating the coefficient of variation by making repeated measurements in the same sample is a preferred method for testing the reliability of the measurement method (26, 52). The values of the coefficients of variation ranged from 0.20% to 6.15% in the study. The results from the test of repeatability suggest that the method of measurement is reliable for the study. The inter-observer reproducibility has not been evaluated because the measurements were carried out by the same observer (25).

In conclusion, although the toothless area, defined as the diastema, seems to be a suitable area for experimental applications, the incisive tooth roots extend along this area in rabbits, as does the presence of the mandibular canal in sheep and goats. Rabbits have a thin bone structure in the ramus region, which can complicate the application of screws, etc. The cortical bone thicknesses on the medial and lateral sides may differ according to the animal species. It is undoubtedly accepted that sheep and goats have a wider working area and thicker cortices in all three regions of the mandible for experimental implant, screw, prosthesis, or bone defect applications. Besides, they are beneficial to the surgeons in pre-operative planning or directly for in vitro studies because they are easily available as slaughtered animals. The morphologic and geometric data of the mandible may help a study with the critical size defects and screw, plate, or other implantations in rabbits and small ruminants to avoid problems or mistakes during experimental oral surgery. Also, the supplementary files can be used by researchers to investigate mandible x-ray images and CT sections of that animal species, as well as sections in different planes based on the intended position during pre-operative planning.

Acknowledgements

The authors declare no conflict of interest related to this report. This research was a part of the unpublished master's thesis. The study was supported by the ADU-BAP (VTF-18021) and the mandibles in this study were taken from part of an unrelated and unpublished research project (TUBİTAK- COST 115-O830). The study was carried out with the permission of the Adnan Menderes University Animal Experiments Ethics Committee (2008/037 and 2014/188).

References

1. Campillo VE, Langonnet S, Pierrefeu A, Chaux–Bodard AG. Anatomic and histological study of the rabbit mandible as an experimental model for wound healing and surgical therapies. Lab Anim 2014; 48(4): 273–7. doi: 10.1177/0023677214540635

2. Carvalho PH, Saavedra MSFA, Ballester RY, Luz JGC. Biomechanical evaluation of the sheep mandible as a model for studying fixation methods. 2018; 36(3): 926–30. doi: 10.4067/S0717-95022018000300926

3. Pearce AI, Richards RG, Milz S, Schneider E, Pearce SG. Animal models for implant biomaterial research in bone: a review. Eur Cell Mater 2007; 13: 1-10. doi: 10.22203/ecm.v013a01

4. Monfared AL. Applied anatomy of the rabbit's skull and its clinical application during regional anesthesia. Global Vet 2013; 10(6): 653–7. doi: 10.5829/idosi.gv.2013.10.6.72111

5. Cheng G, Li Z, Wan Q, Lv K, Li D, Xing X, Li Z. A novel animal model treated with tooth extraction to repair the full-thickness defects in the mandible of rabbits. J Surg Res 2015; 94(2): 706–16. doi: 10.1016/j.jss.2014.11.010

6. Borie E, Calzzani R, Dias FJ, Fuentes R, Salamanca C. Morphometry of rabbit anatomical regions used as experimental models in implantology and oral surgery. Biomed Res(India) 2017; 28(12): 5468–72

7. Bottogisio M, Coman C, Lovati BA. Animal models of orthopaedic infections. A review of rabbit models used to induce long bone bacterial infections. Journal of Medical Microbiology 2019; 68: 506–37 DOI 10.1099/jmm.0.000952

8. Frosch S, Buchhorn GH. Considerations on the animal model and the biomechanical test arrangements for assessing the osseous integration of orthopedic and dental implants. MethodsX 2021; 8: 101352. doi: 10.1016/j.mex.2021.101352

9. Alvites RD, Branquinho MV, Sousa AC, et al. Small ruminants and its use in regenerative medicine: recent works and future perspectives. Biology (Basel) 2021; 10: 249 doi: 10.3390/biology10030249

10. Wittenberg JM, Mukherjee DP, Smith BR, Kruse RN. Biomechanical evaluation of new fixation devices for mandibular angle fractures. Int J Oral Maxillofac Surg 1997; 26(1): 68–73. doi: 10.1016/S0901-5027(97)808521

11. Alshehri F, Alshehri M, Sumague T, et al. Evaluation of peri-implant bone grafting around surface-porous dental implants: an in vivo study in a goat model. Materials 2019; 12(21): 3606. doi: 10.3390/ma12213606

12. Cancedda R, Giannoni P, Mastrogiacomo M. A tissue engineering approach to bone repair in large animal models and in clinical practice. Biomaterials 2007; 28(29): 4240–50. doi: 10.1016/j.biomaterials.2007.06.023

13. Szabelska A, Tatara MR, Krupski W. Morphological, densitometric and mechanical properties of mandible in 5-month-old Polish merino sheep. BMC Vet Res 2017; 13(1): 1–7. doi: 10.1186/s12917-016-0921-3

14. McLaughlin CA, Chiasson RB. Laboratory anatomy of the rabbit. Briston: Mc Graw Hill, 1990.

15. Dyce K, Sack W, Wensing CJG. Veteriner Anatomi Konu Anlatımı ve Atlas. 4, 13987, R. Amsterdam: Elsevier, 2018.

16. Pal TK, Chakraborty A, Banerjee S. A micro-anatomical comparison of goat jaw cancellous bone with human mandible: histomorphometric study for implant dentistry. J Int Clin Dental Res Orga 2014; 6(1): 20. doi: 10.4103/2231-0754.139088

17. Leary S, Underwood W, Anthony R, et al. AVMA guidelines for the euthanasia of animals: 2013 edition. Schaumburg: American Veterinary Medical Association, 2013.

18. Flecknell, P. Laboratory animal anaesthesia. London: Elsevier , 2009.

19. Cornick–Seahorn, JL. Veterinary anesthesia. Woburn: Butterworth–Heinemann, 2000.

20. Gencer RC, Ozel A, Uckan IS, Bilateral sagittal split ramus osteotomy using a conventional osteotome-hammer and a magnetic mallet device: an in vitro comparison. Eur Rev Med Pharmacol Sci 2023; 27 (Suppl. 4): 58–65. doi: 10.26355/eurrev_202307_32745

21. Kim MK, Ham MJ, Kim WR, et al. Investigating the accuracy of mandibulectomy and reconstructive surgery using 3D customized implants and surgical guides in a rabbit model. Maxillofac Plast Reconstr Surg 2023; 45(1): 8. DOI 10.1186/s40902-023-00375-9

22. Wang SH, Shen YW, Fuh LJ, Peng SL, Tsai MT et al. Relationship between Cortical Bone Thickness and Cancellous Bone Density at Dental Implant Sites in the Jawbone. Diagnostics (Basel) 2020; 10(9): 710. doi: 10.3390/diagnostics10090710

23. Arsan B. Cone beam computed tomography analysis of mandibular inferior cortical thickness and bone texture in cemento-osseous dysplasia. Oral Surg Oral Med Pathol Oral Radiol 2022; 134(1): 110–8. doi: 10.1016/j.oooo.2022.02.008

24. Hsu JT, Chen YJ, Ho JT, et al. A comparison of micro-ct and dental ct in assessing cortical bone morphology and trabecular bone microarchitecture. PLoS One 2014; 9(9): e107545. doi: 10.1371/journal.pone.0107545

25. Özdamar K, Yayinlari, NK. SPSS ile Biyoistatistik. Ankara: Nisan kitabevi, 2015.

26. Sevil-Kilimci F, Kara ME. The geometry of the proximal femoral medullary canal in German shepherd and Kangal dogs. J Fac Vet Med Istanbul Univ 2017; 43: 52–60. doi: 10.16988/iuvfd.270288

27. Olivera LB, Sant´ana E, Manzato AJ, Guerra FLB, Arnett GW. Biomechanical in vitro evaluation of three stable internal fixation techniques used in sagittal osteotomy of the mandibular ramus: a study in sheep mandibles. J Appl Oral Sci 2012; 20(4). 419–26 doi: 10.1590/S1678-77572012000400006

28. Bavitz JB, Harn SD, Hansen CA, Lang M. An anatomical study of mental neurovascular bundle-implant relationships. Int J Oral Maxillofac Implants 1993; 8(5): 563–7.

29. Watanabe H, Abdul MM, Kurabayashi T, Aoki H. Mandible size and morphology determined with CT on a premise of dental implant operation. Surg Radiol Anat 2010; 32(4): 343–9. doi:10.1007/s00276-009-0570-3

30. Gomes PP, Filho RG, Mazzonetto R, Evaluation of the bending strength of rigid internal fixation with absorbable and metallic screws in mandibular ramus sagittal split osteotomy – in vitro study. Pesqui Odontol Bras 2003;17(3): 267–72. doi:10.1590/S1517-74912003000300012

31. Shah SR, Young S, Goldman JL, Jansen JA, Wong ME, Mikos AG. A composite critical-size rabbit mandibular defect for evaluation of craniofacial tissue regeneration. Nature Protocols 2016; 11(10): 1889–2009. doi: 10.1038/nprot.2016.122

32. Nuntanaranont T, Promboot T, Sutapreyasri S. Effect of expanded bone marrow-derived osteoprogenitor cells seeded into polycaprolactone/tricalcium phosphate scaffolds in new bone regeneration of rabbit mandibular defects. J Mater Sci Mater Med 2018; 29(3): 24. doi: 10.1007/s10856-018-6030-z

33. Gandur IV, Walton VT, Lobato PC, Luaces VL, Céspedes MVM. Mandible measurements and dental midline deviation after alveolar nerve transection in growing rabbits. Int J Morphol 2011; 29(1): 52–6. doi: 10.4067/S0717-95022011000100008

34. Lee SW, Gyorgy S, Choi JB, Choi JY, Kim SG. Carbon plate shows even distribution of stress, decreases screw loosening, and increases recovery of preoperative daily feed intake amount in a rabbit model of mandibular continuity defects. J Craniomaxillofac Surg 2014; 42(5): e245–51. doi: 10.1016/j.jcms.2013.09.006

35. Liebich HG, König HE. Skeleton axiale In: Liebich HG, König HE, eds. Veterinary Anatomy of Domestic Mammals, Textbook and Color atlas. New York: Schattauer, 2007; 69–106.

36. Wu Z, Liu Y, Singare S, Li D. Animal model for evaluation of strain gauge in mandibular distraction osteogenesis in rabbits. British J Oral Maxillofac Surg 2007; 45(8): 633–6. doi: 10.1016/j.bjoms.2007.04.004

37. Motoyoshi M, Yoshida T, Ono A, Shimizu N. Effect of cortical bone thickness and implant placement torque on stability of orthodontic mini-implants. Int J Oral Maxillofac Implants 2007; 22(5): 779–84.

38. Khan K, Sevil Kilimci F, Kara ME. (2021). Biomechanical tests: applications and their reliability for the prediction of bone strength in broiler chicken. Vet J Mehmet Akif Ersoy Uni 2021; 6(2): 85–92.

39. Jiang GZ, Matsumoto H, Hori M, et al. Correlation among geometric, densitometric, and mechanical properties in mandible and femur of osteoporotic rats. J Bone Miner Metab 2008; 26(2): 130–7. doi: 10.1007/s00774-007-0811-7

40. Tingart MJ, Apreleva M, von Stechow D, Zurakowski D, Warner JJ. The cortical thickness of the proximal humeral diaphysis predicts bone mineral density of the proximal humerus. J Bone Joint Surg Br 2003; 85, 611–7. doi: 10.1302/0301-620x.85b4.12843

41. Wescott DJ. Effect of mobility on femur midshaft external shape and robusticity. Am J Phys Anthropol 2006; 130(2): 201–13. doi: 10.1002/ajpa.20316

42. Kiminki A, Tammisalo EH. Cortical ratio as an indicator of the mineral content of human mandibular bones. Acta Odontol Scand 1969; 27(4): 409–15. doi: 10.3109/00016356909040420.

43. Santos IG, Ramos de Faria F, da Silva Campos MJ, de Barros BÁC, Rabelo GD, Devito KL. Fractal dimension, lacunarity, and cortical thickness in the mandible: Analyzing differences between healthy men and women with cone-beam computed tomography. Imaging Sci Dent 2023; 53(2): 153–9. doi: 10.5624/isd.20230042.

44. Elovic RP, Hipp JA, Hayes WC. A Method for measuring the structural properties of the rat mandible. Arch Oral Biol 1994; 39(12): 1029–33. doi: 10.1016/0003-9969(94)90054-x

45. Bulut T, Durmus E, Mihmanlı A, Dolanmaz D, Kalaycı A, Sağlam H. Distracted mandible does not reach the same strength as normal mandible in rabbits. Oral Surg Oral Med Oral Pathol Oral Radiol 2012; 114(Suppl. 5): S140–5. doi: 10.1016/j.oooo.2011.09.024

46. An YH, Draughn RA. Mechanical Testing of Bone and the Bone-Implant Interface.Boca Raton: CRC Press, 1999. doi: 10.1201/9781420073560

47. Halstead P, Collins P, Isaakidou V. Sorting the sheep from the goats: morphological distinctions between the mandibles and mandibular teeth of adult ovis and capra. J Archaeol Sci 2002; 29(5): 545–53 doi: 10.1006/jasc.2001.0777

48. Wang Y, Zhang X, Mei S, Li Y, Khan AA, Guan S, Li X. Determination of critical-sized defect of mandible in a rabbit model: micro-computed tomography, and histological evaluation. Heliyon 2023; 9(7): e18047. doi: 10.1016/j.heliyon.2023.e18047

49. Corte GM, Hünigen H, Richardson KC, Niehues SM, Plendl J. Cephalometric studies of the mandible, its masticatory muscles and vasculature of growing Göttingen Minipigs-A comparative anatomical study to refine experimental mandibular surgery. PLoS One. 2019; 25; 14(4): e0215875. doi: 10.1371/journal.pone.0215875.

50. Abu-Serriah M, Kontaxis A, Ayoub A, Harrison J, Odel E, Barbenel J. Mechanical evaluation of mandibular defects reconstructed using osteogenic protein-1 (rhOP-1) in a sheep model: a critical analysis. Int J Oral Maxillofac Surg 2005; 34: 287–93. doi: 10.1016/j.ijom.2004.09.008

51. Decaup PH, Couture C, Garot E. Is the distribution of cortical bone in the mandibular corpus and symphysis linked to loading environment in modern humans? A systematic review. Arch Oral Biol 2023; 152: 105718. doi: 10.1016/j.archoralbio.2023.105718

52. Klipstein-Grobusch K, Georg T, Boeıng H, Interviewer variability in anthropometric measurements and estimates of body composition. Int J Epidemiol 1997; 26(Suppl. 1): S174–80. doi: 10.1093/ije/26.suppl_1.s174

Morfometrična analiza spodnje čeljustnice pri ovci, kozi in kuncu

B. Evcim, M. E. Kara

Izvleček: 10-letna sterilizirana škotska mačka z ravnimi ušesi je imela trdno, nepremično maso na desni spodnji čeljusti. V zadnjem mesecu se je masa postopoma večala, kar je povzročilo težave pri prehranjevanju in posledično izgubo telesne mase. Računalniška tomografija (CT) je pokazala, da je bila masa omejena na telo spodnje čeljusti, z izrazito periostalno reakcijo, za katero je bil značilen koničast vzorec. Obsežna in nepravilna morfologija periostalne reakcije je nakazovala malignost. Klinični pregled ali diagnostično slikanje ni odkrilo znakov, ki bi nakazovali na metastaze. Zaradi hitre rasti mase in s tem povezanih kliničnih znakov je bila kirurška resekcija prednostna pred pridobitvijo dokončne diagnoze. Za diagnostične in terapevtske namene je bila opravljena razširjena subtotalna mandibulektomija, ki je razkrila alveolarni osteomielitis. Po operaciji je imela mačka boljšo žvečilno funkcijo brez očitnih znakov bolečine v ustih, kar kaže na dober kirurški izid. V 16-mesečnem obdobju spremljanja je mačka ostala v dobrem splošnem in fizičnem stanju brez ponovitve tvorbe. Po našem vedenju je to prvo poročilo, ki kaže, da se osteomielitis lahko kaže z obsežno, nepravilno periostalno reakcijo z radiacijskimi črtami (podtip »sunburst«), ki je običajno povezana z malignimi tumorji. Poleg tega je kirurška resekcija lahko ključna za povrnitev žvečilne funkcije in lajšanje bolečin v ustih, tudi v primerih benignih lezij mandibule.

Ključne besede: spodnja čeljustnica; anatomija; meritve; živalski modeli; eksperimentalna oralna kirurgija

Slov Vet Res

DOI 10.26873/SVR-1829-2024
UDC 611.018.46:615.849:616-089.23:616-091.8:637.412:639.112
Pages: 201–7

Original Research Article

The Effect of Eggshell Hydroxyapatite Powder and Autologous Bone Marrow on the Healing of Bone Defects in Rabbits

Key words

hydroxyapatite;
avian eggshell powder;
autologous bone marrow aspiration;
bone gap

Received: 5 August 2023
Accepted: 28 March 2024

Nadia Hameed Rija AL-Falahi[1], Ali Ghazi Atiyah[2]*

[1]Department of Surgery and Obstetrics, College of Veterinary Medicine, University of Baghdad, Baghdad, [2]Department of Surgery and Obstetrics, College of Veterinary Medicine, University of Tikrit, Tikrit, Iraq

***Corresponding author:** alighazivet@tu.edu.iq

Abstract: The repair of bone defects remains a challenge for clinical orthopedic surgery. Therefore, the present study was designed to evaluate the effect of using eggshell hydroxyapatite (eHA), which was prepared previously from avian eggshell by hydrothermal method and autologous bone marrow aspirated from the femoral bone, on the healing of bone gap defect on the radius bone of the right forelimb in rabbits. This study was conducted on 28 male rabbits divided randomly into four groups each (n=7); in all experimental animals (10 mm length × 2mm width), a bone gap was induced at the mid-shaft of the radius bone reaching the marrow cavity at the right forelimb. The defect in GI was left open as a control group without any additives. In GII, the bone gap was filled with eHA powder; in GIII, it was filled with eHA powder. The bone gap was filled with autologous bone marrow, and in GIV, the bone defect was equally filled with a combination of eHA and bone marrow. Experimental animals were followed up clinically, radiographically at (2, 4, 6, 8) weeks post-operatively, and histopathologically at (4, 6) weeks post-operatively. The radiological and histopathological findings revealed promising results in treated groups compared to a control group, with the best results in the combination of eHA and autologous bone marrow. In conclusion, the use of eHA and autologous bone marrow is considered a beneficial graft material in bone defect regeneration.

Introduction

Bones have potential healing and regeneration, but the healing of bones cannot be accomplished by themselves in case of large bone defects, which remain a considerable challenge in orthopedic surgery and may result from infections, trauma, tumors, and congenital abnormalities (11). A primary goal for orthopedic surgery is to avoid the requirement of a second surgical bone harvest site through synthetic biomaterials as an alternative method for reconstructing or repairing missing bone (1). These materials are used to promote the healing of bone defects. Traditionally, when there is missing bone, it is replaced with material from the patient or a donor. Different sources of bone grafts have been utilized to stimulate bone healing in cases of bone defects (2). Hydroxyapatite (HA) is a biomaterial comprising calcium and phosphorous, vital minerals found in bones (3). Hydroxyapatite can be synthesized from organic-based materials or inorganic components. The conventional method of obtaining HA involves working with reagent chemicals, making these synthetic routes expensive and time-consuming (4). Natural HA is believed to have metabolic activity and a dynamic response to the environment compared to synthetic HA (5, 6). Calcium-rich Eggshells have promising possibilities as sources of HA; In fact, processed eggshell HA has already demonstrated encouraging results in bone regeneration (5).

Recently, Synthetic biomaterials alone do not have sufficient osteoinductive or angiogenic properties for healing bone defects. Therefore, many recent studies have illustrated that

osteoprogenitor cells, especially cells derived from bone marrow (BMSCs), alone or combined with biomaterials, have successfully regenerated bone tissue (7, 8). The bone marrow serves as a source of stem cells responsible for regularly regenerating blood components and non-hematopoietic stem cells, like mesenchymal stem cells (MSCs). Multiple reports have highlighted the plasticity of stem cells derived from the bone marrow and their capacity to differentiate into cell lines (9). This study aims to assess how effective avian eggshell powder and autologous bone marrow aspiration (BMA) are in promoting the healing process of radius bone gaps in sexually mature male rabbits.

Materials and methods

Ethical statement

Animal management procedures were undertaken following the guideline requirements of the Animal Care and Use Committee at the College of Veterinary Medicine, Tikrit University, Iraq (369 -10/2/2022).

Rabbits care and experimental design

The study used twenty-eight New Zealand White male rabbits, aged between 6- 8 months and weighing 1- 1.8 kg, obtained from the animal house center at the College of Veterinary Medicine Tikrit University, who was in good health. These rabbits were kept in separate cages (1 × 0.5 meters) and fed on commercial pellets (Lone Star, Netherland). They provided water ad libitum under the same conditions for 15 days before the surgery to allow them to acclimatize. Before the surgery, they were treated with a deworming medication (0.02 mg/kg), ivermectin. A bone gap defect measuring 10 mm in length and 2mm in width was created using a speedy electrical drill, and irrigation was done using sterile saline solution (0.9%). These defects were created in the midshaft of the radius bone in all experimental animal groups, and then the animals were divided into four groups. In GI, the bone defect was left open without any additives as a control. In group GII, the defects were filled with eggshell hydroxyapatite powder prepared using hydrothermal methods described by Atiyah and coauthors. (10). In group GIII, the bone gaps were filled with bone marrow aspirated from the femoral bone of each animal of the same group used a bone marrow aspiration needle directed along the medial aspect of the greater trochanter inside the femur then aspirate approximately 1 ml of bone marrow with a sterile syringe and apply 0.5 ml to fill the defect. Lastly, in group GIV, a combination of eggshell hydroxyapatite powder (0.5 mg) with autologous bone marrow aspirated (0.5 ml) in each animal of the same group was used to fill the bone gaps

Surgical protocol

The experimental animals were first tranquilized using Acepromazine at a dosage of 1 mg/kg. After ten minutes, they were further anesthetized using a combination of 2% of Xylazine hydrochloride at a dosage of (5mg/kg), and 10% of Ketamine at a dose (50mg/kg) through intramuscular injections. The surgeons made an incision of 3- 4 cm long on the inside of the right forelimb by carefully using blunt scissors; they separated the muscles to reveal the radius bone. To create a gap in the shaft of the radius bone (10 mm long by 2mm wide), they used a drill and flushed it with sterile saline solution (0.9%) to reach the marrow cavity. The bone gap was left empty in the GI, while in GII, the defect was filled with eHA powder, and in GIII, the bone defect was filled with 0.5ml autologous bone marrow aspirated from the femoral bone. In GIV, the bone defect was filled with an equal mixture of autologous bone marrow aspirated from the femoral bone with eHA powder. The muscles were approximated with 3/0 polydioxanone (PDS) by a simple continuous suture, and the skin was closed using 3/0 silk by a simple interrupted suture pattern. Meloxicam was given as analgesia at a dosage of 0.5 mg/ kg for three days, and enrofloxacin antibiotic was given at a dose of 5-10 mg/kg IM for three days postoperatively. Experimental animals were followed up clinically (daily for the first week post-surgery) and radiographically at (2, 4, 6,8) weeks postoperatively using an X-ray machine (65 kV) and (8 mAs) to observe the bone reaction. After the operation, bone specimens were taken from euthanized animals in all groups using an overdose of 10% Ketamine HCL anesthesia administered through intramuscular injection of 5 ml and evaluated histopathologically at the fourth and sixth weeks post-operative. The specimens were preserved in 10% neutral buffer formalin (NBF) for 48 hours. After that, they were decalcified using a 10% formic acid solution for two weeks. Following several chemical processes, the samples were sectioned into 5µm with a microtome (Leica SP 1600; Leica Microsystems, Germany), and finally stained with Hematoxylin and Eosin. They were then viewed under a light microscope (AX80T; Olympus, Tokyo, Japan).

Results

Clinical Evaluation

All experimental animals could not bear weight on the operative limb during the first three days post operation without any indications of infection or rejection at the fractured site post-surgery, and all wounds healed with first intention.

Radiological evaluation

In the GI (control group) at the 2nd-week post-operation, the bone gap appeared in the shaft of the radius bone with a slight periosteal reaction at the bone gap margins (Fig. 1.

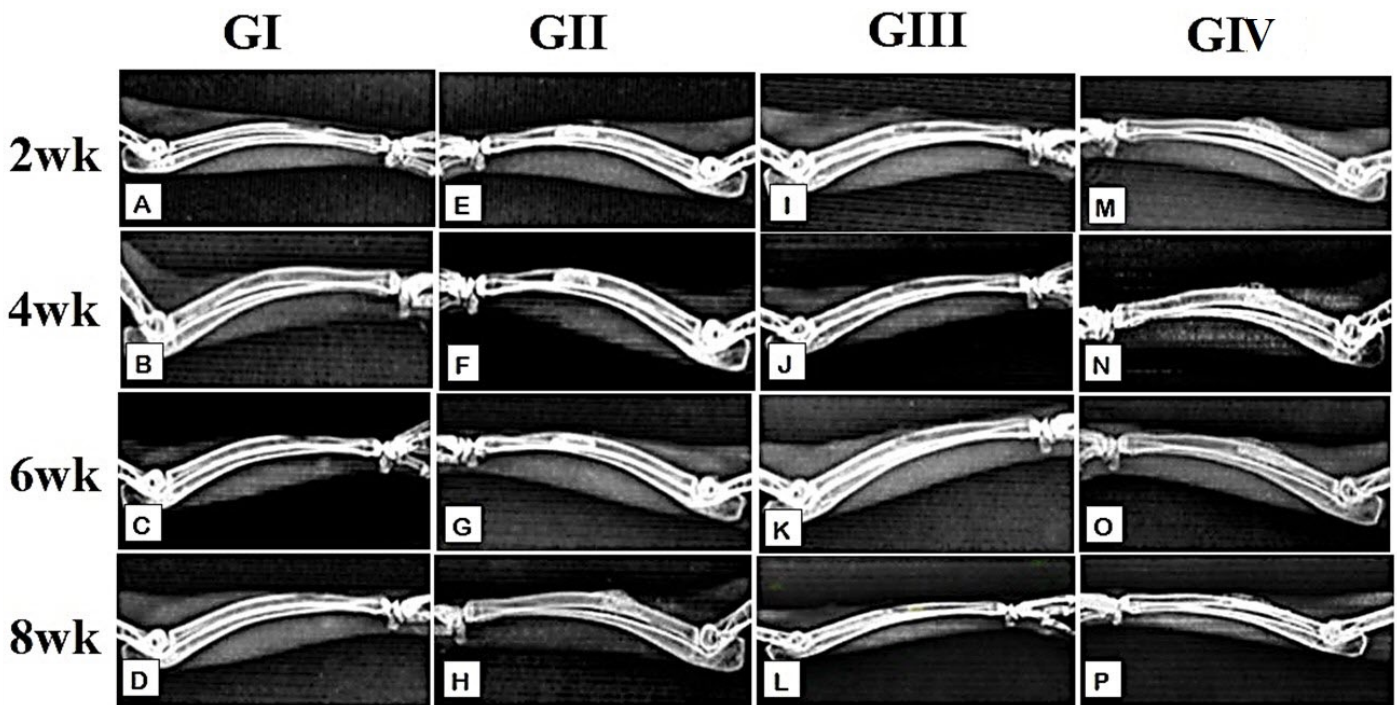

Figure 1: Lateral view radiographs of radius bone in rabbits at (2,4, 6,8) weeks post operatively. (A, B, C, D) GI group. (E, F, G, H) The GII group. (I, J, K, L). The GIII group. (M, N, O, P) the GIV group

A), which increased with time progress and partially closed at the 8th-week post operation (Fig. 1. B, C and D). In the GII, the eggshell powder that filled the radius gap appeared as a radiopaque area compared to normal bone with a slight periosteal reaction, specifically at the distal end of the bone gap at 2 weeks postoperatively (Fig. 1. E). The periosteal reaction increased in the fourth week, and the powder still appeared as a radiopaque material that filled the radius bone gap (Fig. 1. F). In the sixth week, there was a radiolucent area in the middle of the eggshell powder (Fig. 1. G). In the eighth week, the periosteal reaction increased, and the powder appeared less opaque in the bone gap (Fig. 1. H). In the GIII, the bone gap appeared in the shaft of the radius bone with a slight periosteal reaction in the second week (Fig. 1. I). In the fourth week, the bone gap still appeared at the shaft of the radius bone (Fig. 1. J). In the sixth week, the bone gap partially closed from the distal part of the bone gap (Fig. 1. K). At 8 weeks, the bone gap closed, and the marrow cavity appeared along the mid-shaft of the bone (Fig. 1. L). In the GIV in the second week, the composite of eggshell powder with bone marrow appeared as a radiopaque area in the bone gap (Fig. 1.M). In the fourth and sixth weeks, the periosteal reaction appeared at the gap periphery (Fig. 1. N and O). In the eighth week, the composite appeared remodeled with the bone gap and took on the regular shape of the normal bone (Fig.1.P).

Histopathological Evaluation

The histopathological sections of bone defect in the control group GI at the fourth week post operation showed excessive granulation tissue formation surrounded by newly formed thin irregular bone trabeculae. Other sections showed the formation of new cartilage and irregular, thin bone trabeculae (Fig. 2A). In the GII at the same period, the histopathological sections of bone defect showed calcified cartilage that formed variably thickened of anastomosed bone trabeculae, with thick bone trabeculae at the fracture site lined by osteoblasts (Fig. 2B). In the GIII at fourth week post operation, the histopathological sections of the bone defect showed newly formed irregular fragments of bone trabeculae and areas of hemorrhage with normal appearance of adipocytes and bone marrow cells (Fig. 2C). In the GIV at the same time, the histopathological sections of the bone defect showed a marked network of fibrovascular tissue and variably sized bone trabeculae lined by osteoblasts that surrounded non- absorbable eHA powder particles that appeared as a golden-brown particle (Fig. 2D).

In the sixth week post-operation, the histopathological sections in the control group GI showed granulation tissue bound fragment bone, with thickening trabecular and lamellar bone at the end of the fracture speared into granulation tissue, which infiltrated by mononuclear cells (Fig. 3A). In GII, Sections in the bone at sixth week post-operation showed thickening trabecular bone elongated from one side of the fractured bone (Fig. 3B). In GIII, sections in the bone at the same period showed marked fibrin-rich blood clots with inflammatory cells filling the site of the defect (Fig. 3C). While in GIV, sections in the bone at the same period showed markedly different sizes of bone

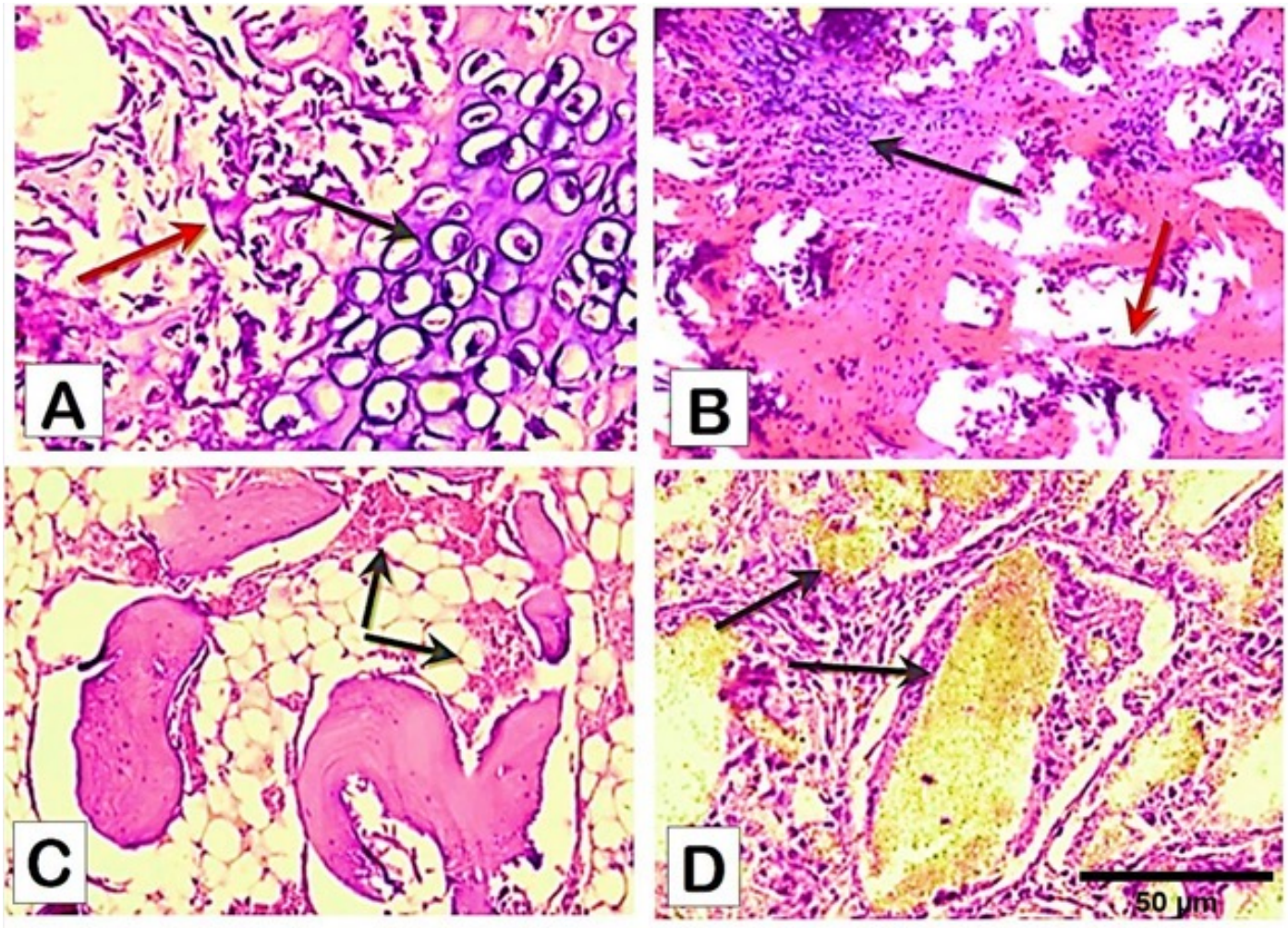

Figure 2: Histopathological sections of bone defect at fourth week post-operation. (A) The GI group shows the formation of new cartilage (black arrow) and irregular thin bone trabeculae (red arrow) (H&E 40X). (B) The GII group shows calcified cartilage (black arrow) that formed variably thickened of anastomosed bone trabeculae with thick bone trabeculae at the fracture site lined by osteoblasts (red arrow) (H&E 20X). (C) The GIII group shows marked fibrin-rich blood clots with inflammatory cells filling the defect site (black arrows) (H&E 20X). (D) The GIV group shows a marked network of fibrovascular tissue and variably sized bone trabeculae lined by osteoblasts surrounding nonabsorbable eHA powder particles that appeared as a golden brown particle (black arrows) (H&E 40X)

trabeculae lined by osteoblasts, surrounded by the residue of non-absorbable eHA powder particles, and spaces between the bone trabeculae filled with blood (Fig. 3D).

Discussion

Autografts are considered the gold standard in orthopedic reconstructive surgeries. They have a high success rate because of their disadvantages, which include restricted supply, donor site dismalness, and inflated costs. Another option is allografts, which wipe out the likely downsides of the autografts. However, their related constraints incorporate sickness transmission chance and a high disappointment rate in vivo because of decellularization and disinfection strategies (12). These drawbacks lead to a requirement for an elective uniting choice for bone reconstruction and regeneration. Thus, due to its profitable, plentiful stockpile and adaptable elements, Tissue engineering has emerged as a promising choice for bone medicines.

The current treatment choice uses bone tissue engineering through biomaterials, stem cells, or a combination (13). In the current study, eHA powder and autologous bone marrow aspirated were used as bone gap-filling material to heal bone defects. The clinical observations of experimental animals in the current study showed that they could bear weight on the operative limb after three days post-operation. This may be attributed to the supporting of the ulna bone to the fractured radius bone in the present study, and this was confirmed by some authors who said that when the fracture includes both the radius and ulna, the lameness appears more clinically than in cases of distal radial fracture with intact ulna (14, 15). Also, other clinical observations in the current study showed no signs of infection or rejection at the operation site, indicating the similarity of hydroxyapatite to an inorganic component of natural bone (16). Also, hydroxyapatite components, including calcium and phosphate ions, do not cause adverse local or systemic toxicity (10, 17).

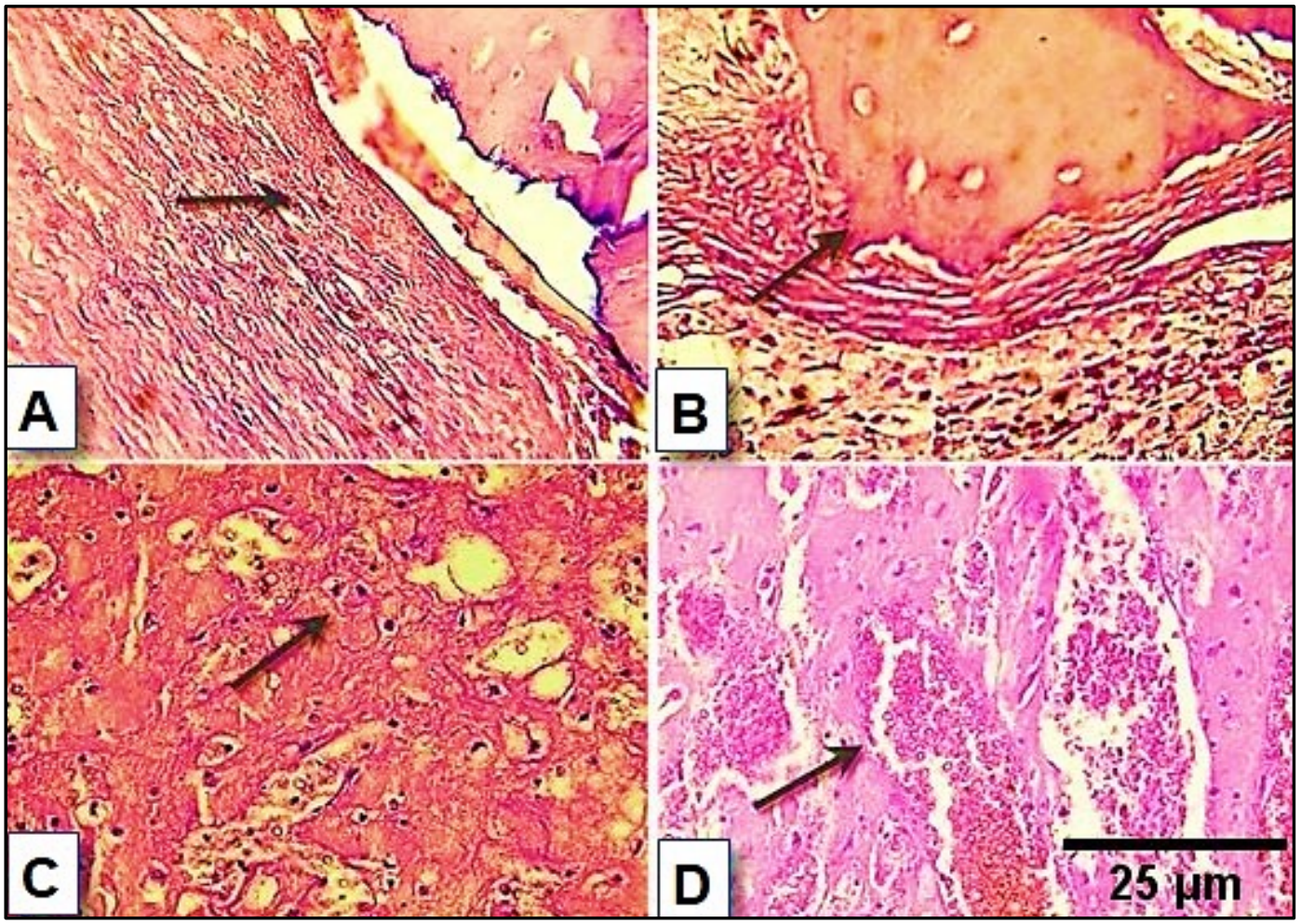

Figure 3: Histopathological sections of bone defect at the sixth week post-operation. (A) The GI group shows granulation tissue bound fragment bone, with thickening trabecular and lamellar bone at the end fracture speared into granulation tissue, which infiltrated by mononuclear cells (black arrow) (H&E 10X). (B) The GII group shows thick trabecular bone elongated from one side of the fractured bone (black arrow) (H&E 10X). (C) The GIII group shows a marked fibrin-rich blood clot with inflammatory cells filling the site of the defect (black arrow) (H&E 40X). (D) The GIV group shows marked variably sized bone trabeculae lined by osteoblasts surrounded by residue of non-absorbable eHA powder particles and spaces between the bone trabeculae filled with blood (black arrow) (H&E 40X)

The radiological findings of the present study showed adequate healing in the bone gap in all treated groups compared to the untreated control group, which appeared to have little bone formation. The eHA in treated groups GII and GIV showed a radiopaque eHA material occupying the bone gap, and the bone gap margin partially resorbed at the end of the eighth week. These results were confirmed by other studies (18, 19). Some authors explained that the improvement of bone repair could be because of the capacity of the HA to work with bone adsorption and calcium discharge, which stimulate osteoblast differentiation and bone development (20). Other studies indicated that the bioceramic scaffold architecture utilized in bone repair, such as porous structures, should be similar to natural bone to encourage cell ingrowth, proliferation, and differentiation (21). In the present study, using autologous bone marrow alone in GII and combination with eHA in GIV gave better bone gap regeneration results than the control group. These outcomes were explained by some authors (22, 23), who said that the cellular content of bone marrow, such as blood cells, cytokines, growth factors, and stem cells, all types of cells involved in the enhancement of rapid responses for inflammatory processes with an early huge role in bone fracture repair; and these results were confirmed by other researchers (15). Other studies confirmed that using bone marrow in transverse fractures in the distal radius of dogs gives good results in its reaction to fractured bone regeneration in the sixth and tenth weeks.

The histopathological findings in the present study showed markedly different sizes of bone trabeculae lined by many osteoblasts in groups planted with eHA. Some authors explained that egg shells contain large amounts of calcium carbonate, which can serve as a hydroxyapatite source and promote osteoblast cell formation and differentiation. Thus, the number of osteoblasts in eHA- the eHA-treated group will be much higher (24-26). These results come from the results of other authors (27). On the other hand, other studies concluded that Hydroxyapatite has biocompatible properties that can down-regulate and

migrate macrophages. This will lead to a decrease in the number of osteoclasts and an increase in the number of osteoblasts so that the bone healing process can occur faster (26). Other researchers indicated hydroxyapatite in the bone defect area stimulates osteoprogenitor cells to become osteoblasts. Hydroxyapatite also makes it easier for osteoprogenitor cells to occupy a suitable medium with actual bone conditions to proliferate and differentiate into osteoblast cells (27). In addition, the use of autologous bone marrow in combination with eHA powder in the present study showed the best healing of bone gaps, and this may be related to the characteristics of eHA in addition to the ability of bone marrow in bone defect regeneration due to its components of MSCs, hematopoietic stem cells, blood cell components, stromal cells populations, and growth factors (28). Others expressed that the injection of bone marrow percutaneously at the fractured site with the use of a composite graft gives good results in the treatment of simple bone cysts, congenital tibial pseudoarthrosis, and delayed bone union in troublesome clinical conditions such as cancer patients (29, 30).

Conclusion

We concluded that the use of avian eHA powder and autologous bone marrow aspiration is a beneficial grafting material that can fill the bone holes without immune rejection and have the ability to promote healing activity at the site of bone defects, and further studies will needed for clinical application of these grafting materials as a scaffold applications.

Acknowledgments

The authors are grateful to Dr. Omar Husian Kalaf in the Pathology Department at the College of Veterinary Medicine, University of Baghdad, for his help and valuable notice in completing this study.

Author's Contribution. NH and AG made contributions to the idea of the publication and organization of work and writing the manuscript.

Competing interest. The authors declare that they have no competing interests.

References

1. Pawelec K, eds. Bone repair biomaterials: regeneration and clinical applications. 2nd ed. Cambridge: Woodhead Publishing, 2018.
2. Kattimani VS, Chakravarthi PS, Kanumuru NR, et al. Eggshell derived hydroxyapatite as bone graft substitute in the healing of maxillary cystic bone defects: a preliminary report. J Int Oral Health 2014; 6(3): 15–9.
3. Agbeboh NI, Oladele IO, Daramola OO, Adediran AA, Olasukanmi OO, Tanimola MO. Environmentally sustainable processes for the synthesis of hydroxyapatite. Heliyon 2020; 6(4): e03765. doi: 10.1016/j.heliyon.2020.e03765
4. Szcześ A, Hołysz L, Chibowski E. Synthesis of hydroxyapatite for biomedical applications. Adv Colloid Interface Sci 2017; 249: 321–30. doi: 10.1016/j.cis.2017.04.007
5. 5. Ahmad Fara ANK, bin Yahya MA, Abdullah HZ. Preparation and characterization of biological hydroxyapatite (HAp) obtained from Tilapia fish bone. Adv Mat Res 2015; 1087: 152–6. doi: 10.4028/www.scientific.net/AMR.1087
6. Sobhi BM, Ismael EY, Mansour AS, Elsabagh M, Fahmy KNE. Effect of nano-hydroxyapatite as an alternative to inorganic dicalcium phosphate on growth performance, carcass traits, and calcium and phosphorus metabolism of broiler chickens. J Adv Vet Res 2020; 10(4): 250–6.
7. Vidal L, Brennan MÁ, Krissian S, et al. In situ production of pre-vascularized synthetic bone grafts for regenerating critical-sized defects in rabbits. Acta Biomat 2020; 114: 384–94. doi: 10.1016/j.actbio.2020.07.030
8. Stamnitz S, Klimczak A. Mesenchymal stem cells, bioactive factors, and scaffolds in bone repair: from research perspectives to clinical practice. Cells 2021; 10(8): 1925. doi: 10.3390/cells10081925
9. Jiang Y, Jahagirdar BN, Reinhardt RL, et al. Pluripotency of mesenchymal stem cells derived from adult marrow. Nature 2002; 418(6893): 41–9. doi: 10.1038/nature00870
10. Atiyah A, Al-Falahi N, Farhan F. Synthesis and structure of eggshell hydroxyapatite bone implant. Online J Vet Res 2018; 22(6): 495–500.
11. Alonzo M, Primo FA, Kumar SA, et al. Bone tissue engineering techniques, advances, and scaffolds for treatment of bone defects. Curr Opin Biomed Eng 2021; 17: 100248. doi: 10.1016/j.cobme.2020.100248
12. Andric T, Taylor BL, Whittington AR, Freeman JW. Fabrication and characterization of three-dimensional electrospun scaffolds for bone tissue engineering. Regen Eng Transl Med 2015; 1: 32–41. doi: 10.1007/s40883-015-0004-1
13. Szpalski C, Wetterau M, Barr J, Warren SM. Bone tissue engineering: current strategies and techniques—part I: scaffolds. Tissue Eng Part B Rev 2012; 18(4): 246–57. doi: 10.1089/ten.TEB.2011.0427
14. Manchi G, Brunnberg MM, Shahid M, et al. Radial and ulnar fracture treatment with paraosseous clamp-cerclage stabilisation technique in 17 toy breed dogs. Vet Rec Open 2017; 4(1): e000194. doi: 10.1136/vetreco-2016-000194
15. Thanoon M, Eesa M, Abed E. Effects of platelets rich fibrin and bone marrow on the healing of distal radial fracture in local dogs: comparative study. Iraqi J Vet Sci 2019; 33(2): 419–25. doi: 10.33899/ijvs.2019.163169
16. Goel SC, Singh D, Rastogi A, Kumaraswamy V, Gupta A, Sharma N. Role of tricalcium phosphate implant in bridging the large osteoperiosteal gaps in rabbits. Indian J Exp Biol 2013; 51(5): 375–80.
17. Dorozhkin SV. Calcium orthophosphate (CaPO4)-based bioceramics: preparation, properties, and applications. Coatings 2022; 12(10): 1380. doi: 10.3390/coatings12101380
18. Park JW, Bae SR, Suh JY, et al. Evaluation of bone healing with eggshell-derived bone graft substitutes in rat calvaria: a pilot study. J Biomed Mater Res A 2008; 87(1): 203–14. doi: 10.1002/jbm.a.31768

19. Kim SH, Kim W, Cho JH, Oh NS, Lee MH, Lee SJ. Comparison of bone formation in rabbits using hydroxyapatite and β-tricalcium phosphate scaffolds fabricated from egg shells. Adv Mat Res 2008; 47: 999–1002. doi: 10.4028/www.scientific.net/AMR.47-50.999

20. El-Ghannam A, Amin H, Nasr T, Shama A. Enhancement of bone regeneration and graft material resorption using surface-modified bioactive glass in cortical and human maxillary cystic bone defects. Int J Oral Maxillofac Implants 2004; 19(2): 184–91.

21. Chocholata P, Kulda V, Babuska V. Fabrication of scaffolds for bone-tissue regeneration. Materials (Basel) 2019; 12(4): 568. doi: 10.3390/ma12040568

22. Travlos GS. Normal structure, function, and histology of the bone marrow. Toxicol pathol 2006; 34(5): 548–65. doi: 10.1080/01926230600939856

23. Korf-Klingebiel M, Kempf T, Sauer T, et al. Bone marrow cells are a rich source of growth factors and cytokines: implications for cell therapy trials after myocardial infarction. Eur Heart J 2008; 29(23): 2851–8. doi: 10.1093/eurheartj/ehn456

24. Woeckel VJ, Alves RDAM, Swagemakers SMA, et al. 1α, 25-(OH) 2D3 acts in the early phase of osteoblast differentiation to enhance mineralization via accelerated production of mature matrix vesicles. Journal of cellular physiology. 2010; 225(2): 593–600. doi: 10.1002/jcp.22244

25. Lu H, Cui L, Zuo C, Lin S, Wu T. Evaluation of morphological parameters of bone formation in Sprague–Dawley rats of different ages by in vivo fluorochrome labeling. Ital J Zool (Modena) 2015; 82(1): 33–40. doi: 10.1080/11250003.2014.984781

26. Shafiu Kamba A, Zakaria ZAB. Osteoblasts growth behaviour on bio-based calcium carbonate aragonite nanocrystal. BioMed Res Int 2014; 2014: 215097. doi: 10.1155/2014/215097

27. Fuadiyah D, Ratnawati R, Kurniawati S, et al. Effect of chicken eggshell powder on osteoblast, osteocyte, and osteoprotegerin (OPG) expressions in alveolar bone defect healing of wistar rats. Mal J Med Health Sci 2023; 19(suppl. 5): 58–65.

28. Gayathri SB, Kamaraj P. Macrophage and osteoblast response to micro and nano hydroxyapatite: a review. Nano Vis 2011; 1(1): 1–13.

29. Ardhiyanto HB. Stimulasi osteoblas oleh hidroksiapatit sebagai material bone graft pada proses penyembuhan tulang. Stomatognatic 2012; 9(3): 162–4.

30. Sugaya H, Yoshioka T, Kato T, et al. Comparative analysis of cellular and growth factor composition in bone marrow aspirate concentrate and platelet-rich plasma. Bone Marrow Res 2018; 2018: 1549826. doi: doi: 10.1155/2018/1549826

Vpliv prahu hidroksiapatita iz jajčne lupine in avtolognega kostnega mozga na celjenje kostnih poškodb pri kuncih

N. H. R. AL-Falahi, A. G. Atiyah

Izvleček: Sanacija kostnih defektov ostaja izziv za klinično ortopedsko kirurgijo. Zato je bil namen te raziskave oceniti učinek uporabe hidroksiapatita iz jajčne lupine (eHA), predhodno pripravljenega iz jajčne lupine ptic s hidrotermalno metodo, in avtolognega kostnega mozga, pridobljenega iz stegnenice, na celjenje kostnega defekta na radialni kosti desne sprednje okončine pri kuncih. Študija je bila izvedena na 28 samcih kuncev, naključno razdeljenih v štiri skupine (n = 7); pri vseh poskusnih živalih (dolžina 10 mm × širina 2 mm) je bila ustvarjena kostna vrzel na sredini desne koželjnice, ki je segala do kostnega mozga. Vrzel v skupini GI je ostala odprta kot kontrolna skupina brez kakršnihkoli dodanih snovi. V skupini GII je bila kostna vrzel zapolnjena s prahom eHA. V skupini GIII je bila kostna vrzel zapolnjena z avtolognim kostnim mozgom, v GIV pa s kombinacijo eHA in kostnega mozga. Poskusne živali so bile klinično spremljane, rentgensko pregledane 2 tedna ter 4, 6 in 8 tednov po operaciji, histopatološko pa 4 tedne in 6 tednov po operaciji. Radiološke in histopatološke ugotovitve so pokazale obetavne rezultate v zdravljenih skupinah v primerjavi s kontrolno skupino, pri čemer so bili najboljši rezultati pri kombinaciji eHA in avtolognega kostnega mozga. Sklenemo lahko, da uporaba eHA in avtolognega kostnega mozga velja za koristen presadni material pri regeneraciji kostnih defektov.

Ključne besede: hidroksiapatit; prah iz lupine ptičjih jajc; avtologna aspiracija kostnega mozga; kostna vrzel

Slov Vet Res
DOI 10.26873/SVR-2033-2024
UDC 591.8:616.341:622.363.1:636.52/.58
Pages: 209–22

Original Research Article

Immunohistochemical and Histomorphometric Related Small Intestine Changes Associated With Sodium Butyrate Supplement in Chickens

Key words

IL-22;
TLR8;
intestinal villi;
sodium butyrate; goblet cells;
lymphoid nodules

Mohamed A.M. Alsafy[1]*, Samar M. Ez Elarab[2], Islam A. Abdellatif[1], Yaser H. Elewa[4,5], Heba A. Basha[3], Naglaa F. Bassuoni[1], Samir A. El-Gendy[1], Mohamed A. Abumandour[1], Catrin Sian Rutland[6]*, Karam Roshdy[2]

[1]Department of Anatomy and Embryology, [2]Department of Histology and Cytology, [3]Department of Animal Husbandry and Animal Wealth Development, Faculty of Veterinary Medicine, Alexandria University, Alexandria, [4]Histology and Cytology Department, Faculty of Veterinary Medicine, Zagazig University, Zagazig, Egypt, [5]Laboratory of Anatomy, Faculty of Veterinary Medicine, Basic Veterinary Sciences, Hokkaido University, Sapporo, Japan, [6]School of Veterinary Medicine and Science, University of Nottingham, Nottingham, United Kingdom

***Corresponding authors:** mohamed.alsafy@alexu.edu.eg; catrin.rutland@nottingham.ac.uk

Abstract: This study evaluated the effects of sodium butyrate (SB) supplementation on small intestine development in broiler chickens. Periodic acid-Schiff (PAS) and immunohistochemistry were used to undertake histological examinations of the duodenum, jejunum, and ileum. Duodenum, jejunum, and ileum histomorphometric data (villus length, crypt depth, goblet cell count), and interleukin-22 (IL-22) and toll-like receptor 8 (TLR8) immuno-stained area tissue coverage were quantified in control and SB supplemented groups. The histological changes in the SB supplemented group compared to the control group were as follows: There were increased villi lengths, widths, and crypt depths in the small intestine (duodenum, jejunum, and ileum). Increased numbers of goblet cells were observed, especially in the ileum. In addition, the lymphoid tissue within the small intestine was significantly larger (cross-section area=SB 34.8±0.5m2 vs control 13.2±0.5m2) and presented with more lymphoid nodules and more diffuse lymphoid tissue in the tunica submucosa, in the SB supplemented group compared to controls. Chickens do not have lymph nodes, therefore the mucosal-associated lymphoid tissue plays a major immunological role. Significant immunohistochemistry expression of IL-22 and TLR8 proteins were observed in the intestinal epithelial layer of the small intestine, which may play a role in protecting against many pathogens and gastrointestinal cancers.

Received: 3 April 2024
Accepted: 6 June 2024

Introduction

Broilers are meat-producing chickens and are popular worldwide for their growth efficiency, and therefore low production cost. They grow in six weeks from an average hatching weight of around 40 g to a weight of around 2.4 kg. Conventionally farmed broilers are typically slaughtered from 42 days whereas slower growing or organic chickens are culled at 8-12 weeks (1). Broiler breeders have also concentrated on producing rapidly growing broilers in order to maintain gut health in antibiotic-free rearing programs (2). Intestinal health is critical for maximizing feed efficiency and growth rates (3, 4). Previous studies have already found a link between the development of intestinal anatomical characteristics and animal weight gains and feed conversion ratios (5).

The chicken's small intestine has three compartments (duodenum, jejunum, and ileum), each with a tunica mucosa, tunica submucosa, tunica muscularis, and tunica serosa (6). Previous histological studies have shown that the tunica mucosa is composed of surface epithelium

and lamina propria and may lack a well-developed lamina muscularis mucosae (7). The height of the villi gradually decreases from the duodenum, jejunum then ileum, and microvilli are present on the apical edge of columnar cells (8, 9). The crypts, containing intestinal stem cells and Paneth cells, have a basic tubular structure with a bulging base that opens into the lumen between the villi's bases, the interiors of the villi have multiple nodules. Previous studies have indicated that longer villi and deeper crypts increase tissue regeneration and nutrient absorption (8-10). The lamina propria consists of loose connective tissue and contains blood capillaries, a few smooth muscle cells, and lymph nodules. The tunica muscularis in chickens is divided into three layers of smooth muscle cells: the inner longitudinal, middle circular, and outer longitudinal layer. The thickness of the tunica muscularis increases as you navigate from the duodenum through to the ileum. The tunica serosa contains mostly loose connective tissue, blood vessels, and mesothelial cells (11-13).

Butyrate (a straight-chain alkyl carboxylic acid also called butyric acid and butanoic acid) and other short-chain fatty acids are widely used in animal nutrition because they assist weight gain and have a variety of other beneficial digestive tract effects (14). Sodium salt from butyric acid is commonly called sodium butyrate (SB). SB has been linked to protective effects against Salmonella enteritidis in birds (15) and butyrate has been shown to aid in the development of the intestinal epithelium (16).

Previous studies (16-18) have indicated links between enhanced immunity and SB supplementation, therefore protein expression of interleukin-22 (IL-22) and toll-like receptor 8 (TLR8) were investigated in the present study. IL-22, a cytokine involved in many processes ranging from innate immune responses to tissue regeneration, helps to regenerate many organs, including the intestine, thymus, liver, lung, and pancreas (19, 20). Agonists to TLR8, an endosomal receptor that recognizes single stranded RNA, have been used in clinical trials as immune enhancers in combination therapy for a variety of cancers (21). Despite studies reporting marked enhancements in chicken growth performance due to the use of food supplemented with sodium butyrate (22-24), the major histological changes within the small intestine have not been elucidated and requires further study.

The present study outlines the histological changes in chickens supplemented with SB relating to small intestine architecture and goblet cell count, in addition to showing the intestinal immunohistochemistry expression of IL-22 and TLR8.

Material and methods

Animal and experimental design

The study was conducted with ethical permission from the Faculty of Veterinary Medicine, Alexandria University and approved by Institutional Animal Care and Use Committee (ALEXU-IACUC; Approval code: 013/2022/12/12/189). A total of 60 one-day-old male Cobb 500 broilers were obtained from the Integrated Management and Hatching Laboratory (Desert Road Facility, Alexandria governorate). A completely randomized design was used to randomly allocate the chickens into one of two groups: the control group (n=30) and the SB supplemented group (n=30). Each group was represented by two replicates with 15 chicks per replicate, and each group of n=15 was housed in separate, controlled environment pens in accordance with Directive 2010/63/EU, separated by wooden chipboard. Control chickens received water free from sodium butyrate and SB supplemented received water containing 0.98 mg sodium butyrate (West Bengal Chemical Industries Ltd., India) per 1 ml of drinking water from days 1-28 (based on a previous study (25)).

The chicks were housed on litter (mainly wood chippings) on the floor at a depth of 5 cm and brooded at 32 °C for the first week, which was reduced by 3 °C weekly, then maintained at 20 °C by week four. Relative humidity was maintained at between 65% and 75%. Following standard healthcare regimes, the chicks were vaccinated against Newcastle disease and infectious bronchitis at the 8th and 18th days (using the Hitchner, IB, and HIPRAVIAR Clon live vaccine CL/79 clon), in their drinking water. They were also vaccinated against infectious bursal disease (IBD) on the 14th day using an intermediate strain in drinking water (26). Both groups received minerals and vitamins in their *ad lib* feed (full ingredients shown Table 1) as per Nutrient Requirements of Poultry guidelines (27) with a starter diet provided on days 0 to 14, then a grower diet containing from day 15 to until the end. Fosfomycin antibiotics were added to their water as standard animal care (therefore bacterial load was not investigated in the present study). The chicks had daily health checks and underwent cervical dislocation and decapitation on day 30.

Histological and immunohistochemical (IHC) examination of the small intestine

Fresh samples from the duodenum, jejunum, and ileum were collected from n=5 per replicate control and n=5 per replicate SB supplemented groups for histological examination. The specimens (duodenum, jejunum, and ileum) were fixed in 10% phosphate-buffered formaldehyde, processed into paraffin blocks and 5µm sections cut then stainedLayton, Bancroft and Suvarna (28). The periodic acid-Schiff technique (PAS) was used to identify goblet cells using a previously published protocol (29). In brief this consisted of 0.5 % periodic acid for 10 min, Schiff's Reagent

Table 1: Ingredients and nutrient composition (% dry mass) in broiler starter and grower food

Ingredient	Starter (%) days 1-14	Grower (%) days 15-30
Yellow corn	53.5	66.5
Soybean meal (48% starter mix)	34.38	24
Corn gluten	5.82	3.6
Salt	0.3	0.3
Dicalcium phosphate[A]	2.7	2.48
Vitamin premix[B]	0.3	0.3
Corn oil	3.00	2.82
Total	100%	100%
Calculated values		
Metabolizable Energy (ME) (kcal/kg)	2976.83	3096.31
Crude protein	22.97	18.07
Calcium	1.08	0.9
Available phosphorus	0.52	0.45
Methionine[C]	0.52	0.51
Lysine[D]	1.29	1.13

A) Dicalcium phosphate, 18% granular phosphate, and 23% calcium. B) Supplied per kg of diet: vitamin A 12,000 IU, vitamin D3 3,000 IU, vitamin E 40mg, vitamin K3 3mg, vitamin B1 2mg, vitamin B2 6mg, vitamin B6 5 mg, vitamin B12 0.02mg, niacin 45mg, biotin 0.075mg, folic acid 2mg, pantothenic acid 12mg, manganese 100mg, zinc 600mg, iron 30mg, copper 10mg, iodine 1mg, selenium 0.2mg, cobalt 0.1mg. C) DL-Methionine, Met AMINO® (DL-2- - amino-Y-methyl-oily acid)amino-4-(methyl-thio)-butane acid, DL-methionine, by Feed Grade 99% (EU). D) L-Lysine HCL 99% (Feed Grade) L-Lysine: 78.0% Min (Indonesia)

Table 2: List of antibodies, their sources, working dilutions and antigen retrieval

Antibody	Catalogue number and Source	Dilution	Antigen retrieval
Rabbit polyclonal anti-IL-22	ab18564, Abcam, UK	1:100	Tris-HCl, 110°C 15 min microwave
Rabbit polyclonal anti-TLR-8	ab24185, Abcam, UK	1:1000	10 mM citrate buffer (pH 6.0), 105°C 20 min microwave
Biotin-conjugated goat anti-rabbit IgG antiserum (secondary)	Histofine kit 424032, Nichirei Biosciences Inc. Japan		

Table 3: Histomorphometric changes in the small intestine following administration of dietary sodium butyrate

	Villus length (µm) ± SEM		Crypt depth (µm) ± SEM		Goblet cell count/10,000 µm² ± SEM	
	SB group	Control group	SB group	Control group	SB group	Control group
Duodenum	374.67±0.83[a]	360.00±0.94[b]	244.000±0.54[a]	173.000±0.47[b]	1306.66±15.15[a]	294.67±3.18[b]
Jejunum	574.67±0.83[a]	400.67±1.44[b]	163.666±2.16	150.666±3.66	702.66±0.57[a]	531.67±0.98[b]
Ileum	1000.00±2.72[a]	421.33±5.19[b]	623.666±0.57[a]	335.000±0.47[b]	924.00±0.54[a]	479.67±8.04[b]

a and b = values differed significantly between the control and sodium butyrate (SB) groups, where $P < 0.05$ using ANOVA with post-hoc testing. SEM = standard error of the mean. N=10 chickens per group (control and SB).

for 20 min at 65 °C, and hematoxylin for visualization of nuclei. The goblet cells were counted using image J/Fiji in ten different fields of view for each intestinal region from each specimen at x400 magnification.

The immunohistochemical technique used for the intestinal sections was as previously published (30). The antibodies used for immunohistochemistry, and their sources and working dilutions, in addition to antigen retrieval methods, are listed in Table 2. In brief 0.5% TritonX-100 was applied for 20 min, followed by antigen retrieval (Table 2), washed in distilled water, followed by 0.3% H_2O_2/methanol for 20 min to deactivate endogenous peroxidase. Then 5% bovine serum albumin in PBS was applied followed by primary antibody incubation (Table 2).

Negative control sections were maintained in the 5% bovine serum. Followed a wash in PBS the sections were incubated for 30 min in, biotin-conjugated goat anti-rabbit IgG antiserum (Histofine kit, Cat: 424032, lot: H1401; Nichirei, Tokyo, Japan), then washed in PBS, then incubated in streptavidin–peroxidase conjugate for 30 min at room temperature. Peroxidase/3,3'-Diaminobenzidine (DAB; ChemMate Detection Kit; Cat: K5007, lot: 00054660A, Dako, Carpinteria, CA, USA) was used to visualise the conjugate and Mayer's hematoxylin was used to counterstain.

Imaging, measurements, and statistical analysis

Micrographs of the stained sections (10 systematically randomly chosen fields from every specimen for the duodenum, jejunum, and ileum respectively) were taken with a digital camera (Leica EC3, Leica, Germany) connected to a light microscope (DM500, Leica, Germany). The histomorphometric data, consisting of villi lengths, crypt depths, goblet cell counts, from within the duodenum, jejunum, and ileum, and the Peyer's patch areas and numbers in cross sections of the ileum, in both the control and SB supplemented groups were measured with the aid of image J software (National Institutes of Health, USA; Table 3). Goblet cell count was calculated on PAS sections at X400 magnification using ten different fields (each measuring 10,000 μm^2) per chick per tissue type. For quantification of immunostaining intensities, Image J software was used as described previously (31). In brief, the mean density of staining was determined in the 10 systematically randomly chosen fields from each section from the five birds in each group, as previously published by Vis and coauthors (32). This was presented as a percentage of positive immune-stained area (brown colour for DAB) for both IL-22 and TLR 8 from small intestine tissue in the control and SB supplemented groups.

Data measured as lengths and areas were statistically analyzed with one-way analysis of variance (ANOVA) and Bonferroni post-hoc testing (SPSS version 26, IBM). This enabled concomitant comparisons between the two groups (Control vs SB) and the three different tissue types (duodenum, jejunum, and ileum). Immunostaining was calculated as percentage coverage. Data are expressed as mean ± standard error of the mean (SEM), P values <0.05 were considered significant. Analyses of the significant main effects of experimental treatments were performed using multiple range comparisons with Duncan's multiple range test.

Results

Histological examination of the small intestine

The small intestines from the 60 day old chicks from both the control and SB supplemented groups had a small intestine structures consisting of four layers, the tunica mucosa, tunica submucosa (Fig.1a,e/SU), tunica muscularis (Fig.1a,e/TM), and tunica serosa (Fig.1a,e/TS). The duodenum in these chicks lacked the Bruner's gland (Fig.1a/IG) and had finger-like projecting intestinal villi (Fig.1a,b). The jejunum contained tube-like villi (Fig.1c,d), and the ileum had leaf-like villi with broad bases and pointed ends (Fig.1e,f).

Histomorphometry changes were observed in the SB groups compared to the control chicks at day 60. The length of villi (Fig.1a-f/VL, Table 3) increased in the SB group duodenum, jejunum, and ileum compared to controls ($P < 0.05$). Crypt depth (Figs.1a-f/CD; 2a-b, Table 3), increased in the SB group duodenum and ileum compared to controls ($P < 0.05$) but not the jejunum ($P > 0.05$). The goblet cells had a characteristic magenta-red color and had a flask shape between epithelial cells of the intestinal villi (Figs. 2 and 3). The number of goblet cells significantly increased in the duodenum (control 360.00±0.94, SB 374.67±0.83) jejunum (control 400.67±1.44, SB 574.67±0.83) and ileum (control 421.33±5.19, SB 1000.00±2.72) with the administration of sodium butyrate in the supplemented group (Figs.2c and 3b/arrowheads) in comparison with the control group (Figs.2c and 3a/arrowheads; $P < 0.05$; Table 3).

The surface area of each of the lymphoid nodules, known as Peyer's patches within the ileum, increased in the SB supplemented group to 34.3±0.5 μm^2 in comparison with the control group at 13.3±0.3 μm^2 (Figs.1e&f arrows and 4a–b/LN; $P < 0.05$). Concomitantly, the number of Peyer's patches was higher in the SB group compared to controls (19±0.45 in SB versus 10.8±0.49 in controls; Fig.4b/LN; $P < 0.05$). The combined surface area with number of nodules resulted in an increased nodule area in the SB group (651.68 μm^2 in controls versus 143.56 μm^2 in SB supplemented per cross section of the ileum; $P < 0.05$). Microscopic qualitative observation of the sections indicated that the SB supplemented group showed a few regressed intestinal glands (Fig.4b/arrows), and instead of diffuse glands, aggregated lymphoid tissue was observed (Fig.4b/DL). Qualitative analysis also showed that in the SB supplemented group ileums, there were diffuse

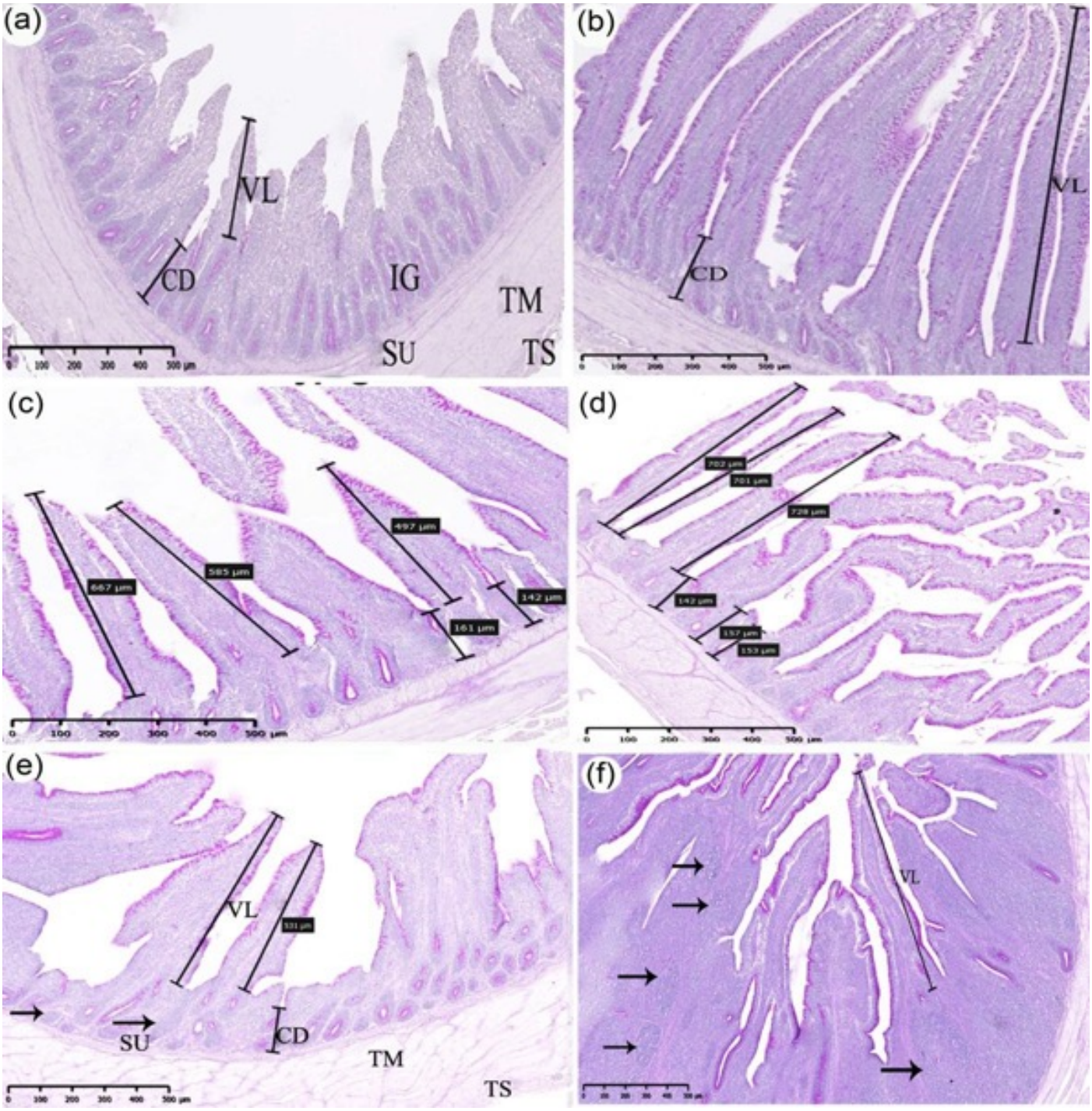

Figure 1: Photomicrographs of the duodenum, jejunum and ileum in control and SB supplemented chickens

a) Control group duodenum showing villi (finger-like shape). b) SB supplemented duodenum showing increased villus length and crypt depth. c) Control group jejunum showing villi length and crypt depth. d) SB supplemented group jejunum with increased villi length and crypt depth. e) Control group ileum indicating villus length and crypt depth, with associated tunica submucosa, tunica muscularis, tunica serosa, and fewer numbers of lymphoid nodules (arrow). f) SB supplemented group ileum with increased villus length, increased numbers of lymphoid nodules which were larger in size (arrow). Villus length (VL). Crypt depth (CD). Intestinal gland (IG). Tunica submucosa (SU). Tunica muscularis (TM). Tunica serosa (TS). Stain = PAS, Magnification = 40X, scale bars represent 500 µm

lymphocytes present (Fig.4c/I), penetration of lymphocytes into the diffuse lymphoid tissue had occurred and the cells were located next to enterocytes (Fig.4c/arrows), desquamated epithelium were observed (Fig.4c/DS), and mucous secretion was observed in the lumen near the tip of the villi in the ileum (magenta-red color in Fig.4c/MU and arrowhead). In addition, a lymph vessel lined with simple squamous endothelial cells each containing a flat and elongated nucleus (Fig.4d/arrowheads) was observed, the lymph vessel was filled with lymphocytes (Fig.4d/L). Cells

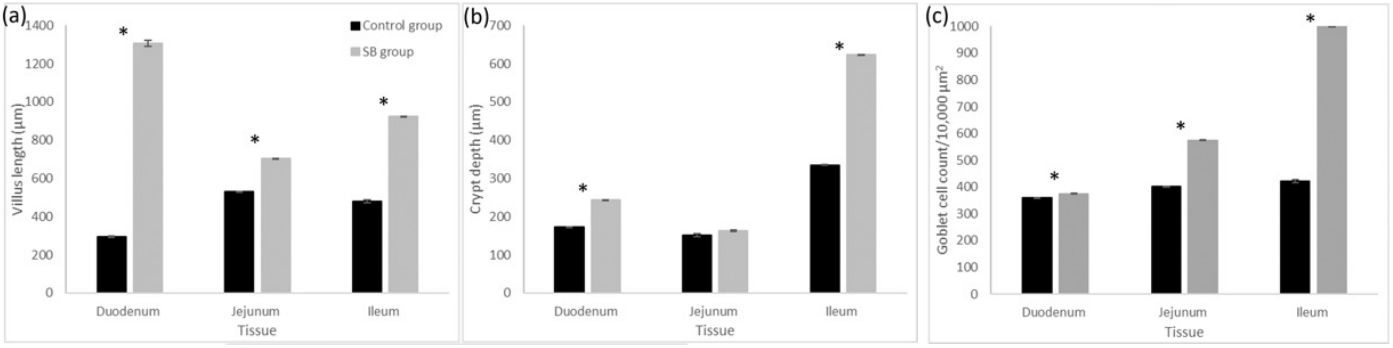

Figure 2: Villus length, crypt depth, and goblet cell number measurements within the small intestine. a) Villus length, b) crypt depth and c) goblet cell quantification in the duodenum, jejunum, and ileum. Calculated on PAS sections at X400 magnification using ten different fields (each measuring 10,000 µm²) per chick per tissue type (duodenum, jejunum, and ileum). Values represent mean ± SEM. * indicates significant differences P < 0.05 between control and SB supplemented groups

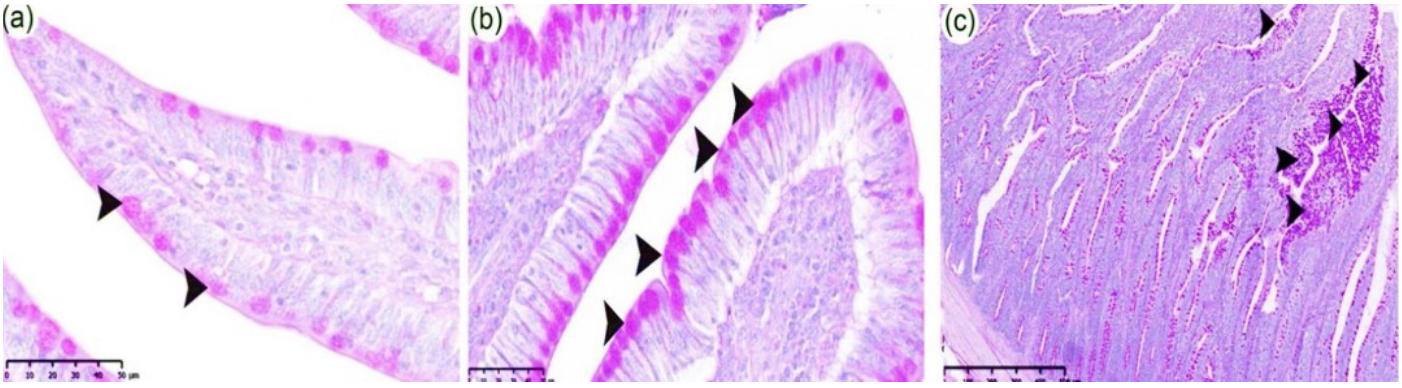

Figure 3: Goblet cells within the ileum and jejunum. (a) Control group ileum had a low density of goblet cells (arrowheads). (b) SB supplemented group ileum exhibiting increased numbers of goblet cells, with a higher density in a typical cup shape-like structure (arrowheads). (c) SB supplemented group jejunum showing hyperplasia of goblet cells within the jejunal villi (arrowheads). Stain = PAS. a+b) Magnification = X400, scale bars represent 50µm, c) Magnification = X40, scale bars represent 500 µm

that looked like macrophages with kidney shaped nuclei (Fig.4d/arrow) and diffuse lymphoid tissue were located under the lamina epithelial of the dome structure of Peyer's patches in the lamina propria, known as loose connective tissue (Fig.4d/DL), were also observed. Following SB supplementation for 60 days, a high number of reticular fibers (Fig.4e/arrows) were noted, potentially acting as a scaffold for diffuse lymphoid tissues (Fig.4e/DL) in the lamina propria of the ileum (Fig.4e).

Immunohistochemistry analysis and immune response

Expression of IL-22 in the small intestine tissue (duodenum, jejunum, and ileum) was observed in both the SB supplementation group and the control group (Fig.5, Supp Table 1). The duodenum, jejunum, and ileum intestinal tissue in the control group revealed weak expression of IL-22 (Fig.5a,c,e). Conversely, SB supplemented chickens exhibited noticeable darker IL-22 staining in the duodenum, jejunum, and ileum, within the epithelium lining the villi (Figs.5b,d,f/arrows and 6a) and crypts (Fig.5b,d,f/arrowheads). TLR8 protein expression was present in the epithelium lining of the small intestine (duodenum, jejunum, and ileum) tissue. As observed with IL-22, the control group revealed weak expression of TLR8 (Fig.7a,c,e/arrows), whereas the SB supplemented group exhibited notably darker TLR8 expression in the epithelium lining of

Supplementary Table 1: Quantification of interleukin-22 (IL-22) and Toll-like receptor 8 (TLR8) expression

	SB supplemented (%)	Control (%)
IL-22 - Duodenum	16.23±0.12	1.33±0.03
- Jejunum	13.43±0.03	1.87±0.03
- Ileum	16.07±0.07	2.07±0.07
TLR8 - Duodenum	23.68±0.33	5.40±0.06
- Jejunum	22.16±0.09	4.30±0.11
- Ileum	24.83±0.44	5.37±0.09

Immunohistochemical positive staining was measured as total area (expressed as a percentage of tissue) across ten different fields per tissue sections. Values represent mean±SEM.

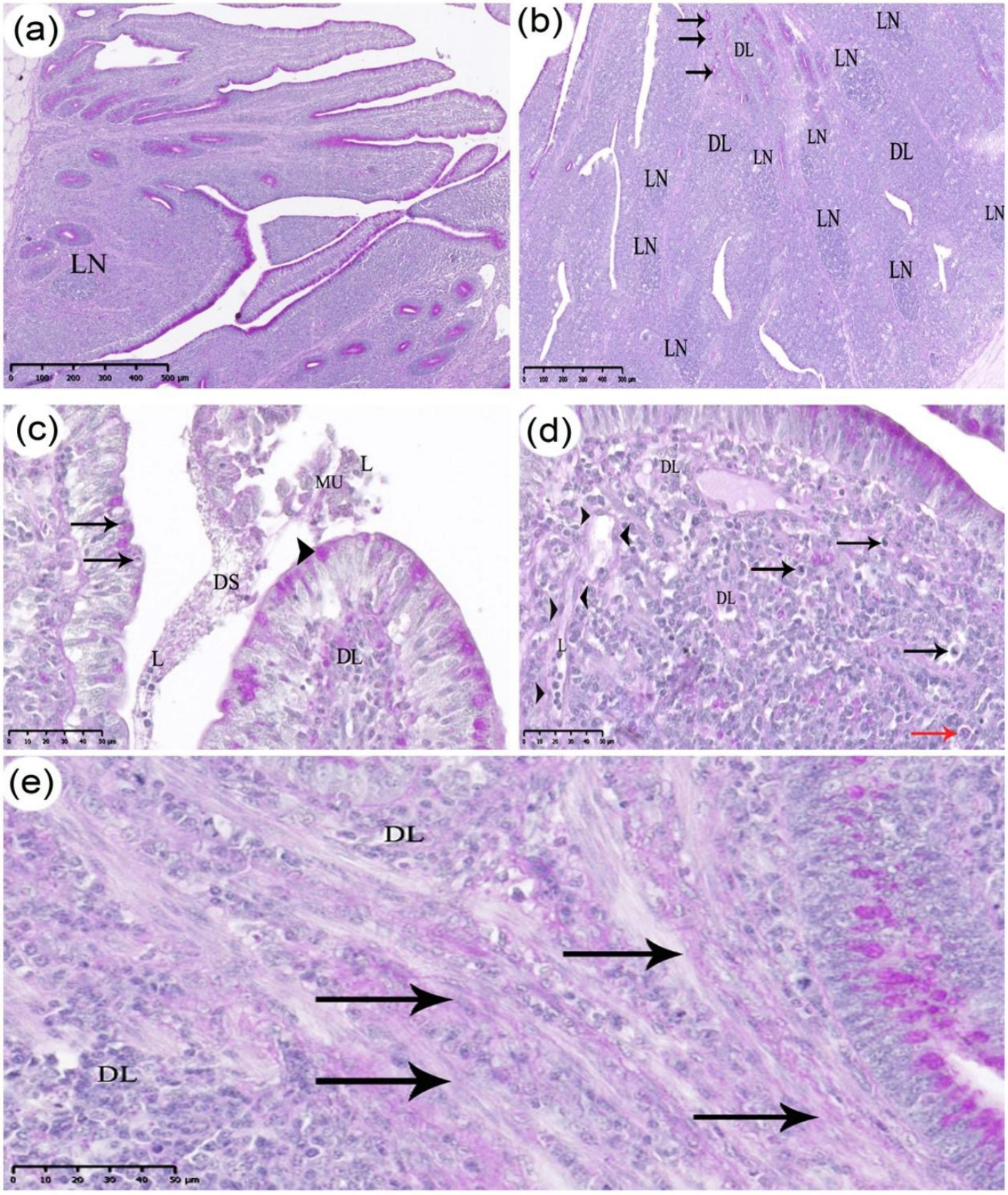

Figure 4: Histological observations in the ileum tissue. a) The control group ileum exhibited very few lymphoid nodules (LN). b) In the SB supplemented group the ileum contained a few regressed intestinal glands (arrows), as most had been replaced by diffuse lymphoid tissue (DL) and a high number of Peyer's patches (LN). c) In the SB supplemented group ileum there was penetration of lymphocytes into the diffuse lymphoid tissue (arrows), desquamated epithelium (DS), lymphocytes (L), magenta-red color mucous secretion (MU) near to tip of the villi of the ileum (arrowhead), and diffuse lymphoid tissue in lamina propria (DL). d) In the SB supplemented groups ileum lymph-vessel (arrowheads), lymphocytes were present inside the lymph vessel (L), beneath the dome structure, and between diffuse lymphocytes in the lamina propria (DL), and macrophages with kidney shape nuclei (arrows). e) The SB supplemented ileum also exhibited reticular fibers-stained magenta-red in color (arrows), with diffuse lymphoid tissue in the lamina propria (DL). Staining = PAS. a+b) Magnification = X40, scale bars represent 500 µm. c-e) Magnification = X400, scale bars represent 50 µm

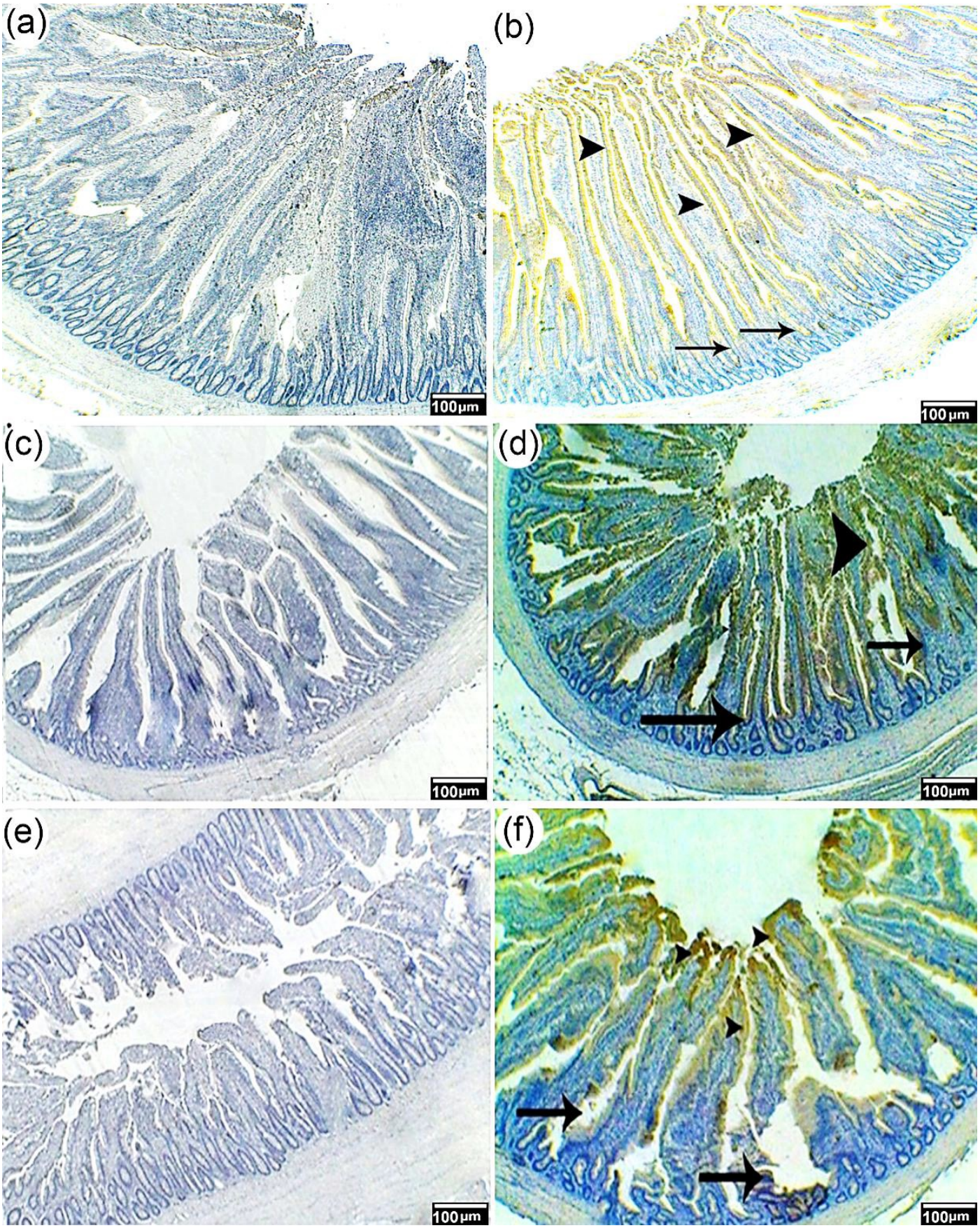

Figure 5: Mucosal cell immunohistochemical staining for interleukin-22 (IL-22) in the small intestinal (duodenum, jejunum, and ileum) in the epithelium lining the villi (arrows) and crypts (arrowheads). a) Control group duodenum, b) SB supplemented group duodenum, c) Control group jejunum, d) SB supplemented group jejunum, e) Control group ileum and f) SB supplemented group ileum. Note the DAB brown color denoting IL-22 expression in the SB supplemented intestinal tissue. Magnification = X40, scale bar represents 100 µm

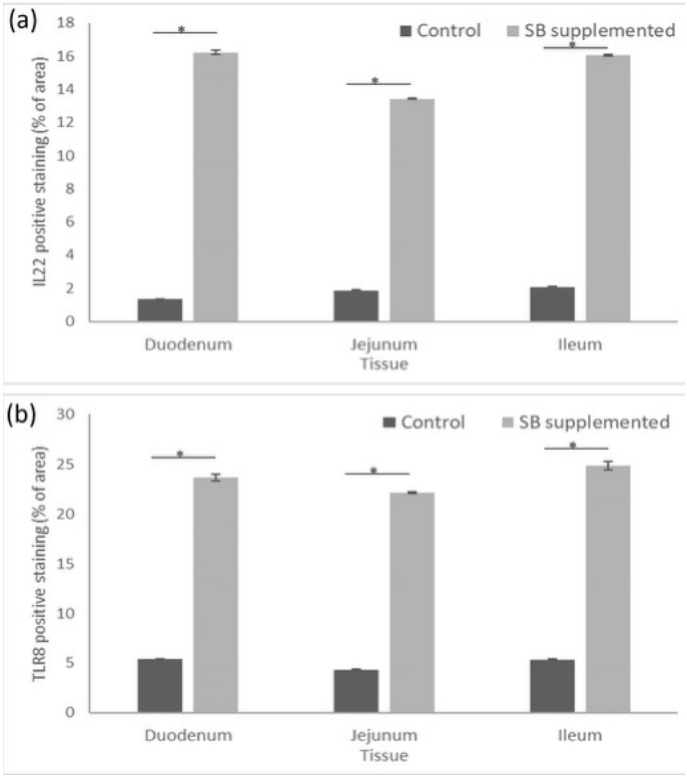

Figure 6: Quantification of a) interleukin-22 (IL-22) and b) Toll-like receptor 8 (TLR8) expression. Immunohistochemical positive staining was measured as total area (expressed as a percentage of tissue) across ten different fields per tissue section. Values represent mean ± SEM. * indicates significant differences between control and SB supplemented groups ($P < 0.05$)

the duodenum, jejunum, and ileum epithelium (Fig.7b,d,f/ arrows, dark brown immune-positive staining).

Concomitant with the qualitative changes described above, there was a quantitative increase in the mean area (expressed as a percentage of total tissue) of IL-22 positive immuno-stained tissue in the SB supplemented group compared to the control group. The percentage of immunostained areas were control 1.33±0.03 vs SB 16.23±0.12% in the duodenum, control 1.87±0.03 vs SB 13.43±0.03% in the jejunum, and control 2.07±0.07 vs SB 16.07±0.07 in the ileum. Quantification of TLR8 protein expression also showed more tissue area was immunostained in the SB supplement intestinal tissues compared to control tissues (duodenum control 5.40±0.06 vs SB 23.68±0.33%, jejunum control 4.30±0.11 vs SB 22.16±0.09%, ileum control 5.37±0.09 vs SB 24.83±0.44%.

Discussion

In this study, the administration of sodium butyrate significantly increased duodenal, jejunal, and ileum villi lengths and crypt depths, similar to previous reports in broiler chickens using coated SB (33, 34). Longer villi are thought to support larger surface areas, enabling higher absorption capacities and healthier intestinal development, resulting in the gut's optimal state (35-37). Butyrate is the active ingredient within sodium butyrate which was absorbed by enterocytes as a source of energy, it has therefore been implemented to support faster intestinal development and function as well as facilitating improved overall health (38, 39). Furthermore, in the present study microscopic analysis of the villi revealed that SB supplements increased the number of goblet cells by 4% in the duodenum, 43% in the jejunum and 137% in the ileum compared to controls. Microscopic observations also indicated the SB supplemented group chicks exhibited potential hyperplasia of the goblet cells within the jejunal villi (Fig.3c/arrowheads, qualitative observation). Goblet cells are responsible for the production and stimulation of mucus (40) and the mucus layer is often considered the first line of defense in the intestinal mucosa. The mucins were controlled by changing the number of goblet cells or mucin gene expression, especially MUC2 (41). Therefore, it is of interest that SB supplementation increased the number of goblet cells, therefore potentially impacting mucus production and immunity.

Chicks do not have lymph nodes, and the present study confirmed the lack of lymph nodes, therefore it has been asserted that the mucosal-associated lymphoid tissue has a major immunological role. Eren and coauthors (42) explained the role of cecal tonsils as one mucosal associated lymphoid tissue in chicken and highlighted its role in TLR2 and TLR4. An important finding of the present research related to the ileum lymphoid nodules, known as Peyer's patches, which increased in both number and size, resulting in an overall increase in tissue following SB supplementation. The surface area of each of the Peyer's patches within the ileum increased by 2.5-fold in the SB supplemented group in comparison with the control group. Concomitantly, the number of Peyer's patches was 75% higher in the SB group compared to controls, and when the surface areas and number of nodules were considered together, this resulted in a 4.5 increase in nodule area in the SB group. This finding agrees with Sikandar *et al.*, (34) who recorded that coated SB increased the size and number of lymphoid nodules in the bursa and that SB also enhanced immune system function. In the present study the lymph vessels within the ileum were lined with a single layer of endothelium and filled with lymphocytes. This finding agrees with the review written by Pepper and Skobe (43) which suggested that the lymph vessels had significant importance for the entrance of leukocytes and serving immunological functions. In the present study relatively high numbers of macrophages were observed in the lamina propria of the ileum. This finding concurs with concepts as previously reviewed (44) which explained the role of macrophages in the immunological defense in Peyer's patches of the ileum of mammals known for phagocytic activities.

Reticular fibers were evident in the Peyer's within the ileum of both control and SB supplemented, but more evident in

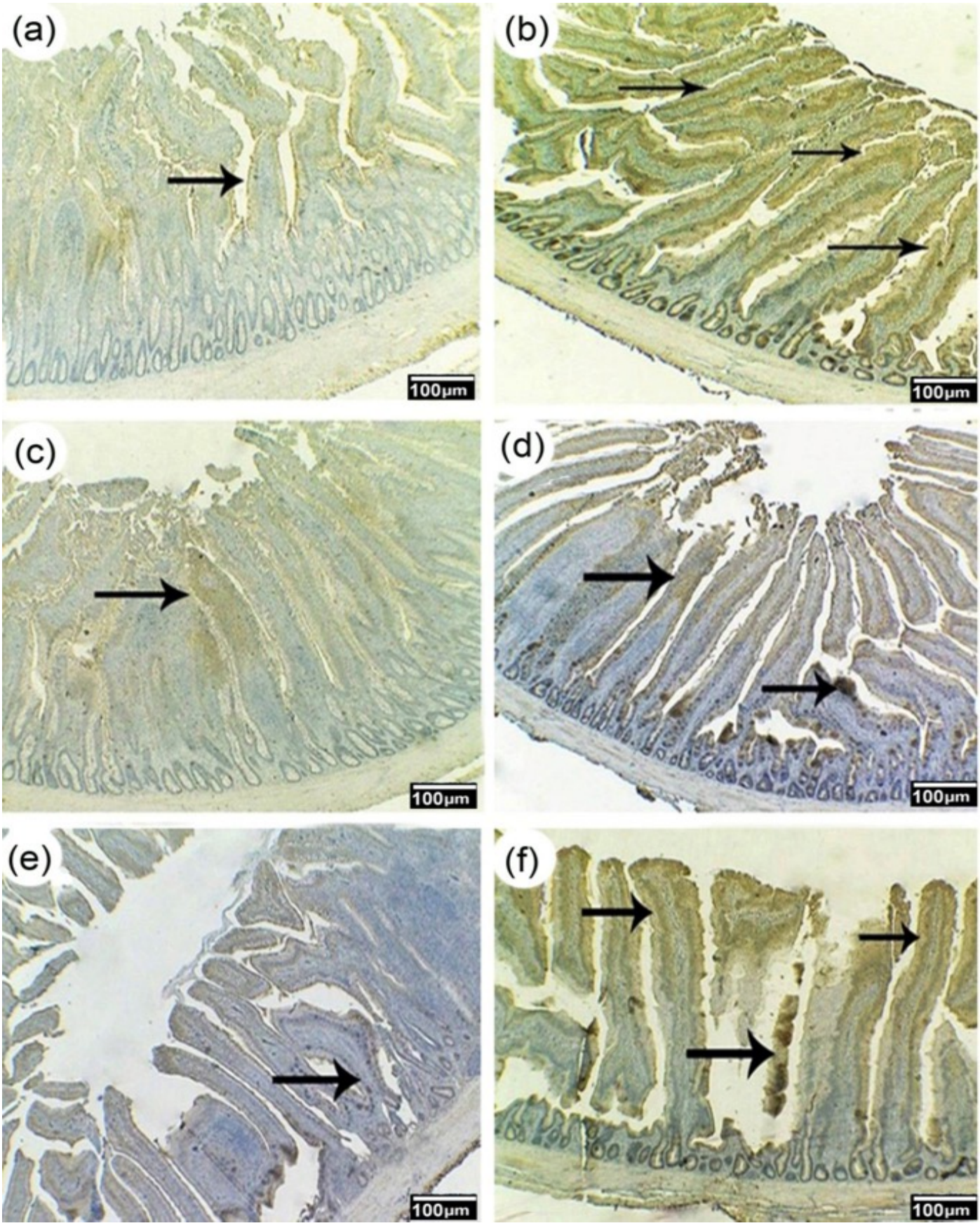

Figure 7: Immunohistochemical staining of Toll-like receptor 8 (TLR8) in the epithelium lining and intestinal mucosal cells in the duodenum, jejunum, and ileum - arrows. a) Control duodenum, b) SB supplemented duodenum, c) Control jejunum, d) SB supplemented jejunum, e) Control ileum, f) SB supplemented ileum. Note the pale brown DAB immunostaining expression of TLR8 in the control group compared to the darker dark brown in the SB supplemented group. Magnification = X40, scale bar represents 100 µm

the SB chickens. The reticular fibers were visualized as a magenta-red color following PAS application, indicating their structure rich with heparin sulfate, which belong to the glycosaminoglycans (a polysaccharide), as explained by Montes and coauthors (45). The lymphocytes in the present study, which move from the submucosa to the epithelium tissue, were found between the enterocytes in the ileum lamina epithelial layer. This finding agreed with Lundqvist *et al.*, (46) who observed a similar situation in the human small intestine. They summarized that the immunological role of intraepithelial lymphocytes, a lytic role and had potential effects as T-helper and T-cytotoxic lymphocyte functions, which had a cytolytic role in tumor cells. The intestinal epithelium also played a barrier role, that was enhanced by sodium butyrate, in a mouse model of diabetes and obesity, helping to ameliorate diabetic-endotoxemia (37).

Sodium butyrate supplementation had a positive relationship with interleukin-22 immunostaining expression in the intestinal epitheliums in the small intestines of the SB supplemented group chicks. This finding agrees with Yang and coauthors (47), who reported that butyrate enhanced IL-22 production in vivo (in mice) and played a role in the inhibition of colitis via IL-22 action. Both our present study, and the previous work in mice, have indicated that SB supplementation therefore plays a positive role in intestinal immunity. For example Keir et al., (48), reviewed the role of IL-22 in intestinal health and disease, and discussed the role of IL-22, functioning as an intestinal barrier, with roles in intestinal hemostasis, complement production, and cancer. Patnaude and colleagues (49) concluded that the mechanisms behind IL-22 in human intestinal organoids and resections, and mice, by showing enhanced expression of the stem of intestinal cells, cell division, the intestinal mucous layer, and barrier activities against many pathogens. A review by Chen and coauthors (50) discussed that butyrate, T cells, and intestinal epithelium cooperated in environmental harmony to act in an anti-apoptosis, pro-proliferation, and anti-inflammation manner. As IL-22 responses were found in both healthy and diseased states, they suggested that IL-22 had a significant role in the initiation of defense action and cell regeneration. They also suggested that further studies should occur in diseased states to help with IL-22 based therapy. However, the previous studies relating to intestinal epithelium permeability are limited, and it has been suggested that in mice IL-22 has limited action on permeability in some junctional molecules. IL-22 has also been shown to induce the action of claudin-2 regulation, as reported in many studies (51, 52). The significant increases in IL-22 expression in the present study therefore indicate potentially beneficial changes following SB supplementation in the chicken.

Sodium butyrate, a supplement, had a positive correlation with the immune expression of TLR8 in the intestinal epithelium in the developing chicks in the present study. This finding agrees those shown previously (53) in bovine mammary epithelial cells and in intestinal porcine enterocyte cultures (54). They found that the administration of sodium butyrate enhanced the expression of TLR8 and TLR2, which played a significant role in the production of antimicrobial agents to protect against many pathogens such as *Staphylococcus aureus*. SB has also been shown to alleviate the action of lipopolysaccharides, which are the main factor in intestinal injury and microflora disturbance in rats. Dou and coauthors (55) explained the mechanism of sodium butyrate action by decreasing mRNA expression of cytokines to decrease the inflammatory process, thus enhancing the microbiota's action to decrease apoptosis of the intestinal epithelium which decreased inflammation. In people, TLR8 is found intracellularly in the normal state and has a known role in innate and acquired immunity (56, 57). TLR8 has also been used to induce the activity of natural killer cells against tumors, and has been used in both tumor adjuvant and immunotherapy (58).

Conclusion

Administration of supplemental sodium butyrate (SB) via drinking water induced significant histological changes and immunological increases during intestinal development. Sodium butyrate dietary supplementation had a potentially beneficial effect on the chicken small intestine (duodenum, jejunum, and ileum) by increasing the lengths of villi, depths of crypt, number of intestinal goblet cells, the amount of diffuse lymphoid tissue, and the number and sizes of Peyer's patches. Expression levels of both IL-22 and TLR8 were also increased in the sodium butyrate supplemented group. These characteristics produced by SB supplementation may enhance the optimal intestinal microstructure and provide additional intestinal protection against many pathogens.

Acknowledgements

We thank Alexandria University for its help in completing this work. The current study has not received any funds from any organizations or institutions, but the University of Nottingham funded Open Access.

Authors declare no Conflict of Interests for this article.

The datasets used and/or analyzed during the current study are available from the corresponding author on reasonable request.

Abbreviations. SB Sodium butyrate, IL-22 Interleukin-22, TLR8 Toll-like receptor 8.

References

1. Nielsen SS, Alvarez J, Bicout DJ, et al. Welfare of broilers on farm. EFSA J 2023; 21(2): e07788. doi: 10.2903/j.efsa.2023.7788

2. Cervantes, H.M., Antibiotic-free poultry production: is it sustainable? J Appl Poult Res 2015; 24(1): 91–7. doi: 10.3382/japr/pfv006

3. Abd El-Naby, FS, Naiel Mohammed AE, Al-Sagheer AA, Negm SS. Dietary chitosan nanoparticles enhance the growth, production performance, and immunity in Oreochromis niloticus. Aquaculture 2019;501: 82–9. doi: 10.1016/j.aquaculture.2018.11.014

4. Alagawany M, Abd El-Hack ME, Al-Sagheer AA, Naiel MA, Saadeldin IM, Swelum AA. Dietary cold pressed watercress and coconut oil mixture enhances growth performance, intestinal microbiota, antioxidant status, and immunity of growing rabbits. Animals(Basel) 2018; 8(11): 212. doi: 10.3390/ani8110212

5. Elnesr S, Alagawany M, Elwan HA, Fathi MA, Farag MR. Effect of sodium butyrate on intestinal health of poultry–a review. Ann Anim Sci 2020; 20(1): 29–41. doi: 10.2478/aoas-2019-0077

6. Alshamy Z, Richardson KC, Hünigen H, Hafez HM, Plendl J, Al Masri S. Comparison of the gastrointestinal tract of a dual-purpose to a broiler chicken line: A qualitative and quantitative macroscopic and microscopic study. PLoS One 2018; 13(10): e0204921. doi: 10.1371/journal.pone.0204921

7. Kadhim KK, Zuki AB, Noordin MM, Babjee SM. Histomorphology of the stomach, proventriculus and ventriculus of the red jungle fowl. Anat Histol Embryol 2011; 40(3): 226–33. doi: 10.1111/j.1439-0264.2010.01058.x

8. Adibmoradi M, Navidshad B, Seifdavati J, Royan M. Effect of dietary garlic meal on histological structure of small intestine in broiler chickens. J Poult Sci 2006; 43(4): 378–83. doi: 10.2141/jpsa.43.378

9. Elhassan MMO, Ali AM, Blanch A, Kehlet AB, Madekurozwa MC. Morphological responses of the small intestine of broiler chicks to dietary supplementation with a probiotic, acidifiers, and their combination. J Appl Poult Res 2019; 28(1): 108–17. doi: 10.3382/japr/pfy042

10. Hamedi S, Rezaian M, Shomali T. Histological changes of small intestinal mucosa of cocks due to sunflower meal single feeding. Amer J Anim Vet Sci 2011; 6(4): 171–5. doi: 10.3844/ajavsp.2011.171.175

11. Kachave C, Bhosle N, Mamde CS, Lambate L. Histological observations on small intestine in broiler and layer of poultry birds. R Vet J India 2009; 5(1/2): 5–9.

12. Janardhana V, Broadway MM, Bruce MP, et al., Prebiotics modulate immune responses in the gut-associated lymphoid tissue of chickens. J Nutr 2009; 139(7): 1404–9. doi: 10.3945/jn.109.105007

13. Jamroz D, Wiliczkiewicz A, Skorupińska J, Orda J, Kuryszko J, Tschirch H. Effect of sweet chestnut tannin (SCT) on the performance, microbial status of intestine and histological characteristics of intestine wall in chickens. Br Poult Sci 2009; 50(6): 687–99. doi: 10.1080/00071660903191059

14. Robles R, Lozano AB, Sevilla A, Márquez L, Nuez-Ortín W, Moyano FJ. Effect of partially protected butyrate used as feed additive on growth and intestinal metabolism in sea bream (Sparus aurata). Fish Physiol Biochem 2013; 39(6): 1567–80. doi: 10.1007/s10695-013-9809-3

15. Fernández-Rubio C, Ordóñez C, Abad-González J, et al., Butyric acid-based feed additives help protect broiler chickens from Salmonella Enteritidis infection. Poult Sci 2009. 88(5): 943–8. doi: 10.3382/ps.2008-00484

16. Bortoluzzi C, Pedroso AA, Mallo JJ, Puyalto M, Kim WK, Applegate TJ. Sodium butyrate improved performance while modulating the cecal microbiota and regulating the expression of intestinal immune-related genes of broiler chickens. Poult Sci 2017; 96(11): 3981–93. doi: 10.3382/ps/pex218

17. Ahsan U, Cengiz Ö, Raza I, et al., Sodium butyrate in chicken nutrition: the dynamics of performance, gut microbiota, gut morphology, and immunity. World's Poult Sci J 2016; 72(2): 265–75. doi: 10.1017/S0043933918000090

18. Zhang WH, Gao F, Zhu QF, et al. Dietary sodium butyrate alleviates the oxidative stress induced by corticosterone exposure and improves meat quality in broiler chickens. Poult Sci 2011; 90(11): 2592–9. doi: 10.3382/ps.2011-01446

19. Dudakov JA, Hanash AM, van den Brink MR. Interleukin-22: immunobiology and pathology. Annu Rev Immunol 2015; 33: 747–85. doi: 10.1146/annurev-immunol-032414-112123

20. Lindemans CA, Calafiore M, Mertelsmann AM, et al., Interleukin-22 promotes intestinal-stem-cell-mediated epithelial regeneration. Nature 2015; 528(7583): 560–4. doi: 10.1038/nature16460

21. Abou-Bakr S. Genetic and phenotypic trends of 305-day milk yield of Holstein cows raised at commercial farm in Egypt. Egyptian J Anim Product 2009; 46(2): 85–92. doi: 10.21608/ejap.2009.94031

22. Mallo JJ, Sol C, Puyalto M, Bortoluzzi C, Applegate TJ, Villamide MJ. Evaluation of sodium butyrate and nutrient concentration for broiler chickens. Poult Sci 2021; 100(12): 101456. doi: 10.1016/j.psj.2021.101456

23. Morkhade SJ, Deshpande KY, Thakare SO, Mandale NR, Badukale DM. Influence of dietary sodium butyrate supplementation on performance, nutrient digestibility and economics of broiler chicken. Anim Nutr Feed Technol 2022;22(2): 287–96. doi: 10.5958/0974-181X.2022.00023.3

24. Hu Z, Guo Y. Effects of dietary sodium butyrate supplementation on the intestinal morphological structure, absorptive function and gut flora in chickens. Anim Feed Sci Technol 2007; 132(3/4): 240–9. doi: 10.1016/j.anifeedsci.2006.03.017

25. Belih S, EL-Hadad S, Amen G, Basiony MR. Influence of sodium butyrate on salmonella infection in broiler chicks. Benha Vet Med J 2016; 31(2): 21–32. doi: 10.21608/bvmj.2016.31255

26. Saleh N, Allam T, El-Latif AA, Ghazy E. The effects of dietary supplementation of different levels of thyme (Thymus vulgaris) and ginger (Zingiber officinale) essential oils on performance, hematological, biochemical and immunological parameters of broiler chickens. Glob Vet 2014; 12(6): 736–44. doi: 10.5829/idosi.gv.2014.12.06.83189

27. Council NR. Nutrient requirements of poultry. 9th ed. Washington: The National Academies Press, 1994.

28. Layton, C, Bancroft JD, Suvarna SK. 4—Fixation of tissues. In: Suvarna SK, eds. Bancroft's Theory and Practice of Histological Techniques. 8th ed. Amsterdam: Elsevier, 2019: 40–63.

29. McManus, J. Histological and histochemical uses of periodic acid. Stain Technol 1948; 23(3): 99–108. doi: 10.3109/10520294809106232

30. Alsanosy AA, Noreldin AE, Elewa YHA, Mahmoud SF, Elnasharty MA, Aboelnour A. Comparative features of the upper alimentary tract in the domestic fowl (Gallus gallus domesticus) and kestrel (Falco tinnunculus): a morphological, histochemical, and scanning electron microscopic study. Microsc Microanal 2021; 27(1): 201–14. doi: 10.1017/S1431927620024812

31. Sysel AM, Valli VE, Nagle RB, Bauer JA. Immunohistochemical quantification of the vitamin B12 transport protein (TCII), cell surface receptor (TCII-R) and Ki-67 in human tumor xenografts. Anticancer Res 2013; 33(10): 4203–12.

32. Vis AN, Kranse R, Nigg AL, van der Kwast TH. Quantitative analysis of the decay of immunoreactivity in stored prostate needle biopsy sections. Amer J Clin Pathol 2000; 113(3): 369–73. doi: 10.1309/CQWY-E3F6-9KDN-YV36

33. Chamba F, Puyalto M, Ortiz A, Torrealba H, Mallo JJ. Effect of partially protected sodium butyrate on performance, digestive organs, intestinal villi and E. coli development in broilers chickens. Int J Poult Sci 2014; 13(7): 390–6. doi: 10.3923/ijps.2014.390.396

34. Sikandar A, Zaneb H, Younus M, et al. Effect of sodium butyrate on performance, immune status, microarchitecture of small intestinal mucosa and lymphoid organs in broiler chickens. Asian-Australas J Anim Sci 2017; 30(5): 690–9. doi: 10.5713/ajas.16.0824

35. Galfi P, Bokori J. Feeding trial in pigs with a diet containing sodium n-butyrate. Acta Vet Hung 1990; 38(1/2): 3–17.

36. Olukosi O, Dono N. Modification of digesta pH and intestinal morphology with the use of benzoic acid or phytobiotics and the effects on broiler chicken growth performance and energy and nutrient utilization. J Anim Sci 2014; 92(9): 3945–53. doi: 10.2527/jas.2013-6368

37. Xu YH, Gao CL, Guo HL, et al. Sodium butyrate supplementation ameliorates diabetic inflammation in db/db mice. J Endocrinol 2018; 238(3): 231–44. doi: 10.1530/JOE-18-0137

38. Józefiak D, Rutkowski A, Martin S. Carbohydrate fermentation in the avian ceca: a review. Anim Feed Sci Technol 2004; 113(1/4): 1–15. doi: 10.1016/j.anifeedsci.2003.09.007

39. Moquet P, Onrust L, Van Immerseel F, Ducatelle R, Hendriks W, Kwakke RP. Importance of release location on the mode of action of butyrate derivatives in the avian gastrointestinal tract. Worlds Poult Sci J 2016; 72(1): 61–80. doi: 10.1017/S004393391500269X

40. Strous GJ, Dekker J. Mucin-type glycoproteins. Crit Rev Biochem Mol Biol 1992; 27(1/2): 57–92. doi: 10.3109/10409239209082559

41. Corfield AP, Myerscough N, Longman R, Sylvester P, Arul S, Pignatelli M. Mucins and mucosal protection in the gastrointestinal tract: new prospects for mucins in the pathology of gastrointestinal disease. Gut 2000; 47(4): 589–94. doi: 10.1136/gut.47.4.589

42. Eren U, Kum S, Nazligul A, et al. TLR2 and TLR4 molecules and antigen-presenting cell compositions in cecal tonsils of broiler chicks (Gallus gallus domesticus) in the first two weeks of the post-hatch period. Anat Histol Embryol 2022; 51(1): 125–35. doi: 10.1111/ahe.12773

43. Pepper MS, Skobe M. Lymphatic endothelium: morphological, molecular and functional properties. J Cell Biol 2003; 163(2): 209–13. doi: 10.1083/jcb.200308082

44. Da Silva C, Wagner C, Bonnardel J, Gorvel JP, Lelouard H. The Peyer's patch mononuclear phagocyte system at steady state and during infection. Front Immunol 2017; 8: 1254. doi: 10.3389/fimmu.2017.01254

45. Montes GS, Krisztán RM, Shigihara KM, Tokoro R, Mourão PA, Junqueira LC. Histochemical and morphological characterization of reticular fibers. Histochemistry 1980; 65(2): 131–41. doi: 10.1007/BF00493161

46. Lundqvist C, Melgar S, Yeung M, Hammarström S, Hammarström ML. Intraepithelial lymphocytes in human gut have lytic potential and a cytokine profile that suggest T helper 1 and cytotoxic functions. J Immunol 1996; 157(5): 1926–34.

47. Yang W, Yu T, Huang X, et al., Intestinal microbiota-derived short-chain fatty acids regulation of immune cell IL-22 production and gut immunity. Nat Commun 2020; 11(1): 4457. doi: 10.1038/s41467-020-18262-6

48. Keir ME, Yi T, Lu TT, Ghilardi N. The role of IL-22 in intestinal health and disease. J Experiment Med 2020; 217(3): e20192195. doi: 10.1084/jem.20192195

49. Patnaude L, Mayo M, Mario R, et al. Mechanisms and regulation of IL-22-mediated intestinal epithelial homeostasis and repair. Life Sci 2021; 271: 119195. doi: 10.1016/j.lfs.2021.119195

50. Chen Z, Downing S, Tzanakakis ES. Four decades after the discovery of regenerating islet-derived (Reg) proteins: current understanding and challenges. Front Cell Dev Biol 2019; 7: 235. doi: 10.3389/fcell.2019.00235

51. Tsai PY, Zhang B, He WQ, et al. IL-22 upregulates epithelial claudin-2 to drive diarrhea and enteric pathogen clearance. Cell Host Microbe 2017; 21(6): 671-81, e4. doi: 10.1016/j.chom.2017.05.009

52. Wang Y, Mumm JB, Herbst R, Kolbeck R, Wang Y. IL-22 increases permeability of intestinal epithelial tight junctions by enhancing claudin-2 expression. J Immunol 2017; 199(9): 3316–25. doi: 10.4049/jimmunol.1700152

53. Alva-Murillo, N, Medina-Estrada I, Báez-Magaña M, Ochoa-Zarzosa A, López-Meza JE. The activation of the TLR2/p38 pathway by sodium butyrate in bovine mammary epithelial cells is involved in the reduction of Staphylococcus aureus internalization. Molec Immunol 2015; 68(2): 445–55. doi: 10.1016/j.molimm.2015.09.025

54. Dou X, Gao N, Lan J, Han J, Yang Y, Shan A. TLR2/EGFR are two sensors for pBD3 and pEP2C induction by sodium butyrate independent of HDAC inhibition. J Agric Food Chem 2019; 68(2): 512–22. doi: 10.1021/acs.jafc.9b06569

55. Dou X, Ma Z, Yan D, et al., Sodium butyrate alleviates intestinal injury and microbial flora disturbance induced by lipopolysaccharides in rats. Food Funct 2022; 13(3): 1360–9. doi: 1360–9. 10.1039/D1FO03183J

56. Triantafilou K, Vakakis E, Orthopoulos G, et al. TLR8 and TLR7 are involved in the host's immune response to human parechovirus 1. Eur J Immunol 2005; 35(8): 2416–23. doi: 10.1002/eji.200526149

57. Brownlie R, Allan B. Avian toll-like receptors. Cell Tissue Res 2011; 343(1): 121–30. doi: 10.1007/s00441-010-1026-0

58. Veneziani I, Alicata C, Pelosi A, et al. Toll-like receptor 8 agonists improve NK-cell function primarily targeting CD56brightCD16– subset. J Immunother Cancer 2022; 10(1): e003385. doi: 10.1136/jitc-2021-003385

Imunohistokemične in histomorfometrične spremembe tankega črevesa, povezane z dodatkom natrijevega butirata pri piščancih

M. A.M. Alsafy, S. M. Ez Elarab, I. A. Abdellatif, Y. H. Elewa, H. A. Basha, N. F. Bassuoni, S. A. El-Gendy, M. A. Abumandour, C. S. Rutland, K. Roshdy

Izvleček: Raziskava je ocenila učinke dodajanja natrijevega butirata (SB) na razvoj tankega črevesa pri piščancih brojlerjih. Za histološke preiskave dvanajstnika, teščega in vitega črevesa sta bili uporabljeni periodična kislina-Schiff (PAS) in imunohistokemija. Histomorfometrični podatki za dvanajstnik, tešče in vito črevo (dolžina resic, globina kripte, število čašastih celic) ter imunohistokemična obarvanost tkiva z interlevkinom-22 (IL-22) in Tollu podobnim receptorjem 8 (TLR8) so bili izmerjeni v kontrolni skupini in skupini, ki je prejemala dodatek SB. Histološke spremembe v skupini z dodatkom SB so bile v primerjavi s kontrolno skupino naslednje: v tankem črevesu (dvanajstniku, teščem in vitem črevu) so se povečale dolžine, širine in globine kript. Povečano je bilo število čašastih celic, zlasti v vitem črevesu. Poleg tega je bilo limfatično tkivo v tankem črevesu v skupini z dodatkom SB v primerjavi s kontrolno bistveno večje (površina prečnega prereza = SB 34,8 ± 0,5 m2, pri kontrolni skupini pa 13,2 ± 0,5 m2) in je pokazalo več limfatičnih vozličev ter bolj razpršeno limfatično tkivo v podsluznici. Piščanci nimajo bezgavk, zato ima limfatično tkivo sluznice črevesa pomembno imunološko vlogo. V epiteliju tankega črevesa smo opazili značilno imunohistokemično izražanje proteinov IL-22 in TLR8, kar lahko ima vlogo pri zaščiti pred številnimi patogeni in rakom prebavil.

Ključne besede: IL-22; TLR8; črevesne resice; natrijev butirat; čašaste celice; limfatični vozliči

Slov Vet Res
DOI 10.26873/SVR-1809-2023
UDC 665.526:612.887:639.21
Pages: 223–31

Original Research Article

Tea Tree (*Melaleuca alternifolia*) and Geranium (*Pelargonium graveolens*) Essential Oils as new Anesthetics in Rainbow Trout (*Oncorhynchus mykiss*)

Key words

Oncorhynchus mykiss;
anesthesia;
histopathology;
tea tree;
geranium

Hakan Didinen

Yalvaç Vocational School of Technical Sciences, Isparta University of Applied Sciences, Yalvaç, Isparta, Turkey

Corresponding author: hakandidinen@isparta.edu.tr

Abstract: In the present study was investigated anesthetic and histopathological effects of tea tree (*Melaleuca alternifolia*) and geranium (*Pelargonium graveolens*) essential oils in rainbow trout. These essential oils were applied at 20, 50, 70, 100, 150, 200, 300, 400, 500 and 600 mg L-1 concentrations to determine the anesthetic effect. As a result of this study, major components were found as beta-citronellol (27.52%) for geranium oil and 4-terpineol (40.77%) for tea tree oil. The lowest effective doses of geranium and tea tree oils were 400 mg L^{-1} and 300 mg L^{-1} for deep anesthesia of fish, respectively. At these doses, anesthesia induction and recovery times were 129.00 and 247.00 s for geranium essential oil, 118.67 and 65s for tea tree essential oil, respectively. No histopathological findings in liver, kidney and gill tissues were observed in anesthetized fish for each essential oil. In conclusion, geranium and tea tree oils can use as safe and effective anesthetics for rainbow trout.

Received: 11 July 2023
Accepted: 20 November 2023

Introduction

Anesthetics are used for preventing physical injury and stress during aquaculture procedures (1, 2). Drugs, such as quinaldine, etomidate, phenoxyethanol and MS-222 have been often used for anesthesia in aquaculture (3). These agents cause side effects such as excessive mucus and secretion gill irritation (4). Therefore, studies on natural anesthetics in fish have increased recently.

Tea tree (*Melaleuca alternifolia*) is a native plant of Australia. Tea tree is mainly composed of terpinen-4-ol, g-terpinene, α-terpinenene and 1.8-cineole (5,6). The anesthetic activity of *M. alternifolia* essential oil has been investigated in different fish species: common carp (*Cyprinus carpio*) (6), silver catfish (*Rhamdia quelen*) (7), *Astyanax bimaculatus* (8) and gilthead seabream (*Sparus aurata*) (9) In addition, tea tree essential oil was recommended as anesthetic agent for transport in tambaqui (*Colossoma macropomum*) (10) and nil tilapia (*Oreochromis niloticus*) (11).

Geranium (*Pelargonium graveolens*) exists naturally in South Africa and is generally cultivated in many countries of the world (12,13). The major components of geranium are citronellol, geranoil and citronellal. These components have sedative and antidepressant effects (14,15,16). There is a limited number of studies about the anesthetic efficiency of geranium essential oil in fish. Can et al. (17) showed that geranium oil was an effective anesthetic in *Labidochromis caeruleus* and *Sciaenochromis fryeri*.

In this study, use of geranium (*P. graveolens*) and tea tree (*M. alternifolia*) essential oils in rainbow trout as anesthetic agents and their histopathologic effects were investigated for the first time.

Table 1: Anesthesia stages in fish

Stage	Description	Behaviour exhibited
I	Light sedation	Equilibrium normal. slow swimming. decreased reactivity to external stimuli. slight decrease in opercular rate
II	Deep sedation	Restlessness. equilibrium normal. voluntary swimming still possible; slight decrease in opercular rate no response to weak external stimulus
III	Light anesthesia	Partial loss of equilibrium; swimming erratic. increased opercular rate; reactive only to strong tactile and vibrational stimuli
IV	Deep anesthesia	Total loss equilibrium. lying on one side without movement. opercular movements slow and irregular; loss of all reflexes
	Recovery	Regaining equilibrium and active swimming

Materials and methods

Eessential oil

Tea tree (*Melaleuca alternifolia*) and geranium (*Pelargonium graveolens*) essential oils were purchased from Botalife company (Isparta, Turkey). Analysis of essential oils for determination of their components was performed by GC-MS (Gas chromatography–mass spectrometry).

Experimental design

Fish (10 g) were provided from a rainbow trout farm (Isparta, Turkey). 200 trout were placed in two tanks (450 L) in flowing water system. Fish were fed ad libitum with commertial feed for 15-day adaptation period. Water temperature, pH and dissolved oxygen were measured as 8.2°C, 7.9 and 9.06 mg/L, respectively. Essential oils of tea tree (*M. alternifolia*) and geranium (*P. graveolens*) were dissolved in ethyl alcohol (95%) at 1:10 ratio. After adaptation, anesthetic effects of these essential oils at 20, 50, 70, 100, 150, 200, 300, 400, 500 and 600 mg L^{-1} concentrations were determined in fish. Induction and recovery stages were evaluated according to Keene et al. (18) (Table 1). Each fish was considered replicate (n=10 for each concentration). For anesthesia induction, each fish (one at a time) were caught with hand net from the adaptation tanks and taken in to the aquariums (10 L). After anasthesia, fish were placed to the aquarium (10 L) containing clean water for recovery times. Each stage was recorded with a stopwatch. After recovery, abnormal behavior (swimming, position in the water column, etc.) and mortalities were observed. This study was taken permission by Isparta Applied Sciences University, Animal Experimentation Ethics Committee (No: 77211729-804.01/694).

Histopathological examination

Five fish anesthezed with both essantial oils at 600 mg L^{-1} concentration were euthanized by severing the spinal cords and sampled from tissues (gill, kidney, liver). Tissue samples were fixed in 10% neutral formalin and processed. The samples were embedded in paraffin, and 5µm sections were taken by a Leica RM 2155 rotary microtome (Leica Microsystem). Then, sections were stained with hematoxylin and eosin (HE) examined under a light microscope and microphotographed.

Statistical analysis

The homogeneity of variances by Levene's test and normality of data by Shaphiro-Wilk test were controlled. Then, data were analyzed by one-way ANOVA and significant variations were tested with the Duncan test ($p < 0.05$). Regression equations were used to determination of a relationship between anesthetic concentrations and induction/ recovery times.

Results

Essential oil compounds

The compounds of tea tree (*Melaleuca alternifolia*) and geranium (*Pelargonium graveolens*) essential oils were given in Table 2, 3. Beta.-citronellol (27.52%), citronellyl formate (13.92) in geranium and 4-terpineol (40.77%), gama terpinene (20.18 %) and alpha. terpinene (10.96 %) in tea tree were found as major compounds.

Anesthesia induction and recovery times

Anesthesia induction time decreased with rising of the concentration of tea tree (Melaleuca alternifolia) and geranium (Pelargonium graveolens) essential oils. Recovery time rised with increasing of dose of these oils. These essential oils did not cause any abnormal behavior or mortalities in rainbow trout.

The lowest effective concentration for deep anesthesia in fish for tea tree essential oil was found as 300 mg L-1 (Table 4). Anesthesia induction and recovery times at this concentration were 118.67 and 65 s respectively . There is a correlation between the anesthesia induction and recovery times with tea tree essential oil concentrations (R2: 0.86 for

Table 2: Components of tea tree essential oil (%)

Name	Retention time	Area%
Furan. Tetrahydro-2.5-dimethyl-	2.509	0.02
Alpha.-pinene. (-)-	6.684	4.30
Camphene	7.249	0.05
Beta.-phellandrene	8.086	0.23
2-.beta.-pinene	8.293	0.30
3-menthene	8.567	0.05
L-Phellandrene	9.479	0.11
Alpha. Terpinene	10.011	10.96
Benzene. Methyl(1-methylethyl)- (CAS) Cymol	10.341	4.79
L-Limonene	10.566	2.86
1.8-cineole	10.716	1.96
Beta. Ocimene y	11.403	0.51
Gama terpinene	12.101	20.18
3.8-p-Menthadiene	12.667	0.41
3-Methyl-4-cyclohexene-1.2-dicarboxylic anhydride	12.765	0.19
Alpha.-terpinolene	13.457	2.63
Alpha.-fenchone	13.600	0.24
Dimethylstyrene <alpha-para->	13.690	0.07
Cyclopentanol. 1.2-dimethyl-3-(1-methylethenyl)-. [1R-(1.alpha..2.beta..3.beta.)]	16.959	
4-Terpineol (terpinen-4-ol)	19.377	40.77
3.6-Dimethyl-2.3.3a.4.5.7a-hexahydrobenzofuran	19.545	0.01
Alpha. Terpıneol	20.142	6.33
Terpineol <gamma->	20.403	0.30
7-Oxabicyclo[4.1.0]heptane. 1-methyl-4-(2-methyloxiranyl)-	23.759	0.16
Gurjunene <alpha->	33.601	0.41
Alpha.-guaiene	38.669	0.59
Viridiflorene	38.891	1.03
Alpha.-selinene	39.139	0.16
Alloaromadendrene	44.591	0.19
		100.00

Table 3: Compounds of geranium (Pelargonium graveolens) essential oil (%)

Name	Retention time	Area%
Alpha-pinene. (-)-	6.663	1.10
Beta-myrcene	8.720	0.25
L-Phellandrene	9.457	0.11
Benzene Methyl(1-methylethyl)- (CAS) Cymol	10.296	0.25
Limonene	10.529	0.36
3.6-dimethyl-3.5-cycloheptadienone	10.610	0.07
1.3.6-Octatriene. 3.7-dimethyl-. (E)- (CAS) .BETA. OCIMENE Y	11.377	0.13
Linalool oxide cıs	12.666	0.24
Linalool l	14.319	7.33
Rose oxide A	14.849	1.77
Rose oxide A	15.789	0.70
6-Octenal. 3.7-dimethyl-. (R)-	17.337	0.29
P-Menthan-3-one. (1R.4R)-(+)-	18.086	10.70
Beta. Fenchyl alcohol	20.013	0.38
Beta.-citronellol	22.451	27.52
Z-citral	22.880	2.29
2.6-Octadien-1-ol. 3.7-dimethyl-. (Z)-	23.942	4.07
E-citral	24.810	0.64
6-Octen-1-ol. 3.7-dimethyl-. Formate (CAS) Citronellyl formate	25.251	13.92
Geranyl bromide	26.830	6.49
Alpha.-cubebene	29.801	0.27
Citronellyl acetate	30.182	0.37
Copaene <alpha->	31.585	0.98
Beta. Bourbonene	32.064	2.80
Caryophyllene	34.310	2.36
Beta.-cubebene	34.996	0.19
Aristolen	35.786	0.30
Citronellyl propionate	35.973	0.19
Gurjunene <alpha->	36.214	0.77
Alpha.-humulene	36.565	0.32
Cadina-1(6).4-diene <10betah->	37.695	0.20
Germacrene-d	38.202	2.35
Bicyclogermacrene	39.124	0.51
Cadinene <delta->	40.628	0.90
Citronellyl butyrate	41.282	0.47
Isospathulenol	42.168	0.26
Geranyl butyrate	43.134	1.04
2-Butenoic acid. 2-methyl-. 2-phenylethyl ester. (E)-	44.560	1.01
Eudesmol <epi-gamma->	46.728	5.87
Citronellyl tiglate <(E)->	49.331	0.22
		100.00

Table 4: Anesthesia induction and recovery times for tea tree essential oil

Concentration (mg L^{1})	Induction Time (s) AnaeAnesthesiael				Recovery Time (s)
	I	II	III	IV	
20	58.33±7.51^{a}	-	-	-	
50	52.67±5.51^{a}	236.00±4.58^{a}	-	-	
70	50.00±6.24^{a}	120.33±7.51^{b}	-	-	
100	35.67±4.04^{b}	87.33±5.51^{c}	-	-	
150	34.67±5.51^{bc}	85.33±4.51^{c}	129.33±6.66^{a}	-	
200	28.00±2.65^{abc}	55.00±7.21^{d}	116.67±4.04^{b}	300.67±7.37^{a}	66.00±4.58^{a}
300	26.33±4.04^{cd}	51.00±6.24^{d}	103.00±7.21^{c}	118.67±6.03^{b}	65.00±8.19^{b}
400	25.67±4.51^{d}	49.00±8.19^{d}	75.33±4.51^{d}	117.67±3.21^{bc}	149.00±7.00^{c}
500	22.00±3.00^{d}	48.00±4.58^{de}	67.67±4.04^{d}	107.33±6.51^{c}	237.67±3.21^{d}
600	20.67±2.52^{d}	38.00±3.00^{e}	46.67±5.51^{e}	64.67±5.51^{d}	330.33±7.09^{d}
R^2	0.95	0.89	0.92	0.87	0.99
Equation	$y=175.18x^{-0.33}$	$y=1826.2x^{-0.614}$	$y=0.0005x^{2}-0.5158x+198.05$	$y=148218x^{-1.198}$	$y=0.0014x^{2}-0.3971x+81.4$

Table 5: Anesthesia induction and recovery times for geranium essential oil

Concentration (mg L^{1})	Induction Time (s) AAnesthesialevel				Recovery Time (s)
	I	II	III	IV	
20	67.33±5.69^{a}	-	-	-	
50	63.00±6.08^{a}	145.00±8.89^{a}	272.33±10.97^{a}	-	
70	61.00±9.54^{a}	147.00±4.36^{a}	261.67±5.69^{a}	-	
100	60.00±3.00^{ab}	144.67±7.51^{a}	259.67±8.50^{a}	572.67±12.01^{a}	94.67±9.07^{d}
150	59.00±7.21^{ab}	94.67±10.21^{b}	220.00±9.17^{b}	534.67±7.51^{b}	122.0±12.12^{c}
200	48.00±6.00^{bc}	65.00±8.89^{c}	133.67±10.07^{c}	225.00±11.14^{c}	222.67±9.29^{b}
300	47.67±8.62^{bc}	64.67±13.50^{c}	105.33±6.66^{d}	227.67±9.29^{c}	245.33±11.02^{a}
400	38.33±10.02^{d}	58.00±8.19^{c}	94.33±11.72^{de}	129.00±9.54^{d}	247.00±9.17^{a}
500	21.00±6.00^{e}	57.33±9.29^{c}	84.67±7.09^{e}	115.33±11.93^{de}	246.33±17.56^{a}
600	19.33±3.79^{e}	34.67±7.51^{d}	56.00±7.55^{f}	100.33±12.01^{f}	264.33±10.21^{a}
R^2	0.97	0.90	0.95	0.93	0.89
Equation	$y=-2E-05x^{2}-0.0701x+67.362$	$y=1463.2x^{-0.551}$	$y=0.0009x^{2}-0.9692x+326.75$	$y=74097x^{-1.04}$	$y=-0.0014x^{2}+1.2283x-7.8595$

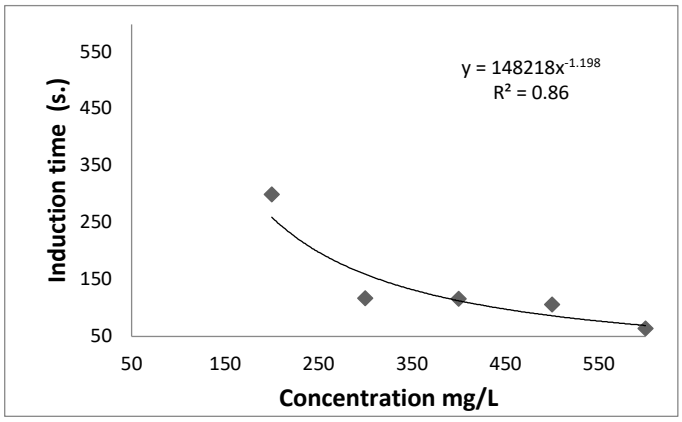

Figure 1: Relationship between tea tree oil concentration with anesthesia induction time of rainbow trout (stage 4).

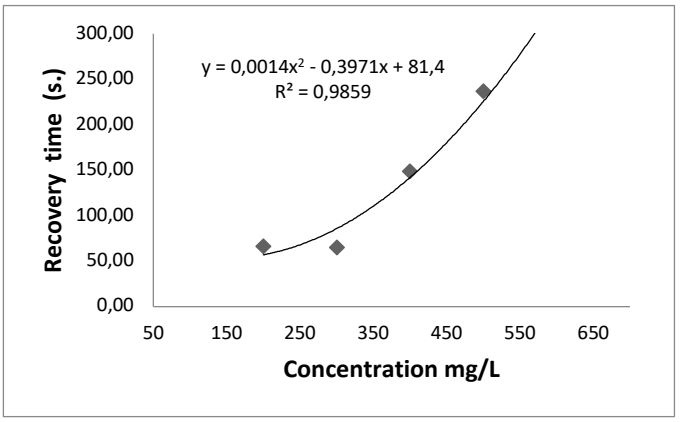

Figure 2: Relationship between tea tree oil concentration with recovery time of rainbow trout

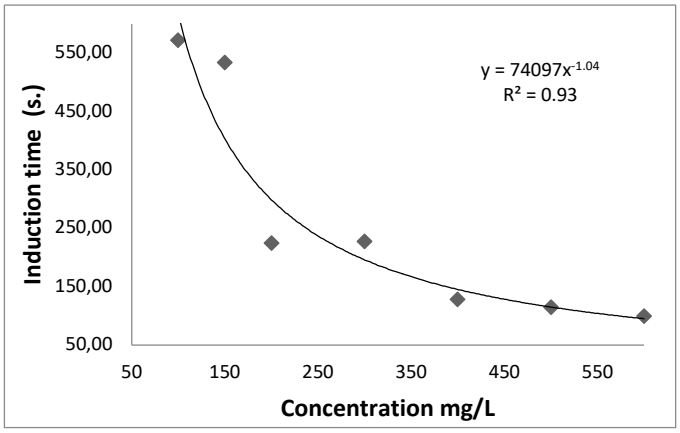

Figure 3: Relationship between geranium oil concentration with anesthesia induction time of rainbow trout (stage 4).

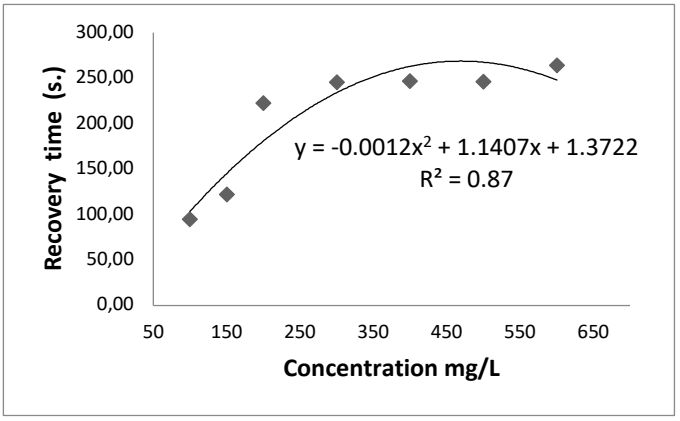

Figure 4: Relationship between geranium oil concentration with recovery time of rainbow trout

anesthesia induction time; 0.99 for recovery time) (Figures 1 and 2).

The lowest effective dose of geranium essential oil in trout was found as 400 mg L -1 for deep anesthesia (anesthesia induction: 129s s and recovery times: 247s) (Table 5). There is a correlation between the anesthesia induction and recovery times with geranium essential oil concentrations (R2: 0.93 for anesthesia induction time; 0.87 for recovery time) (Figures 3 and 4).

Histopathological results

No histopathological findings were detected in gill, liver and kidney of fish anesthetized with each of the essential oils (Figure 5 and 6).

Discussion

Beta citronellol (27.52%), citronellyl formate (13.92%) for geranium (*Pelargonium graveolens*) essential oil and 4-terpineol (40.77%), gama terpinene (20.18 %) and alpha terpinene (10.96 %) for tea tree were found as the primary components in this study. Simalarly, the major components of essential oils have been reported as citronellol (33.49%), geraniol (*synonym* citronellyl formate) (15.08%) for geranium (*Pelargonium graveolens*) (17) and terpinen-4-ol for tea tree *Melaleuca alternifolia*. (7).

Ideal deep anesthesia should occur in approximately 5 minutes and recovery time should not be longer than 10 minutes (19). According to these criteria, the lowest effective dose for deep anesthesia of geranium essential oil in rainbow trout was found as 400 L^{-1} (induction: 129s and recover time: 247s) in the present study. There was one study on the anesthetic effect of geranium essential oil in fish. Can et al. (17) determined that optimal concentration of geranium oil for deep anesthesia in *Sciaenochromis fryeri* and *Labidochromis caeruleus* was 75 µl L^{-1}. Differences can be due to different fish species.

Tea tree (*Melaleuca alternifolia*) essential oil at 300 mg L^{-1} (induction time: 118,67 s and recovery time: 65s) was ideal concentration for deep anesthesia in this study. Simalarly, da Silva et al. (8) noted that *M. alternifolia* at 300

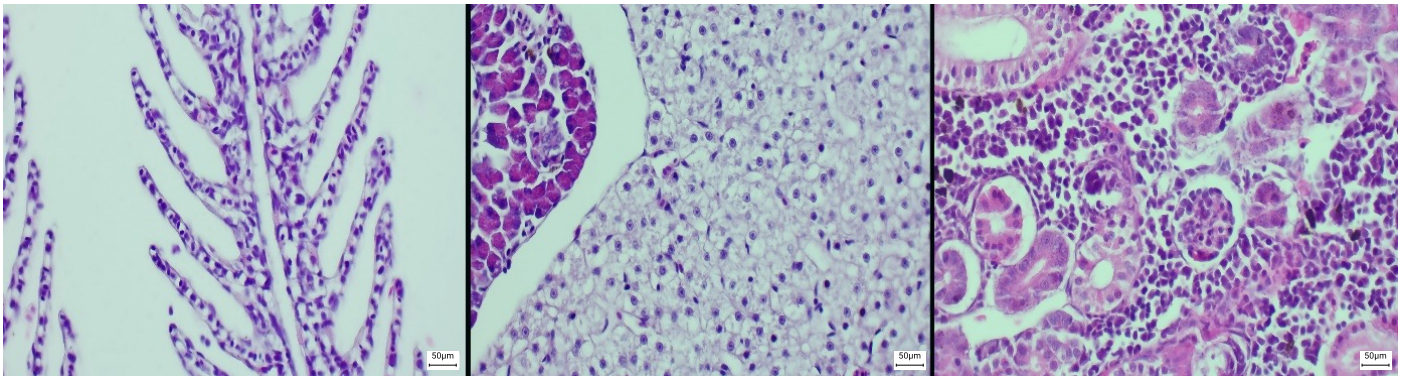

Figure 5: Gill, liver and kidney histology of fish exposed to 600 mg L tea tree essantial oil HE, scale bars =50µm, x20

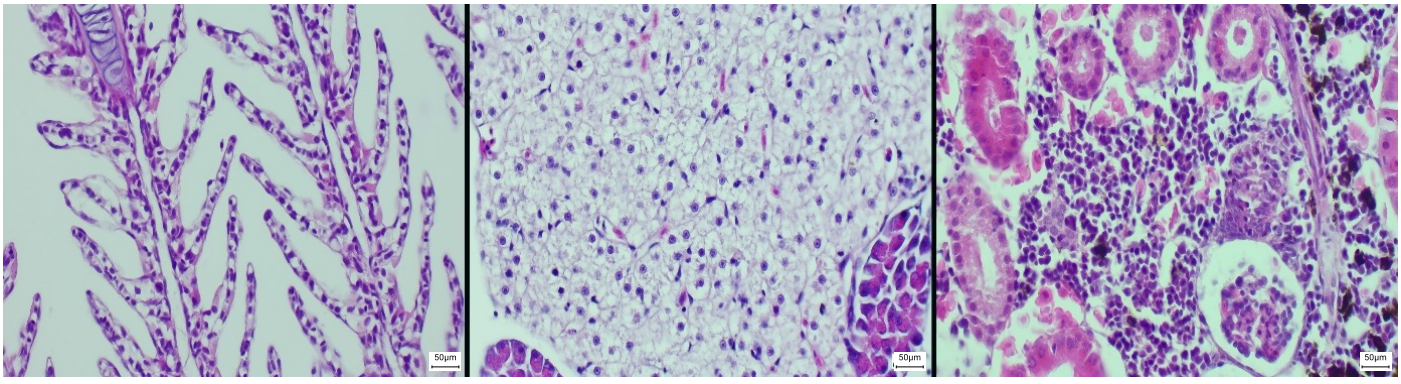

Figure 6: Gill, liver and kidney histology of fish exposed to 600 mg L geranium essantial oil. HE, scale bars =50µm, x20

µl L^{-1} concentration has effective anesthetic properties in Astyanax bimaculatus. Golomazou et al. (9) also observed anesthetic effect at 200 µl L^{-1} concentration (induction time: 691.25 s and recovery time: 302.00) of *M. alternifolia* oil in gilthead seabream (*Sparus aurata*). Hajek (6) informed that *M. alternifolia* at 0.2 to 0.6 ml L^{-1} concentrations provided sedation and immobilization in common carp. Souza et al. (7) showed that tea tree (*Melaleuca alternifolia*) essential oil provided deep anesthesia at concentrations ranging from 500 (316 s) to 1000 µL L^{-1} (185 s) in silver catfish.

In this study, no pathological finding in gill, liver and kidney was observed in fish anesthetized with *Melaleuca alternifolia* and *Pelargonium graveolens* essential oil. Similarly, Santos et al. (10) reported that harmful morphological alterations to the gill epithelium did not observed in tambaqui anesthtezed with tea tree oil during transport. No histopathological effects also reported in liver, kidney and gill of rainbow trout anesthetized with basil (*Ocimum basilicum*), eucalyptus (*Eucalyptus globulus*), coriander (*Coriandrum sativum*), lavender (*Lavandula angustifolia*) and laurel (*Laurus nobilis*) essential oils at 600 mg L^{-1} concentration (20,21,22). Metin et al. (23) reported no lesion in gill, skin, hepatopancreas in common carp anesthetized with lavender (*L. angustifolia*) and cumin (*Cuminum cyminum*) essential oils at 400 and 500 mg L^{-1} concentrations. However, unlike these studies, Yigit and Kocaayan (22) observed marked hyperemia, edema, inflammatory cell infiltrations and desquamation in gills of rainbow trout anesthezied with thyme (*Origanum onites*) essential oil at 600 mg L^{-1} concentration. Brandão et al. (24) also noted that hypertrophy and hyperplasia in gills were observed with use as anesthetics of *Mentha piperita*, *Lippia sidoides* and *Aloysia triphylla* essential oils in tambaqui. Differences among these studies may be due to differences in essential oils and main components in essential oils.

In the present study, the lowest effective concentrations for deep anesthesia in rainbow trout were 400 mg L^{-1} for geranium essential oil and 300 mg L^{-1} for tea tree essential oil. Additionally, these essential oils do not cause tissue damage in fish. Concequently, geranium and tea tree essential oils are suitable using as safely and effectively herbal anesthetics for rainbow trout.

Acknowledgments

We would like to thank Prof. Dr. Ozlem Ozmen for her support during histological examinations in research.

Authorship Contributions. Hakan DIDINEN designed and performed the experiment.

Conflict of Interest. No conflict of interest was declared by the authors.

Data Availability Statement. Data are available on request due to privacy or other restrictions.

References

1. Inoue LAKA, Santos Neto CD, Moraes G. Clove oil as anaesthetic for juveniles of matrinxã Brycon cephalus (Gunther, 1869). Ciênc Rural 2003; 33(5): 943–7. doi: 10.1590/S0103-84782003000500023
2. Facanha MF, Gomes LDC. A eficácia do mentol como anestésico para tambaqui (Colossoma macropomum, Characiformes: Characidae). Acta Amazon 2005; 35: 71–5.
3. Bressler K, Ron B. Effect of anesthetics on stress and theinnate immune system of gilthead seabream (Sparus aurata). Isr J Aquacult Bamid 2004; 56: 5-13.
4. Aydın B, Barbas LAL. Sedative and anesthetic properties of essential oils and their active compounds in fish: a review. Aquaculture 2020; 520: 1–9. doi: 10.1016/j.aquaculture.2020.734999
5. Carson CF, Riley TV. Safety, efficiency and provenance of tea tree (Melaleuca alternifolia) oil. Contact Dermatitis 2001; 45: 65-7. doi: 10.1034/j.1600-0536.2001.045002065.x
6. Hajek GJ. The anaesthetic-like effect of tea tree oil in common carp Cyprinus carpio L. Aquac Res 2011; 42: 296–300. doi: 10.1111/j.1365-2109.2010.02625.x
7. Souza CF, Baldissera MD, Silva LDL, Geihs MA, Baldisserotto B. Is monoterpene terpinen-4-ol the compound responsible for the anesthetic and antioxidant activity of Melaleuca alternifolia essential oil (tea tree oil) in silver catfish. Aquaculture 2018; 486: 217–23. doi: 10.1016/j.aquaculture.2017.12.025
8. da Silva E, Aldegunde M, da Silva DF, Lopes C, Bertoldi FC, Weber RA. Assessment of induction and recovery times of anesthesia in Astyanax bimaculatus using 2-phenoxyethanol and the essential oils of Melaleuca alternifolia and Ocimum gratissimum. Aquac Res 2020; 51: 577–83. doi: 10.1111/are.14404
9. Golomazou E, Malandrakis EE, Kavouras M, et al. Anaesthetic and genotoxic effect of medicinal plant extracts in gilthead seabream (Sparus aurata L.). Aquaculture 2016; 464: 673–82. doi: 10.1016/j.aquaculture.2016.08.017
10. Santos ELR, Rezende FP, Moron SE. Stress-related physiological and histological responses of tambaqui (Colossoma macropomum) to transportation in water with tea tree and clove essential oil anesthetics. Aquaculture 2020; 523: 735164. doi: 10.1016/j.aquaculture.2020.735164
11. Rezende FP, Pascoal LM, Vianna RA, Lanna EAT. Sedation of Nile tilapia with essential oils: tea tree, clove, eucalyptus, and mint oils. Rev Caatinga 2017. 30: 479–86. https://doi.org/10.1590/1983-21252017v30n223rc
12. Boukhris M, Simmonds MSJ, Sayadi S, Bouaziz M. Chemical Composition and biological activities of polar extracts and essential oil of rose-scented geranium, Pelargonium graveolens: chemical composition and biological activities of geranium. Phytother Res 2013; 27: 1206–13. doi: 10.1002/ptr.4853
13. Al-Mijalli SH, Mrabti HN, Assaggaf H, et al. Chemical profiling and biological activities of pelargonium graveolens essential oils at three different phenological stages. Plants (Basel) 2022; 11(7): 2226. doi: 10.3390/plants11172226
14. Sousa DP, de Sousa Oliveira F, de Almeida RN. Evaluation of the central activity of hydroxydihydrocarvone. Biol Pharm Bull 2006; 29: 811–12. doi: 10.1248/bpb.29.811
15. Quintans-Júnior L, Rocha RFD, Caregnato FF, et al. Antinociceptive action and redox properties of citronellal, an essential oil present in lemongrass. J Med Food 2011; 14: 630–9. doi: 10.1089/jmf.2010.0125
16. Sayowan W, Siripornpanich V, Piriyapunyaporn T, Hongratanaworakit T, Kotchabhakdi N, Ruangrungsi N. The harmonizing effects of citronella oil on mood states and brain activities. J Health Res 2012; 26: 69–75.
17. Can E, Kızak V, Can SS, Ozcicek E. Anesthetic potential of geranium (Pelargonium graveolens) oil for two cichlid species, Sciaenochromis fryeri and Labidochromis caeruleus. Aquaculture 2018; 491: 59–64. doi: 10.1016/j.aquaculture.2018.03.013
18. Keene JL, Noakes DLG, Moccia RD, Soto CG. The efficacy of clove oil as an anaesthetic for rainbow trout, Oncorhynchus mykiss (Walbaum). Aquac Res 1998; 29: 89-101. doi: 10.1046/j.1365-2109.1998.00927.x
19. Tsantilas H, Galatos AD, Athanassopoulou F, Prassinos NN, Kousoulaki K. Efficacy of 2-phenoxyethanol as an anaesthetic for two size classes of white sea bream, Diplodus sargus L., and sharp snout sea bream, Diplodus puntazzo. Aquaculture 2006; 253: 64–70. doi: 10.1016/j.aquaculture.2005.07.034
20. Yigit NO, Metin S, Sabuncu OF, et al. Efficiency of Ocimum basilicum and Eucalyptus globulus essential oils on anesthesia and histopathology of rainbow trout, Oncorhynchus mykiss. J World Aquac Soc 2022; 53: 1051–61. doi: 10.1111/jwas.12911
21. Yigit NO, Metin S, Didinen BI, Didinen H, Ozmen O. Effect of lavander (Lavandula angustifolia) and laurel (Laurus nobilis) essential oils as anesthesics in rainbow trout (Oncorhynchus mykiss). Aquacult 2022; 557: 738328. doi: 10.1016/j.aquaculture.2022.738328
22. Yigit NO, Kocaayan H. Efficiency of thyme (Origanum onites) and coriander (Coriandrum sativum) essential oils on anesthesia and histopathology of rainbow trout (Oncorhynchus mykiss). Aquaculture 2023; 562: 738813. doi: 10.1016/j.aquaculture.2022.738813
23. Metin S, Yigit NO, Balkaya M, Didinen BI, Didinen H, Ozmen O. Efficacy of cumin (Cuminum cyminum) and lavender (Lavandula angustifolia) essential oils as anaesthesics in common carp (Cyprinus carpio L. 1758). Aquac Res 2022; 53: 3598–607. doi:10.1111/are.15864
24. Brandão FR, Farias CFS, de Melo Souza DC, et al. Anesthetic potential of the essential oils of Aloysia triphylla, Lippia sidoides and Mentha piperita for Colossoma macropomum. Aquaculture 2021; 534: 736275. doi: 10.1016/j.aquaculture.2020.736275

Eterična olja čajevca (*Melaleuca alternifolia*) in pelargonije (*Pelargonium graveolens*) kot nova anestetika pri šarenki (*Oncorhynchus mykiss*)

H. Didinen

Izvleček: Študija je preučevala anestetične in histopatološke učinke eteričnih olj čajevca (*Melaleuca alternifolia*) in pelargonije (*Pelargonium graveolens*) na šarenko. Ti eterični olji sta bili uporabljeni v koncentracijah 20, 50, 70, 100, 150, 200, 300, 400, 500 in 600 mg L^{-1} za določitev anestetičnega učinka. Na podlagi te študije so bile ugotovljene naslednje glavne sestavine: beta-citronelol (27,52 %) za olje geranije in 4-terpineol (40,77 %) za olje čajevca. Najnižji učinkoviti odmerki olja geranije in čajevca so bili 400 mg L^{-1} oziroma 300 mg L^{-1} za globoko anestezijo rib. Pri teh odmerkih sta bila čas indukcije anestezije in čas prebujanja iz anestezije 129,00 in 247,00 s za eterično olje geranije ter 118,67 in 65 s za eterično olje čajevca. Pri anesteziranih ribah pri nobenem eteričnem olju niso opazili histopatoloških sprememb v tkivih jeter, ledvic in škrg. Iz tega sledi, da se olji geranije in čajevca lahko uporabljata kot varna in učinkovita anestetika za šarenko.

Ključne besede: *Oncorhynchus mykiss*; anestezija; histopatologija; čajevec; geranija

Slov Vet Res
DOI 10.26873/SVR-2147-2025
UDC 636.8:616.72-002:617-089
Pages: 233–9

Case Report

Extended Subtotal Mandibulectomy in a Cat with Alveolar Osteomyelitis Characterized by a Spiculated Periosteal Reaction

Key words

mandibular mass;
alveolar osteomyelitis;
periosteal reaction;
mandibulectomy

Eun-Jae Cho[1], Min-Jung Ko[1], Jae-Eun Hyun[2], Aryung Nam[2], Yun Young Go[3], Hun-Young Yoon[1, 4]*

[1]Department of Veterinary Surgery, [2]Department of Veterinary Internal Medicine, College of Veterinary Medicine, Konkuk University, 120 Neungdong-ro, Gwangjin-gu, Seoul 05029, Republic of Korea, [3]Laboratory of Large Animal Clinical Science, College of Veterinary Medicine, Konkuk University, 120 Neungdong-ro, Gwangjin-gu, Seoul 05029, [4]KU Center for Animal Blood Medical Science, Konkuk University, Seoul 05030, Republic of Korea

***Corresponding author:** yoonh@konkuk

Abstract: A 10-year-old spayed female Scottish Straight cat presented with a firm, non-movable mass in the right mandible. Over the past month, it had progressively enlarged, leading to difficulty eating and subsequent weight loss. Computed tomography (CT) scans revealed that the mass was confined to the body of the mandible, with a prominent periosteal reaction characterized by a spiculated pattern. The extensive and irregular morphology of the periosteal reaction strongly suggested malignancy. No evidence suggestive of metastasis was identified on physical examination or diagnostic imaging. Surgical resection was prioritized over obtaining a definitive diagnosis, owing to the rapid increase in mass size and associated clinical signs. An extended subtotal mandibulectomy was performed for diagnostic and therapeutic purposes, revealing alveolar osteomyelitis. Postoperatively, the patient showed improved masticatory function with no apparent signs of oral pain, indicating a good surgical outcome. During the 16-month follow-up period, the patient remained in good general and physical condition without recurrence of the mass. To the best of our knowledge, this is the first report suggesting that osteomyelitis can present with an extensive, irregular periosteal reaction with radiating lines ("sunburst" subtype), typically associated with malignant tumors. Additionally, surgical resection may be critical for recovery of masticatory function and alleviation of oral pain, even in cases involving benign mandibular lesions.

Received: 26 November 2024
Accepted: 23 May 2025

Introduction

Feline mandibular swelling has a 50% malignancy rate, and benign lesions mostly manifest as osteomyelitis (1). Mandibular bone lesions are expected to be more biologically aggressive when cortical margins are ill-defined, when the zone of transition is broad and indistinct, and when the periosteal reaction is irregular on diagnostic imaging (2, 3). Unfortunately, both malignant tumors and osteomyelitis can exhibit these aggressive characteristics (2, 3, 4, 5). Mandibulectomy is commonly recommended for malignant mandibular tumors because complete surgical excision is the only curative method (6).

Moreover, despite variations in the extent of distant metastasis among different types, most malignant tumors have low metastatic potential (6, 7, 8, 9), suggesting a higher likelihood of achieving curative ablation. Conversely, the extent of local invasion is similar among the different types of mandibular tumors (2). Therefore, there is a general consensus that a minimum margin of 1 cm should be aimed for when planning for surgery with curative intent (2, 7). When surgery is not appropriate, palliative care may temporarily improve quality of life but often leads to euthanasia due to tumor progression (6).

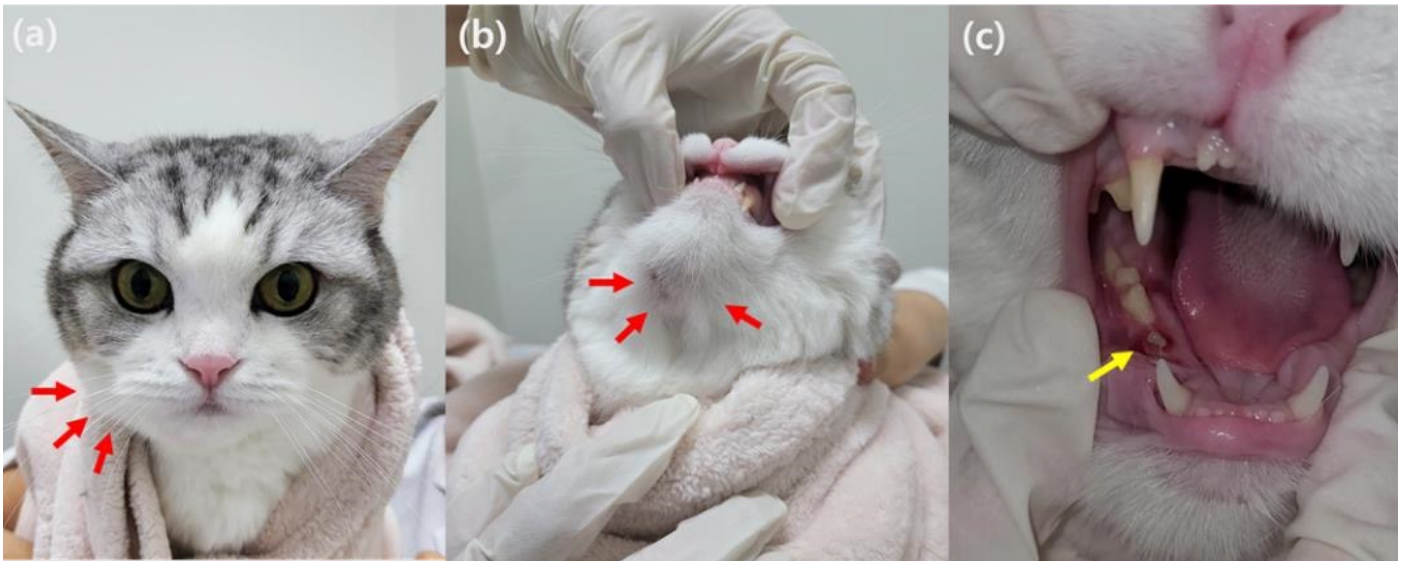

Figure 1: Preoperative examination reveals a firm mandibular mass (red arrow) and gingival erythema around the mandibular right third premolar (Triadan 407) (yellow arrow)

In the treatment of osteomyelitis, while general principles are followed, clinical decisions are often adapted to the patient's specific condition (10, 11). Antibiotic therapy alone may be sufficient, but surgical excision is required in more advanced cases (4, 12). When radical excision is chosen for mandibular osteomyelitis, at least 1 cm margin is generally recommended, although this remains controversial (6, 12). Ultimately, regardless of the presence of malignant tumors or osteomyelitis, mandibular excisions with margins >1 cm are believed to yield a good prognosis.

Among the various mandibulectomy methods, total mandibulectomy is the most invasive and technically demanding procedure (7, 13). It involves removal of the entire mandibular body and ramus with disarticulation of the temporomandibular joint (TMJ), requiring detachment of the masseter, temporalis, medial and lateral pterygoid, and digastricus muscles. Disarticulation of the TMJ can increase surgical risks and anesthesia time due to its technical complexity (13). Although typically reserved for more severe cases, total mandibulectomy has a complication rate of approximately 38%, exceeding that of partial resections (33% for segmental mandibulectomy and 12% for unilateral rostral mandibulectomy) (14). In contrast, subtotal mandibulectomy allows removal of the mandibular body while preserving the vertical ramus associated with TMJ, offering a balance between therapeutic efficacy and functional preservation. A recently described variation, the extended subtotal mandibulectomy, further refines this approach by enabling complete excision of the mandibular canal (13). This technique may minimize surgical morbidity without compromising therapeutic goals, making it an increasingly preferred alternative in appropriately selected cases.

Alveolar osteomyelitis refers to infection or inflammation involving the alveolar bone, including the mandibular canal and medullary spaces, which support the teeth and are commonly affected in association with dental or periodontal disease (4, 15). This case report presents a situation where alveolar osteomyelitis manifests with a spiculated periosteal pattern, a distinctive sign of malignancy. Surgery was required to alleviate the clinical signs, and a wide surgical resection in the form of an extended subtotal mandibulectomy allowed for successful control of the mandibular osteomyelitis.

Case description

A 10-year-old spayed female Scottish Straight cat weighing 3 kg was admitted for evaluation of a right mandibular mass. The patient had difficulty eating, leading to recent weight loss. On history taking, the owner reported that the patient had been diagnosed with a feline odontoclastic resorption lesion (FORL) affecting the right mandible teeth four years earlier. Although tooth extraction is the primary treatment for FORLs, it was not pursued in this case due to concerns regarding anesthesia. Instead, the patient was treated with doxycycline, meloxicam, and alendronate, as reported by the owner. The patient continued antibiotics and nonsteroidal anti-inflammatory drugs (NSAIDs) for the past four years until admission to our hospital.

Physical examination revealed a firm, non-movable mass of size 2 × 3 × 2 cm (W x L x H) in the right mandible. Gingival erythema was also observed, particularly around the mandibular right third premolar (Triadan 407) (Figure 1). The patient exhibited no systemic signs such as fever or lethargy. No abnormalities were detected on superficial lymph node palpation. Blood analysis revealed no significant findings. Radiography demonstrated an extensive, irregular periosteal reaction with radiating lines (the "sunburst" appearance) localized to the right mandibular body, with

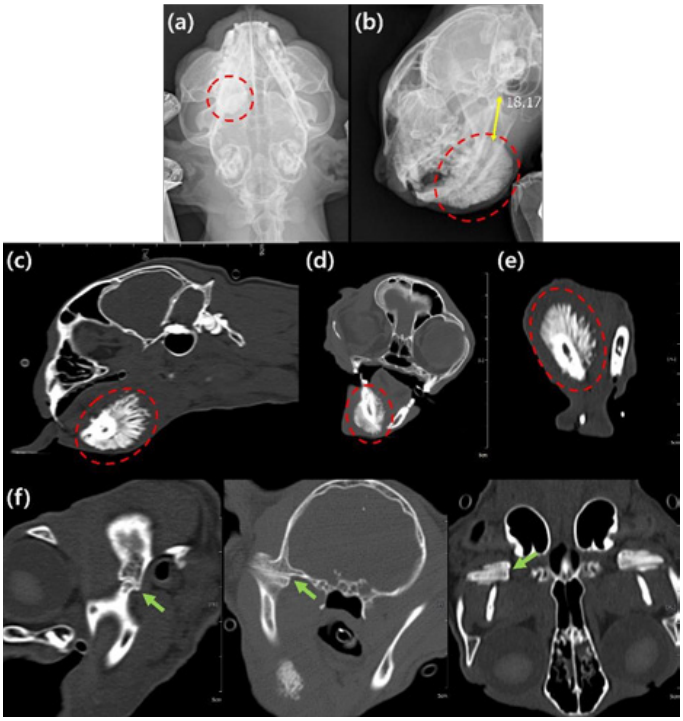

Figure 2: Radiography (a-b) and CT (c-f) reveal a spiculated periosteal reaction ("sunburst" type) on the right mandibular body (red dotted circle), 18.2 mm rostral to the TMJ (yellow arrow). The TMJ shows no evidence of involvement on CT (green arrow)

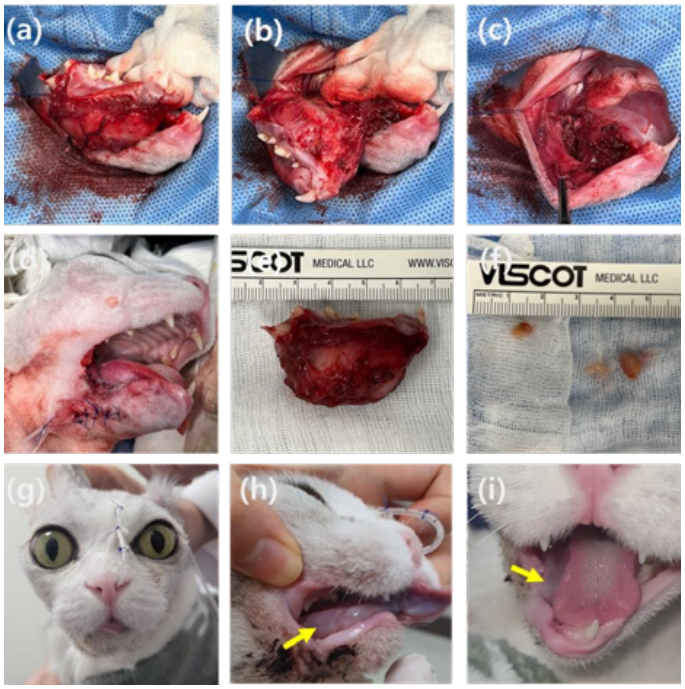

Figure 3: Intraoperative (a-f) and postoperative (g-i) photographs. The mandible is resected approximately 1 cm caudal from the mass (a-c), and a Penrose drain tube is placed (d). The right mandibular lymph nodes are also excised for metastasis evaluation (f). For postoperative care, a nasoesophageal tube is temporarily placed (g). A ranula-like lesion (yellow arrow) is noticeable after surgery (h-i)

the temporomandibular joint (TMJ) unaffected (Figure 2). The caudal border of the periosteal reaction was located approximately 18.2 mm rostral to the right TMJ, specifically the condylar process. Thoracic and abdominal radiography, abdominal ultrasonography, and computed tomography (CT) were performed to evaluate for possible metastasis and to better characterize the bony lesion. CT reconfirmed the periosteal reaction in the right mandibular body without evidence of additional bone involvement or distant metastasis (Figure 2). No signs of possible metastasis were noted across all imaging modalities. Due to the extent and irregularity of the periosteal reaction, a preliminary diagnosis of malignancy was strongly considered, although benign tumors and inflammatory conditions could not be entirely ruled out.

Although preoperative biopsy was considered, extended subtotal mandibulectomy was prioritized to address the rapid growth of the lesion and the potential risk of temporomandibular joint involvement. The mandible was resected approximately 1 cm caudal from the mass. Considering the high possibility of malignancy, the right mandibular lymph nodes were also excised to evaluate possible metastasis (Figure 3). The entire resected mandible and mandibular lymph nodes were sent for histopathological analysis.

General anesthesia was maintained with isoflurane following propofol induction. Analgesia was achieved with fentanyl CRI. The patient was positioned in left lateral recumbency, and inferior alveolar nerve block was performed using bupivacaine. A labial mucosal incision was made, extending from the mandibular symphysis to the caudal boundary of the planned ostectomy. Dissection was carried along the mandibular body, including the sublingual aspect, to expose the mandibular symphysis rostrally and the caudal boundary of the planned ostectomy. The anterior belly of the digastricus muscle was detached to access the mandibular body. Care was taken to avoid laceration of the inferior alveolar neurovascular structures. The mandibular symphysis was transected and the mandibular body was excised approximately 1 cm caudal to the gross lesion, using a combination of an osteotome and an oscillating saw. The ostectomy was extended caudally towards the angular process to include the mandibular foramen, enabling en bloc removal of the mandibular canal, consistent with an extended subtotal mandibulectomy technique. The vertical ramus, including the coronoid and condylar processes, was preserved, and disarticulation of the temporomandibular joint was not required. Margins were planned based on preoperative CT imaging and intraoperative gross appearance, aiming to achieve 1 cm of grossly normal tissue around the lesion. Margin evaluation was based on intraoperative gross assessment, as histologic confirmation of clean margins is inherently challenging in chronic osteomyelitis due to diffuse inflammatory remodeling. Wound closure was performed using 4-0 PDS® II (polydioxanone, Ethicon, Johnson & Johnson, USA) for the digastricus, oral mucosa,

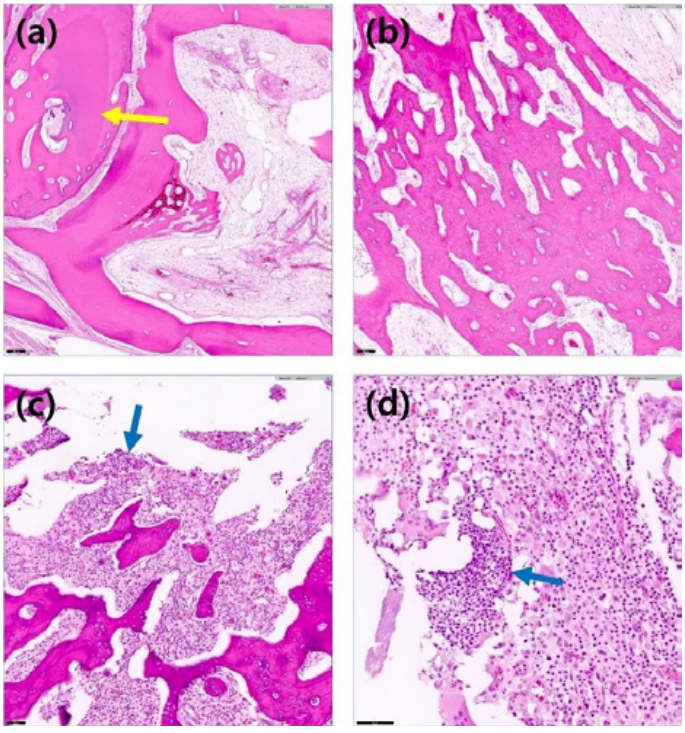

Figure 4: Histopathology of the resected mandibular specimen (H&E, 5x (a), 10x (b), 20x (c), 40x (d) magnifications). Alveolar osteomyelitis manifests as suppurative, marked, chronically active areas with microabscess formation (blue arrow), granulation tissue, chronic bony reorganization, and intratrabecular edema. Periosteal woven bone proliferation is observed in the mandible (a, b, c) and tooth (yellow arrow).

and subcutaneous layers, and 3-0 Dafilon® (monofilament polyamide, B. Braun, Melsungen, Germany) for the skin.

A Penrose drain tube was placed to manage the anticipated dead space, secured using two interrupted sutures, and removed on postoperative day 5 due to marked reduction in drainage and to minimize the risk of retrograde infection. A nasoesophageal tube was temporarily placed for postoperative care to support enteral nutrition (Figure 3). Return of voluntary appetite was confirmed on postoperative day 7. However, oral ingestion was postponed and the nasoesophageal tube was maintained until the day of suture removal (postoperative day 17), to minimize the risk of dehiscence caused by food-related trauma.

Histopathological examination of the resected mandibular specimen revealed alveolar osteomyelitis with periodontitis (Figure 4), as well as reactive lymphadenopathy of the right mandibular lymph nodes. Alveolar osteomyelitis manifested as suppurative, marked, chronically active areas with microabscess formation, granulation tissue, chronic bony reorganization, and intratrabecular edema. Marked chronic periosteal new woven bone formation was also observed. The mandibular lymph As a wide resection was performed and no clinical signs were observed postoperatively, the likelihood of residual disease was considered low. However, given the chronicity and extent of the lesion, and the inherent difficulty in assessing complete surgical margins in chronic osteomyelitis, adjunctive clindamycin therapy (22 mg/kg PO BID for 6 weeks) was administered postoperatively to minimize the risk of residual infection and recurrence.

After surgery, a transient ranula-like lesion developed and spontaneously resolved within 2 weeks. Persistent minor drooling was noted but required minimal care. (Figure 3) Although cheiloplasty was considered, further intervention was not pursued due to the owner's concern about anesthesia. The cosmetic changes associated with extended subtotal mandibulectomy were minimal (Figure 3), and no major complications were identified.

Postoperatively, the patient showed improved masticatory function, with no apparent signs of oral pain. Clinical improvement was clearly evident by the time of suture removal and remained stable throughout the 16-month follow-up period. The patient remained in good general and physical condition without recurrence, as assessed through periodic phone interviews with the owner. Although the patient did not return for in-clinic re-evaluation beyond the early postoperative period, the overall surgical outcome was deemed successful, with complete resolution of clinical symptoms and no major complications.

Discussion

In this case, the extensive periosteal reaction, typically characteristic of malignancy, led to the initial assumption of a neoplasm. Periosteal and endosteal new bone formation (reactive bone formation) is a common feature of neoplasia and osteomyelitis, along with osteolysis and osteosclerosis (3, 4, 5). However, although bone infections may also have an active periosteal reaction, extremely aggressive periosteal reactions are more commonly associated with tumors (3, 16). Furthermore, the immense degree of periosteal reaction observed in this case, is rare even in tumors, let alone in osteomyelitis. In cats, the “sunburst” subtype of periosteal reaction in the mandible has been described in a few cases of osteosarcoma (17), and squamous cell carcinoma (6), but not in osteomyelitis. In humans, strong periosteal reaction has been described in osteomyelitis but typically manifests as an “onion-skin” (laminated) appearance (18, 19, 20, 21). The spiculated pattern, including both “hair-on-end” and “sunburst” subtypes, is highly suggestive of Ewing’s sarcoma and osteosarcoma (20), respectively. To our knowledge, this is the first report to show that the aggressiveness of mandibular osteomyelitis can be equal to or even exceed that of neoplastic changes.

The need for surgery and the extent of surgical resection are typically guided by biopsy results and the patient's response to initial medical management, such as antimicrobial therapy. Advanced imaging modalities such as CT can improve biopsy accuracy by identifying the most representative areas for sampling. However, biopsy results may still be misleading due to non-representative sampling, particularly in heterogeneous or necrotized bone lesions.

Furthermore, initial medical therapy is often ineffective in osteomyelitis due to antimicrobial resistance or poor drug penetration caused by local ischemia and the presence of a "blood-bone" barrier (22). In this case, although preoperative biopsy was considered, surgical resection was prioritized because of the rapid progression of the lesion over one month and the risk of TMJ involvement. Recognizing the potential for sarcoma, wide resection margins were intentionally obtained, including complete removal of the mandibular canal, to mitigate the risk of incomplete excision. In feline patients, achieving margins greater than 1 cm is challenging due to their small craniofacial dimensions (6). Since wide resection was attainable without exposure of the TMJ, surgery was considered a better option than waiting for a definitive diagnosis. Additionally, no remission was observed with previous long-term administration of antibiotics and NSAIDs prescribed for presumed FORL, further supporting the need for surgical management. Thus, while preoperative biopsy remains the gold standard, in extensive bone lesions where wide resection is achievable without significant morbidity, direct surgical excision may be justified to preserve anatomical function and optimize outcomes.

Several classification systems exist; however, osteomyelitis of the jaw is generally classified according to its chronicity and etiology (4, 5, 12). In humans, the arbitrary standard between acute/subacute and chronic is 4 weeks (4, 5, 12, 23). Although no set standard exists in veterinary medicine, the long-term recognition of mandibular swelling and the histological findings of bony reconstruction in this patient fits the criteria for chronic osteomyelitis.

The underlying cause of osteomyelitis in this case was unclear. Although no microorganisms were observed on histopathology, the exclusion of infectious agents was difficult because culture and sensitivity testing were not performed. However, cultures are often unrewarding (23, 24) because oral microbiota is detected in most cases of mandibular osteomyelitis, indicating the possibility of sample contamination. In addition, negative culture results may result from inadequate techniques (4, 5, 12, 23). Osteomyelitis of the jaw may occur as a secondary consequence of periodontal disease, endodontic disease, or smoldering regional bacterial infections following extraction, trauma, or systemic inflammatory/metabolic diseases. In cats, osteomyelitis in the form of alveolar bone expansion commonly occurs with periodontitis and/or FORL (4). This phenomenon has not been extensively investigated and can be expressed in various ways such as "peripheral osteitis, " "alveolar osteitis, " and "peripheral buttressing" (4). Although the causal relationship between osteomyelitis, periodontitis, and FORL has not been fully elucidated, some studies suggest that FORL plays a significant role in causing this phenomenon (4, 25).

The patient's history, as reported by the owner, indicated a prior diagnosis of FORL, though no diagnostic imaging or clinical records were available. Histopathology confirmed periodontitis, suggesting a possible association with the osteomyelitis. However, without definitive diagnostic confirmation, the contribution of FORL remains speculative. Given the absence of other comorbidities, a potential link cannot be entirely excluded.

The possibility of medication-related osteonecrosis of the jaw (MRONJ) associated with long-term bisphosphonate therapy should also be considered. This patient had several risk factors consistent with MRONJ, including a history of prolonged alendronate administration, mandibular involvement, and chronic osteomyelitis associated with periodontitis. However, in the absence of necrotic bone or clinical signs of bone exposure, the likelihood of MRONJ in this case is reduced, although it cannot be entirely excluded. (26)

There were minor complications following extended subtotal mandibulectomy; a ranulalike lesion and increased drooling. A ranula-like lesion can develop from formation of hematoma and/or trauma to the salivary ducts. It is speculated that the ranula-like lesion was only transient because careful dissection was made avoiding inadvertent trauma to the mandibular duct and the major sublingual duct that open on the sublingual caruncle. Drooling was likely a consequence of altered jaw conformation following mandibulectomy. No major complications were identified.

The clinical implications of this case report can be summarized as follows. First, to the best of our knowledge, this is the first report suggesting that mandibular osteomyelitis in cats can present with an extensive, spiculated periosteal reaction ("sunburst" subtype), a pattern typically associated with malignant bone tumors. Second, even in patients with benign mandibular lesions, surgical resection plays an important role in improving masticatory function and alleviating oral pain. Particularly, in fast-growing masses that have not yet invaded the TMJ, timely surgical intervention may be critical to preserve joint function and optimize postoperative outcome. Third, extended subtotal mandibulectomy may offer an effective surgical strategy for managing extensive mandibular lesions associated with osteomyelitis, providing both disease control and functional preservation.

References

1. Kapatkin AS, Marretta SM, Patnaik AK, Burk RL, Matus RE. Mandibular swellings in cats: prospective study of 24 cats. J Am Anim Hosp Assoc 1991; 27(6): 575–80.

2. Dittmer KE, Pemberton S. A holistic approach to bone tumors in dogs and cats: radiographic and histologic correlation. Vet Pathol 2021; 58(5): 841–57. doi: 10.1177/0300985821999832

3. Thrall DE, Widmer WR. Textbook of Veterinary Diagnostic Radiology. 7th ed. St. Louis: Elsevier, 2018.

4. Bell CM, Soukup JW. Histologic, clinical, and radiologic findings of alveolar bone expansion and osteomyelitis of the jaws in cats. Vet Pathol 2015; 52(5): 910–18. doi: 10.1177/0300985815591079

5. Gudmundsson T, Torkov P, Thygesen TH. Diagnosis and treatment of osteomyelitis of the jaw – a systematic review (2002-2015) of the literature. J Dent Oral Disord 2017; 4(4): 1066. doi: 10.26420/jdentoraldisord.2017. 1066

6. Bilgic O, Duda L, Sánchez MD, Lewis JR. Feline oral squamous cell carcinoma: clinical manifestations and literature review. J Vet Dent 2015; 32(1): 30–40. doi: 10.1177/089875641503200104

7. Johnston SA, Tobias KM. Veterinary Surgery: small animal. 2nd ed. St. Louis: Elsevier; 2017.

8. Pavlin D, Dolenšek T, Švara T, Nemec A. Solid type primary intraosseous squamous cell carcinoma in a cat. BMC Vet Res 2018;14(1): 23. doi: 10.1186/s12917-018-1344-0

9. Quigley PJ, Leedale AH. Tumors involving bone in the domestic cat: a review of fiftyeight cases. Vet Pathol 1983;20(6):670–86. doi: 10.1177/030098588302000603

10. Panteli M, Giannoudis PV. Chronic osteomyelitis: what the surgeon needs to know. EFORT Open Rev 2016; 1(5): 128–35. doi: 10.1302/2058-5241.1.000017

11. Marais LC, Ferreira N, Aldous C, Le Roux TLB. The outcome of treatment of chronic osteomyelitis according to an integrated approach. Strat Traum Limb Recon 2016; 11(2): 135–42. doi: 10.1007/s11751-016-0259-1

12. Qaisi M, Montague L. Bone margin analysis for osteonecrosis and osteomyelitis of the jaws. Oral Maxillofac Surg Clin North Am 2017; 29(3): 301–13. doi: 10.1016/j.coms.2017.03.007

13. Fiani N, Peralta S. Extended subtotal mandibulectomy for the treatment of oral tumors invading the mandibular canal in dogs—a novel surgical technique. Front Vet Sci 2019; 6: 339. doi: 10.3389/fvets.2019.00339

14. Liptak J. Partial mandibulectomy. In: Griffon D, ed. Complications in small animal surgery. Hoboken: Wiley, 2016: 229–36. doi: 10.1002/9781119421344.ch31

15. Krakowiak PA. Alveolar Osteitis and Osteomyelitis of the Jaws. Oral Maxillofac Surg Clin North Am 2011; 23(3): 401–13. doi: 10.1016/j.coms. 2011.04.005.

16. Patel SJ. Spiculated periosteal reaction: Radiology reference article. Radiopaedia. https://radiopaedia.org/articles/spiculated-periostealreaction?lang=us.

17. Quigley PJ, Leedale A, Dawson IMP. Carcinoma of mandible of cat and dog simulating osteosarcoma. J Comp Pathol 1972; 82(1) :15–8. doi: 10.1016/0021-9975(72)90021-7

18. Baltensperger M, Grätz K, Bruder E, Lebeda R, Makek M, Eyrich G. Is primary chronic osteomyelitis a uniform disease? Proposal of a classification based on a retrospective analysis of patients treated in the past 30 years. J Cranio-Maxillofac Surg 2004; 32(1): 43–50. doi: 10.1016/j.jcms.2003.07.008

19. Tong ACK, Ng IO, Yeung KM. Osteomyelitis with proliferative periostitis: an unusual case. Oral Surg Oral Med Oral Pathol Oral Radiol Endod 2006; 102(5): e14–9. doi: 10.1016/j.tripleo.2006.03.025

20. Akgül HM, Caglayan F, Yılmaz SG, Açıkgöz G. Garre's osteomyelitis of the mandible caused by infected tooth. Case Rep Dent 2018; 1409539. doi: 10.1155/2018/1409539

21. Rana RS, Wu JS, Eisenberg RL. Periosteal reaction. AJR Am J Roentgenol 2009; 193(4): W259–72. doi: 10.2214/ajr.09.3300

22. Nandi SK, Bandyopadhyay S, Das P, et al. Understanding osteomyelitis and its treatment through local drug delivery system. Biotechnol Adv 2016; 34(8): 1305–17. doi: 10.1016/j.biotechadv.2016.09.005

23. Hudson JW. Osteomyelitis of the jaws: a 50-year perspective. J Oral Maxillofac Surg 1993; 51(12): 1294–301. doi: 10.1016/s0278-2391(10)80131-4

24. Arzi B, Fiani N. Diagnostic imaging in veterinary dental practice. J Am Vet Med Assoc 2009; 235(10): 1149–51. doi: 10.2460/javma.235.10.1149

25. Lewis JR, Okuda A, Shofer FS, Pachtinger G, Harvey CE, Reiter AM. Significant association between tooth extrusion and tooth resorption in domestic cats. J Vet Dent 2008; 25(2): 86–95. doi: 10.1177/089875640802500209

26. Hatunen SL, Anderson JG, Bell CM, Campos HC, Finkelman MD, Shope BH. A retrospective case series on bisphosphonate-related osteonecrosis of the jaw in 20 cats. Front Vet Sci 2024; 11: 1436988. doi: 10.3389/fvets.2024.1436988

Razširjena subtotalna mandibulektoemija pri mački z alveolarnim osteomielitisom, za katerega je značilna spikularna periostalna reakcija

E-J. Cho, M-J. Ko, J-E. Hyun, A. Nam, Y. Y. Go, H-Y. Yoon

Izvleček: 10-letna sterilizirana škotska mačka z ravnimi ušesi je imela trdno, nepremično maso na desni spodnji čeljusti. V zadnjem mesecu se je masa postopoma večala, kar je povzročilo težave pri prehranjevanju in posledično izgubo telesne mase. Računalniška tomografija (CT) je pokazala, da je bila masa omejena na telo spodnje čeljusti, z izrazito periostalno reakcijo, za katero je bil značilen špičast vzorec. Obsežna in nepravilna morfologija periostalne reakcije je nakazovala malignost. Pri kliničnem pregledu ali diagnostičnem slikanju ni bilo ugotovljenih znakov, ki bi nakazovali na metastaze. Zaradi hitre rasti mase in s tem povezanih kliničnih znakov je bila kirurška resekcija prednostna pred pridobitvijo dokončne diagnoze. Za diagnostične in terapevtske namene je bila opravljena razširjena subtotalna mandibulektomija, ki je razkrila alveolarni osteomielitis. Po operaciji je imela mačka boljšo žvečilno funkcijo brez očitnih znakov bolečine v ustih, kar kaže na dober kirurški izid. V 16-mesečnem obdobju spremljanja je mačka ostala v dobrem splošnem in fizičnem stanju brez ponovitve tvorbe. Po našem vedenju je to prvo poročilo, ki kaže, da se osteomielitis lahko kaže z obsežno, nepravilno periostalno reakcijo z radiacijskimi črtami (podtip »sunburst«), ki je običajno povezan z malignimi tumorji. Poleg tega je kirurška resekcija lahko ključnega pomena za povrnitev žvečilne funkcije in lajšanje bolečin v ustih, tudi v primerih benignih lezij mandibule.

Ključne besede: mandibularna masa; alveolarni osteomielitis; periostalna reakcija; mandibulektomija; mačka

Table of Content